



Universiteit
Leiden
The Netherlands

Regulation of BMP and TGF β signaling pathway in cancer progression

Ren, J.

Citation

Ren, J. (2020, June 24). *Regulation of BMP and TGF β signaling pathway in cancer progression*. Retrieved from <https://hdl.handle.net/1887/123057>

Version: Publisher's Version

License: [Licence agreement concerning inclusion of doctoral thesis in the Institutional Repository of the University of Leiden](#)

Downloaded from: <https://hdl.handle.net/1887/123057>

Note: To cite this publication please use the final published version (if applicable).

Cover Page



Universiteit Leiden



The handle <http://hdl.handle.net/1887/123057> holds various files of this Leiden University dissertation.

Author: Ren, J.

Title: Regulation of BMP and TGF β signaling pathway in cancer progression

Issue Date: 2020-06-24

Regulation of BMP and TGF β Signaling Pathway in Cancer Progression

Jiang Ren

ISBN: 978-94-028-2085-0

Cover: *GREM1* RNA staining by using *in situ* hybridization in a breast cancer tissue.

© 2020, Jiang Ren, Leiden, the Netherlands. All rights reserved. No part of this thesis may be reproduced, stored, translated or transmitted in any form or by any means now or hereafter, electronic or mechanical without prior written permission from the author.

Cover design & layout by Jiang Ren.

Printed by Ipskamp Printing

The research presented in this thesis was performed at the Department of Cell and Chemical Biology, Leiden University Medical Center, Leiden, The Netherlands. This research was supported by Cancer Genomics Center Netherlands, Onco institute and China Scholarship Council.

Regulation of BMP and TGF β Signaling Pathway in Cancer Progression

Proefschrift

ter verkrijging van
de graad van Doctor aan de Universiteit Leiden,
op gezag van Rector Magnificus prof.mr. C.J.J.M. Stolker,
volgens besluit van het College voor Promoties
te verdedigen op donderdag, 24 juni, 2020
klokke 10:00 uur

door

Jiang Ren

geboren te Langzhong, China

in 1987

Promotor:

Prof. Dr. P. ten Dijke

Leden promotiecommissie:

Prof. Dr. M. J. Goumans

Prof. Dr. A. Moustakas (Uppsala University)

Prof. Dr. M. M. Maurice (Utrecht University Medical Center)

CONTENTS

Introduction and Outline of the Thesis	7
Chapter 1 Bone Morphogenetic Proteins in the Initiation and Progression of Breast Cancer	15
Chapter 2 Invasive Behavior of Human Breast Cancer Cells in Embryonic Zebrafish	47
Chapter 3 Cancer-associated Fibroblast-derived Gremlin 1 Promotes Breast Cancer Progression	67
Chapter 4 Synergistic Reactivation of BMP Signaling by MEK Inhibitor and FK506 Reduces Breast Cancer Metastasis	109
Chapter 5 JUNB Governs a Feed-forward Network of TGF β Signaling that Aggravates Breast Cancer Invasion	141
Chapter 6 Combined Inhibition of TGF β Signaling and the PD-L1 Immune Checkpoint Is Differentially Effective in Tumor Models	181
Summary and Perspectives	203
Addendum Nederlandse Samenvatting	210
List of Abbreviations	213
List of Publications	216
Curriculum Vitae	217
Acknowledgments	218

Introduction and Outline of the Thesis

TGF β family signaling pathway

The transforming growth factor β (TGF β) family comprises a large family of structurally related secreted dimeric cytokines, which includes TGF β s, bone morphogenetic proteins (BMPs), activins, nodal, growth differentiation factors (GDFs), and anti-Müllerian hormone (AMH), among others. TGF β family members signal via single transmembrane type I and type II serine/threonine kinase receptors. Upon ligand-induced heteromeric complex formation, the constitutively active type II kinases trans-phosphorylate type I receptors. In this way the extracellular signal is transduced across the plasma membrane. The type I receptors act downstream of the type II receptors, and it is the type II receptors that determine signaling specificity in the heteromeric complex. Activated type I receptors subsequently initiate intracellular signaling by phosphorylating downstream effector proteins, of which SMAD proteins play a key role [1].

There is a convergence in signaling; 33 genes encode more than 33 TGF β family ligands, signaling via 5 type II receptors, 7 type I receptors and 2 main intracellular SMAD pathways [2]. Whereas the activated TGF β type I receptor induces phosphorylation of SMAD2 and SMAD3, the activated BMP type I receptor mediates the phosphorylation of SMAD1, SMAD5 and SMAD8. These activation receptor-regulated SMADs (R-SMADs) can form heteromeric complexes with common mediator, *i.e.*, SMAD4, which can act as transcription factor complexes that regulate gene transcriptional responses. The ability of SMADs to directly bind to DNA is weak, and they need to act in concert with other DNA-binding transcription factors, such as AP1 and ETS, *etc.*, to efficiently bind to promoters and enhancers. These SMAD interaction partners are subject to extracellular and intercellular cues, which provides one explanation for how different cells can respond differently to a single TGF β family ligand. Apart from the canonical SMAD signaling pathway that is initiated downstream of TGF β family receptors, other non-SMAD intracellular signaling cascades have been shown to be activated in response to TGF β family receptor activation, such as the phosphoinositide 3-kinase (PI3K) pathway, mitogen-activated protein kinase (MAPK) pathway, and Rho-like GTPase pathway, *etc.*, in a cell type-dependent manner. Therefore, the effects of TGF β s and BMPs are strongly dependent on the cellular context, including the state of differentiation and the presence of other factors/pathways [3-5].

TGF β family members regulate many physiological processes, including early embryogenesis, organ morphogenesis, and stem cell renewal, and maintain tissue homeostasis during the adult life of all multicellular organisms [6]. The signaling activity of each family member is carefully controlled, and positive and negative regulators of each step of the pathway have been identified. Ligand bioavailability, for example, is regulated by ligand-binding proteins that block ligand-receptor interactions and coreceptors without intrinsic enzymatic activity present ligands to type I and type II signaling receptors and thereby promote cellular responsiveness. At the receptor and intracellular levels, TGF β and BMP signaling pathway components are subject to regulation by phosphorylation, ubiquitylation, sumoylation and methylation. Not surprisingly, perturbation of TGF β and BMP signaling has been implicated in various developmental disorders and a broad range of diverse pathological processes [6, 7]. This PhD thesis focuses in particular on the role of dysregulated TGF β /BMP signaling in breast cancer progression.

Targeting TGF β /BMP signaling for cancer therapy

TGF β is thought to play a biphasic role; in normal and premalignant cells, TGF β acts as a tumor suppressor by, for example, inhibiting cell proliferation and promoting apoptosis, while in late stages, TGF β -induced cytostatic effects are blocked by oncogene activation, and TGF β acts as a tumor promotor by stimulating invasion and metastasis of cancer cells [8, 9]. How TGF β promotes breast cancer invasion is still not well understood. Moreover, TGF β contributes to cancer progression by acting on cells in the tumor microenvironment. TGF β activates cancer associated fibroblasts (CAFs), suppresses the immune system and stimulates angiogenesis, thereby creating a niche for rapid tumor growth and metastasis [8]. Anticancer effects have been achieved by taking efforts to inhibit TGF β -SMAD signaling extracellularly via TGF β ligand/receptor blocking antibodies or decoy receptors, or inhibition of TGF β -SMAD signaling intracellularly via small-molecule inhibitors of type I/II serine/threonine receptor kinases, or SMAD transcriptional inhibitory peptide aptamers [10-12]. In addition, overactivation of CAFs mediated by high expression of TGF β leads to immune exclusion in certain cancer types (colorectal and metastatic urothelial cancer). This has been shown to be one reason why immune checkpoint blocking antibodies against programmed death-ligand 1 (PD-L1) fail to achieve beneficial therapeutic effects [13, 14]. Therefore, dual targeting of TGF β and PD-L1 may provide an opportunity for more effective cancer immunotherapy.

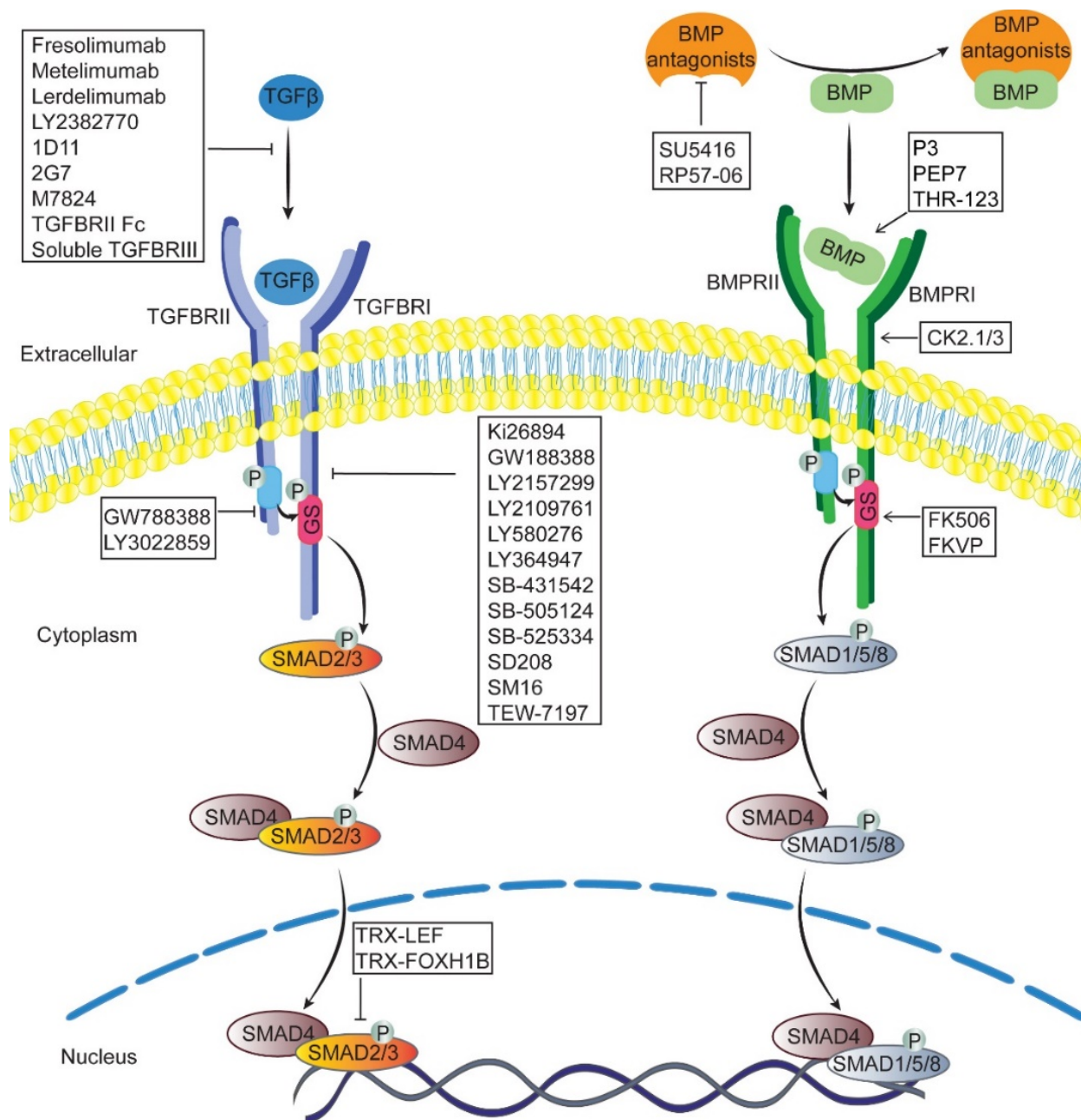


Figure 1. TGFβ and BMP canonical SMAD signaling pathway, and schematic representation of strategies are being utilized to inhibit TGFβ or activate/enhance BMP signaling. Extracellular TGFβ/BMP ligands induce heteromeric complex formation of type II and type I serine/threonine kinase receptors (TGFBRII/BMPRII and TGFBR I/BMPRI, respectively). Cytoplasmic kinase domain of TGFBRII/BMPRII trans-phosphorylates TGFBR I/BMPRI serine and threonine residues in a glycine/serine-rich (GS) domain. The activated TGFBR I/BMPRI phosphorylates regulated SMADs (R-SMADs, SMAD2/3, SMAD1/5/8). R-SMADs form heteromeric complexes with common SMAD4. Then, the complexes translocate into nucleus and bind to target genes promoters to regulate transcription.

TGF β -SMAD2/3 signaling can be inhibited extracellularly by TGF β 1 neutralizing antibody (Fresolimumab, Metelimumab, Lerdelimumab, LY2382770, 1D11, 2G7) or decoy receptor (M7824, soluble TGFBR2 Fc, soluble TGFBR3 (β glycan)); or intracellularly by receptor kinase inhibitors (Ki26894, GW188388, LY2157299, LY2109761, LY580276, LY3022859, LY364947, SB-431542, SB-505124, SB-525334, SD208, SM16, TEW-7197); or by SMAD transcriptional inhibitory peptide aptamers (TRX-LEF, TRX-FOXH1B) [8, 11, 26]. BMP-SMAD1/5/8 signaling can be activated by BMP mimetic peptide (P3, PEP7, THR-123) [23, 24] or BMPRI1A mimetic peptide (CK2.1/3) [19, 25], and enhanced by neutralizing antibody to extracellular BMP antagonists (SU5416, RP57-06) [20-22] or BMPRI1 liberator (FK506, FKVP) [17, 18].

BMPs have been reported to act oppositely of TGF β , promote mesenchymal to epithelial transition (MET), and maintain epithelial identity. BMPs are known to counterbalance the profibrotic role of TGF β , prompting consideration of enhancing BMP signaling to ameliorate chronic fibrotic status [15]. Some neutralizing antibodies targeting extracellular BMP antagonists, synthetic BMP agonists or inducers, and BMP/receptor mimetic peptides can be used to enhance BMP-SMAD1/5 signaling [16-25]. In advanced cancer, therefore, inhibition of TGF β signaling and/or promotion of BMP signaling may provide beneficial and therapeutic effects. However, the interplay between TGF β and BMP during cancer progression and the effects of BMPs on cells in the tumor microenvironment, such as CAFs, are not clear. Elucidating the function of BMP signaling and extracellular and intracellular regulators of this pathway in breast cancer progression and determining how new mechanistic insights can be used for therapeutic intervention have been the main themes of my PhD thesis.

Outline of the thesis

In **Chapter 1**, the current molecular and cellular mechanistic concepts related to BMP signal transduction and regulation are reviewed. An overview of the abnormal expression of BMP signaling components and their potential prognostic value in breast cancer is also presented. In addition, the functions of BMP signaling in breast cancer initiation and progression are discussed, including cancer stem cell self-renewal and tumorigenesis, cancer cell proliferation and apoptosis, the tumor microenvironment, and the processes of metastasis.

There is a need for rapid and efficient breast cancer models to better understand the pathogenesis of cancer metastasis and assess potential treatment strategies *in vivo*. In **Chapter 2**, we introduce step by step protocols to establish two xenograft zebrafish cancer models via

perivitelline space or duct of Cuvier injection. With the use of high-resolution microscopy, human breast cancer cell intravasation and extravasation can be clearly observed.

The misexpression of extracellular BMP antagonists can dysregulate proper BMP signaling. In **Chapter 3**, we report that the BMP antagonist *GREM1* is highly expressed in the tumor stroma and correlates with a poor prognosis of breast cancer patients. Our results demonstrate that Grem1 is a pivotal factor in the reciprocal interplay between breast cancer cells and CAFs that promotes cancer cell invasion. Targeting Grem1 could be beneficial in the treatment of breast cancer patients with high Grem1 expression.

BMP-SMAD1/5 signaling can counteract the promoting role of TGF β -SMAD3 signaling in breast cancer metastasis. In **Chapter 4**, we discovered a negative correlation between BMP signaling and the invasiveness of tumor cells. Sustained ERK activation by TGF β is specifically observed in aggressive cells and contributes to BMP signaling inhibition. In our study, we demonstrate that synergistic activation of BMP signaling by two small chemical compounds at suboptimal doses can achieve a robust decrease in breast cancer metastasis.

It is well known that TGF β signaling switches from tumor-suppressing to tumor-promoting during cancer progression. To define the pro-oncogenic events underlying the interactions between SMAD2/3 and other transcription factors, we performed *de novo* motif analysis of the SMAD2/3 binding regions by chromatin immunoprecipitation with SMAD2/3 antibodies after prolonged TGF β stimulation, as presented in **Chapter 5**. We present a model in which JUNB creates a TGF β signaling feed-forward network, and the secreted cytokine WNT7B plays an effector role in this network in breast cancer to promote breast cancer invasion.

Cancer immunotherapy with programmed death-ligand 1 (PD-L1) checkpoint-blocking antibodies has displayed impressive responses in clinical trials, albeit in approximately 15% of cancer patients. TGF β is a potent immunosuppressive cytokine. Therefore, we investigated whether a TGF β type I receptor kinase inhibitor (LY364947) could enhance the antitumor effect of an anti-PD-L1 mouse monoclonal antibody (mAb) in **Chapter 6**. Our data suggest that whether an additive antitumor effect is seen with dual inhibition of PD-L1 and TGF β signaling is dependent on the tumor model that is used, emphasizing the importance of selecting patients who are suitable for treatment.

In **Chapter 7**, we summarize and provide further perspectives on the results presented in this PhD thesis.

References

1. Shi Y, Massagué J. Mechanisms of TGF β signaling from cell membrane to the nucleus. *Cell* 2003, 113(6):685-700.
2. Heldin CH, Moustakas A. Signaling receptors for TGF β family members. *Cold Spring Harb Perspect Biol* 2016, 8(8):a022053.
3. Massagué J. TGF β signalling in context. *Nat Rev Mol Cell Biol* 2012, 13(10):616-30.
4. Zhang YE. Non-Smad signaling pathways of the TGF β family. *Cold Spring Harb Perspect Biol* 2017, 9(2):a022129.
5. Mu Y, Gudey SK, Landström. Non-Smad signaling pathways. *Cell Tissue Res* 2012, 347(1):11-20.
6. Wu MY, Hill CS. TGF β superfamily signaling in embryonic development and homeostasis. *Dev Cell* 2009, 16(3):329-43.
7. Derynck R, Budi EH. Specificity, versatility, and control of TGF β family signaling. *Sci Signal* 2019, 12(570):eaav5183.
8. Colak S, ten Dijke P. Targeting TGF β signaling in cancer. *Trends Cancer* 2017, 3(1):56-71
9. Massagué J. TGF β in cancer. *Cell* 2008, 134(2):215-30.
10. Neuzillet C, Tijeras-Raballand A, Cohen R, *et al.* (2015) Targeting the TGF β pathway for cancer therapy. *Pharmacol Ther* 2015, 147:22-31.
11. Zhang L, Zhou F, ten Dijke P. Signaling interplay between transforming growth factor- β receptor and PI3K/AKT pathways in cancer. *Trends Biochem Sci* 2013, 38(12):612-20
12. Lan Y, Zhang D, Xu C, *et al.* Enhanced preclinical antitumor activity of M7824, a bifunctional fusion protein simultaneously targeting PD-L1 and TGF β . *Sci Transl Med* 2018, 10(424): ean5488.
13. Mariathasan S, Turley SJ, Nickles D, *et al.* (2018) TGF β attenuates tumour response to PD-L1 blockade by contributing to exclusion of T cells. *Nature* 2018, 554(7693): 544-8.
14. Tauriello DVF, Palomo-Ponce S, Stork D, *et al.* TGF β drives immune evasion in genetically reconstituted colon cancer metastasis. *Nature* 2018, 554(7693): 538-43.
15. Dituri F, Cossu C, Mancarella S, *et al.* The Interactivity between TGF β and BMP Signaling in Organogenesis, Fibrosis, and Cancer. *Cells* 2019, 8(10):E1130.
16. Peiffer BJ, Qi L, Ahmadi AR, *et al.* Activation of BMP signaling by FKBP12 ligands synergizes with inhibition of CXCR4 to accelerate wound healing. *Cell Chem Biol* 2019, 26(5): 652-61.
17. Spiekerkoetter E, Tian X, Cai J, *et al.* FK506 activates BMPR2, rescues endothelial dysfunction, and reverses pulmonary hypertension. *J Clin Invest* 2013, 123(8):3600-13.
18. Akkiraju H, Srinivasan PP, Xu X, *et al.* CK2.1, a bone morphogenetic protein receptor type Ia mimetic peptide, repairs cartilage in mice with destabilized medial meniscus. *Stem Cell Res Ther* 2017, 8(1):82.

19. Ciuculan L, Sheppard K, Dong L, *et al.* Treatment with anti-gremlin 1 antibody ameliorates chronic hypoxia/SU5416-induced pulmonary arterial hypertension in mice. *Am J Pathol* 2013, 183(5):1461-73.
20. Hampton DW, Asher RA, Kondo T, *et al.* A potential role for bone morphogenetic protein signalling in glial cell fate determination following adult central nervous system injury *in vivo*. *Eur J Neurosci* 2007, 26(11):3024-35.
21. Hampton DW, Steeves JD, Fawcett JW, *et al.* Spinally upregulated noggin suppresses axonal and dendritic plasticity following dorsal rhizotomy. *Exp Neurol* 2007, 204(1):366-79.
22. Kang EJ, Kim SK, Eom TG, *et al.* Evaluation of the osteogenic activity of the BMP-2 mimetic peptide, PEP7, *in vitro* and *in vivo*. *Int J Oral Maxillofac Implants* 2013, 28(3):749-56.
23. Tong Z, Guo J, Glen RC, *et al.* A bone morphogenetic protein (BMP)-derived peptide based on the type I receptor-binding site modifies cell-type dependent BMP signalling. *Sci Rep* 2019, 9(1):13446.
24. Akkiraju H, Bonor J, Olli K, *et al.* Systemic injection of CK2. 3, a novel peptide acting downstream of bone morphogenetic protein receptor BMPRIa, leads to increased trabecular bone mass. *J Orthop Res* 2015, 33(2):208-15.
25. Haque S, Morris JC, *et al.* Transforming growth factor- β : A therapeutic target for cancer. *Hum Vaccin Immunother* 2017, 13(8):1741-50.

Chapter 1

Bone Morphogenetic Proteins in the Initiation and Progression of Breast Cancer

Jiang Ren, Peter ten Dijke

Bone Morphogenetic Proteins: Systems Biology Regulators. Springer 2017, p.409-33.

Abstract

Due to their vast roles in human development, differentiation, homeostasis, and disease, bone morphogenetic proteins (BMP) have evolved along with numerous potentiating and inhibitory mechanisms to fine-tune signaling outcomes. As such, this chapter focuses on some of the best-studied and utilized extracellular mechanisms of BMP signal regulation. Due to their inherent binding characteristics, BMP ligands are often found engaged with at least one of these many interacting partners. From a structural and functional perspective, we discuss our current understanding of how BMP ligands interact with these numerous binding partners, including secreted extracellular antagonists, BMP prodomains, and various co-receptors and noncanonical binding partners. Interestingly, while the BMP ligands themselves exhibit very redundant structural features, the composition and structure of their interacting proteins is quite diverse, leading to different ligand-binding modes and mechanisms, which lead to very different biological outcomes. Collectively, biochemical and structural characterization of these important interactions has provided valuable insight into BMP signal regulation.

Keywords: BMP, Breast cancer, Metastasis, Proliferation, DAN family, Follistatin, Chordin, Noggin, Antagonism

Introduction

Bone morphogenetic proteins (BMPs) were originally identified as osteogenic factors with the ability to induce cartilage and bone formation at ectopic sites [1]. Accumulating evidence thereafter showed that BMPs (of which about 20 members have been identified in mammals) can perform versatile functions in embryonic development and in maintenance of adult tissue homeostasis. BMPs were found to regulate proliferation, survival, migration, differentiation, and lineage commitment of many different cell types [2, 3]. Perturbation in BMP signal transduction processes may lead to disease states, including tumorigenesis [3]. BMPs belong to the transforming growth factor β (TGF β) superfamily, which are dimeric ligands that signal via specific transmembrane type I and type II serine/threonine kinase receptors and intracellular SMAD transduction factors. Each step of the BMP signaling pathway is carefully regulated, e.g., through ligand-binding proteins that sequester ligand from binding to receptors and coreceptors that present ligand to these receptors [4]. Recent years have seen an increasing interest in the role of BMP signaling in the development and progression of several cancers [5]. Similar as found for TGF β , BMPs may act as tumor suppressor and/or promoter in a highly contextual manner [5].

BMPs play an important role in the development of embryonic mammary gland [6]. Of interest is also that breast cancer is frequently accompanied by osteolytic metastasis, which accounts for significant morbidity [7]. BMPs are present with high abundance in bone and have the ability to stimulate bone formation [8]. In this review, we aim to overview the recent studies on the relationship between BMPs and breast cancer pathology. After a brief introduction to the key components of BMP signaling pathways and their regulation, we discuss the aberrant expression of canonical BMP/SMAD signaling components and the underlying prognostic value in breast cancer. We then focus on the functions of BMPs in breast cancer initiation, proliferation, apoptosis, tumor microenvironment, as well as the processes of metastasis. The possibilities utilizing these controlling mechanisms of BMPs for therapeutic intervention against breast cancer are also discussed.

BMP signaling and its regulation

BMPs are produced as larger dimeric precursor proteins, which are proteolytically processed thereby generating a carboxy-terminal bioactive domain with highly conserved cysteine residues. This mature dimer may undergo further posttranslational modification such as glycosylation [4, 9]. The BMP signaling cascade is initiated by binding of BMPs to two types of transmembrane

serine/threonine kinase receptors, *i.e.*, BMP type I and type II receptors (BMPRI and BMPRII, respectively) [10]. Generally, initial binding occurs to BMPRI, *i.e.*, activin receptor-like kinase (ALK)1, ALK2 (or ACVR1A), ALK3 (or BMPRIA), and ALK6 (or BMPRIIB), to which BMPs interact with higher affinity as compared to BMPRII. Thereafter, BMPs recruit BMPRII, which is specific for BMPs, or activin type II A receptor (ACVR2A) and activin type IIB receptor (ACVR2B), which are shared type II receptors with the activins (Table 1) [4].

Table 1. BMP subclasses-receptors binding preference

Ligands	Type I receptors	Type II receptors
BMP2/4	ALK3, 6	BMPRII, ACVR2A, ACVR2B
BMP5/6/7/8	ALK2, 3, 6	BMPRII, ACVR2A, ACVR2B
GDF5/6/7	ALK3, 6	BMPRII, ACVR2A, ACVR2B
BMP9/10	ALK1	BMPRII, ACVR2A

As described in Figure 1, upon BMP-induced formation of a heteromeric receptor complex, the constitutively active BMPRII kinase can phosphorylate BMPRI in the highly conserved glycine-serine-rich (GS) juxtamembrane domain. Then, the activated BMP type I receptor in turn can incur intracellular signaling by phosphorylating specific SMADs (R-SMADs), SMAD1/5/8 [9]. These BMP R-SMADs are distinct from TGF β and activin receptor-induced R-SMADs, *i.e.*, SMAD2 and SMAD3. Phosphorylated R-SMADs form heteromeric complexes with common-partner SMAD (Co-SMAD), *i.e.*, SMAD4 [11]. Subsequently, these SMAD complexes can translocate into the nucleus where they serve as transcription factors and recognize specific BMP response elements (BRE) (also termed SMAD-binding elements (SBE)) located within the promoters or enhancers of target genes. In collaboration with other transcription factors and transcriptional coactivators/corepressors, they mediate the transcription of BMP target genes, such as inhibitor of differentiation (ID) 1-3, inhibitory SMAD6, and runt-related transcription factor 2 (RUNX2) [12-14]. Besides the canonical SMAD-dependent pathway, BMPs have also been reported to activate non-SMAD pathways, including stress-activated protein kinase/c-Jun NH2-terminal kinase (JNK), extracellular signal-regulated kinase (ERK), and p38 mitogen-activated protein kinase (MAPK) pathways, as well as phosphoinositide 3-kinase (PI3K)-AKT, protein kinase C (PKC), TGF β -activated kinase 1 (TAK1), and small Rho-GTPases pathways [9, 15].

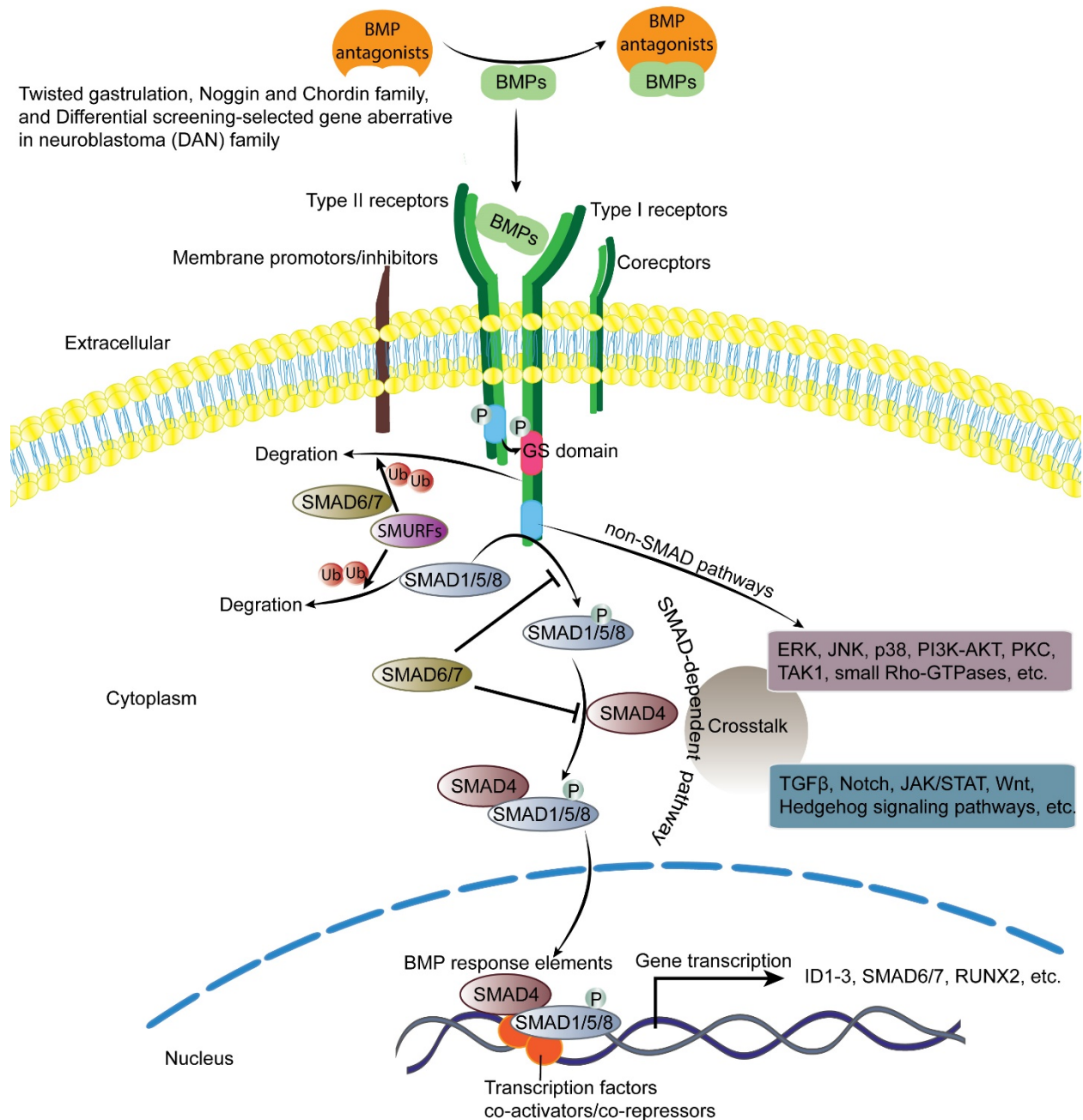


Figure 1. Schematic presentation of the BMP signaling pathway. BMP binds and induces heterotetrameric complex formation of specific single transmembrane-spanning BMP type I and type II receptors. Upon heteromeric complex formation, the extracellular BMP signal is transduced across the membrane by the phosphorylation of BMP type I receptors in the glycine-serine-rich (GS) juxtamembrane domain by the constitutively active type II receptors kinase. The intracellular signal is initiated by the phosphorylation of SMAD1/5/8. These activated R-SMADs can then form heteromeric complexes with SMAD4, which translocate into the nucleus where they collaborate with other DNA-binding transcription factors and transcriptional coactivators/corepressors to regulate the transcription of

BMP target genes (SMAD-dependent pathway). The BMP signal can also be transduced via non-SMAD pathways. BMP signaling is subject to multiple regulations, such as extracellular antagonists, coreceptors, membrane promoters/inhibitors, and inhibitory SMAD6/7. There also exists extensive cross talk between BMP signaling pathways and other signaling pathways

The BMP signaling cascade is subject to intricate regulation at multiple levels. Extracellular antagonists prevent binding of BMPs to receptors either by sequestering the BMP ligands or by binding to the BMP receptors themselves [2]. Like the BMP ligands, the BMP antagonists have a cysteine knot structure, which can be divided into several subclasses: twisted gastrulation, Noggin and Chordin family, and differential screening-selected gene aberrative in neuroblastoma (DAN) family (including DAN, Cerberus, Gremlin 1, protein related to Dan or Cerberus (PRDC), Sclerostin, uterine sensitization-associated gene 1 (USAG1), Caronte, and Coco) [9, 16]. Another type of inhibitors involves soluble receptors in the extracellular environment, which also can sequester BMPs from binding to their transmembrane receptors [17]. Regulation at the cell membrane level is mediated by various membrane proteins. The BMP and activin membrane-bound inhibitor (BAMBI) inhibit BMP signaling by interfering with receptor complex formation [18]. In addition, BMP signaling can be potentiated by some membrane proteins, such as members of the repulsive guidance molecule (RGM) family [19], and coreceptors betaglycan [20] and endoglin (CD105) [21, 22].

Within the cell, Endofin acts as an anchor between SMAD1 and activated BMPRI_s to facilitate SMAD1 phosphorylation. Meanwhile, Endofin can mediate the dephosphorylation and inactivation of BMPRI_s by its motif for protein phosphatase binding [23]. FK506 binding protein 12 (FKBP12) can bind to the GS domain of BMPRI_s, thereby shielding the serine and threonine residues from being phosphorylated by BMPRI_{II}s and stabilizing the inactive conformation [24, 25]. The drug FK506 (tacrolimus) that binds FKBP12 was shown to relieve this inhibition and to potentiate BMP signaling [24, 25]. BMP signaling is also restricted intracellularly by the inhibitory SMADs (I-SMADs), i.e., SMAD6 and SMAD7, which compete with SMAD1/5/8 for interaction with BMPRI_s and with SMAD4 for complex formation with SMAD1 [26, 27]. Both SMAD1 and SMAD5 can be targeted for proteasomal degradation via addition of ubiquitin chains by SMAD ubiquitin regulatory factors (SMURFs). Additionally, by interacting with I-SMADs that can be recruited to activated BMPRI, SMURFs are also capable of decreasing the stability of BMPRI [28].

Importantly, many of the (negative) regulators of BMP signaling themselves are BMP target genes, creating auto-feedback loops that ensure increased fine-tuning of signaling [2, 28, 29]. Additional facets of BMP signaling include cross talk with other signaling pathways, such as TGF β , Notch, Janus kinase/signal transducers and activators of transcription (JAK/STAT), Wnt, and Hedgehog, which further broaden the cellular responses to BMP signaling [30]. Thus, the actual outcome of BMP signaling results from levels and activities of all those cellular context-dependent components mentioned above, explaining the diversity of observed effects.

Aberrant expression of BMP signaling components in breast cancer

In the normal breast, all the necessary components of the canonical BMP signaling pathway (*i.e.*, BMP ligands, BMP receptors, and SMADs) are expressed [31]. Aberrant expression of these components has been observed for breast cancer cell lines with different characteristics and/or has been detected in breast cancer cell lines compared to normal cell lines, in primary tumor tissues compared to normal tissues, and in recurrent tumor tissues compared to primary tumor tissues, however, often with inconsistent and frequent contradictory results. In part, this may be caused by cell lines that were cultured under different conditions and tumors that were not characterized and, for example, not subdivided based upon their genetic alterations and stroma content.

In the forthcoming section, we have listed some examples. Significant lower levels of BMP2 transcript and protein were detected in both noninvasive and invasive breast cancer cell lines and/or cancer cells in breast cancer tissues [31-33]. There were no significant differences in the percentage of BMP2-positive tumors found with respect to cancer cell subtype [31] and grades [33]. What is intriguing, BMP2 protein levels were found to be increased significantly in luminal tumor tissues compared to normal tissues [31]. Immunohistochemical (IHC) staining revealed that BMP2 protein was mainly produced by endothelial cells, fibroblasts, and other stromal cells in luminal tumor microenvironment, not by tumor cells themselves [31]. BMP2 is also highly enriched in bone marrow microenvironment during the process of breast cancer bone metastases [34]. These results indicate that breast tumor cells are the target of BMP2, rather than the source of overexpression.

BMP4 is expressed with wide variation in levels among breast cancer cell lines and/or primary cancer tissues [32, 33, 35-39]. While low levels of BMP4 protein were observed only in normal mammary gland tissue, it was strongly stained in 25 % of patients and more frequent in

lobular carcinoma compared to the ductal carcinoma, suggesting that strong expression is cancer specific [39]. Breast cancer patients with strong BMP4 staining suffered from increased frequency of local and distant tumor recurrence [39]. Another study showed that a four-marker panel with low methylation in breast cancer (paired-like homeodomain 2 (PITX2), BMP4, fibroblast growth factor (FGF) 4, and family with sequence similarity 110, member A (FAM110A)) is associated with a longer duration to distant metastasis [36]. However, opposite results were reported in a study by Kretschmer and coworkers indicating that BMP4 mRNA and protein are clearly reduced in ductal carcinoma *in situ* (DCIS) and invasive ductal carcinoma (IDC) compared to nonmalignant human and murine mammary tissues [40]. A negative correlation between BMP4 mRNA level and tumor grade was reported by Ketolainen *et al.* [37]. Accordingly, lower BMP4 mRNA expression correlated with poor disease-free survival in breast cancer patients [41].

BMP6 mRNA and/or protein expression was consistently found to be significantly downregulated in breast cancer cell lines or primary cancer tissues [33, 42-46]. Downregulation of BMP6 mRNA correlated with the increase in breast tumor histologic grade [46]. Interestingly, compared to estrogen receptor-positive (ER⁺) breast cancers, BMP6 mRNA level is significantly higher in estrogen receptor-negative (ER⁻) breast cancers [43, 45, 46].

BMP7 has been described as being amplified at the gene levels [47, 48] and overexpressed at the mRNA and/or protein levels [33, 47, 49-51] frequently in breast cancer cell lines and/or tissues. BMP7 protein expression was also found to be tumor subtype dependent; 57% of the lobular carcinomas but only 37% of the ductal carcinomas are BMP7 positive [50]. Increased BMP7 DNA copy number was reported to show significant correlation with a high Ki67 proliferation index and high histological tumor grade [47]. In addition, BMP7 overexpression was regarded as an independent prognostic marker for early bone metastasis development by multivariate analysis, especially in ductal carcinomas [50]. But contradicting results for BMP7 expression in breast cancer to those just mentioned have also been reported. For example, extreme low levels of BMP7 mRNA were detected in aggressive cells [52, 53]. Moreover, BMP7 mRNA levels in primary breast cancers involving bone metastases were found lower when compared with those involving visceral (lung and liver) metastases [52]. In addition, lower BMP7 levels in patients show a moderate and poor clinical outcome [33].

Relatively few studies have appeared on the expression of other BMP ligands in breast cancer. No difference in BMP3 mRNA levels between breast tumors and normal tissues was detected, but lower BMP3 transcript levels correlated with a poorer prognosis [33]. Lower BMP5 mRNA levels were observed in breast tumors compared to normal breast tissues [54] and correlated with cancer recurrence, particularly in patients with ER α -negative cancers [54]. In contrast, another study showed that patients with higher levels of BMP5 transcript were associated with moderate and poor prognosis [33]. Moreover, decreased expression of BMP9 [55], BMP10 [56], growth and differentiation factor (GDF) 9a [57], GDF-9b/BMP15 [57], and BMP12 [58] along with poor prognosis was observed in breast cancer compared with matched normal tissues.

Investigations into the expression profiles of BMP receptors and downstream SMAD signaling components have been conducted rather infrequently for breast cancer. BMPRI_s, BMPRII_s, and SMAD4 and inhibitory SMAD6 and 7 were found expressed rather uniformly in breast cancer cells or tissues [35, 38, 59]. DNA homozygous deletion and mRNA downregulation of BMP receptors are rare in breast cancer according to the provisional breast in The Cancer Genome Atlas (TCGA, Provisional) database [60]. BMPRIA [31, 35, 61] and BMPRIB [31, 35, 62] expressions were found overall increased in tumors compared to normal breast tissues. BMPRIB and BMPRII expression is significantly increased in highly metastatic breast cancer cells [51]. Tissue microarrays demonstrated that high expression of BMPRIA [48, 63] and BMPRII [48] correlated with poor relapse-free survival (RFS) or survival. Strong expression of BMPRIB is associated with high proliferation, cytogenetic instability, high grade, and poor prognosis in ER⁺ breast cancer [62]. However, the results from Bokobza *et al.* [64] showed that a decreased level of BMPRIB in breast cancer is associated with poor prognosis.

Only a small portion of breast cancer cell lines and clinical samples were identified as homozygous deletion and reduced mRNA and/or protein expression of SMAD4 [48, 65]. But SMAD4 mutations, which are usually found in pancreatic [66] and colorectal [67] cancer, are rare in breast cancer [65]. Secreted BMP antagonists, such as Gremlin 1 [40, 48, 68, 69], Noggin [31, 48], and Chordin [48], are amplified and/or expressed at higher levels in breast cancer tissues compared to nonmalignant tissues. Of which, Gremlin 1 expression was below detection in breast cancer cells [70] but frequently found expressed in stromal cells within the microenvironment of human breast cancers [68]. In addition, a study conducted by Tarragona et

al. indicated that higher levels of Noggin were found in breast cancer bone metastatic tissues compared to lung, brain, and liver metastatic tissues [71].

Taken together, the results of the studies above on the expression of BMP signaling components suggest a highly context-dependent and multifunctional role of BMPs in breast cancer.

Status of BMP/SMAD signaling in breast cancer

Even though the expression frequencies and levels of BMPs and other BMP signaling components varied considerably among different studies, human breast cancers and their metastases retain BMP/SMAD signaling [48, 61, 72], as well as several mouse models of breast cancer [61].

Strong phospho-SMAD1/5/8 staining, indicative for active BMP receptor signaling, was demonstrated in human breast cancer tissues [48, 61, 72] and not confined to specific cancer cell types within the tumor tissue [48, 61]. This is consistent with the already mentioned finding that the core BMP canonical signaling components were found to be expressed in breast cancer cells. Metastatic breast cancer to the brain, bone, liver, lymph node, and lung was also found to be positive for phospho-SMAD1/5/8 [48, 72]. Lymph node metastasis tissues were demonstrated to be weaker in phospho-SMAD1/5/8 levels than bone metastasis tissues [72]. Moreover, BMP/SMAD signaling is specifically absent in the stroma of human ductal and lobular carcinoma *in situ* (DCIS and LCIS). Yet after progression to invasion, breast cancers of many distinct subtypes contained a stroma active for BMP signaling [73].

Regulation of the expression of BMP signaling components by other factors in breast cancer

The expression of BMPs and other pathway components has been shown to be regulated by several other factors, such as estrogen [43, 45, 46, 49], epidermal growth factor (EGF) [49], and p53 [74]. Estrogen represents the primary stimulant in the development and progression of breast cancers. ER status is a determinant for selecting endocrine therapies to block estrogen signaling [75]. A possible relationship between BMP signaling and ER is therefore an interesting area of research. Estrogen has been shown to alter BMP signaling by downregulating specific BMPs and their receptors in ER⁺ MCF-7 cells, including BMP7, BMPRIA, BMPRIB, ACVR2A, and ACVR2B, but no effect was detected on ACVR1 and BMPRII [59, 76]. In addition, estrogen can

suppress BMP2-induced activation of the SMAD pathway and BMP-mediated gene expression [77]. This effect probably depends on the direct physical interaction of SMAD4 with ER α /ER β [78]. The antiestrogen modulator raloxifene can increase the promoter activity of BMP4 in U2OS osteoblast-like cells in the presence of ER α [79]. In contrast, promoter hypermethylation was found to lead to BMP6 downregulation in ER $^{-}$ breast cancer tissues, while lower methylation frequency was detected in ER $^{+}$ cases [43, 45, 46, 80]. Moreover, BMP6 gene expression can be upregulated by estrogen-mediated demethylation of the BMP6 promoter in ER $^{+}$ MCF-7 cells in a dose-dependent manner [81].

Apart from upregulation of BMP2 and BMP6, a derivative of vitamin D can reduce inhibitory SMAD6 expression and enhance SMAD1/5 phosphorylation [82, 83]. EGF treatment can also lead to elevated levels of BMP6 mRNA in a dose-dependent manner [42]. FGF8 was found to inhibit BMP receptor-mediated SMAD1/5/8 phosphorylation and mitigate BMP target gene ID1 promoter activity by suppressing BMPRII expression and by increasing I-SMAD expression [84]. Parathyroid hormone-related protein (PTHrP) can function as the upstream regulator of BMP6 through the protein kinase A (PKA) pathway and exert its anti-mitogenic effect through downregulating BMP6 mRNA expression [85]. Furthermore, BMP7 is a target gene of the p53 family [61, 74] and LIM domain only protein 4 (LMO-4) [86], which activate BMP signaling by inducing the expression of BMP7 in breast cancer.

In short, many different signaling pathways regulate BMP signaling; these findings explain in part the contextual functions of BMPs.

BMP signaling in stem cell self-renewal and initiation of breast cancer

In human breast cancer, a subpopulation of cancer cells with an ALDH^{high}/CD44^{high}/CD24^{low} phenotype is highly enriched for cancer stem cells (CSCs), also termed tumor initiating cells (TICs), which are capable of initiating and sustaining tumorigenesis [87]. CSCs may be generated from the adult somatic stem cell by disturbing the processes of normal self-renewal or from more differentiated cells through certain processes to reacquire stem cell-like characteristics, such as epithelial to mesenchymal transition (EMT) [87, 88]. BMPs are indispensable for tissue homeostasis in adults, regulating somatic stem cells and controlling differentiation. Aberrant regulation of the BMP signaling pathway could therefore be a target in early phases of tumorigenesis [5].

The evidence points activation of BMP signaling as an early event during primary breast cancer initiation from malignant transformation [31, 48, 61]. Clinically defined samples demonstrate increased BMP signaling in premalignant luminal epithelial cells within the area of DCIS lesions [61]. BMP signaling is also hyperactivated in both epithelium and surrounding stroma in the premalignant mammary gland of transgenic mice model with mouse mammary tumor virus (MMTV)-derived oncogene expression [48, 61]. Chapellier *et al.* [31] showed that stimulation with BMP2 rapidly induced sustained upregulation of a well-known luminal differentiation regulator, GATA3, and progressive switch of the forkhead box (FOX)A1/FOXC1 balance in favor of FOXA1 through BMPRII-dependent signaling, thereby leading to differentiation of normal mammary epithelial cell to luminal and expansion of luminal immature progenitors. In addition, abnormal high levels of BMP2 are produced in the mammary microenvironment upon exposure to common carcinogens. Chronic exposure of MCF10A breast epithelial cells to high levels of BMP2 thus initiates transformation of luminal immature progenitor cells toward a luminal tumorlike phenotype *in vitro* [31].

The small-molecule BMPRI kinase inhibitor Dorsomorphin and its more selective analogs LDN193189 and DMH1 provide the chance to evaluate the effects of BMP type I receptor signaling on tumorigenesis. *In vitro* analysis revealed that suppressing BMP signaling in premalignant murine mammary cells or immortalized mammary epithelial cells (IMECs) repressed mammosphere formation [89] and clonogenic capacity and diminishes the CSC-enriched ALDH1^{high} population [61]. Accordingly, the expression of stem markers, spinocerebellar ataxia type 1(SCA1) and NOTCH1, are markedly reduced [89]. Consistently, BMP4 stimulation increased the number and size of primary mammospheres [89]. Thus, BMP signaling is essential for maintenance of CSCs in breast cancer. Importantly, the BMP receptor kinase inhibitor blocks the ability of ALDH1^{high} fraction to resubstitute the mixed ALDH1^{high}/ALDH1^{low} parental culture, implicating that BMP signaling may control the aspects of cellular plasticity within tumor hierarchies [61]. Furthermore, LDN193189 restricts the tumorigenic capacity of allografts and increases tumor latency *in vivo* [61]. Therefore, these data implicate that BMP signaling is central to regulating mammary epithelial cell stemness, plasticity, and potentially supports maintenance and progression of tumorigenesis.

Interestingly, BMPs also seem to pose a substantial barrier to tumor stemness, when it comes to aggressive and metastatic breast cancers, or rather metastasis-initiating cells. Besides

reduced BMP7 expression, an aggressive clone from MCF-7 cell line shows CD44 upregulation and CD24 downregulation, indicative of a CSC phenotype [90]. BMP4 inhibits mammosphere-forming and tumor-initiating ability in IMEC-transformed derivatives with high motility and high percentage of CD44^{high}/CD24^{low} subpopulation [91]. Multiple BMPs (BMP2, BMP7, BMP2/7) decrease the size of ALDH^{high}/CD44^{high}/CD24^{low} stem/progenitor subpopulation in MDA-MB-231 [92]. Elevated expression of BMP6 in MDA-MB-231 cells results in decreased tumorigenesis *in vivo* [93]. Furthermore, colonization of metastatic cancer cells in the target organs is thought of as another type of tumor initiation, while CSCs are commonly considered as the culprits [94]. High-metastatic cells expressing high levels of the BMP antagonist Noggin [71] or Coco [95] are associated with CSCs traits, with the ability to form more tumor spheres and a higher CD44^{high}/CD24^{low} population that display a higher capacity for metastatic colonization. Mechanistically, Coco induces CSC traits of metastatic cells by sustaining the expression of stem cell transcription factors, NANOG, SRY-related HMG-box (SOX) 2, octamer-binding transcription factor (OCT) 4, and transcriptional coactivator TAFAZZIN (TAZ). BMP4 suppresses their expression [95].

Taken together, with respect to CSCs development and tumorigenesis, it can be concluded that BMP signaling can act as promoter of premalignant mammary cells and as suppressor of aggressive mammary cancer cells.

Effects of BMPs on breast cancer proliferation and apoptosis

BMPs have been reported to regulate breast cancer cell growth with context pleiotropy. For the same BMP ligand, the responses can vary within different tumor types. For example, BMP7 was reported to promote cell proliferation of BT-474 and MDA-MB-231 breast cancer cells but to decrease cell proliferation of other breast cancer cell lines (including MDA-MB-361, HCC1954, ZR-75-30, and T-47D) [53]. Even for the same BMP ligand and cell line, different conditions may cause a different response. BMP4 does not have any inhibitory effects on the proliferation of MDA-MB-231 cells in two-dimensional (2D) cell culture but inhibits proliferation in 3D [96]. BMP2 was found to inhibit the hormone-independent growth of MCF-7 *in vitro* [97-99], but the contrary was reported *in vivo* [100]. BMP4 and BMP7 have also been shown to promote anchorage-independent MCF-7 cell proliferation [51, 89].

In most of the studies, BMP2 [31, 97-103], BMP4 [31, 37, 96], BMP6 [46, 93, 104], BMP9 [105, 106], and BMP10 [56] were found to trigger cytostatic effects on multiple breast

cancer cells. The underlying mechanism could be that BMP signaling has evident effects on the expression of mitotic checkpoint proteins. Chemical inhibition of BMP signaling by BMPRI kinase inhibitor Dorsomorphin abrogates Nocodazole-mediated mitotic arrest [107]. Simultaneously, levels of mitotic checkpoint proteins, budding uninhibited by benzimidazoles 3 (BUB3), highly expressed protein in cancer (HEC1), monopolar spindle 1 (MPS1), and mitotic arrest deficient 2 (MAD2), which ensures proper chromosome segregation during mitosis, were dramatically downregulated. Overexpressing these proteins significantly recovers the defect in mitotic arrest caused by BMP inhibition [107]. Some of BMPs are demonstrated to delay cell cycle reentry in breast cancer cells. BMP2 [99, 102, 108, 109], BMP4 [37, 96], and BMP6 [46, 93, 104] induce G1 cell cycle arrest caused by increased expression of the cell cycle inhibitor p21 [96, 99, 102, 108, 109]. p21 protein activity in turn inactivates cyclin D1 and cyclin E and results in retinoblastoma protein (pRb) hypophosphorylation [101]. The process of cell cycle arrest requires active BMPRI, and the cytoplasmic signal transducers SMAD1/5 and SMAD4 are indispensable [102]. Upregulation of protein tyrosine phosphatases (PTPs), such as protein tyrosine phosphatase gamma (PTPRG), MAPK phosphatase (MKP), and phosphatase and tensin homolog (PTEN), may also contribute to increased levels of p21 in cells where BMP induced antiproliferative effects [110, 111]. In addition, BMP7 [84] and BMP9 [105] can lead to an accumulation of the G2/M phase in breast cancer cells.

BMPs can also influence the effect of other factors on breast cancer cell proliferation. BMP4 itself cannot significantly stimulate the proliferation but potently enhances the mitogenic activity of EGF, FGF, and hepatocyte growth factor (HGF) on murine mammary epithelial cells [112]. BMP2, in contrast to BMP4, prevents EGF-induced proliferation of MDA-MB-231 cells [108]. The estrogen-induced mitotic effects can be suppressed by BMP2 [59, 101], BMP4 [59], BMP6 [59], and BMP7 [59, 84], with the effects of BMP6 and BMP7 being more potent than those of BMP2 and BMP4 [59]. AB215, an activin A/BMP2 chimera, has increased BMP2-like signaling potency via the SMAD1/5/8 pathway and exerts stronger inhibitory effects on estradiol-induced proliferation in ER⁺ breast cancer cells than BMP2 [113]. Estradiol rapidly activates MAPK phosphorylation including ERK1/2, p38, and JNK pathways [59, 84]. BMP6 and 7 can preferentially inhibit estradiol-induced p38 phosphorylation [59]. BMP6 is also believed to decrease the chemoresistance of MCF-7 breast cancer cells to doxorubicin through inactivation of ERK signaling and upregulation of P-glycoprotein (P-GP) [46]. Furthermore,

BMP9 can inhibit expression of HER2, phosphorylation of ERK1/2 (without effect on p38 and JNK), and PI3K/AKT in SK-BR-3 cells, thereby suppressing the growth of HER2⁺ SK-BR-3 cells in vitro and in vivo [106].

Obviously, the distinct BMP receptors present also explain the diversity of effects of BMP signaling on breast cancer proliferation. BMPRIA was identified as a positive regulator of breast cancer at primary and secondary sites through activation of the SMAD pathway [72]. In contrast, another type I receptor, BMPRIB, plays a negative role in the proliferation of breast cancer cells. Downregulation of BMPRIB in MDA-MB-231 cells leads to promotion of cell growth in vitro [64]. Overexpression of a BMPRII-dominant negative (DN) mutant interferes with the phosphorylation of SMAD1, resulting in G1 phase cell cycle arrest of T-47D cells [109]. However, in the MMTV polyoma middle T antigen mice model of spontaneous mammary tumor formation, BMPRII-DN-expressing tumor cells have higher proliferation rates [114].

A few studies have pointed out pro-apoptotic roles for BMPs in breast cancer cells [86, 99, 105, 115]. BMP2 regulates the expression of apoptosis-related genes, especially protein kinase R (PKR) and activates its substrate α -subunit of eukaryotic initiation factor 2, thereby showing a pro-apoptotic effect in MCF-7 cells under normal culture conditions [115]. However, when these cells are deprived of serum, BMPs display a contrasting function by exerting an anti-apoptotic effect. BMP2 increases the resistance to hypoxia-induced apoptosis in MCF-7 cells via activation of the MAPK and ID1 pathways and suppression of caspase-3 [116, 117]. In parallel, BMP6, which can inhibit the proliferation of MDA-MB-231 cells, inhibits serum starvation-induced apoptosis through SMAD-dependent upregulation of Survivin and non-SMAD-dependent activation of p38 MAPK [104].

BMPs and the tumor microenvironment

Accumulating evidence indicates that the tumor microenvironment is a pathologically active niche that shapes tumor evolution. Hypoxia, low pH, immune evasion, chronic inflammation, and neovasculature can be considered as enabling characteristics [118]. Disruption of BMP signaling brings about alterations in the breast tumor microenvironment and accelerates tumor progression [41, 114, 119]. Deletion of BMPRII in mammary tumors [114] or in fibroblasts within the tumor stroma [119] can result in increased expression of chemokines, such as chemokine (C-C motif) ligand 5 and 9 (CCL5, 9), interferon gamma-induced protein 10 (IP-10), and granulocyte colonystimulating factor (G-CSF), which facilitate inflammation by a sustained

increase of myeloid cells infiltration, especially myeloid-derived suppressor cells (MDSCs) [114, 119]. Accordingly, the T-cell population is reduced due to a main function of MDSCs in the inhibition of T-cell proliferation [114]. As a classical stress response pathway, nuclear factor- κ B (NF- κ B) activation can be detected in a majority of cancers [120]. BMP4 has been shown to attenuate NF- κ B activity in breast cancer [41]. Thereby lower levels of chemokines result from the attenuation of its known regulator NF- κ B, leading to reduced numbers and immunosuppressive activity of MDSCs [41, 114]. Meanwhile, increased T-cell populations are observed within stromal tissues, and many immune-related genes are significantly upregulated by BMP4, indicating BMP4 triggers an enhanced antitumor immune response [41]. Therefore, it can be concluded that BMP signaling could inhibit inflammatory infiltrates and tumor progression through suppressing an inflammatory chemokine profile in tumor microenvironment.

Intriguingly, BMP signaling could also induce a series of cytokines which trigger CAF-mediated pro-tumorigenic stimulation on epithelial cells directly. BMP4 treatment of normal mammary fibroblasts or carcinoma-associated mammary fibroblasts (CAFs) induces an increase in secreted matrix metalloproteases (MMPs) and proinflammatory cytokines, which enhance mammary carcinoma cell invasion [73, 121]. Furthermore, inhibition of BMP signaling alters fibroblasts, macrophages, and lymphatic vessels to be less tumor promoting in vivo [48].

It has been reported that BMPs can promote endothelial cell (EC) proliferation and migration [122]. Consistent with this notion, BMP signaling is required for appropriate angiogenesis [123]. BMP2 promotes vascularization by stimulating the ID1 and p38 MAPK pathways. Overexpression of BMP2 in MCF-7 cells induces vascularized tumors eventually upon injection in vivo [124]. The signaling mediated by BMP type I receptor ALK1 has a critical role in regulation of both developmental and pathologic blood vessel formation [125]. ALK1 is mainly expressed at the sites of angiogenesis during embryogenesis and is expressed at lower levels in adult vasculature. Yet its expression increases in neoangiogenic vessels of wounds and cancer [125]. BMP9 binds to ALK1 in ECs with high affinities [126]. There have been divergent results with respect to the effects of BMP9/ALK1 signaling on ECs. Some reports demonstrate that high-dose BMP9/ALK1 signaling exhibits antiangiogenic effects, by inhibiting FGF-induced angiogenesis [127, 128], while other reports have shown induction of proliferation by low dose of BMP9 in several types of ECs and proangiogenic effects of BMP9 in Matrigel plug assays [129, 130]. The apparent discrepancy between these reports might reflect the contextual function

of BMPs, in which the concentration plays an important role. In addition, common proangiogenic factors (VEGF-A and bFGF) can stimulate ALK1-mediated BMP/SMAD-like signaling, leading to cell spreading, and tubulogenesis of ECs [131]. Inhibition of ALK1 signaling by gene silencing, ligand traps, or antibodies can significantly suppress the growth and progression of tumors, including breast cancer, with substantial reduction of angiogenesis, supporting the notion that ALK1 is an important target for antiangiogenic treatment [131, 132].

Roles of BMPs in the migration, invasion, and metastasis of breast cancer

It is clear that BMPs and their receptors modulate key pathways mediating breast cancer cell invasion and migration, critical parameters of metastatic dissemination. But the conclusions also seem paradoxical, indicating dependence on particular cell types and contexts.

BMPs and EMT

The development of metastasis involves the replacement with new phenotypes in cancer cells to facilitate detachment from the primary site [133]. Many epithelial cancer cells can acquire sufficient phenotypic plasticity by EMT, which implies the conversion of a proliferative epithelial state into nonproliferative mesenchymal state with the ability to migrate and invade adjacent tissue [134]. Restriction in BMP signaling level is frequently needed for efficient EMT [54, 91, 135]. Significant downregulation of some BMPs and upregulation of two secreted BMP antagonists, Chordin-like (CHRD) 2 and Gremlin, were observed when human mammary epithelial cells pass through an EMT [91]. A subsequent study showed that the transcription factor zinc finger E-box-binding homeobox 1 (ZEB1) which mediates EMT can directly upregulate the expression of the BMPs antagonists Noggin, Follistatin, and CHRD1 [135]. Likewise, a newly identified EMT pathway mediated by the transcriptional repressor Blimp-1 (PRDM1) leads to SNAIL induction via repression of BMP5 [54]. Of note, during acquisition of metastatic ability, EMT in mammary cells is strongly correlated with a CD44^{high}/CD24^{low} stem cell phenotype [90, 91, 136]. These studies thus support a mechanistic link between BMP downregulation, EMT, and stem cell signature in cancer.

In addition, some BMPs are capable of reversing EMT or EMT markers in breast cancer cells [52, 80, 137]. E-cadherin-mediated cell-to-cell adhesion can be restored through inhibition of ZEB1 by BMP6 in breast cancer cells [44, 137, 138]. Stimulation with exogenous BMP7, which can decrease vimentin and increase cytokeratin expression in vitro and in vivo, gives rise

to an epithelial-like phenotype [52]. BMPs can also oppose EMT inducers, e.g., TGF β , in normal mammary epithelial cells or IMECs [54, 91, 139-142] and in breast cancer cells [52, 92, 140]. For example, the loss of E-cadherin expression on the surface of NMuMG cells in response to TGF β 1 is largely overridden by BMP5, and the fibroblastoid phenotype is also substantially reversed [54]. BMP7 has also been shown to reverse TGF β -induced EMT [139-141], which increases E-cadherin expression through upregulation of ID2 and ID3. Interestingly, when knocking down ID2 or ID3, BMP7 actually induces the expression of α -smooth muscle actin (α SMA) and stimulates EMT [140, 141]. Thus, BMP signaling impedes the progression of breast cancer to an invasive state and prevents metastasis in the aforementioned studies. However, the BMP pathway was found to maintain a mesenchymal stem cell phenotype of breast cancer cells and render cells more migratory, invasive in other in vitro [89, 143, 144] and in vivo [61, 143] studies. BMP2 transforms MCF-7 cells from a round-like shape into a spindle-like shape with some specialized structures, such as filopodia, lamellipodia, and membrane protrusions, which are essential for cell migration and spreading [100, 144]. BMP4 blocks the capacity of mammary epithelial cells to form polarized lumen-containing structures and renders them invasive properties [145]. Of note, in 4T1.2 cells expressing BMP4, genes associated with EMT are upregulated but no change was observed in their migratory capacity [41].

BMPs and components of the extracellular matrix (ECM)

EMT is not an “all-or-nothing” event; it’s highly dynamic. Studies have shown that BMPs induce MMP-dependent migration and invasion of breast cancer [48, 96, 121]. MMPs are known for degrading surrounding ECM components during cancer invasion and metastasis [146]. Treatment of primary tumors with BMPRI kinase inhibitor DMH1 reduced MMP2 and CCL9 in CAFs [48]. BMP4 induces the expression of multiple MMPs in mouse mammary fibroblasts and in cancer-associated human mammary fibroblasts [121] and dramatically increases MMP3 and MMP4 expression in 3D-cultured MDA-MB-231 cells [96]. However, another study showed that BMP4 suppresses the activity of MMP9 in 2D culture, rather than MMP1 and MMP3 [147]. Moreover, BMP6 was found to inhibit MMP9 activation via SMAD-dependent induction of heme oxygenase 1 (HO1) in MCF-7 cells [148]. BMP9 can inhibit MMP9 by inhibiting the AKT signaling pathway [106, 149].

ECM-associated protein Wnt1-inducible secreted protein 3 (WISP-3/CCN6) binds directly to BMP4 to antagonize BMP4-induced SMAD-independent activation of TAK1/p38 kinases,

decreases the invasiveness of breast cancer cells in 3D, and also reduces distant metastasis in xenografts [143]. In contrast, the expression of ECM proteins tenascin-W, which can promote the motility of breast cancer cells expressing $\alpha 8$ integrin, is induced by BMP2-mediated p38 MAPK and JNK signaling pathways [150].

Interplay Between BMPs and TGF β

Apart from EMT as previously mentioned, other features of cancer cells such as migration and invasion are also affected by a mutual antagonism between BMPs and TGF β . Overexpression of type III TGF β receptor inhibited BMP-mediated SMAD1/5/8 phosphorylation and BMP-induced migration [151]. BMP7 treatment significantly increases migration and invasion in MDA-MB-231 cells [53, 152]. This effect is substantially inhibited by costimulation with TGF β by inducing the formation of complexes involving phosphorylated SMAD1/5 and SMAD3 [152]. Moreover, BMP2-mediated upregulation of ID1 may be a contributing factor in BMP2-related aggressiveness of breast cancer cells. Aberrant activation of SRC kinase resulting in increased SMAD1/5 signaling can change ID1 expression, which is positively controlled via SMAD1/5 by BMP2 and negatively via SMAD2/3 by TGF β [153]. Conversely, BMP7 inhibits TGF β -induced expression of $\alpha v\beta 3$ integrin and invasion of the metastatic breast cancer cell line MCF-10CA1a in a spheroid model [154].

BMPs and metastasis

Common sites of metastatic dissemination, such as the bone and lung, are the main targets of metastatic breast cancer [7]. In the process of bone metastasis, breast cancer triggers predominantly an osteoclast-mediated osteolytic lesion [155]. BMP signaling is shown to shift the osteoblast/osteoclast differentiation balance in favor of stimulating osteoblast differentiation [70, 71, 156]. By inactivating BMP signaling, BMP antagonists, such as Noggin, Follistatin, and CHRDL1, have been linked to the induction of osteoclast differentiation, as well as the formation of osteolytic bone metastases [71, 135, 156]. Lack of Noggin expression by breast cancer cells is a determinant of osteoblastic activities [70]. In an intracardiac xenograft model, evidence was found that Noggin is expressed in metastatic breast cancer cells during the late events of metastasis. In particular, it facilitates the metastatic capabilities of breast cancer cells to the bone by promoting osteoclast differentiation and bone degradation [71].

In contrast, when MCF-7 or MDA-MB-231 cells are cocultured with osteoblast-like cells, Noggin effectively inhibits migration and invasion of breast cancer cells by downregulating MMP1 and CXCR4 and improves bone remodeling by increasing the ratio of osteoprotegerin (OPG)/nuclear factor kappa B ligand (RANKL) [38]. The BMP target gene and cofactor RUNX2 are required for breast cancer osteolytic metastases [157, 158]. miR-135 impairs the BMP-RUNX2 axis by directly targeting SMAD5 and subsequently reduces the osteolytic properties of breast cancer cells [158]. Likewise, expression of dominant-negative receptors (DN-ALK3) for BMPs reduces interleukin-11 (IL-11) expression and inhibits bone metastasis in xenograft model [72].

As for individual BMP, BMP9, which is one of the most effective BMPs in osteogenesis, can inhibit osteolytic injury and bone metastasis caused by MDA-MB-231 cells by downregulating PTHrP, IL6, RANKL, and connective tissue growth factor (CTGF) [55, 149]. BMP2, 7, and 2/7 heterodimer inhibits bone metastases formation in MDA-MB-231 cells [52, 92]. Contradicting results showed that BMP7 overexpression could lead to accelerated bone metastasis formation of breast cancer cells [50, 51, 53].

BMP signaling can also prevent the colonization of metastatic cells in the lung by repressing key CSCs traits and enforcing cancer cells into dormancy. Overexpression of the BMP antagonist Coco permits a few dormant cancer cells to break through the barrier imposed by BMP signaling and to establish clinically meaningful metastases [95].

Conclusions and perspectives

As discussed above, there are conflicting views regarding the significance of BMPs in breast cancer, based both on in vitro and in vivo studies. This has been attributed to multiple factors, including the (dose- and context-dependent) differential effects of different BMP ligands and differences in the genetic patterns of breast cancer subtypes, as well as differences in the research models that were used. Most results are obtained using only a few types of cancer cell lines or single and different animal models and are therefore difficult to compare to each other. What is clear is that BMPs are emerging as key factors in many aspects of breast cancer. Aberrant changes in BMP signaling/components have been detected in breast cancer and metastatic recurrence and have deepened our understanding of the pathogenesis of breast cancer. The majority of studies indicate that BMP signaling is a critical negative regulator in multiple breast

cancer cell lines both in vitro and in vivo. Restoration or amplification of specific aspects of BMP signaling may be potentially exploited for therapeutic intervention strategies.

To this point, context is critical. For instance, even an agonist or coactivator with precisely delivered BMP signaling input will not make any contribution to overcome the shortages that derive from functional deficiency of BMP receptors or any critical downstream components. It is therefore necessary to identify more potential targets or markers of the specific signaling defect(s). This might be pursued by using the latest types of high-throughput (epi)genetic, proteomic, and metabolomic analysis to systematically investigate the BMP responses to multiple cell types of the different breast cancer subclasses and/or patient-derived (organoid) (co)cultures grown in 3D and investigating the effect of misexpression of BMP receptor components or pharmacological inhibition of BMP receptor signaling in relevant transgenic mouse models and patient-derived xenografts with clear classification of histological pathology. This may provide effective principles to better illuminate the context-dependent roles of BMP family signaling in breast cancer. Via these approaches the opportunities for pharmacological intervention to rectify aberrant BMP family signaling in specific contexts are likely to be increased.

Acknowledgments We are grateful to Philip Owens, Miriam de Boeck, and Hans van Dam for critical reading and comments. Our studies on BMP in cancer and vascular diseases are supported by the Cancer Genomics Centre, Netherlands, and Swedish Cancerfonden (090773).

References

1. Urist MR. Bone: formation by autoinduction. *Science* 1965,150(3698):893-9.
2. Brazil DP, Church RH, Surae S, *et al.* BMP signalling: agony and antagonism in the family. *Trends Cell Biol* 2015, 25:249-64.
3. Wang RN, Green J, Wang Z, *et al.* Bone Morphogenetic Protein (BMP) signaling in development and human diseases. *Genes Dis* 2014, 1(1):87-105.
4. Miyazono K, Kamiya Y, Morikawa M. Bone morphogenetic protein receptors and signal transduction. *J Biol Chem* 2010, 1(1):87-105
5. Ehata S, Yokoyama Y, Takahashi K, Miyazono K. Bi-directional roles of bone morphogenetic proteins in cancer: another molecular Jekyll and Hyde? *Pathol Int* 2013, 63(6):287-96.
6. Robinson GW. Cooperation of signalling pathways in embryonic mammary gland development. *Nat Rev Genet* 2008, 8(12):963-72.

7. Lorusso G, Rüegg C. New insights into the mechanisms of organ-specific breast cancer metastasis. *Semin Cancer Biol* 2012, 22(3):226-33.
8. Long F. Building strong bones: molecular regulation of the osteoblast lineage. *Nat Rev Mol Cell Biol* 2012, 13(1):27-38.
9. Bragdon B, Moseychuk O, Saldanha S, *et al.* Bone morphogenetic proteins: a critical review. *Cell Signal* 2011, 23(4):609-20.
10. Wakefield LM, Hill CS. Beyond TGF β : roles of other TGF β superfamily members in cancer. *Nat Rev Cancer* 2013, 13(5):328-41.
11. Heldin CH, Miyazono K, Ten Dijke P. TGF β signalling from cell membrane to nucleus through SMAD proteins. *Nature* 1997, 390(6659):465-71.
12. López-Rovira T, Chalaux E, Massagué J, Rosa JL, Ventura F. Direct binding of Smad1 and Smad4 to two distinct motifs mediates bone morphogenetic protein-specific transcriptional activation of Id1 gene. *J Biol Chem* 2002, 277(5):3176-85.
13. Ishida W, Hamamoto T, Kusanagi K, *et al.* Smad6 is a Smad1/5-induced Smad inhibitor characterization of bone morphogenetic protein-responsive element in the mouse Smad6 promoter. *Trends Cell Biol* 2000, 275(9):6075-9.
14. Lee KS, Kim HJ, Li QL, *et al.* Runx2 is a common target of transforming growth factor β 1 and bone morphogenetic protein 2, and cooperation between Runx2 and Smad5 induces osteoblast-specific gene expression in the pluripotent mesenchymal precursor cell line C2C12. *Mol Cell Biol* 2000, 20(23):8783-92.
15. Zhang YE. Non-Smad pathways in TGF β signaling. *Cell Res* 2009, 19(1):128-39.
16. Walsh DW, Godson C, Brazil DP, *et al.* Extracellular BMP-antagonist regulation in development and disease: tied up in knots. *Trends Cell Biol* 2010, 20(5):244-56.
17. Singhatanadgit W, Salih V, Olsen I. Shedding of a soluble form of BMP receptor-IB controls bone cell responses to BMP. *Bone* 2006, 39(5):1008-1017.
18. Onichtchouk D, Chen YG, Dosch R, *et al.* Silencing of TGF β signalling by the pseudoreceptor BAMBI. *Nature* 1999, 401(6752):480-5.
19. Halbrooks PJ, Ding R, Wozney JM, *et al.* Role of RGM coreceptors in bone morphogenetic protein signaling. *J Mol Signal* 2007, 2:4.
20. Kirkbride KC, Townsend TA, Bruinsma MW, *et al.* Bone morphogenetic proteins signal through the transforming growth factor- β type III receptor. *J Biol Chem* 2008, 283(12):7628-37.
21. Scherner O, Meurer SK, Tihaa L, *et al.* Endoglin differentially modulates antagonistic transforming growth factor- β 1 and BMP-7 signaling. *J Biol Chem* 2007, 282(19):13934-43.

22. Alt A, Miguel-Romero L, Donderis J, *et al.* Structural and functional insights into endoglin ligand recognition and binding. *PLoS One* 2012, 7:e29948.
23. Shi W, Chang C, Nie S, *et al.* Endofin acts as a Smad anchor for receptor activation in BMP signaling. *J Cell Sci* 2007, 120(Pt 7):1216-24.
24. Kugimiya F, Yano F, Ohba S, *et al.* Mechanism of osteogenic induction by FK506 via BMP/Smad pathways. *Biochem Biophys Res Commun* 2005, 338(2):872-9.
25. Spiekerkoetter E, Tian X, Cai J, *et al.* FK506 activates BMPR2, rescues endothelial dysfunction, and reverses pulmonary hypertension. *J Clin Invest* 2013, 123(8):3600-13.
26. Ten Dijke P, Goumans MJ, Itoh F, *et al.* Regulation of cell proliferation by Smad proteins. *J Cell Physiol* 2002, 191(1):1-16.
27. Massagué J, Seoane J, Wotton D. Smad transcription factors. *Genes Dev* 2005, 19:2783-2810
28. Itoh S, ten Dijke P (2007) Negative regulation of TGF β receptor/Smad signal transduction. *Curr Opin Cell Biol* 19:176-184
29. Massagué J, Chen YG. Controlling TGF β signaling. *Genes Dev* 2000, 19(23):2783-810.
30. Guo X, Wang XF. Signaling cross-talk between TGF β /BMP and other pathways. *Cell Res* 2009, 19(1):71-88.
31. Chapellier M, Bachelard-Cascales E, Schmidt X, *et al.* Disequilibrium of BMP2 levels in the breast stem cell niche launches epithelial transformation by overamplifying BMPR1B cell response. *Stem Cell Rep* 2015, 4(2):239-54.
32. Reinholz MM, Iturria SJ, Ingle JN, *et al.* Differential gene expression of TGF β family members and osteopontin in breast tumor tissue: analysis by real-time quantitative PCR. *Breast Cancer Res Treat* 2002, 74(3):255-69.
33. Davies SR, Watkins G, Douglas-Jones A, *et al.* Bone morphogenetic proteins 1 to 7 in human breast cancer, expression pattern and clinical/prognostic relevance. *J Exp Ther Oncol* 2008, 7(4):327-38.
34. Zhang XHF, Wang Q, Gerald W, *et al.* Latent bone metastasis in breast cancer tied to Src-dependent survival signals. *Cancer Cell* 2009, 16(1):67-78.
35. Alarmo EL, Kuukasjärvi T, Karhu R, *et al.* A comprehensive expression survey of bone morphogenetic proteins in breast cancer highlights the importance of BMP4 and BMP7. *Breast Cancer Res Treat* 2007, 103(2):239-46.
36. Hartmann O, Spyrtos F, Harbeck N, *et al.* DNA methylation markers predict outcome in node-positive, estrogen receptor-positive breast cancer with adjuvant anthracycline-based chemotherapy. *Clin Cancer Res* 2009, 15(1):315-23.

37. Ketolainen JM, Alarmo EL, Tuominen VJ, *et al.* Parallel inhibition of cell growth and induction of cell migration and invasion in breast cancer cells by bone morphogenetic protein 4. *Breast Cancer Res Treat* 2010, 124(2):377-86.
38. Guo D, Huang J, Gong J. Bone morphogenetic protein 4 (BMP4) is required for migration and invasion of breast cancer. *Mol Cell Biochem* 2012, 363(1-2):179-90.
39. Alarmo EL, Huhtala H, Korhonen T, *et al.* Bone morphogenetic protein 4 expression in multiple normal and tumor tissues reveals its importance beyond development. *Mod Pathol* 2013, 26(1):10-21.
40. Kretschmer C, Conradi A, Kemmner W, *et al.* Latent transforming growth factor binding protein 4 (LTBP4) is downregulated in mouse and human DCIS and mammary carcinomas. *Cell Oncol* 2011, 34(5): 419-434.
41. Cao Y, Slaney CY, Bidwell BN, *et al.* () BMP4 inhibits breast cancer metastasis by blocking myeloid-derived suppressor cell activity. *Cancer Res* 2014, 74(18):5091-102.
42. Clement JH, Sanger J, Hoffken K. Expression of bone morphogenetic protein 6 in normal mammary tissue and breast cancer cell lines and its regulation by epidermal growth factor. *Int J Cancer* 1999, 80(2):250-256.
43. Zhang M, Wang Q, Yuan W, *et al.* Epigenetic regulation of bone morphogenetic protein-6 gene expression in breast cancer cells. *J Steroid Biochem Mol Biol* 2007, 105(1-5):91-7.
44. Du J, Yang S, An D, *et al.* BMP-6 inhibits microRNA-21 expression in breast cancer through repressing δ EF1 and AP-1. *Cell Res* 2009, 19(4):487-96.
45. Barekati Z, Radpour R, Lu Q, *et al.* Methylation signature of lymph node metastases in breast cancer patients. *BMC Cancer* 2012, 12:244.
46. Lian WJ, Liu G, Liu YJ, *et al.* Downregulation of BMP6 enhances cell proliferation and chemoresistance via activation of the ERK signaling pathway in breast cancer. *Oncol Rep* 2013, 30(1):193-200.
47. Alarmo EL, Rauta J, Kauraniemi P, *et al.* Bone morphogenetic protein 7 is widely overexpressed in primary breast cancer. *Genes Chromosomes Cancer* 2006, 45(4):411-9.
48. Owens P, Pickup MW, Novitskiy SV, *et al.* Inhibition of bmp signaling suppresses metastasis in mammary cancer. *Oncogene* 2014, 34(19):2437-49.
49. Schwalbe M, Sanger J, Eggers R, *et al.* Differential expression and regulation of bone morphogenetic protein 7 in breast cancer. *Int J Oncol* 2003, 23(1):89-95.
50. Alarmo EL, Korhonen T, Kuukasjarvi T, *et al.* Bone morphogenetic protein 7 expression associates with bone metastasis in breast carcinomas. *Ann Oncol* 2007, 19(2):308-14.

51. Sakai H, Furihata M, Matsuda C, *et al.* Augmented autocrine bone morphogenic protein (BMP) 7 signaling increases the metastatic potential of mouse breast cancer cells. *Clin Exp Metastasis* 2012, 29(4):327-38.
52. Buijs JT, Henriquez NV, Van Overveld PG, *et al.* Bone morphogenetic protein 7 in the development and treatment of bone metastases from breast cancer. *Cancer Res* 2007, 67(18):8742-51.
53. Alarmo EL, Pärssinen J, Ketolainen JM, *et al.* BMP7 influences proliferation, migration, and invasion of breast cancer cells. *Cancer Lett* 2009, 275(1):35-43.
54. Romagnoli M, Belguise K, Yu Z, *et al.* Epithelial-to-mesenchymal transition induced by TGF β 1 is mediated by Blimp-1-dependent repression of BMP-5. *Cancer Res* 2012, 72(23):6268-78.
55. Ren W, Sun X, Wang K, *et al.* BMP9 inhibits the bone metastasis of breast cancer cells by downregulating CCN2 (connective tissue growth factor, CTGF) expression. *Mol Biol Rep* 2014, 41(3):1373-83.
56. Ye L, Bokobza S, Li J, *et al.* Bone morphogenetic protein-10 (BMP-10) inhibits aggressiveness of breast cancer cells and correlates with poor prognosis in breast cancer. *Cancer Sci* 2010, 101(10):2137-44.
57. Hanavadi S, Martin T, Watkins G, *et al.* The role of growth differentiation factor-9 (GDF-9) and its analog, GDF-9b/BMP-15, in human breast cancer. *Ann Surg Oncol* 2007, 14(7):2159-66.
58. Li J, Ye L, Parr C, *et al.* The aberrant expression of bone morphogenetic protein 12 (BMP-12) in human breast cancer and its potential prognostic value. *Gene Ther Mol Biol* 2009, 13(13):186-193.
59. Takahashi M, Otsuka F, Miyoshi T, *et al.* Bone morphogenetic protein 6 (BMP6) and BMP7 inhibit estrogen-induced proliferation of breast cancer cells by suppressing p38 mitogen-activated protein kinase activation. *J Endocrinol* 2008, 199(3):445-455.
60. Network CGA. Comprehensive molecular portraits of human breast tumours. *Nature* 2012, 490(7418):61-70.
61. Balboni AL, Hutchinson JA, DeCastro AJ, *et al.* Δ Np63 α -mediated activation of bone morphogenetic protein signaling governs stem cell activity and plasticity in normal and malignant mammary epithelial cells. *Cancer Res* 2013, 73:1020-30.
62. Helms MW, Packeisen J, August C, *et al.* First evidence supporting a potential role for the BMP/SMAD pathway in the progression of oestrogen receptor-positive breast cancer. *J Pathol* 2005, 206(3):366-76.
63. Pickup MW, Hover LD, Guo Y, *et al.* Deletion of the BMP receptor BMPRIa results in EMT and impairs mammary gland tumor formation and metastasis. *Oncotarget* 2015, 6(26): 22890-904.

64. Bokobza SM, Ye L, Kynaston HE, *et al.* Reduced expression of BMPR-IB correlates with poor prognosis and increased proliferation of breast cancer cells. *Cancer Genom Proteom* 2009, 6(2):101-8.
65. Zhong D, Morikawa A, Guo L, *et al.* Homozygous deletion of SMAD4 in breast cancer cell lines and invasive ductal carcinomas. *Cancer Biol Ther* 2006, 5(6):601-7.
66. Valero V III, Saunders TJ, He J, *et al.* Reliable detection of somatic mutations in fine needle aspirates of pancreatic cancer with next-generation sequencing. *Ann Surg* 2015, 263(1):153-61.
67. Voorneveld PW, Kodach LL, Jacobs RJ, *et al.* Loss of SMAD4 alters BMP signaling to promote colorectal cancer cell metastasis via activation of Rho and ROCK. *Gastroenterology* 2014, 147(1):196-208.
68. Sneddon JB, Zhen HH, Montgomery K, *et al.* Bone morphogenetic protein antagonist gremlin 1 is widely expressed by cancer-associated stromal cells and can promote tumor cell proliferation. *Proc Natl Acad Sci U S A* 2006, 103(40):14842-7.
69. Ma X-J, Dahiya S, Richardson E, *et al.* Gene expression profiling of the tumor microenvironment during breast cancer progression. *Breast Cancer Res* 2009, 11(1):R7.
70. Schwaninger R, Rentsch CA, Wetterwald A, *et al.* Lack of noggin expression by cancer cells is a determinant of the osteoblast response in bone metastases. *Am J Pathol* 2007, 170(1):160-75.
71. Tarragona M, Pavlovic M, Arnal-Estapé A, *et al.* Identification of NOG as a specific breast cancer bone metastasis-supporting gene. *J Biol Chem* 2012, 287(25):21346-55.
72. Katsuno Y, Hanyu A, Kanda H, *et al.* Bone morphogenetic protein signaling enhances invasion and bone metastasis of breast cancer cells through Smad pathway. *Oncogene* 2008, 27(49):6322-33.
73. Owens P, Polikowsky H, Pickup MW, *et al.* Bone morphogenetic proteins stimulate mammary fibroblasts to promote mammary tumorigenesis. *PLoS One* 2013; 8(6): e67533.
74. Yan W, Chen X. Targeted repression of bone morphogenetic protein 7, a novel target of the p53 family, triggers proliferative defect in p53-deficient breast cancer cells. *Cancer Res* 2007, 67(19):9117-24.
75. Huang B, Warner M (2015) Gustafsson J-Å. Estrogen receptors in breast carcinogenesis and endocrine therapy. *Mol Cell Endocrinol* 2014, 418:240-244.
76. Kusumegi T, Tanaka J, Kawano M, *et al.* BMP7/ActRIIB regulates estrogen-dependent apoptosis: New biomarkers for environmental estrogens. *J Biochem Mol Toxicol* 2004, 18(1):1-11.
77. Yamamoto T, Saatcioglu F, Matsuda T. Cross-talk between bone morphogenic proteins and estrogen receptor signaling. *Endocrinology* 2002, 143(7):2635-42.

78. Páez-Pereda M, Giacomini D, Refojo D, *et al.* Involvement of bone morphogenetic protein 4 (BMP-4) in pituitary prolactinoma pathogenesis through a Smad/estrogen receptor crosstalk. *Proc Natl Acad Sci U S A* 2003, 100(3):1034-9.
79. Van den Wijngaard A, Mulder W, Dijkema R, *et al.* Antiestrogens specifically up-regulate bone morphogenetic protein-4 promoter activity in human osteoblastic cells. *Mol Endocrinol* 2000 14(5):623-33.
80. Liu G, Liu YJ, Lian WJ, *et al.* Reduced BMP6 expression by DNA methylation contributes to EMT and drug resistance in breast cancer cells. *Oncol Rep* 2014, 32(2):581-8.
81. Zhang M, Yan JD, Zhang L, *et al.* Activation of bone morphogenetic protein-6 gene transcription in MCF-7 cells by estrogen. *Chin Med J (Engl)* 2005, 118(19):1629-36.
82. Lee HJ, Liu H, Goodman C, *et al.* Gene expression profiling changes induced by a novel Gemini Vitamin D derivative during the progression of breast cancer. *Biochem Pharmacol* 2006, 72(3):332-43.
83. Lee HJ, Wislocki A, Goodman C, *et al.* (2006) A novel vitamin D derivative activates bone morphogenetic protein signaling in MCF10 breast epithelial cells. *Mol Pharmacol* 2006, 69(6):1840-8.
84. Masuda H, Otsuka F, Matsumoto Y, *et al.* Functional interaction of fibroblast growth factor-8, bone morphogenetic protein and estrogen receptor in breast cancer cell proliferation. *Mol Cell Endocrinol* 2011, 343(1-2):7-17.
85. Mi D, Zhang M, Yan JD, *et al.* PTHrP inhibits BMP-6 expression through the PKA signaling pathway in breast cancer cells. *J Cancer Res Clin Oncol* 2011, 137(2):295-303.
86. Wang N, Lin K, Lu Z, *et al.* The LIM-only factor LMO4 regulates expression of the BMP7 gene through an HDAC2-dependent mechanism, and controls cell proliferation and apoptosis of mammary epithelial cells. *Oncogene* 2007, 26(44):6431-41.
87. Wei W, Lewis MT. Identifying and targeting tumor-initiating cells in the treatment of breast cancer. *Endocr Relat Cancer* 2015, 22(3):R135-55.
88. Oshimori N, Fuchs E. The harmonies played by TGF β in stem cell biology. *Cell Stem Cell* 2012, 11(6): 751-764.
89. Garulli C, Kalogris C, Pietrella L, *et al.* Dorsomorphin reverses the mesenchymal phenotype of breast cancer initiating cells by inhibition of bone morphogenetic protein signaling. *Cell Signal* 2014, 26(2):352-62.
90. Uchino M, Kojima H, Wada K, *et al.* Nuclear β -catenin and CD44 upregulation characterize invasive cell populations in non-aggressive MCF-7 breast cancer cells. *BMC Cancer* 2010, 10:414

91. Scheel C, Eaton EN, Li SH-J, *et al.* Paracrine and autocrine signals induce and maintain mesenchymal and stem cell states in the breast. *Cell* 2011, 145(6):926-40.
92. Buijs J, Van Der Horst G, Van Den Hoogen C, *et al.* The BMP2/7 heterodimer inhibits the human breast cancer stem cell subpopulation and bone metastases formation. *Oncogene* 2012, 31(17):2164-74.
93. Hu F, Meng X, Tong Q, *et al.* BMP-6 inhibits cell proliferation by targeting microRNA-192 in breast cancer. *Biochim Biophys Acta* 2013, 1832(12):2379-90.
94. Clevers H. The cancer stem cell: premises, promises and challenges. *Nat Med* 2011, 17(3):313-9.
95. Gao H, Chakraborty G, Lee-Lim AP, *et al.* The BMP inhibitor Coco reactivates breast cancer cells at lung metastatic sites. *Cell* 2012, 150(4):764-79.
96. Ampuja M, Jokimäki R, Juuti-Uusitalo K, *et al.* BMP4 inhibits the proliferation of breast cancer cells and induces an MMP-dependent migratory phenotype in MDA-MB-231 cells in 3D environment. *BMC Cancer* 2013, 13:429.
97. Arnold S, Tims E, McGrath B. Identification of bone morphogenetic proteins and their receptors in human breast cancer cell lines: importance of BMP2. *Cytokine* 1999, 11(12):1031-7.
98. Wang D, Huang P, Zhu B, *et al.* Induction of estrogen receptor α -36 expression by bone morphogenetic protein 2 in breast cancer cell lines. *Mol Med Rep* 2012, 6 (3):591-6.
99. Chen A, Wang D, Liu X, *et al.* Inhibitory effect of BMP-2 on the proliferation of breast cancer cells. *Mol Med Rep* 2012, 6(3):615-20.
100. Clement JH, Raida M, Sängers J, *et al.* Bone morphogenetic protein 2 (BMP-2) induces in vitro invasion and in vivo hormone independent growth of breast carcinoma cells. *Int J Oncol* 2005, 27(2):401-7.
101. Ghosh-Choudhury N, Ghosh-Choudhury G, Celeste A, *et al.* Bone morphogenetic protein-2 induces cyclin kinase inhibitor p21 and hypophosphorylation of retinoblastoma protein in estradiol-treated MCF-7 human breast cancer cells. *Biochim Biophys Acta* 2000, 1497(2):186-96.
102. Pouliot F, Labrie C. Role of Smad1 and Smad4 proteins in the induction of p21WAF1, Cip1 during bone morphogenetic protein-induced growth arrest in human breast cancer cells. *J Endocrinol* 2002, 172(1):187-98.
103. Dumont N, Arteaga CL. A kinase-inactive type II TGF β receptor impairs BMP signaling in human breast cancer cells. *Biochem Biophys Res Commun* 2003, 301(1):108-12.
104. Du J, Yang S, Wang Z, *et al.* Bone morphogenetic protein 6 inhibit stress-induced breast cancer cells apoptosis via both smad and P38 pathways. *J Cell Biochem* 2008, 103(5):1584-97.
105. Wang K, Feng H, Ren W, *et al.* BMP9 inhibits the proliferation and invasiveness of breast cancer cells MDA-MB-231. *J Cancer Res Clin Oncol* 2011, 137(11):1687-96.

106. Ren W, Liu Y, Wan S, *et al.* BMP9 Inhibits proliferation and metastasis of HER2-positive SK-BR-3 breast cancer cells through ERK1/2 and PI3K/AKT pathways. *PLoS One* 2014, 9 (5):e96816.
107. Yan H, Zhu S, Song C, *et al.* Bone morphogenetic protein (BMP) signaling regulates mitotic checkpoint protein levels in human breast cancer cells. *Cell Signal* 2012, 24(4):961-8.
108. Ghosh-Choudhury N, Woodruff K, Qi W, *et al.* Bone morphogenetic protein-2 blocks MDA MB 231 human breast cancer cell proliferation by inhibiting cyclin-dependent kinase-mediated retinoblastoma protein phosphorylation. *Biochem Biophys Res Commun* 2000, 272(3):705-11.
109. Pouliot F, Blais A, Labrie C. Overexpression of a dominant negative type II bone morphogenetic protein receptor inhibits the growth of human breast cancer cells. *Cancer Res* 2003, 63 (2), 277-81.
110. Waite KA, Eng C. BMP2 exposure results in decreased PTEN protein degradation and increased PTEN levels. *Hum Mol Genet* 2003, 12(6):679-84.
111. Rodriguez-Martinez A, Alarmo EL, Saarinen L, *et al.* Analysis of BMP4 and BMP7 signaling in breast cancer cells unveils time-dependent transcription patterns and highlights a common synexpression group of genes. *BMC Med Genomics* 2011, 4:80.
112. Montesano R, Sarközi R, Schramek H. Bone morphogenetic protein-4 strongly potentiates growth factor-induced proliferation of mammary epithelial cells. *Biochem Biophys Res Commun* 2008, 374(1):164-8.
113. Jung JW, Shim SY, Lee DK, *et al.* An Activin A/BMP2 chimera, AB215, blocks estrogen signaling via induction of ID proteins in breast cancer cells. *BMC Cancer* 2014, 14:549.
114. Owens P, Pickup MW, Novitskiy SV, *et al.* Disruption of bone morphogenetic protein receptor 2 (BMPR2) in mammary tumors promotes metastases through cell autonomous and paracrine mediators. *Proc Natl Acad Sci U S A* 2012, 109(8):2814-9.
115. Steinert S, Kroll TC, Taubert I, *et al.* Differential expression of cancer-related genes by single and permanent exposure to bone morphogenetic protein 2. *J Cancer Res Clin Oncol* 2008, 134(11):1237-45.
116. Clement JH, Marr N, Meissner A, *et al.* Bone morphogenetic protein 2 (BMP-2) induces sequential changes of Id gene expression in the breast cancer cell line MCF-7. *J Cancer Res Clin Oncol* 2000, 126(5):271-9.
117. Raida M, Clement JH, Ameri K, *et al.* Expression of bone morphogenetic protein 2 in breast cancer cells inhibits hypoxic cell death. *Int J Oncol* 2005, 26(6):1465-70.
118. Hanahan D, Weinberg RA. Hallmarks of cancer: the next generation. *Cell* 2011, 144(5):646-74.
119. Pickup MW, Hover LD, Polikowsky ER, *et al.* BMPR2 loss in fibroblasts promotes mammary carcinoma metastasis via increased inflammation. *Mol Oncol* 2015, 9(1):179-91.

120. Perkins ND. The diverse and complex roles of NF- κ B subunits in cancer. *Nat Rev Cancer* 2012, 12(2):121-32.
121. Owens P, Polikowsky H, Pickup MW, *et al.* Bone morphogenetic proteins stimulate mammary fibroblasts to promote mammary carcinoma cell invasion. *PLoS One* 2013, 8(6):e67533.
122. Cai J, Pardali E, Sánchez-Duffhues G, *et al.* BMP signaling in vascular diseases. *FEBS Lett* 2012, 586(14):1993-2002.
123. David L, Feige JJ, Bailly S. Emerging role of bone morphogenetic proteins in angiogenesis. *Cytokine Growth Factor Rev* 2009, 20(3):203-12.
124. Raida M, Clement JH, Leek RD, *et al.* Bone morphogenetic protein 2 (BMP-2) and induction of tumor angiogenesis. *J Cancer Res Clin Oncol* 2005, 131(11):741-50.
125. Cunha SI, Pietras K. ALK1 as an emerging target for antiangiogenic therapy of cancer. *Blood* 2011, 117(26):6999-7006.
126. Brown MA, Zhao Q, Baker KA, *et al.* Crystal structure of BMP-9 and functional interactions with pro-region and receptors. *J Biol Chem* 2005, 280(26):25111-8.
127. Scharpfenecker M, van Dinther M, Liu Z, *et al.* BMP-9 signals via ALK1 and inhibits bFGF-induced endothelial cell proliferation and VEGF-stimulated angiogenesis. *J Cell Sci* 2007, 120(Pt 6):964-72.
128. David L, Mallet C, Keramidas M, *et al.* Bone morphogenetic protein-9 is a circulating vascular quiescence factor. *Circ Res* 2008, 102(8):914-22.
129. Suzuki Y, Montagne K, Nishihara A, *et al.* BMPs promote proliferation and migration of endothelial cells via stimulation of VEGF-A/VEGFR2 and angiopoietin-1/Tie2 signalling. *J Biochem* 2008, 143(2):199-206.
130. Suzuki Y, Ohga N, Morishita Y, *et al.* BMP-9 induces proliferation of multiple types of endothelial cells in vitro and *in vivo*. *J Cell Sci* 2010, 123(Pt 10):1684-92.
131. Hu-Lowe DD, Chen E, Zhang L, *et al.* Targeting activin receptor-like kinase 1 inhibits angiogenesis and tumorigenesis through a mechanism of action complementary to anti-VEGF therapies. *Cancer Res* 2011, 71(4):1362-73.
132. Cunha SI, Pardali E, Thorikay M, *et al.* Genetic and pharmacological targeting of activin receptor-like kinase 1 impairs tumor growth and angiogenesis. *J Exp Med* 2010, 207(1):85-100.
133. Chaffer CL, Weinberg RA. A perspective on cancer cell metastasis. *Science* 2011, 331(6024):1559-64.
134. Polyak K, Weinberg RA. Transitions between epithelial and mesenchymal states: acquisition of malignant and stem cell traits. *Nat Rev Cancer* 2009, 9(4):265-73.

135. Mock K, Preca B, Brummer T, *et al.* The EMT-activator ZEB1 induces bone metastasis associated genes including BMP-inhibitors. *Oncotarget* 2015, 6(16):14399-412.
136. Mani SA, Guo W, Liao MJ, *et al.* The epithelial-mesenchymal transition generates cells with properties of stem cells. *Cell* 2008, 133(4):704-15.
137. Yang S, Du J, Wang Z, *et al.* BMP-6 promotes E-cadherin expression through repressing δ EF1 in breast cancer cells. *BMC Cancer* 2007, 7:211.
138. Yang S, Du J, Wang Z, *et al.* Dual mechanism of δ EF1 expression regulated by bone morphogenetic protein-6 in breast cancer. *Int J Biochem Cell Biol* 2009, 41(4):853-61.
139. Zeisberg M, Ji H, Sugimoto H, *et al.* BMP-7 counteracts TGF β 1-induced epithelial-to-mesenchymal transition and reverses chronic renal injury. *Nat Med* 2003, 9(7):964-968.
140. Kowantetz M, Valcourt U, Bergström R, *et al.* Id2 and Id3 define the potency of cell proliferation and differentiation responses to transforming growth factor β and bone morphogenetic protein. *Mol Cell Biol* 2004, 24(10):4241-54.
141. Valcourt U, Kowantetz M, Niimi H, *et al.* TGF β and the Smad signaling pathway support transcriptomic reprogramming during epithelial-mesenchymal cell transition. *Mol Biol Cell* 2005, 16(4):1987-2002.
142. Buijs JT, Henriquez NV, van Overveld PG, *et al.* TGF β and BMP7 interactions in tumour progression and bone metastasis. *Clin Exp Metastasis* 2007, 24(8):609-17.
143. Pal A, Huang W, Li X, *et al.* Ccn6 modulates BMP signaling via the Smad-independent TAK1/p38 pathway, acting to suppress metastasis of breast cancer. *Cancer Res* 2012, 72(18):4818-28.
144. Jin H, Pi J, Huang X, *et al.* BMP2 promotes migration and invasion of breast cancer cells via cytoskeletal reorganization and adhesion decrease: an AFM investigation. *Appl Microbiol Biotechnol* 2012, 93(4):1715-23.
145. Montesano R. Bone morphogenetic protein-4 abrogates lumen formation by mammary epithelial cells and promotes invasive growth. *Biochem Biophys Res Commun* 2007, 353(3):817-22.
146. Friedl P, Alexander S. Cancer invasion and the microenvironment: plasticity and reciprocity. *Cell* 2011, 147(5):992-1009.
147. Shon SK, Kim A, Kim JY, *et al.* Bone morphogenetic protein-4 induced by NDRG2 expression inhibits MMP-9 activity in breast cancer cells. *Biochem Biophys Res Commun* 2009, 385(2):198-203.
148. Wang C, Hu F, Guo S, *et al.* BMP-6 inhibits MMP-9 expression by regulating heme oxygenase-1 in MCF-7 breast cancer cells. *J Cancer Res Clin Oncol* 2011, 137(6):985-95.

149. Wan S, Liu Y, Weng Y, *et al.* BMP9 regulates cross-talk between breast cancer cells and bone marrow-derived mesenchymal stem cells. *Cell Oncol* 2014, 37(5):363-75.
150. Scherberich A, Tucker RP, Degen M, *et al.* Tenascin-W is found in malignant mammary tumors, promotes $\alpha 8$ integrin-dependent motility and requires p38MAPK activity for BMP-2 and TNF- α induced expression *in vitro*. *Oncogene* 2005, 24(9):1525-32.
151. Gatza CE, Elderbroom JL, Oh SY, *et al.* The balance of cell surface and soluble type III TGF β receptor regulates BMP signaling in normal and cancerous mammary epithelial cells. *Neoplasia* 2014, 16(6):489-500.
152. Grönroos E, Kingston IJ, Ramachandran A, *et al.* Transforming growth factor β inhibits bone morphogenetic protein-induced transcription through novel phosphorylated Smad1/5-Smad3 complexes. *Mol Cell Biol* 2012, 32(14):2904-16.
153. Gautschi O, Tepper CG, Purnell PR, *et al.* Regulation of Id1 expression by SRC: implications for targeting of the bone morphogenetic protein pathway in cancer. *Cancer Res* 2008, 68(7):2250-58.
154. Naber HP, Wiercinska E, Pardali E, *et al.* BMP-7 inhibits TGF β -induced invasion of breast cancer cells through inhibition of integrin $\beta 3$ expression. *Cell Oncol* 2012, 35(1):19-28.
155. Roodman GD. Mechanisms of bone metastasis. *N Engl J Med* 2004, 350(16):1655-64.
156. Bunyaratavej P, Hullinger TG, Somerman MJ. Bone morphogenetic proteins secreted by breast cancer cells upregulate bone sialoprotein expression in preosteoblast cells. *Exp Cell Res* 2000, 260(2):324-33.
157. Javed A, Barnes GL, Pratap J, *et al.* Impaired intranuclear trafficking of Runx2 (AML3/CBFA1) transcription factors in breast cancer cells inhibits osteolysis *in vivo*. *Proc Natl Acad Sci U S A* 2005, 102(5):1454-59.
158. Taipaleenmäki H, Browne G, Akech J, *et al.* Targeting of Runx2 by miR-135 and miR-203 impairs progression of breast cancer and metastatic bone disease. *Cancer Res* 2015, 75(7):1433-44.

Chapter 2

Invasive Behavior of Human Breast Cancer Cells in Embryonic Zebrafish

Jiang Ren*, Sijia Liu*, Chao Cui, and Peter ten Dijke

Journal of visualized experiments 2017, (122):e55459.

*These authors contributed equally

Abstract

In many cases, cancer patients do not die of a primary tumor, but rather because of metastasis. Although numerous rodent models are available for studying cancer metastasis *in vivo*, other efficient, reliable, low-cost models are needed to quickly access the potential effects of (epi)genetic changes or pharmacological compounds. As such, we illustrate and explain the feasibility of xenograft models using human breast cancer cells injected into zebrafish embryos to support this goal. Under the microscope, fluorescent proteins or chemically labeled human breast cancer cells are transplanted into transgenic zebrafish embryos, Tg (*flil:EGFP*), at the perivitelline space or duct of Cuvier (Doc) 48 h after fertilization. Shortly afterwards, the temporal-spatial process of cancer cell invasion, dissemination, and metastasis in the living fish body is visualized under a fluorescent microscope. The models using different injection sites *i.e.*, perivitelline space or Doc are complementary to one another, reflecting the early stage (intravasation step) and late stage (extravasation step) of the multistep metastatic cascade of events. Moreover, peritumoral and intratumoral angiogenesis can be observed with the injection into the perivitelline space. The entire experimental period is no more than 8 days. These two models combine cell labeling, micro-transplantation, and fluorescence imaging techniques, enabling the rapid evaluation of cancer metastasis in response to genetic and pharmacological manipulations.

Keywords: Embryonic zebrafish, Human breast cancer, Metastasis, Intravasation, Extravasation, Perivitelline space, Duct of Cuvier

Video Link: The video component of this article can be found at <https://www.jove.com/video/55459/>

Introduction

Overt cancer metastasis in the clinic comprises a series of complex and multi-step events known as the ‘metastatic cascade’. The cascade has been extensively reviewed and can be dissected into successive steps: local invasion, intravasation, dissemination, arrest, extravasation, and colonization [1, 2]. A better understanding of the pathogenesis of cancer metastasis and the development of potential treatment strategies *in vivo* require robust host models of cancer cell spread. Rodent models are well established and widely used to evaluate metastasis [3], but these approaches have low efficiency, ethical limitations, and are costly as a forefront model to determine whether a particular manipulation could affect the metastatic phenotype. Other efficient, reliable, low-cost models are needed to quickly access the potential effect of (epi)genetic changes or pharmacological compounds. Due to the high genetic homology to humans and transparency of the embryos, the zebrafish (*Danio rerio*) has emerged as an important vertebrate model and is being applied increasingly in studying developmental processes, microbe-host interactions, human disease, drug screening, *etc.* [4]. The cancer metastasis models established in zebrafish may provide ideal solutions to the shortcomings of rodent models [5, 6].

Although spontaneous neoplasia is scarcely discovered in wild zebrafish [7], there are several longstanding techniques to induce desired cancer in zebrafish. Carcinogen-induced gene mutations or signaling pathways-activation can model carcinogenesis histologically and molecularly resembling human disease in zebrafish [7-9]. By taking advantage of diverse forward and reverse genetic manipulations of oncogenes or tumor suppressors, (transgenic) zebrafish also have enabled potential studies of cancer formation and maintenance [6, 10]. The induced cancer models in zebrafish cover a broad spectrum of cancer types in digestive, reproductive, blood, nervous systems, and epithelium [6].

The utilization of zebrafish in cancer research has expanded recently due to the establishment of human tumor cell xenograft models in this organism. This was first reported with human metastatic melanoma cells that were successfully engrafted in zebrafish embryos at the blastula stage in 2005 [11]. Several independent laboratories have validated the feasibility of this pioneering work by introducing a diverse range of mammalian cancer cells lines into zebrafish at various sites and developmental stages [5]. For example, injections near the blastodisc and blastocyst of the blastula stage; injections into the yolk sac, perivitelline space,

duct of Cuvier (Doc), and posterior cardinal vein of 6-h- to 5-day old embryos; and injections into the peritoneal cavity of 30-day-old immunosuppressed larvae have been performed [5,12]. Additionally, allogeneic tumor transplantations were also reported in zebrafish [12,13]. One of the great advantages of using xenografts is that the engrafted cancer cells can be easily fluorescently labeled and distinguished from normal cells. Hence, investigations into the dynamic behaviors of microtumor formation [14], cell invasion and metastasis [15-17], tumor-induced angiogenesis [15,18], and the interactions between cancer cells and host factors [17] can be clearly visualized in the live fish body, especially when transgenic zebrafish lines are applied [5].

Inspired by the high potential of zebrafish xenograft models to evaluate metastasis, we demonstrated the transvascular extravasation properties of different breast cancer cell lines in the tailfin area of Tg (*fli:EGFP*) zebrafish embryos through Doc injections [16]. The role of transforming growth factor- β (TGF β) [16] and bone morphogenetic protein (BMP) [19] signaling pathways in pro-/anti-breast cancer cell invasion and metastasis were also investigated in this model. Moreover, we also recapitulated the intravasation ability of various breast cancer cell lines into circulation using xenograft zebrafish models with perivitelline space injections.

This article presents detailed protocols for zebrafish xenograft models based upon the injection of human breast cancer cells into the perivitelline space or Doc. Using high-resolution fluorescence imaging, we show the representative process of intravasation into blood vessels and the invasive behavior of different human breast cancer cells, which move from the blood vessels into the avascular tailfin area.

Protocol

All research using transgenic fluorescent zebrafish Tg (*fli:EGFP*) strain, which has enhanced green fluorescent protein (EGFP) labeled vasculature²⁰, including housing and experiments, was carried out according to the international guidelines and approved by the local Institutional Committee for Animal Welfare (Dier Ethische Commissie (DEC) of the Leiden University Medical Center.

NOTE: As summarized in Figure 1, the protocol is roughly dissected into four steps, embryo collection (Figure 1A), microinjection (Figure 1B), screening (Figure 1C), and analysis (Figure 1D).

1. Prepare the injection needles

1. Prepare injection needles with borosilicate glass microcapillary. Put the microcapillary in a micropipette puller device with the following settings: air pressure 500; heat 650; pull 100; velocity 200; time 40. Keep the injection needles in a needle holder plate until used for injection.

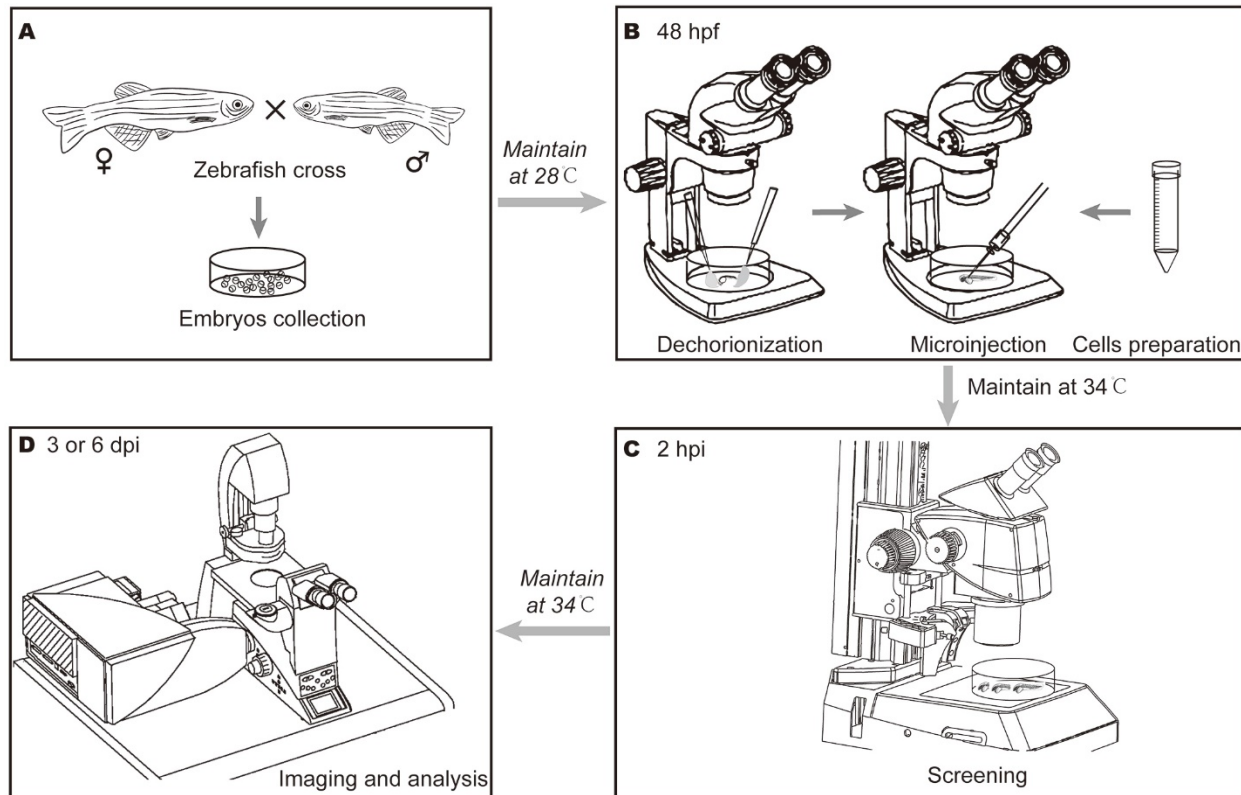


Figure 1. Main steps for investigating the invasive behavior of breast cancer cells in embryonic zebrafish. **A**, After crossing parental zebrafish overnight, Tg (*fli:EGFP*) zebrafish embryos were collected the following morning and maintained at 28 °C. **B**, The embryos were dechorionated with fine tweezers under a stereo microscope 48 h post fertilization (hpf). The labeled breast cancer cells were collected and re-suspended in a small amount of PBS. After well-preparation, suspended cells were loaded into one needle. Approximately 400 cells were injected into the duct of Cuvier (Doc) of the perivitelline space under a stereo microscope. The injected embryos were maintained at 34 °C. **C**, 2 hours post injection (hpi), the embryos were subjected to careful screening under a fluorescence stereo microscope. The embryos were maintained at 34 °C for 3 or 6 d. During the interval, embryos could be subjected to designed treatment. **D**, Cancer cell dissemination by perivitelline space injection or invasion

by Doc injection was detected, counted, and imaged by confocal microscopy 3 or 6 days post injection (dpi).

2. Prepare of the fluorescent genetically labeled breast cancer cells for injection

1. Culture human breast cancer MDA-MB-231 cells at 37 °C in DMEM-high glucose media containing L-glutamine, 10% fetal bovine serum and 1:100 Penicillin-Streptomycin (Pen-Strep).
2. Culture the breast epithelial cell line MCF10A (M1), MCF10A-Ras (M2) at 37 °C in DMEM/F12 media containing L-glutamine, with 5% horse serum, 20 ng/mL epidermal growth factor, 10 mg/mL insulin, 100 ng/mL cholera enterotoxin, 0.5 mg/mL hydrocortisone, and 1:100 Pen-Strep.
3. Produce mCherry lentivirus by co-transfecting PLV-mCherry, pCMV-VSVG [21], pMDLg-RRE (gag/pol) [22], and pRSV-REV [22] plasmids into HEK293T cells. Harvest cell supernatants 48 h after transfection and store at -80 °C.
4. Infect MDA-MB-231, M1 and M2 cells at 30% confluence for 24 h with lentiviral supernatants diluted 1:1 with normal culture medium in the presence of 5 ng/mL polybrene.
5. Select single cell clones by diluting cells in a 96-well plate, which allows the outgrowth of isolated cell clones, until obtaining the stable mCherry-expressing cell lines.
6. Culture one T75 flask of cells for injection. Harvest the cells at 80% confluence with a 0.5% trypsin-EDTA treatment. Wash the cells with 1× PBS 2-3 times.
7. Re-suspend the cells in about 200 µL PBS. Store at 4 °C for less than 5 h before injection.

3. Prepare zebrafish embryos for injection

1. Set up zebrafish breeding pairs and collect embryos as shown in a previous Jove article by Rosen *et al.* [23].
2. Select the embryos that are at 0-4 hpf by removing the unfertilized and abnormal embryos. Keep the embryos in a petri-dish filled with egg water (60 µg/mL sea salts; about 60 embryos/dish) and incubate at 28 °C.
3. Dechorionate the embryos with fine tweezers at 48 hpf.
4. Anesthetize the embryos by transferring them to 40 µg/mL Tricaine (3-aminobenzoic acid) containing egg water approximately 2 min prior to injection, but no longer than 2 h prior to injection.

NOTE: Tricaine stock solution (4 mg/mL, 100×) is prepared as 400 mg tricaine powder in 97.9 mL double-distilled water and 2.1 mL 1 M Tris-base (pH 9), adjust pH to 7.4. Store in the -20 °C freezer.

4. Inject human breast cancer cells into the perivitelline space

1. Load 15 μ L of the cell suspension into an injection needle. Mount the needle onto the micromanipulator and break off the needle tip with fine tweezers to obtain a tip opening diameter of 5-10 μ m.
2. Use a pneumatic picopump and a manipulator to perform microinjection. Adjust the picopump to inject 400 cells each time. Prior to injection, count the cell numbers manually by injecting the cells on the top of a petri-dish containing 1% agarose.
3. Line up anesthetized embryos (2-3 days post fertilization (dpf)) on a flat 1% agarose injecting plate, around 10 embryos each time.
4. Orient the injection plate by hand during injections to place the embryos in the preferred position for inserting the needle (*i.e.*, diagonally).
5. Point the needle tip to the injection site and gently insert the needle tip into the perivitelline space between the yolk sac and the periderm of the zebrafish embryo (Figure 2A).

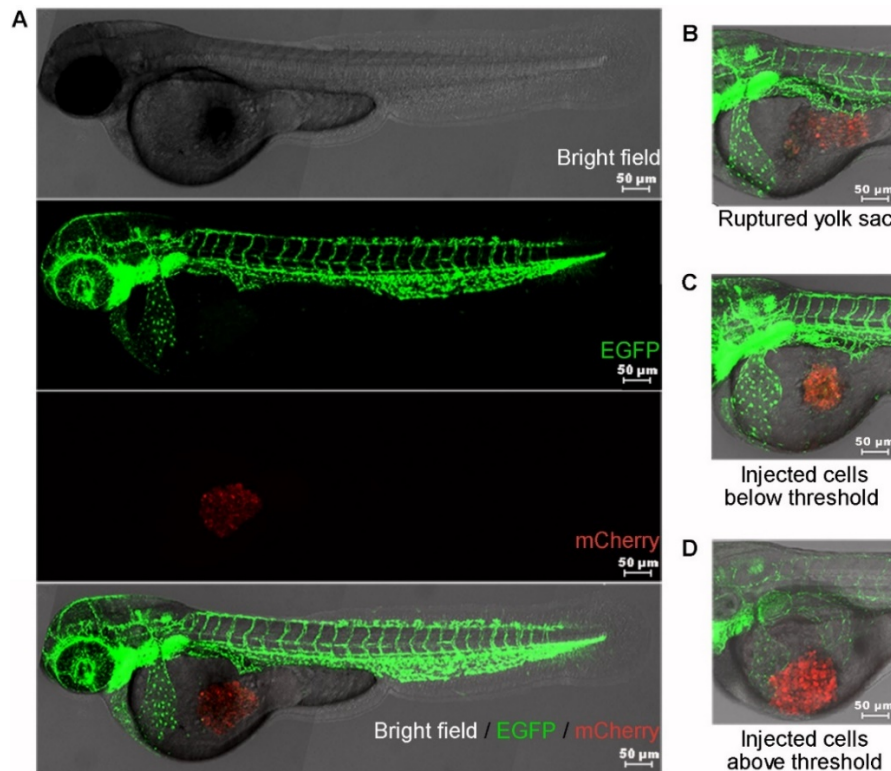


Figure 2. Perivitelline space injection site and common errors. **A**, Approximately 400 mCherry-labeled cells (MDA-MB-231) were injected into the perivitelline space. The brightfield (upper most), green vasculature (middle upper), and red cell mass (middle lower) of injected zebrafish embryos were captured by confocal microscope. The merged image (lower most) of three channels shows the stereo location of the cell mass in the embryo. **B**, The cells did not target the perivitelline space appropriately. The yolk sac was ruptured. **C**, Injected cells below threshold (much less than 400). **D**, Injected cells above threshold (much more than 400). The cell mass was too close to the duct of Cuvier, which has a broad blood stream. Scale bar = 50 μ m.

6. Inject approximately 400 mCherry-labeled tumor cells. Make sure that the yolk sac is not ruptured to avoid implantation into the yolk sac.

5. Inject human breast cancer cells into the Doc

1. Prepare injection needle and zebrafish embryos as described in protocol steps 1, 2, and 3.
2. Use a 45° needle angle so that the Doc can be approached from the dorsal side of the embryo.
3. Insert the needle into the starting point of the Doc (Figure 3A) just dorsal to where the duct starts broadening over the yolk sac and inject approximately 400 cells. The injection is correct if the volume within the duct expands directly after the pulse and the yolk sac.

NOTE: Several consecutive injections can be performed without extracting the needle.

4. Transfer the injected zebrafish embryos to egg water.

NOTE: As considerable variation exists among individual zebrafish embryos, as well as the death of embryos after injection, relatively large number of zebrafish embryos (around 100) should be injected with cancer cells.

5. Maintain the zebrafish embryos at 34 °C to accommodate the optimal temperature requirements for fish and mammalian cells.

6. Screen the injected embryos

1. Screen each fish under a fluorescence stereo microscope at 2 h post-injection (hpi) for perivitelline space injection (Figure 2) or at 2-24 hpi for Doc injection (Figure 2), to ensure all the embryos are injected with similar number of tumor cells. Remove the embryos with injection errors, such as rupture (Figure 2B) or injection (Figure 3B) of yolk sac, and pick

out embryos with injected cells below (Figure 2C and Figure 3B) or above (Figure 2D and Figure 3B) threshold. Keep only the embryos with approximately 400 cells in culture.

2. Rule out the possibility that cells are introduced directly into the circulation during the injection process by removing the embryos with cells already in the circulation from further analysis. Also remove any embryo with a cell mass close to the Doc (Figure 2D).

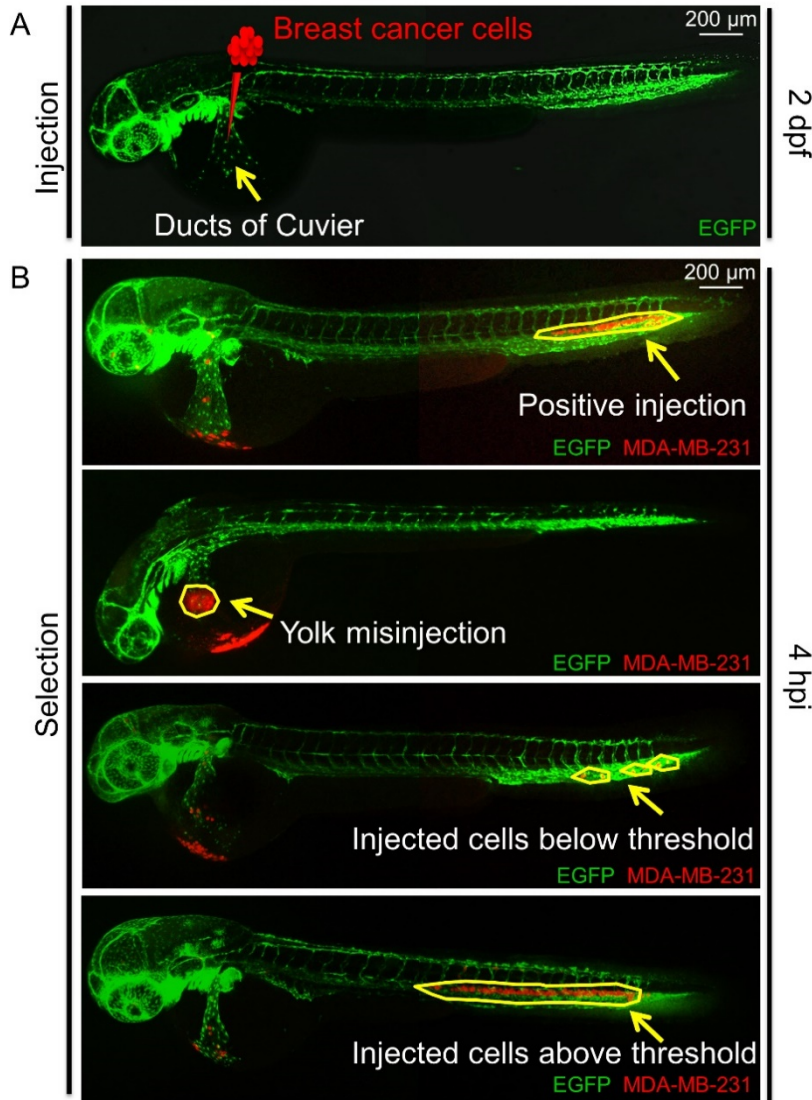


Figure 3. Overview of duct of Cuvier (Doc) injection. A, Schematic of Doc injection at 2 days post-fertilization (dpf) with breast cancer cells in zebrafish embryos. Arrow indicates Doc. B, Examples of positive injection with around 400 breast cancer cells, negative injections including the yolk mis-injection and incorrect number of cells injection at 4 hpi. Arrows and circles indicate injected cells.

7. Image and analyze the metastatic process

1. Collect several anesthetized embryos with a wide-tip Pasteur pipette, and transfer them onto the glass bottom of a polystyrene dish.
2. Remove excess water and keep a limited amount of egg water. Manipulate the embryo into position with a hair loop tool, and place a cover on top of the glass.

3. Use an inverted confocal microscope in combination with water-immersion or long-distance dry objectives. The embryo should be positioned so that the region of interest is as close to the objective as possible.
4. Perform imaging immediately after anesthesia to reduce death risk of embryo due to liquid evaporation.
 1. Capture signals from EGFP-labeled vasculature and mCherry labeled tumor cells at the same position of the embryos to co-register injected cells with blood vessels by merging the two imaging channels.
 2. For each zebrafish embryo, collect two different sets of images from the head region and tail region.
5. Quantify the number of disseminated cells.
 1. For perivitelline space injection, count the number of cells in each fish that disseminated from the cell mass toward the embryonic fish body within the head and tail regions^{4,15}. The regions are beyond the boundaries of the heart cavity frontally, on top of the swim bladder dorsally, and beyond the urogenital opening caudally.
 2. For Doc injection, count the number of individual cells that invade the collagen fibers of the tail fin from circulation (MDA-MB-231) or the number of clusters formed by cells collectively (M2) in the caudal hematopoietic tissue (CHT) of each zebrafish [19].
6. Study invasion and metastasis in more detail, use confocal microscopy (highly recommended).
 1. Use low magnification (4× objective) to image the whole body and obtain an overview of the tumor cell dissemination pattern.

NOTE: Higher magnification (20× and 40× objectives) is suitable for studying intra- and peri-tumoral angiogenesis and precise localization of disseminated cells in the embryo body.
 2. Use a 488-nm laser to scan the zebrafish embryo vasculature, and a 543 nm laser to scan implanted tumor cells labeled with red fluorescence. Obtain a high-quality image, by scanning each embryo in eight to ten steps. Scan and average each step six times.
7. Carefully place the embryo back into the egg water if it is required for further experiments.

8. Perform statistical analysis using one-way analysis of variance (ANOVA) followed by post Hoc analysis

Representative results

In the embryonic xenograft zebrafish model with a perivitelline space injection, the hematogenous dissemination of labeled cancer cells in the fish body is considered as active migration. This process can be detected and quantified under a fluorescent microscope, as described in the methods above. To illustrate this xenograft model, we followed the dissemination process of different breast cancer cell lines with known (or without) invasion/metastasis potential according to in vitro and in vivo mouse studies, including the benign normal breast epithelial M1 cells, HRAS-transformed premalignant M2 cells, and highly metastatic MDA-MB-231 cells, 1 day post injection (dpi) onward. A high-resolution confocal microscopy image showed that MDA-MB-231 cells (red) exhibit an aggressive phenotype, with irregular borders in the perivitelline space. Pseudopodia-like protrusions and invasive fronts were also frequently present (Figure 4A, left). A few cells disseminated into blood circulation as early as 1 dpi (Figure 4A, right). At 2 dpi, clear dissemination was observed in the distal parts of the fish (Figure 4A, right). The number of disseminated cells increased further at 3 dpi (Figure 4A, D). In contrast, when M2 cells were challenged in zebrafish, they exhibited modest spread in the fish body after 2 dpi (Figure 4B). They also showed increased dissemination after time passed (Figure 4F). As shown in Figure 4C and 4G, M1 cells infrequently disseminated into zebrafish circulation, and even active local migration within the perivitelline space was infrequent during the period of observation. The M1 cell mass was virtually detained at the original injection site. If defining positive dissemination or metastasis as >5 cells in the fish body [4], MDA-MB-231 and M2 cell metastasis was observed in 92% and 57% of fish, respectively, at 3 dpi (Figure 4G). In contrast, no positive dissemination was observed with M1 cells. Therefore, this zebrafish model of human cancer cell progression accurately reflects the relative level of metastatic potential of the different cells in mice. Neovascularization (green) that sprouted from the subintestinal plexus of the embryonic zebrafish and penetrated the MDA-MB-231 or M2 cell mass was also present after the perivitelline space injection of tumor cells followed by 3 days of incubation (Figure 4A, B, left). Consistent with the disability in dissemination, only slight neovascularization was detected upon M1 cell implantation (Figure 4C).

In the embryonic xenograft zebrafish model with mCherry-labeled MDA-MB-231 cells and the Doc injection, the labeled cancer cells in the tailfin of the zebrafish are considered representative of active extravasation. The mCherry-labeled MDA-MB-231 cells were injected at

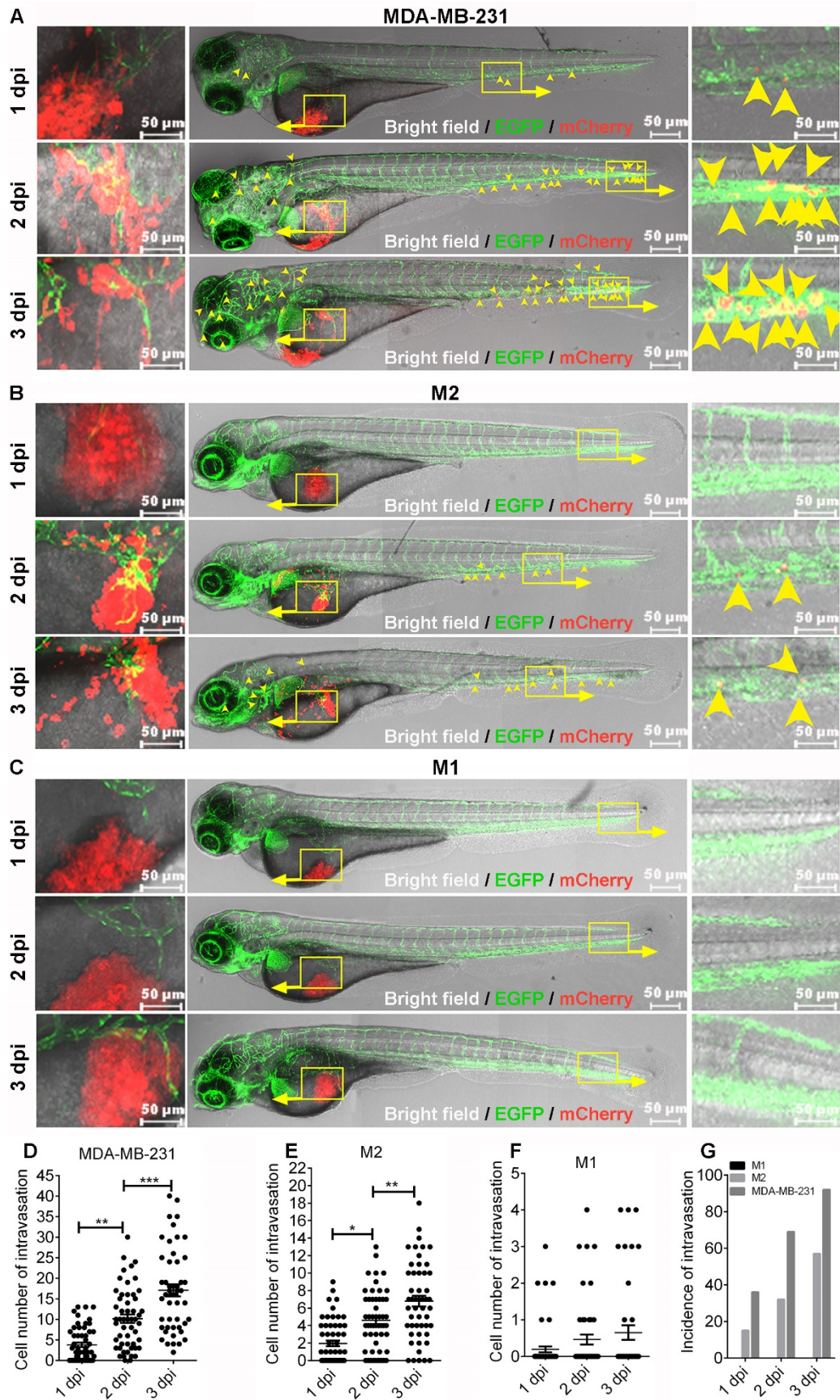


Figure 4. Comparison of dissemination ability among various breast cell lines. Approximately 400 mCherry-labeled MDA-MB-231, MCF10Aras (M2), or MCF10A (M1) cells were injected into the perivitelline space of zebrafish embryos 48 hpf. The injected embryos were followed for 3 days. **A-C**, High-resolution micrographs showing the representative migration and dissemination process of MDA-MB-231 (**A**), M2 (**B**), and M1 (**C**) cells in individual embryonic bodies 1, 2, and 3 days post-injection (dpi). Left, cell migration in the perivitelline space (red) and the peritumoral and intratumoral vasculature (green). Yellow signals indicate the overlap of microvessels and cells. Middle, the whole image of embryo. Right, visualization of disseminated cells in the posterior of embryo. Yellow arrowheads indicate single disseminated cells. Scale bar = 50 μ m. **D-F**, Quantification of the number of disseminated cells in each embryonic body at 1, 2, 3 dpi. Results are expressed as the Mean \pm SEM. Results from one-way analysis of variance (ANOVA) followed by the post hoc analysis are shown. $P < 0.05$ was accepted as statistically significant (* $0.01 < P < 0.05$; ** $0.001 < P < 0.01$; *** $P < 0.001$). **G**, Comparison of the incidence of intravasation for MDA-MB-231, M2, and M1 cells in embryonic bodies at 1, 2, 3 dpi.

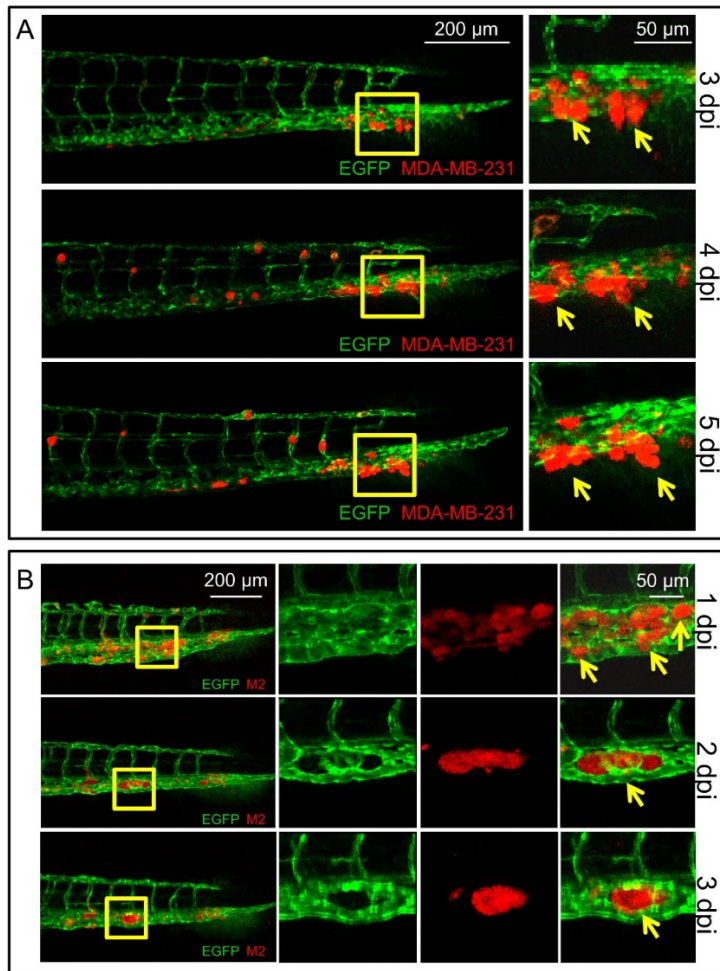


Figure 5. Different behavior of MDA-MB-231 and M2 cell metastasis in zebrafish with duct of Cuvier injection. **A**, Representative confocal images of the zebrafish followed at 3, 4, 5 dpi to show the single cell migration behavior of the MDA-MB-231 cells in zebrafish. Arrows indicate invasive MDA-MB-231 cells that migrated out of the vessels to the tail fins. Scale bar = 200 μ m in the left column, 50 μ m in the right column. **B**, Representative confocal images of the zebrafish followed at 1, 2, 3 dpi to show the cell cluster migration behavior of M2 cells in zebrafish. Arrows indicate invasive M2 cells that migrated out of the vessels to the caudal hematopoietic tissue (CHT) and formed a cluster between the vessels.

2 dpf. At 3 dpi, the cells started to migrate out of the vessels to the tailfin, which is enriched with collagen. Single MDA-MB-231 cells migrated one by one, independently from the vessels, to the distant tailfin (Figure 5A). At 6 dpi, the invasion could be quantified by counting the number of cells that migrated into the tailfin tissue. In the mCherry-labeled M2 cell Doc injection model, the injection was also performed at 2 dpf. However, a clustered phenotype was observed during the active extravasation process. At 1 dpi, M2 cells started to migrate out from the vessels into the CHT of the zebrafish. At 2 dpi, the migrated M2 cells started to form a cluster between the vessels in the CHT (Figure 5B). Quantification of the M2 invasive cell cluster number in the CHT region could be conducted at 6 dpi.

Discussion

Here, we described two methods to investigate the invasive behavior of breast cancer cells in Tg (fli1:EGFP) zebrafish embryos, with perivitelline space and Doc injections. By injecting cancer cells labeled with chemical dye or fluorescent protein into transgenic zebrafish embryos, the dynamic and spatial characteristics of invasion and metastasis can be clearly tracked in real-time at the single-cell or cluster level under a fluorescence microscope. In most cases, the rapid progression of metastasis in zebrafish ensures that the assay can be performed within 1 week after transplantation. Moreover, powerful statistics can be obtained with large cohorts of fish.

Early and late events of the metastatic cascade could be simulated and recapitulated by injecting cancer cells into the perivitelline space or Doc, respectively. The perivitelline space is the confined space between the periderm of the fish and the yolk sac, which allows one to monitor dissemination of single tumor cells from primary sites in the living body. After implantation, the cancer cells undergo local migration and invasion within the perivitelline space (considered the primary site) and then they intravasate into blood vessels and disseminate along with the circulation. At the head and tailfin (considered distant target sites), cancer cells accumulate in narrow capillary beds and extravasate. Therefore, the number of cells that are found at the distant sites in the fish body is a measurement of metastatic capability. In addition, more extravasated cells can be observed at later time points, which is also true of the Doc injection assay.

The Doc is an enlarged common cardinal vein with an extensive blood stream [24]. Directly targeting the Doc as an injection site introduces cancer cells into the circulatory system. In practice, breast cancer cells diffuse throughout the embryonic body via the blood stream

instantly after Doc injection. The cells then arrest at the caudal vein and dorsal aorta. Extravasation, invasion, and micrometastasis formation can be observed successively within 6 days. As reported previously [16], metastatic MDA-MB-231 cells and premalignant mammary M2 cells exhibit different invasive phenotypes. MDA-MB-231 cells undergo single-cell invasion of the collagen matrix-rich tailfin. Thus, the invasion potential of MDA-MB-231 cells can be measured by counting the number of cells that have extravasated and invaded the tailfin tissue. In contrast, M2 cells form clusters of different sizes and undergo collective invasion of the CHT. Quantifying the invasion potential of M2 cells by counting the number of clusters in this protocol is difficult and is preferably performed by making a 3D image using confocal microscopy and determining the volume of clustered tumor cells.

The technical challenge in cancer cell microinjection is successfully targeting the perivitelline space or Doc. The microinjection of large numbers of embryos is a tedious procedure requiring a highly skilled and patient operator. Factors that contribute to variations in the results in individual fish include the developmental stage of the embryo when injecting, differences in the number of cells injected, and the leakage of cells into the yolk sac. Though rare, the manipulation could unintentionally penetrate the vasculature and introduce cells into the circulatory system directly, especially in the perivitelline space injection. To further reduce variation and to ensure the reliability of the analyses, microscopic examination is necessary to exclude unqualified fish at time points throughout the process. In addition, blinded analysis by a professional without knowledge of the setting is strongly suggested to achieve unbiased quantification.

In summary, the two models we introduced here shed light on visualizing the processes of cell invasion and metastasis *in vivo* without invasive procedures. Although we only studied breast cancer cells in two models regarding metastatic potential, they could be extrapolated to other types of cancer. Moreover, the models could have broader applications in determining the mechanisms and new molecular targets controlling cancer cell metastasis using (epi)genetic manipulation. Due to the higher penetrability of zebrafish embryos by small-molecule compounds as compared to the feeding or injection of rodents [25], the two presented models also have advantages in terms of the high-throughput screening of potential new anti-invasion/metastasis drugs.

Disclosures

The authors have nothing to disclose.

Acknowledgements

Studies on TGF β family members are supported by the Cancer Genomics Centre Netherlands. Sijia Liu and Jiang Ren are supported by the China Scholarship Council for 4 years of study at the University of Leiden. We thank Dr. Fred Miller (Barbara Ann Karmanos Cancer Institute, Detroit, MI, USA) for the MCF10A cell lines.

References

1. Wan L, Pantel K, Kang Y. Tumor metastasis: moving new biological insights into the clinic. *Nat Med* 2013, 19(11):1450-64.
2. Obenauf AC, Massagué J. Surviving at a distance: Organ-specific metastasis. *Trends Cancer* 2015, 1(1):76-91.
3. Saxena M, Christofori G. Rebuilding cancer metastasis in the mouse. *Mol Oncol* 2013, 7 (2):283-96.
4. Teng Y, Xie X, Walker, S. *et al.* Evaluating human cancer cell metastasis in zebrafish. *BMC cancer* 2013, 13(1):453.
5. Konantz, M, Balci, TB, Hartwig, UF, *et al.* Zebrafish xenografts as a tool for in vivo studies on human cancer. *Ann N Y Acad Sci* 2012, 1266 (1):124-37.
6. Zhao, S, Huang, J, Ye, J. A fresh look at zebrafish from the perspective of cancer research. *J Exp Clin Cancer Res* 2015, 34(1):80.
7. Stanton, MF. Diethylnitrosamine-induced hepatic degeneration and neoplasia in the aquarium fish, *Brachydanio rerio*. *J Natl Cancer Inst* 1965, 34(1):117-30.
8. Lam SH, Wu YL, Vega VB, *et al.* Conservation of gene expression signatures between zebrafish and human liver tumors and tumor progression. *Nat Biotechnol* 2006, 24(1):73-5.
9. Spitsbergen JM, Kent ML. The state of the art of the zebrafish model for toxicology and toxicologic pathology research-advantages and current limitations. *Toxicol Pathol* 2003, 31(1 suppl):62-87.
10. Stoletov K, Klemke R. Catch of the day: zebrafish as a human cancer model. *Oncogene* 2008, 27(33):4509-20.
11. Lee LM, Seftor EA, Bonde, G, *et al.* The fate of human malignant melanoma cells transplanted into zebrafish embryos: assessment of migration and cell division in the absence of tumor formation. *Dev Dynam* 2005, 233(4):1560-70.
12. Mizgirev I, Revskoy S. Generation of clonal zebrafish lines and transplantable hepatic tumors. *Nat Protoc* 2010, 5(3):383-94.

13. Mizgireuv IV, Revskoy SY. Transplantable tumor lines generated in clonal zebrafish. *Cancer Res* 2006, 66(6):3120-5.
14. Stoletov K, Montel V, Lester RD, *et al.* High-resolution imaging of the dynamic tumor cell-vascular interface in transparent zebrafish. *Proc Natl Acad Sci U.S.A* 2007, 104(44):17406-11.
15. Rouhi P, Jensen LD, Cao Z, *et al.* Hypoxia-induced metastasis model in embryonic zebrafish. *Nat Protoc* 2010, 5 (12):1911-8.
16. Drabsch Y, He S, Zhang L, *et al.* Transforming growth factor- β signalling controls human breast cancer metastasis in a zebrafish xenograft model. *Breast Cancer Res* 2013, 15(6):R106.
17. He, S, Lamers, GE, Beenakker, JW, *et al.* Neutrophil-mediated experimental metastasis is enhanced by VEGFR inhibition in a zebrafish xenograft model. *J Pathol* 2012, 227(4):431-45.
18. Nicoli S, Presta M. The zebrafish/tumor xenograft angiogenesis assay. *Nat Protoc* 2007, 2(11):2918-23.
19. Boeck M, Cui C, Mulder AA, *et al.* Smad6 determines BMP-regulated invasive behaviour of breast cancer cells in a zebrafish xenograft model. *Sci Rep* 2016, 6:24968.
20. Lawson ND, Weinstein BM. In vivo imaging of embryonic vascular development using transgenic zebrafish. *Dev Biol* 2002, 248(2):307-18.
21. Stewart SA, Dykxhoorn DM, Palliser D, *et al.* Lentivirus-delivered stable gene silencing by RNAi in primary cells. *RNA* 2003, 9(4):493-501.
22. Dull T, Zufferey R, Kelly M, *et al.* A third-generation lentivirus vector with a conditional packaging system. *J Virol* 1998, 72 (11):8463-71.
23. Rosen, JN, Sweeney MF, Mably JD. Microinjection of zebrafish embryos to analyze gene function. *J Vis Exp* 2009, (25):e1115.
24. Lawson ND, Weinstein BM. Arteries and veins: making a difference with zebrafish. *Nat Rev Genet* 2002, 3(9):674-82.
25. Zon LI, Peterson RT. *In vivo* drug discovery in the zebrafish. *Nat Rev Drug Discov* 2005, 4(1):35-44.

Materials

Name	Company	Catalog number	Comments
Agarose	MP Biomedicals	AGAF0500	
Borosilicate glass capillary	Harvard Apparatus	300038	
Cholera enterotoxin	Calbiochem	227035	
Confocal microscope	Leica	SP5 STED	
DMEM-high glucose media containing L- glutamine	ThermoFisher Scientific	11965092	
DMEM/F-12 media containing L-glutamine	ThermoFisher Scientific	21041025	
Dumont #5 forceps	Fine Science Tools Inc	11252-20	
Epidermal growth factor	Merck Millipore	01-107	
Fetal bovine serum	ThermoFisher Scientific	16140071	
Fluorescent stereo microscope	Leica	M165 FC	
HEK293T cell line	American Type Culture Collection	CRL-1573	
Hydrocortisone	SigmaAldrich	227035	
Horse serum	ThermoFisher Scientific	26050088	
Insulin	SigmaAldrich	I-6634	
MCF10A (M1) cell line			Kindly provided by Dr. Fred Miller (Barbara Ann Karmanos Cancer Institute, Detroit, MI, USA)
MCF10Aras (M2) cell line			
MDA-MB-231 cell line	American Type Culture Collection	CRM-HTB- 26	
Manual micromanipulator	World Precision Instruments	M3301R	
Micropipette puller	Sutter Instruments	P-97	
Wide-tip Pasteur pipette (0,5-20 ul)	Eppendorf	F276456I	

pCMV-VSVG plasmid			Kindly provided by Prof. Dr. Rob Hoebe (Leiden University Medical Center, Leiden, The Netherlands)
pMDLg-RRE (gag/pol) plasmid			
pRSV-REV plasmid			
Penicillin-Streptomycin (10,000 U/mL)	ThermoFisher Scientific	15140122	
PLV-mCherry plasmid	Addgene	36084	
Pneumatic picoPump	World Precision Instruments	SYS-PV820	
Polybrene	SigmaAldrich	107689	
Prism 4 software	GraphPad Software		
Stereo microscope	Leica	MZ16FA	
Tg (<i>fli:EGFP</i>) zebrafish strain			Kindly provided by Dr. Ewa Snaar-Jagalska (Institute of Biology, Leiden University, Leiden, The Netherlands)
Tris-base	SigmaAldrich	1181427300 1	
Tricaine (3-aminobenzoic acid)	SigmaAldrich	A-5040	
Trypsin-EDTA (0.5%)	ThermoFisher Scientific	15400054	
Petri dishes, polystyrene (60 × 15 mm)	SigmaAldrich	P5481-500EA	
Polystyrene dish with glass bottom	WillCo	GWST-5040	

Chapter 3

Cancer-associated Fibroblast-derived Gremlin 1 Promotes Breast Cancer Progression

Jiang Ren, Marcel Smid, Josephine Iaria, Daniela C. F. Salvatori,
Hans van Dam, Hong Jian Zhu, John W.M. Martens and Peter ten Dijke

Breast Cancer Research 2019, 21(1):1-19.

Abstract

Bone morphogenetic proteins (BMPs) have been reported to maintain epithelial integrity and to antagonize the transforming growth factor β (TGF β)-induced epithelial to mesenchymal transition. The expression of soluble BMPs antagonists is dysregulated in cancers and interrupts proper BMP signaling in breast cancer. In this study, expression analysis of clinical breast cancer datasets revealed that high expression of *GREM1* in breast cancer stroma is correlated with a poor prognosis regardless of the molecular subtype. The large majority of human breast cancer cell lines did not express *GREM1* *in vitro*, but breast CAFs did express *GREM1* both *in vitro* and *in vivo*. Transforming growth factor β (TGF β) secreted by breast cancer cells, and also inflammatory cytokines, stimulated *GREM1* expression in CAFs. Grem1 abrogated BMP/SMAD signaling in breast cancer cells and promoted their mesenchymal phenotype, stemness and invasion. Moreover, Grem1 production by CAFs strongly promoted the fibrogenic activation of CAFs and promoted breast cancer cell intravasation and extravasation in co-injection xenograft zebrafish models. Our results demonstrated that Grem1 is a pivotal factor in the reciprocal interplay between breast cancer cells and CAFs, which promotes cancer cell invasion. Targeting Grem1 could be beneficial in the treatment of breast cancer patients with high Grem1 expression.

Keywords: Gremlin 1, Cancer-associated fibroblasts, Breast cancer, Invasion, Zebrafish

Background

Although carcinomas, which account for approximately 90% of human cancers, are derived from epithelia, the tumor stroma exerts a powerful influence on cancer behavior, such as tumor cell growth, invasion, metastasis and evading immune responses. The tumor stroma consists of cancer-associated fibroblasts (CAFs), vascular, inflammatory and immune cells, and extracellular matrix (ECM) residing within or in the vicinity of a tumor [1]. CAFs are differentiated from quiescent fibroblasts and are associated with increased expression of myofibroblastic markers, such as vimentin, α -smooth muscle actin (α SMA), fibroblast activation protein (FAP) and fibroblast-specific protein 1 (FSP1, also known as S100A4) [2]. Tumors, including those from breast, often display desmoplasia (a fibrillar network) that is mainly caused by CAFs, in that they produce and remodel ECM components, including collagen, fibronectin, and laminin [3]. The increased stiffness and abnormal physical structure of the ECM can promote tumor cell growth and metastatic dissemination and are also critical for the generation and maintenance of the CAF phenotype [3].

Bone morphogenetic proteins (BMPs) are secreted growth factors that belong to the transforming growth factor β (TGF β) family [4]. Signaling by BMPs is initiated by binding their cognate transmembrane serine/threonine kinase receptors, which triggers the phosphorylation of intracellular SMAD1/5/8 (R-SMADs). Activated R-SMADs can form heteromeric complexes with SMAD4 that accumulate in the nucleus, where they can regulate transcriptional responses in concert with other DNA-binding transcription factors [4]. BMP signaling can elicit diverse and complex biological processes in development and disease, including cancer [5]. Many secreted BMP antagonists, which sequester BMP ligands and prevent their binding to receptors, have been identified [6]. Accumulating evidence indicates that several cancer types show dysregulated BMP signaling caused by a disequilibrium of BMPs and their antagonists. For example, BMP antagonists such as Noggin, Follistatin and Chordin like (Chrdl)1 have been linked to inducing osteoclast differentiation and promoting osteolytic bone metastases [7, 8]. The BMP antagonist Coco permits a few dormant breast cancer cells to escape the quiescent state imposed by BMP signaling and thereby establish metastases [9].

Gremlin (Grem) 1 is a highly conserved glycoprotein belonging to the Cerberus and Dan subfamily of secreted BMP antagonists [10]. It preferentially interacts with BMP2, 4, and 7 [11]. Grem1 is the major BMP antagonist that maintains proper outgrowth and patterning during

vertebral limb development [12]. *Grem1* expression is also essential for cellular proliferation and branching morphogenesis in lung development and in kidney organogenesis [12, 13]. Aberrant expression in adults is associated with orofacial clefting [14], osteoarthritis [15], spontaneous bone fractures [16], and liver [17], lung [18], and renal [19] fibrosis. *Grem1*-mediated proangiogenic and proinflammatory activity appears to be independent of its effects on BMP [20, 21].

In several cancers, *Grem1* reduces the negative effect of BMPs on stemness, proliferation, migration and invasion of cancer cells [22-24]. In hereditary mixed polyposis syndrome, *GREM1* is predominantly expressed in the epithelium of the large bowel, where it disrupts homeostatic intestinal morphogen gradients and initiates colonic tumorigenesis [25, 26]. *GREM1* was also detected at the colorectal cancer desmoplastic invasion front, highlighting a potential role in cancer metastasis [27]. High levels of *GREM1* gene expression were observed in the stromal fibroblasts of many types of cancer [23, 28, 29], suggesting that CAFs are a potential source of *Grem1*. However, the effects of *Grem1* on CAFs' function and on the interaction between (breast) cancer cells and fibroblasts are unclear.

The results presented here support the idea that *Grem1* is a clinical predictor of a poor prognosis in breast cancer. Mechanistically, *Grem1* produced by CAFs promoted fibroblast activation in an autocrine manner and stimulated breast cancer cell stemness and invasion in a paracrine manner. *Grem1* could be an attractive therapeutic target to interfere with breast cancer progression.

Methods

Data mining of genes expression in clinical patient samples and 52 breast cancer cell lines

In-house and publicly available gene expression datasets *GSE2034* [30], *GSE5327* [31], *GSE2990* [32], *GSE7390* [33] and *GSE11121* [34] were used for *GREM1* (and *transforming growth factor beta1/2/3* (*TGFB1/2/3*), *interleukin 1 beta* (*IL1B*) and *tumor necrosis factor alpha* (*TNFA*)) expression in lymph node-negative, non-(neo-) adjuvant treated primary breast cancer patients with available metastasis-free survival data, leading to a cohort of 867 patients. Using the *GSE41313* dataset [35], *GREM1*, *BMPs* and *BMP receptors* expression was assessed in silico in 52 breast cancer cell lines. Breast cancer dataset *GSE14548* [28] was investigated to explore *GREM1* expression in breast epithelium and stroma; this data set was obtained using tissues from normal breast, grade I, II, III ductal carcinoma *in situ* (DCIS) and invasive breast cancer tissue

that were micro-dissected using a laser capture technique. In addition, the colorectal cancer dataset *GSE39396* [36] was analysed for *Grem1* expression; epithelial cells, leukocytes, fibroblasts and endothelial cells were isolated by flow cytometry. Data were gathered from Gene Expression Omnibus (<http://www.ncbi.nlm.nih.gov/geo/>). Raw.cel files were processed using Frozen robust multiarray analysis (fRMA) parameters (median polish) [37] , after which batch effects were corrected using ComBat [38].

***GREM1* RNA *in situ* hybridization (ISH)**

A matched breast cancer, adjacent (adenosis or hyperplasia, and cancer free) and adjacent normal tissue microarray (TMA) was purchased from US Biomax (BR724). *GREM1* RNA *in situ* hybridization was conducted with an RNAscope *GREM1* Probe (312831-C2, Advanced Cell Diagnostics) and a 2.5 HD Detection Kit – BROWN (322300, Advanced Cell Diagnostics). All procedures were performed by strictly following the manufacturer's instructions. The ISH results were scanned by a Digital Slide Scanner (Pannoramic 250 Flash III, 3DHISTECH). The presence of intracellular brown punctate dots was considered as positive staining. The signal intensity was scored utilizing a five-point system: 0, no signals visible; 1, weak signals barely visible; 2, visible signals but not intensive; 3, moderate intensive signals; and 4, intensive signals. Scoring was evaluated independently by two observers with similar outcomes.

Cell culture

The human breast cancer cell lines MDA-MB-231 and MCF7 were purchased from ATCC. The human human telomerase reverse transcriptase (hTERT)-immortalized breast CAFs 19TT cells have been previously described [39]. Human foreskin fibroblasts were obtained from Arti A. Ramkisoensing, and have been previously published [40]. These cell lines and human embryonic kidney (HEK) 293T cells were cultured in Dulbecco's modified Eagle's medium (DMEM, 11965092, Thermo Fisher Scientific) supplemented with 10% Fetal Bovine Serum (FBS, 16000044, Thermo Fisher Scientific), 100 U/ml Penicillin/Streptomycin (Pen/Strep, 15140148, Thermo Fisher Scientific). MCF10A (M1) human breast epithelial cell line and MCF10A-derived cell line MCF10A-Ras (M2) were generously provided by Dr. Fred Miller (Barbara Ann Karmanos Cancer Institute, Detroit, USA); both cell lines were cultured in DMEM/F12 medium (11039047, Thermo Fisher Scientific) supplemented with 5% horse serum (26050088, Thermo Fisher Scientific), 20 ng/ml epidermal growth factor (EGF, 01-107, Merck Millipore), 10 mg/ml

insulin (91077C, Sigma-Aldrich), 100 ng/ml cholera enterotoxin (C8052, Sigma-Aldrich), and 0.5 mg/ml hydrocortisone (H0135, Sigma-Aldrich) and 100 U/ml Pen/Strep. Human mesenchymal (HM), W18, W21 fetal mesenchymal stem cells (MSC) were isolated and previously described [40], and cultured in Minimum Essential Medium (MEM) α (32561037, Thermo Fisher Scientific) with 10% FBS, 100 U/ml Pen/Strep. All cell lines were maintained at 37 °C, 5% CO₂, humidified incubator. All fibroblasts and MSCs were routinely cultured in 0.2% gelatin (G9136, Sigma-Aldrich) coated flasks or plates during whole experiment period to avoid possible activation caused by physical rigidity. All cell lines were monthly tested to verify absence of mycoplasma and human cell lines were authenticated by Single nucleotide polymorphism (SNP) analysis.

Plasmids, lentiviral transduction and generation of stable cell lines

The human *GREM1* complementary DNA (cDNA) was cloned from cDNA by PCR and inserted into the pCDH lentiviral vector. pLV-mCherry has been described by our laboratory before [41]. pUltra-Smurf (blue fluorescent protein AmCyan) was obtained from Addgene (48974, Addgene). Human *GREM1* lentiviral shRNAs were obtained from the Sigma MISSION shRNA library. 5 shRNAs were tested, and the two most effective shRNAs TRCN0000063833 (sh#1) and TRCN0000063837 (sh#2) were used.

Lentiviruses were produced by co-transfecting cDNA expression plasmids or shRNAs with helper plasmids pCMV-VSVG, pMDLg-RRE (gag/pol), and pRSV-REV into HEK293T cells using polyethyleneimine (PEI). Cell supernatants were harvested 48 h after transfection and stored at -80°C. MDA-MB-231 and MCF7 cells were labelled with mCherry by infecting for 24 hours (h) with mCherry-expressing lentiviral supernatants diluted 1:1 with normal culture medium in the presence of 5 ng/ml of polybrene (107689, Sigma-Aldrich). 48 h after infection, cells were placed under Neomycin (A1720, Sigma-Aldrich) selection. 19TT and W21 cells were labelled with AmCyan and subjected to positive fluorescence activated cell sorting (FACs). To obtain *GREM1* stable expressing cell lines, M1, M2, MDA-MB-231, W21 cells were infected, and selected with puromycin (P9620, Sigma-Aldrich). Puromycin was used at 1 µg/ml to maintain selection pressure. After infection with *GREM1* targeting shRNAs, 19TT cells were used within short term as 19TT cells are puromycin resistance already.

Stimulation with conditioned medium (CM) or cytokines

MDA-MB-231 and MCF7 cells were grown to 70-80% confluency, washed two times with PBS and incubated in serum-free DMEM for 24 h. Conditioned medium (CM) was then collected and passed through a 0.45 mm syringe filter (SLHP033RB, Merck Millipore).

19TT cells were treated with CM, recombinant human TGF β 3 (5 ng/ml, 8420-B3, R&D SYSTEMS and Andrew P. Hinck, University of Pittsburgh, USA), interleukin 1 β (IL1 β , 10 ng/ml, 201-LB, R&D SYSTEMS), or tumor necrosis factor α (TNF α , 10 ng/ml, 210-TA, R&D SYSTEMS) for 1, 3, 6, 12, and 24 h. Buffer-treated controls were used in parallel. For antibody-neutralization assays, TGF β 3 or CM were incubated with control (13C4) or TGF β (1D11) neutralizing antibody (generously provided by Sanofi Genzyme, Inc.) for 30 minutes (min) before treatment.

For inhibition of BMP signaling by recombinant human Grem1 (rhGrem1, 5190-GR, R&D SYSTEMS), rhGrem1 was pre-incubated with recombinant human BMP2/6 (5 ng/ml, 355-BM/507-BP, R&D SYSTEMS) for 30 min.

Quantitative real-time PCR (qRT-PCR)

Total RNAs were isolated using the NucleoSpin RNA II kit (740955, BIOKE). A total of 1 μ g of RNA was reverse transcribed using the RevertAid First Strand cDNA Synthesis Kit (K1621, ThermoFisher Scientific). Real-time PCR was conducted with GoTaq qPCR Master Mix (A6001, Promega) using CFX Connect Detection System (1855201, Bio-Rad). All target gene expression levels were normalized to *GAPDH*. The sequences of primers used to detect target human genes in qRT-PCR were listed in Table S1.

CAGA-luciferase reporter assay

HEK293T cells were seeded on a 24-well plate at approximately 5×10^4 cells per well. The next day, cells in each well were co-transfected with 0.1 μ g TGF β /SMAD-inducible (CAGA)₁₂ luciferase transcriptional reporter construct [42] and 0.08 μ g β -galactosidase expression construct using PEI. After overnight incubation, cells were starved with serum free medium. 8 h later, serum free media were removed and replaced by CM from breast cancer cell lines. 1 ng/ml TGF β 3 treatment was performed as a standard. After another overnight incubation, luciferase and β -galactosidase activities were measured. The luciferase activity was normalized based on the β -galactosidase activity.

Western blotting

Cells were lysed with RIPA buffer containing 1 × cOmplete Protease Inhibitor Cocktail (11836153001, Roche). Protein concentrations were determined using a bicinchoninic acid protein assay Kit (5000111, Bio-Rad). Proteins were separated by sodium dodecyl sulfate polyacrylamide gel electrophoresis (SDS-PAGE) and transferred onto 45 µm Polyvinylidene difluoride (PVDF) membrane (IPVH00010, Merck Millipore). Membranes were blocked using 5% non-fat dry milk in tris buffered saline with 0.1% Tween 20 (655204, Merck Millipore) and probed with the respective primary and secondary antibodies. The signal was detected using Clarity™ Western ECL Substrate (1705060, Bio-Rad) and ChemiDoc Imaging System (17001402, Bio-Rad). The antibodies used for immunoblotting were raised against the following proteins: phospho-SMAD1/5/8 (pSMAD1/5/8, home-made) [43], αSMA (A2547, Sigma-Aldrich), Fibronectin (F7387, Sigma-Aldrich), FAP (WH0002191M1, Sigma-Aldrich), Collagen I (ab34710, Abcam), Vimentin (5741, Cell signaling), Glyceraldehyde 3-phosphate dehydrogenase (GAPDH, MAB374, Merck Millipore). GAPDH was used as protein loading control.

Flow cytometry

Adherent cells were trypsinized and washed twice with 1% bovine serum albumin (BSA) (A2058, Sigma-Aldrich) in phosphate buffered saline (PBS). The cells were then incubated with fluorescein isothiocyanate (FITC)-conjugated anti-human CD44 (347943, BD Biosciences), R-Phycoerythrin (PE)-conjugated anti-human CD24 (555428, BD Biosciences) antibodies (1:400 dilution) for 30 min at 37 °C in the dark. Fluorescein isothiocyanate (FITC)/PE-conjugated IgG isotypes (560952/560951, BD Biosciences) were used as control. Cells were washed twice with 1% BSA in PBS and resuspended in 500 µl of PBS prior to analysis on a FACS Canto flow cytometer (BD Biosciences).

Phalloidin staining

Cells were fixed in 4% formalin, permeabilized with 0.1% Triton X-100, and blocked with 5% BSA (A2058, Sigma-Aldrich) in PBS for 30 min. Then cells were stained with Alexa Fluor 488 Phalloidin (A12379, Thermo Fisher Scientific) to visualize filamentous (F)-actin. The nuclei were stained with 4',6-diamidino-2-phenylindole (DAPI, 62248, Thermo Fisher Scientific). Images were taken by confocal microscopy (SP8, Leica Microsystems).

Mammosphere formation assays

Single-cell suspensions of M1 cells were prepared in DMEM/F12 medium containing $1 \times$ B27 (17504044, Thermo Fisher Scientific), 20 ng/ml epidermal growth factor (01-107, Merck Millipore), 20 ng/ml fibroblast growth factors (PHG6015, Thermo Fisher Scientific), and 4 mg/ml heparin (H3149, Sigma-Aldrich). Then, 2000 cells/well were seeded into ultralow attachment 24-well plate (CLS3473-24EA, Corning). After 10 days of standard incubation, the numbers of spheres (> 75 μ m diameter) were counted using an inverted microscope (DMI8, Leica Microsystems). For secondary sphere formation, primary spheres were dissociated with Accutase (A1110501, Thermo Fisher Scientific), followed by 25-gauge needles (Z192406, BD Biosciences) mechanically. Next, 2000 cells/well were replated. Sphere-forming efficiency was calculated as the number of spheres (average diameter = 100 μ m) formed divided by the number of single cells originally seeded.

Collagen gel contraction assays

The contraction assay [44] was performed to evaluate the contractility of 19TT cells with *GREM1* knockdown or *GREM1*-overexpressing W21 cells. Collagen gels were prepared by mixing fibroblast cell suspensions in serum-free medium and type I collagen (Corning, 354249) solution. The final cell density was 2.0×10^5 cells/ml with 1 mg/ml collagen. A 0.5 ml mixture was cast into each well of a 24-well plate and allowed to polymerize for 30 min at 37 °C. Following gelatinization, another 0.5 ml of serum-free DMEM was added to the gel. Changes of gels were recorded by using a ChemiDoc Imaging System (17001402, Bio-Rad) at a fixed distance above the gels at 24, 48, and 72 h. The surface area of the gels was quantified by ImageJ software. The percentage of contraction was calculated using the formula $100\% \times (\text{well surface area} - \text{gel surface area}) / \text{well surface area}$.

Three-dimensional (3D) spheroid invasion assay

mCherry-labeled MDA-MB-231 or MCF7 cells and co-culture (1:1 mixture) with W21 or 19TT groups were prepared at 1000 cells/ml in complete DMEM. Drops of the single cell suspension (30 μ l) were placed onto the lids of 10 cm dishes, which were inverted over dishes containing 10 ml PBS. Hanging drop cultures were incubated 7 days allowing sufficient sedimentation and formation of one spheroid per drop. Images were taken by an inverted fluorescent microscope (DMI8, Leica Microsystems).

The 3D spheroid invasion assay was performed according to our previous study [45] with slight modifications. Single spheroids were embedded in the center of each well of a flat-bottom 96-well plate pre-coated with 50 μ l of collagen mixture. Type I collagen (354249, Corning) was neutralized according to the manufacturer's protocol. The collagen mixture was prepared by diluting neutralized collagen with serum-free medium to a final concentration of 2 mg/ml. Eight spheroids generated by each experimental setting were randomly chosen for embedding. After spheroid embedding, another 50 μ l of collagen mixture was overlaid onto the collagen matrix in each well. The plate was incubated for 30 min at 37 °C to solidify the gels. Thereafter, 50 μ l of serum-free medium was added to each well to prevent the surface from dehydrating. Plates were placed under standard cell culture conditions. Images were taken at days 0, 2 and 4 after embedding by using inverted fluorescence microscopy (DMI8, Leica Microsystems). Invasion was quantified by measuring the area occupied by cells using ImageJ software.

Embryonic zebrafish intravasation and extravasation assay

Zebrafish xenograft breast cancer cell experiments were performed by injecting fluorescently labeled breast cancer cells into embryos at 48 h post-fertilization as described before [41]. Briefly, approximately 400 mCherry-labeled MDA-MB-231 cells were injected into the perivitelline space or the duct of Curvier (DoC) of transgenic zebrafish embryos (*fli : enhanced green fluorescent protein (EGFP)*), whose vasculature is marked in green. For co-injection, mCherry-labeled MDA-MB-231 cells and AmCyan-labeled W21 or 19TT cells were mixed at a ratio of 1:1. Then, approximately 400 mixed cells were injected into the zebrafish perivitelline space. Zebrafish embryos were maintained at 34 °C after injection, a compromise for both the fish and the human cell lines. Three days post-injection (dpi) into the perivitelline space, the MDA-MB-231 cells that intravasated from the cell mass toward the embryonic fish body within the head and tail regions were imaged and counted under a confocal microscope (SP5 STED, Leica Microsystems). At 5 dpi into the DoC, the number of MDA-MB-231 cells that extravasated individually from circulation into the collagen fibers of the tail fin or the number of clusters formed by M2 cells collectively was analyzed. At least 200 zebrafish embryos were injected for each condition. After verification by microscopy, only correctly injected and viable zebrafish were used for experimental analysis. All experiments were repeated at least two times independently, and representative experiments are shown.

Statistical analysis

Statistical analyses were performed using GraphPad Prism version 7.0. Numerical data from triplicates are presented as the mean \pm standard deviation (s.d.), except for the analysis of zebrafish experiments, where a representative result is expressed as the mean \pm standard error (s.e.m). Experiments were analyzed with an unpaired Student's t-test. $P < 0.05$ was considered statistically significant.

Results

High *GREM1* expression in breast tumors is associated with a poor prognosis

BMPs have been reported to maintain epithelial integrity and to antagonize TGF β -induced epithelial to mesenchymal transition (EMT), an important process for cancer cell invasion and metastasis [5]. Many soluble BMP antagonists have been described to be misexpressed and to interrupt proper BMP signaling in breast cancer [7-9]. We examined the prognostic role of soluble BMP antagonists in primary breast cancer using an in-house and publicly available cohort of 867 untreated lymph node-negative breast cancer patients (see the 'Methods' section for data sets that were used). The median follow-up time of metastasis-free survival (MFS) was 94.1 months (range from 1 to 299.4 months). High expression of *GREM1* was found to be associated with a poor prognosis among all BMP antagonists that were examined. As shown in Figure 1A, according to the *GREM1* mRNA expression level, the subjects were divided evenly into 3 quantiles: low, middle and high. *GREM1* expression was inversely associated with MFS in this cohort, *i.e.*, higher expression, poorer outcome: (low vs high: HR (hazard ratio) = 1.35, 95% confidence interval (CI) 1.15-1.57, log rank $P = 0.00018$; low vs middle: HR = 1.41, CI 1.02-1.96, $P = 0.036$; middle vs high: HR = 1.31, CI 0.98-1.74, $P=0.065$). A similar association was observed when dividing subjects into 2 quantiles (Figure S1A). Furthermore, high expression of *GREM1* correlated with a poor prognosis in all the breast cancer molecular subtypes examined: human EGF receptor (HER)2⁺, triple⁻, estrogen receptor (ER)⁺, and ER⁻ (Figures S1B-E). Therefore, *GREM1* is a poor prognostic marker of metastasis-free survival in breast cancer regardless of the subtype.

GREM1 is expressed in cancer-associated fibroblasts.

When we examined *GREM1* expression in 52 human breast cancer cell lines by mining previously published datasets (see the 'Methods' section), we found that only 3 breast cancer cell

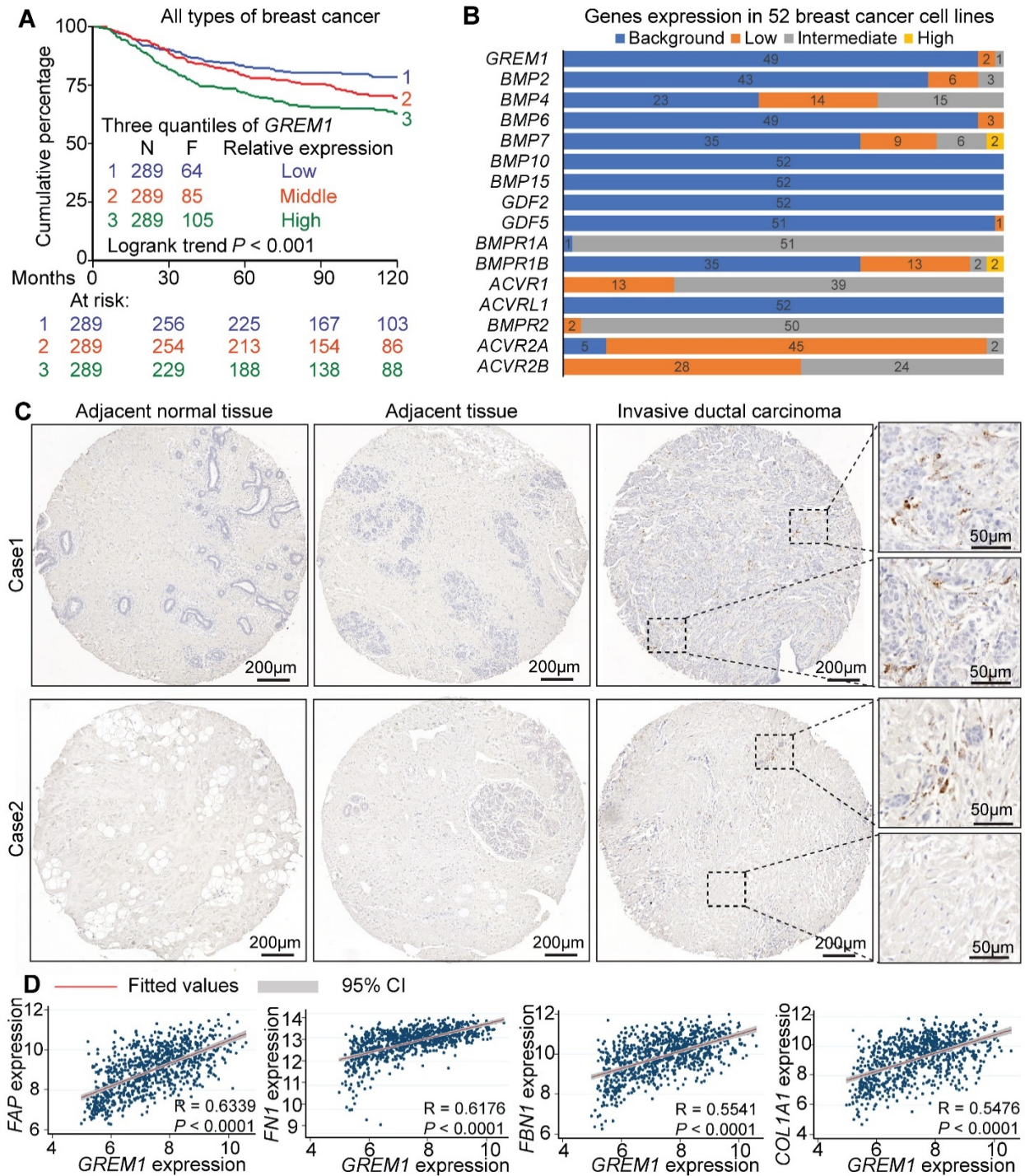


Figure 1. Stromal expression of *GREM1* predicts poor clinical outcome in breast cancer. **A**, Kaplan-Meier survival curve in untreated lymph node-negative breast cancer patients. Based on *GREM1* mRNA expression (low, middle and high), the subjects (N=867) were divided into 3 quantiles. The endpoint is distant metastasis-free survival. **B**, *GREM1*, *BMPs* and *BMP receptors* mRNA expression level in 52 breast cancer cell lines. The expression levels were categorized to 4 group: Background, Low,

Intermediated, High. **C**, Human *GREM1* *in situ* hybridization shows restricted *GREM1* expression in fibroblast-like stromal cells surrounded by malignant breast epithelial cells. **D**, Scatterplot showing positive correlation between the expression of *GREM1* and stromal genes / desmoplastic markers *FAP*, *FN1*, *FBN1*, and *COL1A1* in the clinical datasets. Pearson's coefficient tests were performed to assess statistical significance.

lines express low (MDA-MB-436 and HCC38) or intermediate (SUM149PT) levels of *GREM1*; all other 49 cell lines had no detectable expression (Figure 1B). To explore the source of *GREM1* expression, we stained *GREM1* RNA by using *in situ* hybridization (ISH) in a breast cancer TMA, which comprised 24 matched cases of invasive ductal carcinoma, adjacent tissue and adjacent normal tissue. As shown in Table 1 and Figure 1C, we identified variable amounts of *GREM1* expressed in fibroblast-like cells, *i.e.*, CAFs, whereas there were no detectable levels of *GREM1* in cancer adjacent normal tissues or adjacent cancer free breast tissues. None of the epithelial cells of breast cancers included in this study showed *GREM1*-positive expression. The *GREM1* expression in breast cancer tissue samples is thus mainly caused by the presence of tumor stroma. Moreover, using the in house and publicly available primary breast cancer data sets we observed a significant positive correlation between *GREM1* and markers for CAFs and tumor matrix stiffness/desmoplasia, such as *FAP*, *Fibronectin (FN)1*, *Fibrillin (FBN)1*, *Collagen (COL)1A1*, *Thrombospondin (THBS)2*, and α -*Actin (ACTA)2* (Figure 1D, Figure S1F). Taken together, these results suggest that CAF-derived Grem1 might play a pivotal role in promoting breast tumor progression.

Table 1. RNA ISH scores for *GREM1* in matched breast cancer tissue microassay

RNA ISH score	Adjacent normal tissue (%)	Adjacent tissue (%)	Invasive ductal carcinoma (%)
0	24 (100)	24 (100)	4 (16.67)
1	0 (0)	0 (0)	6 (25.00)
2	0 (0)	0 (0)	5 (20.83)
3	0 (0)	0 (0)	5 (20.83)
4	0 (0)	0 (0)	4 (16.67)

TGF β secreted by cancer cells and inflammatory cytokines induces *GREM1* expression

Analysis of *GREM1* in tissue sections revealed that only the CAFs in close proximity to the cancer cells (tumor-stromal interface) showed high *GREM1* RNA expression (Figure 1C, bottom

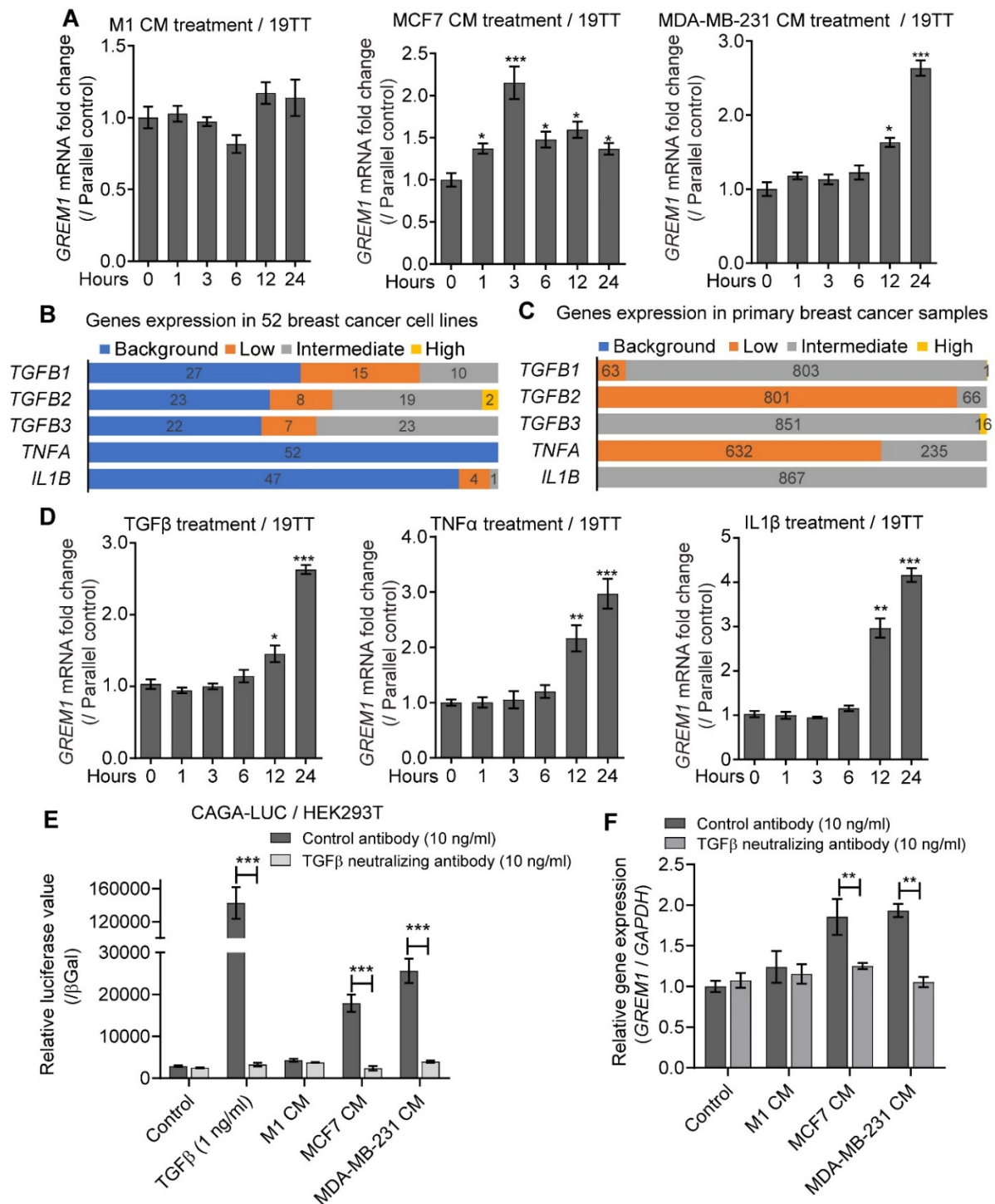


Figure 2. TGFβ secreted by breast cancer cells and inflammatory cytokines induce *GREM1* expression in CAFs. **A**, *GREM1* expression in 19TT CAFs after treatment with conditioned medium (CM) from breast cell lines (M1, MDA-MB-21 or MCF7). Expression was normalized to the parallel time control of normal medium treatment. The results are expressed as the mean \pm s.d, $n = 3$. Student's t test, $*P < 0.05$, $***P \leq 0.001$. **B**, *TGFB1*, *TGFB2*, *TGFB3*, *TNFA*, *IL1B* mRNA levels in 52 breast cancer cell

lines. The expression levels were categorized to 4 groups: Background, Low, Intermediated, High. **C**, *TGFB1/2/3*, *TNFA*, *IL1B* expression in primary breast cancer samples. The expression level was categorized to 4 groups: Background, Low, Intermediated, High. **D**, TGFβ3 (5 ng/ml), or TNFα (10 ng/ml), or IL1β (10 ng/ml) induce *GREM1* expression in 19TT cancer-associated fibroblasts (CAFs). Expression was normalized to the parallel time control of buffer treatment. The results are expressed as the mean ± s.d., n = 3. Student's t test, **P* < 0.05, ***P* ≤ 0.01, ****P* ≤ 0.001. **E**, Measurements of TGFβ activity in CM from breast cancer cell lines using a CAGA luciferase (LUC) reporter assay in HEK293T cells as read out. TGFβ neutralizing antibody (10 ng/ml) was added to demonstrate that luciferase activity in CM is due to TGFβ activation and not activins or nodal. Recombinant TGFβ was added to control for functionality of the assay. The value are normalized to β-galactosidase(βGal) activity. The results are expressed as the mean ± s.d, n = 3. Student's t test, ****P* ≤ 0.001. **F**, The induction of *GREM1* expression in 19TT CAFs by CM from MCF7 and MDA-MB-21 is blocked by TGFβ neutralizing antibody. The results are expressed as the mean ± s.d, n = 3. Student's t test, ***P* ≤ 0.01.

factors secreted by cancer or inflammatory cells. We first collected CM from M1 immortalized normal breast cells, and breast cancer cell lines MCF7 and MDA-MB-231. Treatment of 19TT CAFs (Figure 2A) or W21 MSCs (Figure S2A) with MDA-MB-231 or MCF7 cells CM resulted in a significant increase in *GREM1* mRNA levels. There was no effect of M1 CM on *GREM1* expression. To explore the factors that are responsible for inducing *GREM1* expression in CAFs, we analyzed by data mining the expression of *TGFB1/2/3* and inflammatory cytokines in breast cancer cell lines as well as in breast cancer tissues. We found that *TGFB1/2/3* are highly expressed in both breast cancer cell lines and tissues. Inflammatory cytokines, including *IL1B* and *TNFA*, were expressed in breast cancer tissues but only at very low levels in breast cancer cell lines (Figure 2B and C). *IL1B* and *TNFA* expression in breast cancer tissues is thus likely caused by the stromal cells present in breast cancer tissue samples. Challenging 19TT CAFs (Figure 2D) or W21 MSCs (Figure S2B) with TGFβ3, TNFα, and IL1β promoted *GREM1* mRNA expression. Next we analyzed whether TGFβ is secreted by cancer cells. MDA-MB-231 and MCF7, but not M1, were found to express active TGFβ (Figure 2E). Importantly, the *GREM1* expression-inducing activity of MDA-MB-231 or MCF7 cells could be blocked by a TGFβ neutralizing antibody (Figure 2F). Taken together, TGFβ secreted by cancer cells is the main determinant for inducing *GREM1* expression by CAFs. Within the tumor-stroma niche, inflammatory cells secreting cytokines may also contribute to *GREM1* expression by CAFs.

Grem1 increases mammosphere formation

BMPs are reported to be inhibitors of cell stemness, suggesting that secreted Grem1 might oppositely affect stem traits [9, 22, 46]. First, we confirmed that *BMPs* and *BMP receptors* are indeed expressed in breast cancer cell lines (Figure 1B, Figure S3A and B). Then, mammosphere

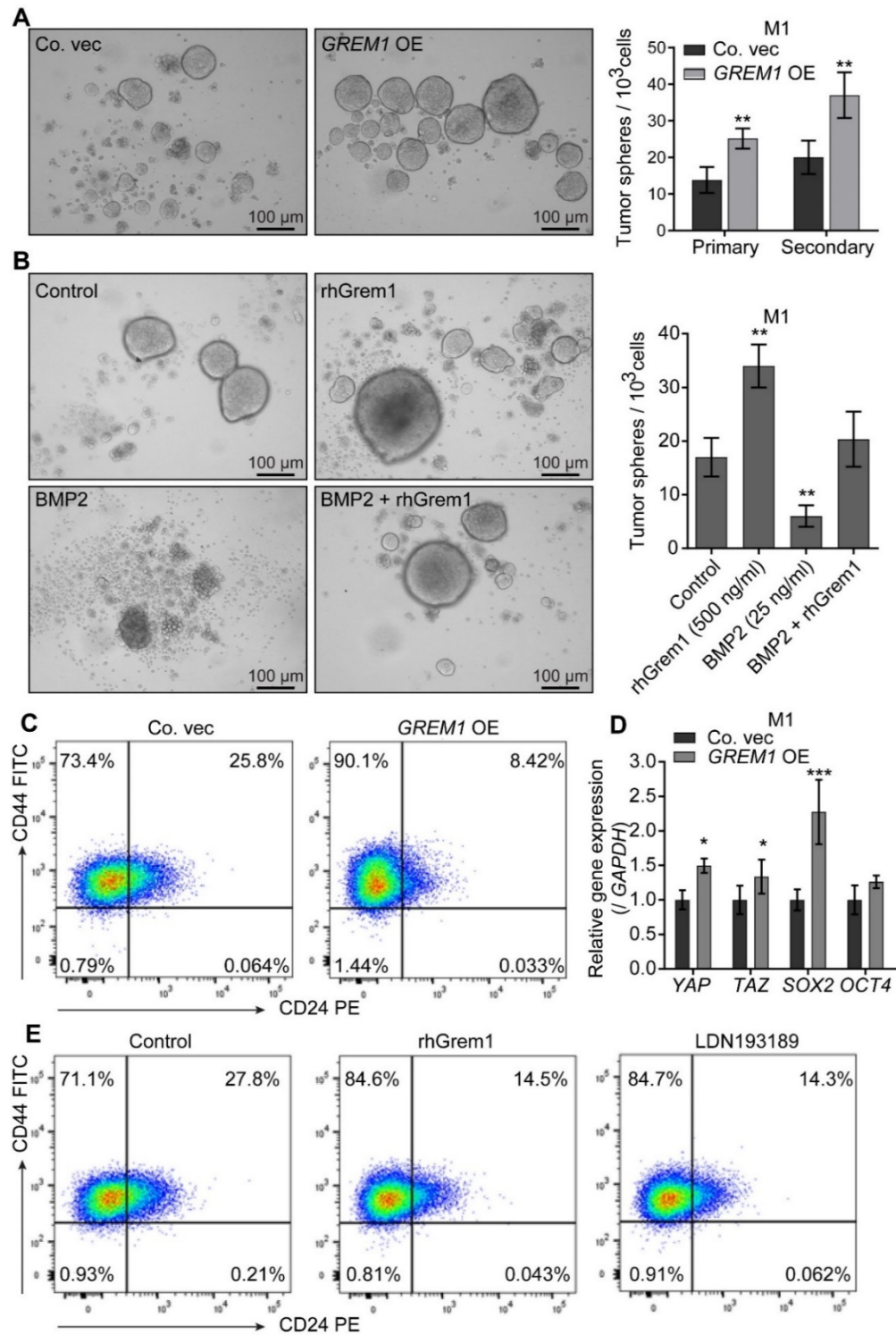


Figure 3. Greml1 maintains stemness in M1 cells. **A**, *GREM1* overexpression (OE) induces more mammosphere formation in M1 cells. Left, representative images of mammospheres at 7 days. Right, number of spheres formed per 1000 cells plated. The primary spheres were disintegrated and replated further. Secondary spheres formed were counted. The results are expressed as the mean \pm s.d., $n = 3$. Student's *t* test, $**P \leq 0.01$. **B**, Pro-mammosphere formation ability of recombinant human Greml1 (rhGreml1) protein (500 ng/ml) can be neutralized by BMP2 (50 ng/ml). Left, representative images of spheres at 7 days; Right, number of spheres formed per 1000 cells plated. The results are expressed as the mean \pm s.d., $n = 3$. Student's *t* test, $**P \leq 0.01$. **C**, Flow cytometry analysis shows that *GREM1* OE in M1 cells increases the stem population (CD44^{+/high} CD24^{-/low}). **D**, *GREM1* OE in M1 cells upregulates stem cell transcription factors. *GAPDH* was used as an internal control. The results are expressed as the mean \pm s.d., $n = 3$. Student's *t* test, $*P < 0.05$, $***P \leq 0.001$. **E**, Flow cytometry analysis showing that 2 days of treatment with rhGreml1 (500 ng/ml) or the BMP type I receptor inhibitor LDN193198 (120 nM) also leads to an increase in the CD44^{+/high} CD24^{-/low} population.

formation assay was performed to assess the effect of Greml1 on mammary stem cell activity *in vitro*. *GREM1*-overexpressing M1 cells exhibited two-fold more sphere formation compared to control cells in each of two subsequent passages (Figure 3A). The administration of exogenous rhGreml1 showed a similar effect on mammosphere formation of M1 cells, whereas the administration of exogenous BMP2 mitigated sphere formation ability. The latter could be reversed by the concurrent administration of rhGreml1 (Figure 3B). The surface expression of CD44^{+/high} CD24^{-/low} cells has been considered a stem population marker of breast cancers or cell lines [46]. Flow cytometry analysis demonstrated a significant increase in the CD44^{+/high} CD24^{-/low} cell subpopulation in *GREM1*-overexpressing M1 cells compared to the control (Figure 3C). qRT-PCR revealed that *GREM1* OE (Figure 3D) or rhGreml1 (Figure S3C) increased the expression of transcriptional regulators *YAP*, *TAZ*, *SOX2*, and *OCT4*, which have been implicated in maintaining breast cancer stemness. Moreover, M1 cells treated with rhGreml1 or the BMP type I receptor inhibitor LDN193189 [47] also displayed more CD44^{+/high} CD24^{-/low} cells than non-treated control cells (Figure 3E). These results suggest that Greml1 enhances the mammosphere formation of M1 cells by repressing BMP signaling.

Greml1 promotes breast cancer cell invasion

To further characterize the role of Greml1 in breast cancer, we stably expressed Greml1 in the breast cancer cell lines M2 and MDA-MB-231 with a lentiviral vector. In a way these transfected

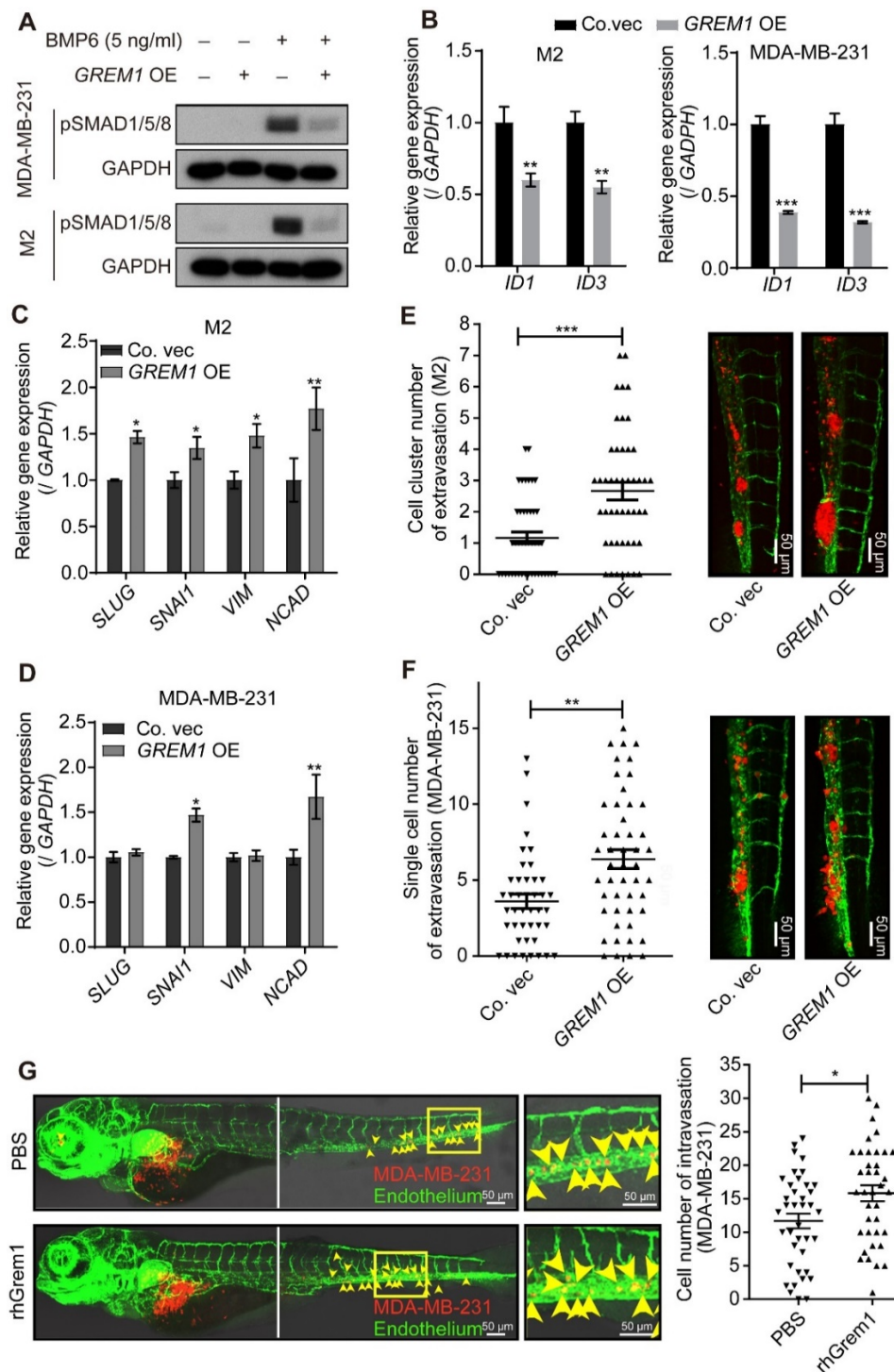


Figure 4. Ectopic expression of *GREM1* promotes cancer cell invasion in a zebrafish model. A, B, *GREM1* overexpression (OE) inhibits BMP-induced SMAD1/5/8 phosphorylation (pSMAD1/5/8, A) and the BMP target genes *ID1* and *ID3* (B) in MDA-MB-231 and M2 cell lines. *GAPDH* was used as an internal control. The results are expressed as the mean \pm s.d., $n = 3$. Student's *t* test, $**P \leq 0.01$. C, D, *GREM1* OE upregulates the expression of EMT transcription factors and markers in M2 (C) and MDA-

MB-231 (**D**) cells. *GAPDH* was used as an internal control. The results are expressed as the mean \pm s.d., $n = 3$. Student's *t* test, $**P \leq 0.01$. **E, F**, *GREM1* OE induces more clusters formation in M2 cells (**E**) and promotes the invasion of MDA-MB-231 cells (**F**) in zebrafish. Left, quantification of the number of extravasated cells/clusters at 5 days post injection (dpi). Right, representative images; Green, vasculature of zebrafish; Red, mCherry-labeled cells. The results are expressed as the mean \pm s.e.m., $n=2$. Student's *t* test, $**P \leq 0.01$, $***P \leq 0.001$. **G**, Perivitelline space injection of MDA-MB-231 cells supplemented with rhGrem1 (1 μ g/ml) increases cell intravasation in zebrafish. Left, representative images. Green, vasculature of zebrafish; Red, mCherry-labeled cells. Right, quantification of the number of intravasated cells in each embryonic body at 3 days post injection (dpi). The results are expressed as the mean \pm s.e.m., $n=2$. Student's *t* test, $*P < 0.05$.

cell lines are somewhat reminiscent to the few breast cancer cell lines that express *GREM1*. In these *GREM1*-overexpressing cell lines, BMP-induced SMAD1/5/8 phosphorylation (Figure 4A) and expression of BMP target genes ID1 and 3 (Figure 4B) were clearly inhibited. Notably, the mRNA levels of the mesenchymal markers *SLUG*, *SNAIL*, *VIM*, and *NCAD* were increased by ectopic *GREM1* expression (Figure 4C and D) or exogenous rhGrem1 treatment (Figure S4B), suggesting that Grem1 induces a slightly more mesenchymal phenotype in these breast cancer cells. To test whether exposure to Grem1 also results in more invasive behavior, we introduced these cells into the blood circulation of embryonic zebrafish via DoC injection and examined extravasation 5 days post injection (dpi) in the avascular tail fin area. Compared to the vector control, the *GREM1* overexpression group showed a higher number of extravasated M2 cell clusters (Figure 4E) or MDA-MB-231 single cells (Figure 4F). The BMP/SMAD signaling could be inhibited by exogenous administration of rhGrem1 (Figure S4B). Next, we injected MDA-MB-231 cells suspended in PBS supplemented with or without rhGrem1 into the perivitelline space of embryonic zebrafish and examined the level of cells in circulation at 3 dpi. Exogenous rhGrem1 increased cellular intravasation significantly, as more cells were found in the head and tail regions of zebrafish embryos (Figure 4G).

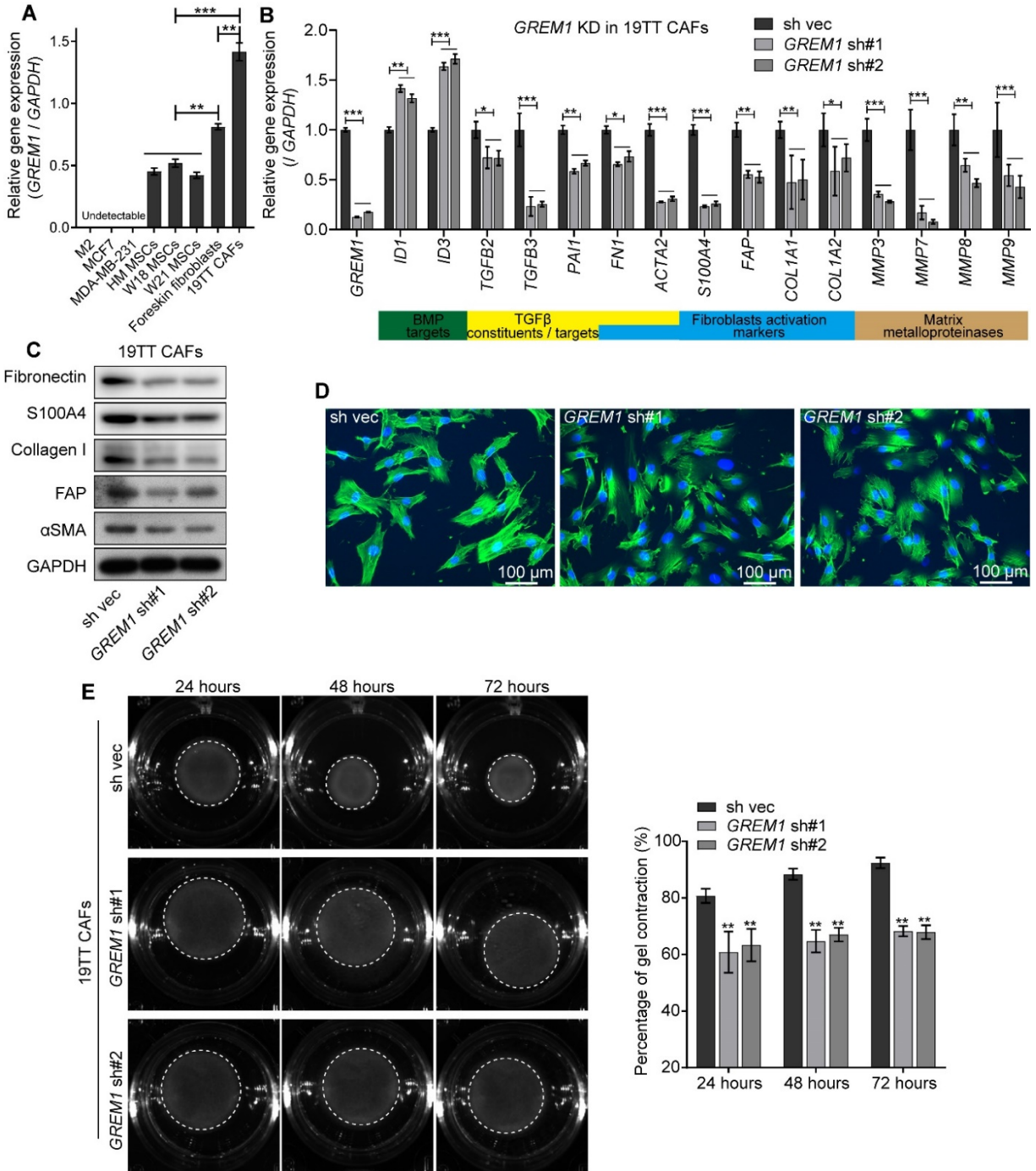
Grem1 promotes fibroblast activation

Grem1 is associated with fibrosis [17-19]. To explore the role of Grem1 in fibroblast activation, we first compared *GREM1* mRNA expression levels in foreskin fibroblasts, 19TT breast cancer CAFs, and HM, W18 and W21 human mesenchymal stem cells (MSCs). M2, MCF7 and MDA-MB-231 cancer cells served as negative control. MSCs, which are considered fibroblast

precursors and can differentiate into fibroblasts [2], showed the lowest expression of *GREM1*; *GREM1* expression in the foreskin fibroblasts, which represent normal fibroblasts, was significantly higher than that in MSCs, and 19TT CAFs showed the highest levels (Figure 5A), indicating that *GREM1* expression increases during different stages of fibroblast activation. We next knocked down *GREM1* in 19TT CAFs. As shown in Figure 5B, two shRNAs-mediated *GREM1* knockdown increased the mRNA expression of both *ID1* and *ID3* and decreased the expression of TGF β signaling components and their target genes (*Plasminogen activator inhibitor (PAI-1)*), fibroblast activation markers and *matrix metalloproteinases (MMPs)*. *GREM1* knockdown in 19TT CAFs also led to decreased protein levels of FN1, S100A4, Collagen I, FAP, and α SMA (Figure 5C). This result suggests that *Grem1* is a pivotal factor in fibroblast activation.

To examine whether *Grem1* affects cytoskeletal changes, we stained the cells with fluorescein-conjugated phalloidin to visualize filamentous (F)-actin. Indeed, *GREM1* knockdown in 19TT CAFs resulted in less prominent stress fibers and less organized bundles in the cytoplasm (Figure 5D). More significantly, the ability of 19TT CAFs to contract collagen gels (a 3D model widely used for evaluating fibroblast-mediated matrix remodeling capacity) decreased significantly with *GREM1* knockdown (Figure 5E). Moreover, *GREM1* overexpression in W21 MSCs (Figure S5A) induced intensive myofibroblast-like characteristics (Figures S5B-E). Consistent with this result, W21 MSCs treated with rh*Grem1* or the selective BMP receptor kinase inhibitor LDN193189 exhibited an upregulation of genes which were inhibited by *GREM1* knockdown in 19TT CAFs (Figure S2F). Overall, these observations imply that *Grem1* is closely associated with the fibrogenic phenotype of breast CAFs.

Figure 5. *GREM1* knockdown in 19TT breast cancer-associated fibroblasts (CAFs) attenuates fibrotic characteristics. **A**, qRT-PCR comparison of relative *GREM1* expression in M2, MCF7, MDA-MB-231, HM, W18, and W21 fetal mesenchymal stem cells (MSCs), foreskin fibroblasts and 19TT CAFs. *GAPDH* was used as an internal control. The results are expressed as the mean \pm s.d., n=3. Student's t test, $**P \leq 0.01$, $***P \leq 0.001$. **B**, qRT-PCR analysis of selected genes, BMP targets, TGF β pathway constituents/targets, fibroblast activation markers, and matrix metalloproteinases in 19TT CAFs with/without shRNA-mediated *GREM1* knockdown. *GAPDH* was used as an internal control. The results are expressed as the mean \pm s.d., n = 3. Student's t test, $*P < 0.05$, $**P \leq 0.01$, $***P \leq 0.001$. **C**, Western blot analysis to detect changes in indicated proteins after *GREM1* knockdown in 19TT CAFs. **D**,



19TT CAFs with/without *GREM1* knockdown were stained with fluorescein-phalloidin (green) to visualize F-actin. DAPI was used for nuclear staining (blue). **E**, Collagen gel contraction assay. 19TT CAFs with/without *GREM1* knockdown were embedded in collagen gels. After 24, 48, and 72 h, the area of each gel (white dash circle) was imaged and quantified. Left, Representative images of contracted gels. Right, percentage of gel contraction. Quantification is shown in the Methods. The results are expressed as the mean \pm s.d., $n = 3$. Student's *t* test, $**P \leq 0.01$.

Fibroblast-derived Grem1 promotes breast cancer cell invasion in a 3D spheroid model

Previous studies have indicated that CAFs are propellants of cancer cell invasion [1, 2]. Prompted by the profibrotic role of Grem1, we further explored the roles of Grem1 in fibroblast-mediated cancer cell invasion using a 3D spheroid model. As illustrated in Figure S6A, spheroids

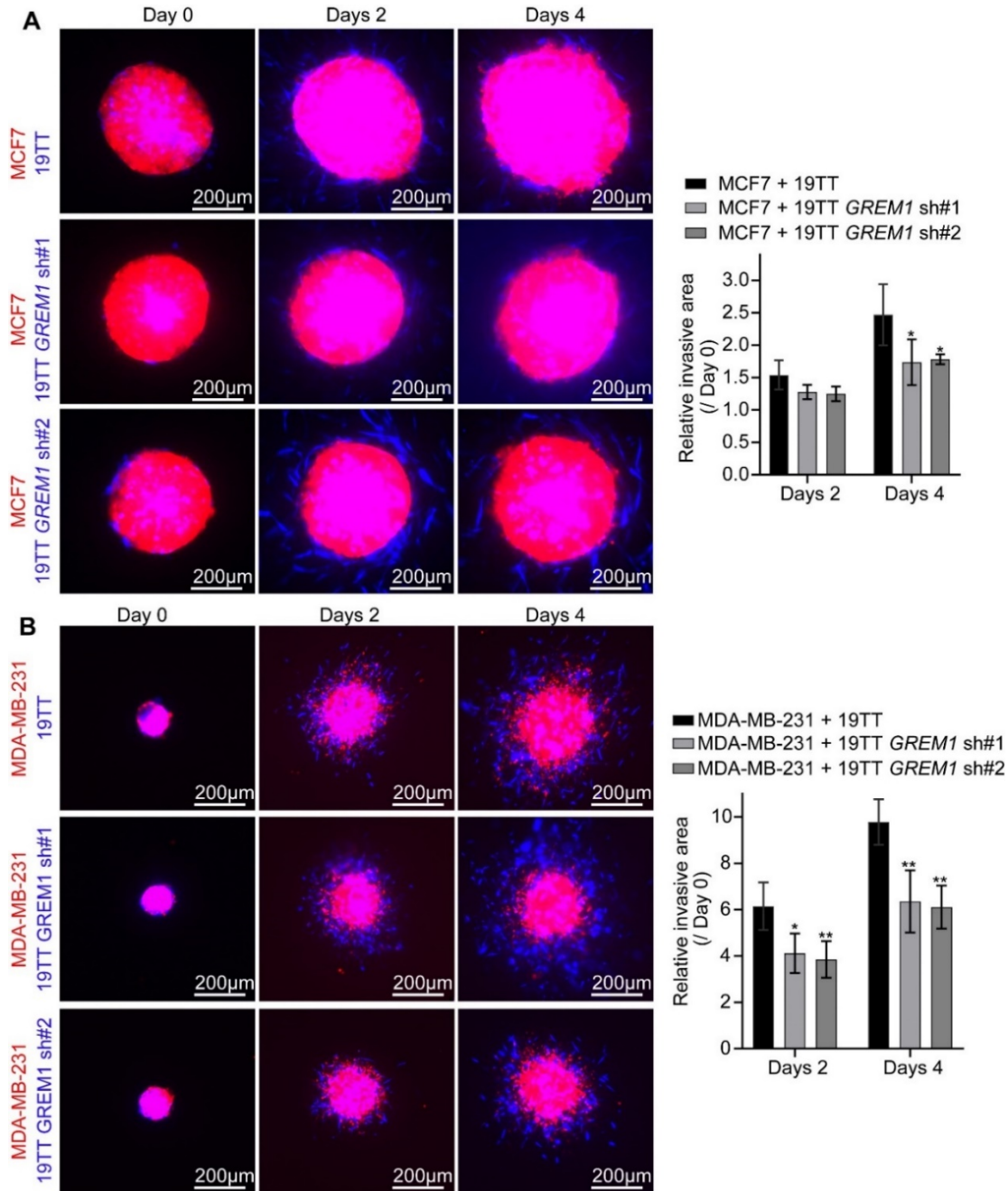


Figure 6. *GREM1* knockdown in 19TT breast cancer-associated fibroblasts (CAFs) impairs breast cancer cells invasion in a 3D spheroid invasion model. A, B, Collagen invasion assay of co-culture spheroids. Eight spheroids per indicated group were embedded into collagen. Left, representative images

of 3D spheroid invasion at days 0, 2, and 4. Red, MCF7 (A) or MDA-MB-231 (B) cells; Blue, 19TT cells with/without *GREM1* knockdown. Right, relative invasion area was quantified as the area difference at days 2 and 4 relative to that at day 0. The results are expressed as the mean \pm s.d., $n = 8$. Student's *t* test, * $P < 0.05$, ** $P \leq 0.01$.

were produced from hanging drop co-cultures of mCherry-labeled breast cancer cells, MCF7 or MDA-MB-231 cells, and AmCyan-labeled 19TT CAFs. CAFs with or without *GREM1* knockdown were mixed with these breast cancer cells at a 1:1 ratio. the various resulting spheroids were embedded in collagen gel. As shown in Figure S6B, the monocultured MCF7 spheroid showed a collective cells invasion phenotype in collagen, and in the presence of 19TT cells, the increased invasion of CAFs was measured at days 4. However, upon *GREM1* depletion in the 19TT CAFs, the coculture spheroids showed strongly reduced invasion (Figure 6A). Likewise, *GREM1* knockdown in the CAFs reduced the invasion of MDA-MB-231 cells in MDA-MB-231 and 19TT co-culture spheroids at days 2 and 4 (Figure 6B).

Fibroblast-derived Grem1 promotes breast cancer cell intravasation

Next, we examined the role of fibroblast-expressed Grem1 in breast cancer cell invasion *in vivo*. We injected mCherry-labeled MDA-MB-231 cells into the perivitelline space of zebrafish in the absence or presence of either AmCyan-labeled W21 MSCs, foreskin fibroblasts, or 19TT CAFs. As depicted in Figure 7A, intravasation of the MDA-MB-231 cells was significantly increased when co-implanted with W21, validating a previous study in which MSCs promoted cancer metastasis [48]. Importantly, this intravasation was much more enhanced by the foreskin fibroblasts and even more so by the 19TT CAFs, suggesting a correlation with their *GREM1* expression level. Indeed, the ectopic expression of *GREM1* in W21 cells resulted in enhanced MDA-MB-231 cells intravasation upon co-injection (Figure S7). Consistent with this result, *GREM1* knockdown mitigated the promotion role of 19TT CAFs on MDA-MB-231 cells intravasation (Figure 7B).

Discussion

Our work has uncovered a strong association between high *GREM1* expression in breast tumor biopsies and a poor prognosis. We provide mechanistic insights into GREM1's key role in facilitating breast cancer progression using *in vitro* and *in vivo* studies. Grem1 is highly expressed by CAFs at the invasion front; its expression can be promoted by factors, such as

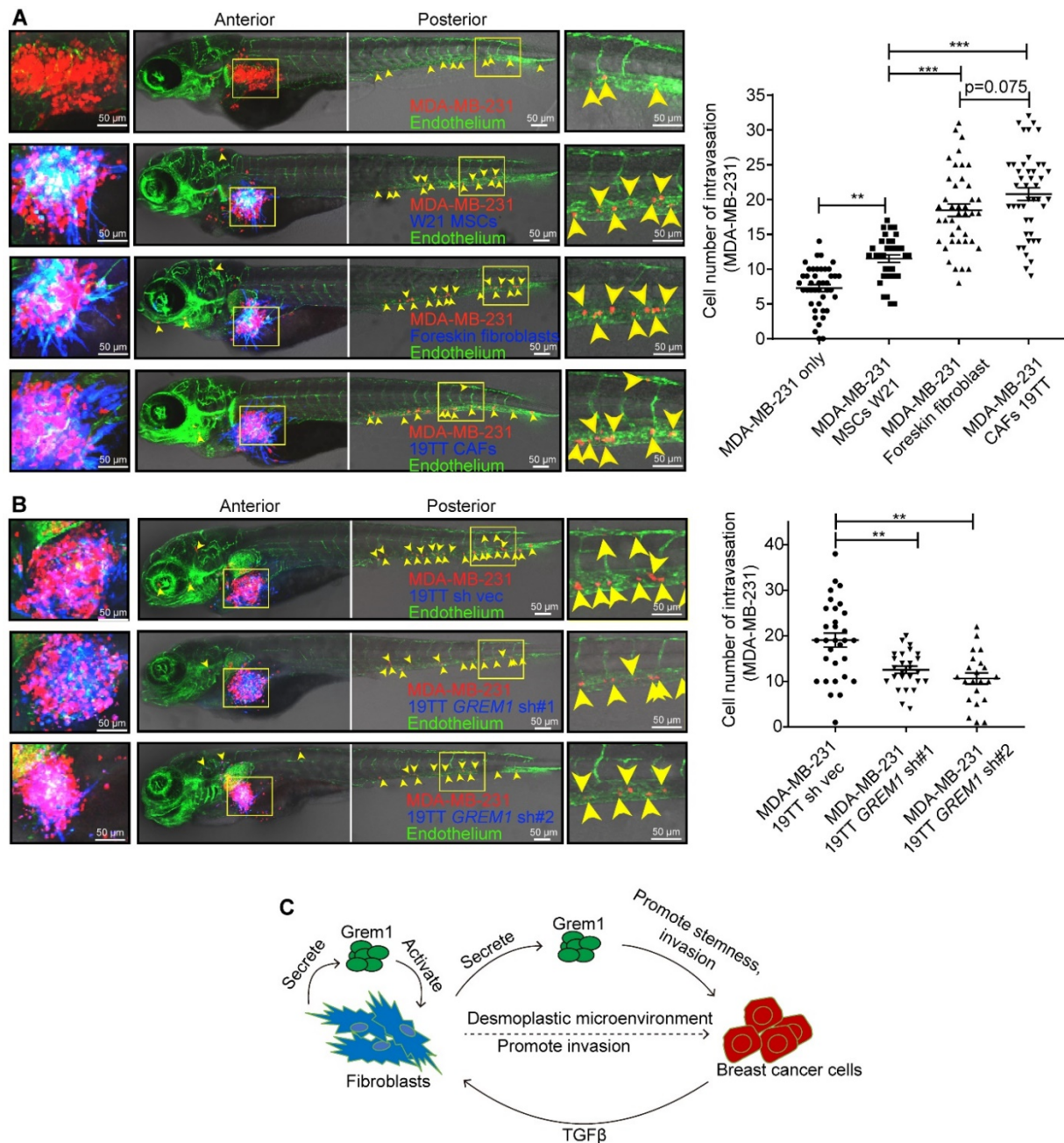


Figure 7. *GREM1* knockdown attenuates the ability of 19TT breast cancer-associated fibroblasts (CAFs) to promote breast cancer cell intravasation in a zebrafish co-injection model. A, Perivitelline space single injection of MDA-MB-231 cells or co-injection of MDA-MB-231 cells and W21 mesenchymal stem cells (MSCs), foreskin fibroblasts or 19TT CAFs, as indicated. The panel shows representative images. Green, endothelium of zebrafish; red, mCherry-labeled MDA-MB-231; Blue, converted from AmCyan-labeled MSCs or fibroblasts. Yellow arrowheads point to single intravasated cells in the head and tail regions of zebrafish. Left, cell migration in the perivitelline space; Middle, image

of a zebrafish embryo body; Right, visualization of intravasated cells in the posterior of the embryo. The graph shows the quantification of the number of intravasated cells in each embryonic body at 3 days post injection (dpi). The results are expressed as the mean \pm s.e.m., $n=2$. Student's t test, $**P \leq 0.01$, $***P \leq 0.001$. **B**, Perivitelline space co-injection of MDA-MB-231 cells and 19TT CAFs with/without *GREM1* knockdown. The panel and graph description are the same as described in (A). The results are expressed as the mean \pm s.e.m., $n=2$. Student's t test, $**P \leq 0.01$. **C**, Schematic of the working model of Greml1 function in breast cancer progression. Greml1 expression in fibroblasts is induced by factors (such as TGF β from breast cancer cells or maybe other stromal cells (that produce inflammatory cytokines). Greml1 could activate fibroblasts into CAFs. CAFs might present a desmoplastic microenvironment, thereby promote cancer cell invasion. Greml1 itself could promote the stemness, and invasion of breast cancer cells.

TGF β released by breast cancer cells and inflammatory cytokines. Greml1 mediates the fibrogenic activation of CAFs in an autocrine manner. Greml1 has a direct effect on cancer cell invasion and stemness, evidenced by the fact that it promoted a slightly more mesenchymal/stemness phenotype in breast cancer cells. It could also contribute indirectly to this process via its potent effects on fibroblast activation. In this way, Greml1 promotes the formation of a microenvironment conducive to breast cancer cell invasion. Thus, Greml1 is a key determinant of the mutual interplay between breast cancer cells and CAFs (Figure 7C).

Although we found an association between Greml1 and poor breast cancer prognosis, the prognostic significance of Greml1 in different cancer types is not consistent. For example, Greml1 expression correlates with progression-free survival in pancreatic neuroendocrine tumors [49] and colorectal cancer [50], but it is an indicator of poor progression-free survival in cervical cancer [51]. Greml1 may have different roles in different tumor types, but this may be dependent on the experimental setup, the analysis of expression in complete tumors versus stromal expression specifically, and/or the determining the levels of RNA versus protein. For instance, when testing commercial antibodies on tissue sections, including sections of *GREM1*-deficient animals, we found that the detected signals may not have been specific for Greml1 (data not shown). To avoid these putatively non-specific measurements, we determined *GREM1* mRNA levels by *in situ* hybridization.

The mRNA detection method revealed that *GREM1* was exclusively expressed by CAFs. Our findings are supported by our data mining of publicly available data sets. We analyzed breast cancer dataset *GSE14548* generated by Ma and colleagues [28], which separated epithelial

and stroma tissues, and in this dataset *GREM1* was found mainly expressed in the (invasive) breast cancer stroma, and there was no *GREM1* expression observed in normal epithelium and stroma (Figures S8a). In addition, we mined a colon cancer dataset *GSE39396* in which epithelial cells, leukocytes, fibroblasts and endothelial cells were separately isolated by FACs and thereafter profiled. Consistent with our results, only fibroblasts were found to express *GREM1* (Figures S8b).

We found that *GREM1* expression in CAFs is particularly high in close vicinity of cancer cells. This is consistent with previous reports in which *Grem1* was found to be highly expressed in CAFs in the microenvironment of basal cell carcinoma (and other tumors) compared to normal tissue counterparts [23], and a study of colorectal cancer, in which *Grem1* was found to be expressed at the invasion fronts in CAFs, and to mediate the loss of cancer cell differentiation [3]. We identified TGF β secreted by cancer cells as a strong driver of *GREM1* expression by CAFs. Moreover, clinical breast cancer samples were also found to highly express *TGFBI/2/3* suggesting that these findings are of clinical relevance. Such invasion fronts are rich in inflammatory cells [52]. Consistent with this result, we found that inflammatory cytokines IL1 β and TNF β induced *GREM1* expression in CAFs. Moreover, *GREM1* expression correlated with mesenchymal marker expression in tumor samples. The latter observation indicates that *Grem1* at the invasion front may contribute to the desmoplastic phenotype (Figure 7C).

We observed a striking activation of fibrogenesis in fibroblasts and in CAFs by *Grem1*. Depletion or ectopic expression of *Grem1* in CAFs demonstrated that *Grem1* expression is positively linked to expression of TGF β ligands and target genes, mesenchymal markers, extracellular matrix proteins and matrix metalloproteinase (MMP) remodeling factors at the mRNA level, as well as with Fibronectin, S100A4, Collagen I, FAP, and α SMA at the protein level. In addition, *Grem1* promoted actin stress fiber formation and collagen gel contraction. These expression patterns are characteristic of a fibrogenic response and fibroblast activation. The *Grem1*-induced responses may be mediated by TGF β pathway activation; TGF β is a strong inducer of fibrogenesis and an activator of fibroblasts [53]. With TGF β being a strong inducer of *Grem1* and *vice versa*, it may act in a feed forward loop.

Multiple studies have shown that CAFs create a microenvironment suitable for cancer cell invasion [1, 2], which we further demonstrated in this study *in vivo* by co-injection of breast cancer cells with fibroblasts/CAF into the zebrafish perivitelline space. Thus, the profibrogenic

ability of Grem1 could contribute to its role in promoting cancer cell invasion mediated by activated fibroblasts and CAFs. 3D coculture of breast cancer cells with CAFs in collagen demonstrated that Grem1 is critical for invasion. In accordance with these results, Grem1 strongly promoted intravasation in a zebrafish co-injection xenograft model. Moreover, by injecting ectopic Grem1-producing M2 and MDA-MB-231 cells into the DoC of zebrafish embryos, we found that Grem1 strongly promoted the extravasation of cancer cells. These results may explain the clinical association between Grem1 expression in tumors and a poor prognosis of MFS.

Mechanistically, Grem1 exerts its effects by antagonizing selective BMPs [11]. Consistent with this notion, we found that BMP-induced SMAD1/5 phosphorylation is inhibited in breast cancer cells and in CAFs. In addition, depletion of endogenous Grem1 in CAFs upregulates BMP/SMAD-dependent *ID1/ID3* expression whilst addition of rhGrem1 has the opposite effect. Moreover, treatment with a selective BMP receptor kinase inhibitor mimicked the effect of exogenous Grem1 protein by promoting mammosphere formation and fibrogenic marker expression. However, our results do not exclude the possibility that Grem1 also can act via BMP-independent pathways [24]. For example, induction of TGF β expression by Grem1 may occur independently of BMP antagonism. Grem1 was found to promote cell viability, migration and invasion in glioma [54] and the invasive phenotype of mesothelioma [55] by activating TGF β /SMAD signaling. Moreover, Grem1 may promote breast tumorigenesis by acting on signaling pathways distinct from TGF β family signaling; in renal tubular cells, Grem1 has been reported to signal via the vascular endothelial growth factor receptor 2 (VEGFR2) pathway [21] to promote angiogenesis [56] and to mediate inflammation and the infiltration of immune-inflammatory cells [57]. Furthermore, Grem1 may act directly or indirectly by sequestering BMP on endothelial cells and immune cells and thereby promote tumorigenesis. Irrespective of the precise mechanisms, our results demonstrate potent pro-tumorigenic effects of Grem1 on cancer cells and CAFs *in vitro* in mono- and in co-culture, as well as a key *in vivo* role for Grem1 in stimulating extravasation and for Grem1-producing CAFs in mediating the intravasation of breast cancer cells. These two processes, extravasation and intravasation, are key steps in the dissemination and distant colonization of primary cancer cells.

Our results identified Grem1 as a driving force of breast cancer progression by affecting the behavior of both cancer cells and neighboring CAFs. Antibodies that neutralize Grem1's

function in the Grem1-BMP interaction have been described which may be beneficial not only for the treatment of pulmonary arterial hypertension [58] but also for breast cancer (by inhibiting breast cancer progression). In addition, BMP agonists that are engineered to prevent interactions with Grem1, as has been performed for Noggin [59], or BMP-mimetic small molecule drugs [60, 61], could be beneficial in the treatment of breast cancer patients with high Grem1 expression.

Acknowledgements

We acknowledge Dr. Derek P. Brazil (Centre for Experimental Medicine, Queen's University Belfast, Belfast, UK) for providing Grem1 deficient mouse colon tissue to test commercial Grem1 antibody and for recommendation to use *in situ* probe for detection of *GREM1* transcripts in tissue sections, Prof. Dr. Slobodan Vukicevic for recombinant BMP6, David Baker for critical reading of manuscript, Maarten van Dinther and Midory Thorikay for technical assistance, Selcuk Colak for advice regarding mammosphere assays and Martijn Rabelink for shRNA constructs.

Funding

This research was supported by Cancer GenomiCs.nl (CGC.nl). Jiang Ren was supported by The China Scholarship Council (CSC) during his PhD study at Leiden University Medical Center.

Availability of data and materials

All remaining data and materials are available from the authors upon reasonable request

Authors' contributions

Conceptualization PtD, JWMM, JR; Methodology: JR; Acquisition of data: PtD, JWMM, JR; Writing, review, and/or revision of the manuscript: JR, PtD, HvD; Administrative, technical, or material support: PtD, JWMM, JR, MS, DCFS, JI, HJZ; Study supervision: PtD.

Ethics approval and consent to participate

All research using zebrafish, including housing and experiments, was carried out according to the international guidelines and was approved by the local Institutional Committee for Animal Welfare (*Dier Ethische Commissie* (DEC)) of the LUMC.

References

1. Madar S, Goldstein I, Rotter V. 'Cancer associated fibroblasts'—more than meets the eye. *Trends Mol Med* 2013, 19(8):447-53.
2. Kalluri R. The biology and function of fibroblasts in cancer. *Nat Rev Cancer* 2016, 16(9):582-8.

3. Karagiannis GS, Poutahidis T, Erdman SE, *et al.* Cancer-associated fibroblasts drive the progression of metastasis through both paracrine and mechanical pressure on cancer tissue. *Mol Cancer Res* 2012, 10(11):1403-18.
4. Katagiri T, Watabe T. Bone morphogenetic proteins. *Cold Spring Harb Perspect Biol* 2016, 8(6):a021899.
5. Ren J, ten Dijke P. Bone morphogenetic proteins in the initiation and progression of breast cancer. *Bone Morphogenetic Proteins: Systems Biology Regulators*, Springer 2017, p.409-33.
6. Brazil DP, Church RH, Surae S, *et al.* BMP signalling: agony and antagonism in the family. *Trends Cell Biol* 2015, 25(5):249-64.
7. Tarragona M, Pavlovic M, Arnal-Estapé A, *et al.* Identification of NOG as a specific breast cancer bone metastasis-supporting gene. *J Biol Chem* 2012, 287(25):21346-55.
8. Mock K, Preca B, Brummer T, *et al.* The EMT-activator ZEB1 induces bone metastasis associated genes including BMP-inhibitors. *Oncotarget* 2015, 6(16):14399-412.
9. Gao H, Chakraborty G, Lee-Lim AP, *et al.* The BMP inhibitor Coco reactivates breast cancer cells at lung metastatic sites. *Cell* 2012, 150(4):764-79.
10. Nolan K, Thompson TB. The DAN family: Modulators of TGF- β signaling and beyond. *Protein Science* 2014, 23(8):999-1012.
11. Church RH, Krishnakumar A, Urbanek A, *et al.* Gremlin1 preferentially binds to bone morphogenetic protein-2 (BMP-2) and BMP-4 over BMP-7. *Biochem J* 2015, 466(1):55-68.
12. Khokha MK, Hsu D, Brunet LJ, *et al.* Gremlin is the BMP antagonist required for maintenance of Shh and Fgf signals during limb patterning. *Nat Genet* 2003, 34(3):303-7.
13. Michos O, Panman L, Vintersten K, *et al.* Gremlin-mediated BMP antagonism induces the epithelial-mesenchymal feedback signaling controlling metanephric kidney and limb organogenesis. *Development* 2004, 131(14):3401-10.
14. Mangold E, Ludwig KU, Birnbaum S, *et al.* Genome-wide association study identifies two susceptibility loci for nonsyndromic cleft lip with or without cleft palate. *Nat Genet* 2010, 42(1):24-6.
15. Tardif G, Pelletier JP, Boileau C, *et al.* The BMP antagonists follistatin and gremlin in normal and early osteoarthritic cartilage: an immunohistochemical study. *Osteoarthritis Cartilage* 2009, 17(2):263-70.
16. Gazzero E, Pereira RC, Jorgetti V, *et al.* Skeletal overexpression of gremlin impairs bone formation and causes osteopenia. *Endocrinology* 2005, 146(2):655-65.

17. Boers W, Aarrass S, Linthorst C, *et al.* Transcriptional profiling reveals novel markers of liver fibrogenesis: gremlin and insulin-like growth factor-binding proteins. *J Biol Chem* 2006, 281(24):16289-95.
18. Koli K, Myllärniemi M, Vuorinen K, S *et al.* Bone morphogenetic protein-4 inhibitor gremlin is overexpressed in idiopathic pulmonary fibrosis. *Am J Pathol* 2006, 169(1):61-71.
19. Walsh DW, Roxburgh SA, McGettigan P, *et al.* Co-regulation of Gremlin and Notch signalling in diabetic nephropathy *Biochim Biophys Acta* 2008, 1782(1):10-21.
20. Corsini M, Moroni E, Ravelli C, *et al.* Cyclic adenosine monophosphate-response element-binding protein mediates the proangiogenic or proinflammatory activity of gremlin. *Arterioscler Thromb Vasc Biol* 2014, 34(1):136-45.
21. Mitola S, Ravelli C, Moroni E, *et al.* Gremlin is a novel agonist of the major proangiogenic receptor VEGFR2. *Blood* 2010, 116(18):3677-80.
22. Yan K, Wu Q, Yan DH, *et al.* Glioma cancer stem cells secrete Gremlin1 to promote their maintenance within the tumor hierarchy. *Genes Dev* 2014, 28(10):1085-100.
23. Sneddon JB, Zhen HH, Montgomery K, v *et al.* Bone morphogenetic protein antagonist gremlin 1 is widely expressed by cancer-associated stromal cells and can promote tumor cell proliferation. *Proc Natl Acad Sci U S A* 2006, 103(40):14842-7.
24. Kim M, Yoon S, Lee S, *et al.* Gremlin-1 induces BMP-independent tumor cell proliferation, migration, and invasion. *PLoS One* 2012, 7(4):e35100.
25. Jaeger E, Leedham S, Lewis A, *et al.* Hereditary mixed polyposis syndrome is caused by a 40-kb upstream duplication that leads to increased and ectopic expression of the BMP antagonist GREM1. *Nat Genet* 2012, 44(6):699-703.
26. Davis H, Irshad S, Bansal M, *et al.* Aberrant epithelial GREM1 expression initiates colonic tumorigenesis from cells outside the stem cell niche. *Nat Med* 2015, 21(1):62-70.
27. Karagiannis GS, Berk A, Dimitromanolakis A, *et al.* Enrichment map profiling of the cancer invasion front suggests regulation of colorectal cancer progression by the bone morphogenetic protein antagonist, gremlin-1. *Mol Oncol* 2013, 7(4):826-39.
28. Ma XJ, Dahiya S, Richardson E, E *et al.* Gene expression profiling of the tumor microenvironment during breast cancer progression. *Breast Cancer Res* 2009, 11(1):R7.
29. Kim HS, Shin MS, Cheon MS, *et al.* GREM1 is expressed in the cancer-associated myofibroblasts of basal cell carcinomas. *PLoS One* 2017, 12(3):e0174565.
30. Wang Y, Klijn JG, Zhang Y, *et al.* Timmermans M, Meijer-van Gelder ME, Yu J *et al.*: Gene-expression profiles to predict distant metastasis of lymph-node-negative primary breast cancer. *Lancet* 2005, 365(9460):671-79.

31. Minn AJ, Gupta GP, Padua D, *et al.* Lung metastasis genes couple breast tumor size and metastatic spread. *Proc Natl Acad Sci U S A* 2007, 104(16):6740-6745.
32. Sotiriou C, Wirapati P, Loi S, *et al.* Gene expression profiling in breast cancer: understanding the molecular basis of histologic grade to improve prognosis. *J Natl Cancer Inst* 2006, 98(4):262-72.
33. Desmedt C, Piette F, Loi S, *et al.* Strong time dependence of the 76-gene prognostic signature for node-negative breast cancer patients in the TRANSBIG multicenter independent validation series. *Clin Cancer Res* 2007, 13(11):3207-14.
34. Schmidt M, Böhm D, Von Törne C, *et al.* The humoral immune system has a key prognostic impact in node-negative breast cancer. *Cancer Res* 2008, 68(13):5405-13.
35. Riaz M, van Jaarsveld MT, Hollestelle A, *et al.* miRNA expression profiling of 51 human breast cancer cell lines reveals subtype and driver mutation-specific miRNAs. *Breast Cancer Res* 2013, 15(2):R33.
36. Calon A, Espinet E, Palomo-Ponce S, *et al.* Dependency of colorectal cancer on a TGF β -driven program in stromal cells for metastasis initiation. *Cancer Cell* 2012, 22(5):571-584.
37. McCall MN, Bolstad BM, Irizarry RA. Frozen robust multiarray analysis (fRMA). *Biostatistics* 2010, 11(2):242-53.
38. Johnson WE, Li C, Rabinovic A. Adjusting batch effects in microarray expression data using empirical Bayes methods. *Biostatistics* 2007, 8(1):118-27.
39. Martens JW, Sieuwerts AM, Bolt-deVries J, *et al.* Aging of stromal-derived human breast fibroblasts might contribute to breast cancer progression. *Thromb Haemost* 2003, 89(2):393-404.
40. Ramkisoensing AA, Pijnappels DA, Askar SF, *et al.* Human embryonic and fetal mesenchymal stem cells differentiate toward three different cardiac lineages in contrast to their adult counterparts. *PLoS One* 2011, 6(9):e24164.
41. Ren J, Liu S, Cui C, *et al.* Invasive Behavior of Human Breast Cancer Cells in Embryonic Zebrafish. *J Vis Exp* 2017(122):e55459.
42. Dennler S, Itoh S, Vivien D, *et al.* Direct binding of Smad3 and Smad4 to critical TGF β -inducible elements in the promoter of human plasminogen activator inhibitor-type 1 gene. *EMBO J* 1998, 17(11):3091-100.
43. Persson U, Izumi H, Souchelnytskyi S, *et al.* The L45 loop in type I receptors for TGF- β family members is a critical determinant in specifying Smad isoform activation. *FEBS Lett* 1998, 434(1-2):83-87.
44. Krause C, Kloen P, ten Dijke P. Elevated transforming growth factor β and mitogen-activated protein kinase pathways mediate fibrotic traits of Dupuytren's disease fibroblasts. *Fibrogenesis Tissue Repair* 2011, 4(1):14.

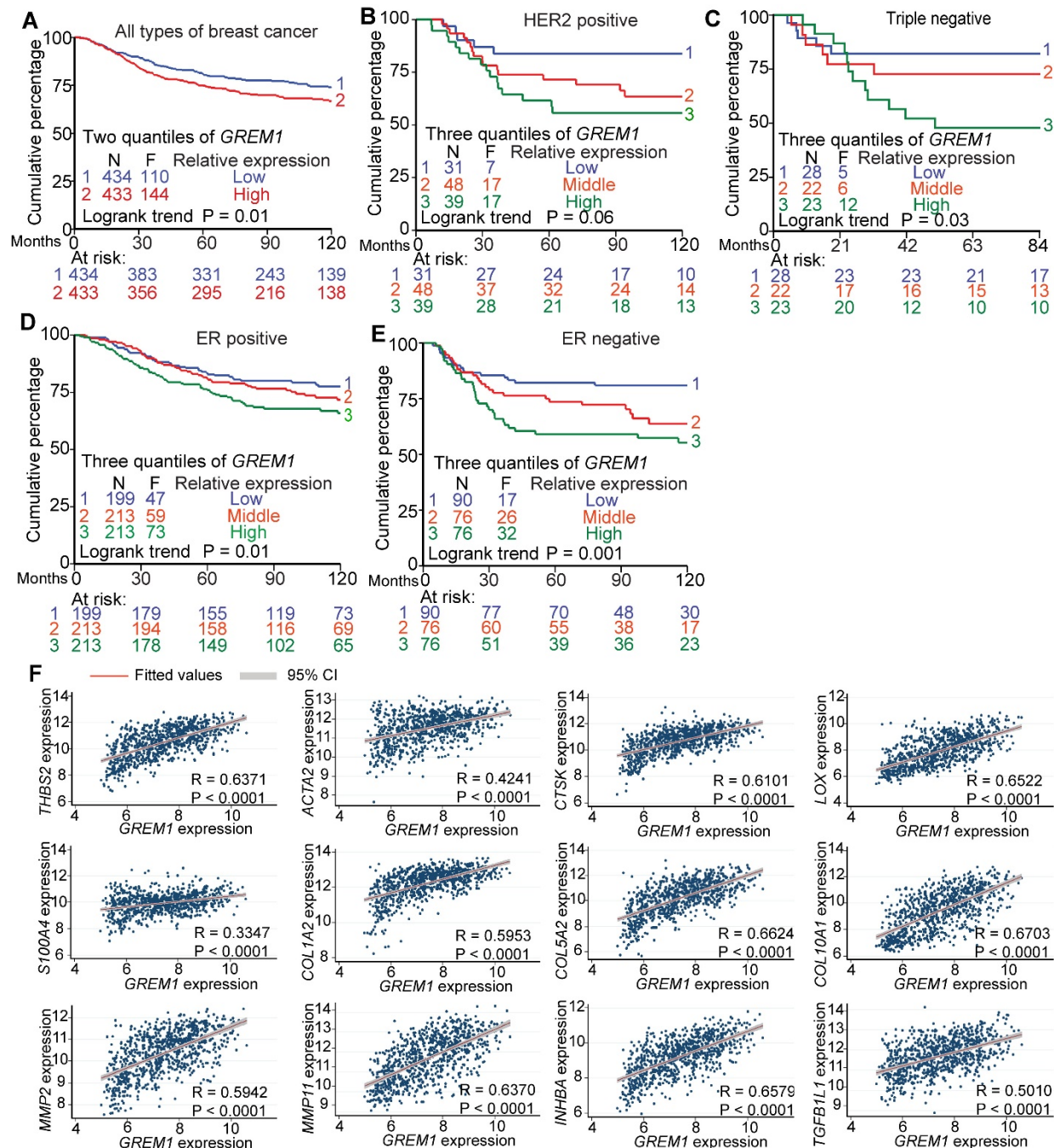
45. Naber HP, Wiercinska E, ten Dijke P, *et al.* Spheroid assay to measure TGF β -induced invasion. *J Vis Exp* 2011(57) :e3337.
46. Buijs J, Van Der Horst G, Van Den Hoogen C, *et al.* The BMP2/7 heterodimer inhibits the human breast cancer stem cell subpopulation and bone metastases formation. *Oncogene* 2012, 31(17):2164-74.
47. Vogt J, Traynor R, Sapkota GP. The specificities of small molecule inhibitors of the TGF β and BMP pathways. *Cell Signal* 2011, 23(11):1831-42.
48. Karnoub AE, Dash AB, Vo AP, *et al.* Mesenchymal stem cells within tumour stroma promote breast cancer metastasis. *Nature* 2007, 449(7162):557-63.
49. Chen MH, Yeh YC, Shyr YM, *et al.* Expression of gremlin 1 correlates with increased angiogenesis and progression-free survival in patients with pancreatic neuroendocrine tumors. 2013 *J Gastroenterol*, 48(1):101-8.
50. Jang BG, Kim HS, Chang WY, *et al.* Prognostic significance of stromal GREM1 expression in colorectal cancer. *Hum Pathol* 2017, 62:56-65.
51. Sato M, Kawana K, Fujimoto A, *et al.* Clinical significance of Gremlin 1 in cervical cancer and its effects on cancer stem cell maintenance. *Oncol Rep* 2016, 35(1):391-7.
52. Grivennikov SI, Greten FR, Karin MJC. Immunity, inflammation, and cancer. 2010, 140(6):883-9.
53. Hawinkels LJ, ten Dijke P. Exploring anti-TGF β therapies in cancer and fibrosis. *Growth factors* 2011, 29(4):140-52.
54. Guan Y, Cheng W, Zou C, *et al.* Gremlin1 promotes carcinogenesis of glioma in vitro. *Clin Exp Pharmacol Physiol* 2017, 44(2):244-56.
55. Yin M, Tissari M, Tamminen J, *et al.* Gremlin-1 is a key regulator of the invasive cell phenotype in mesothelioma. *Oncotarget* 2017, 8(58):98280-97.
56. Ravelli C, Mitola S, Corsini M, *et al.* Involvement of α v β 3 integrin in gremlin-induced angiogenesis. *Angiogenesis* 2013, 16(1):235-43.
57. Lavozy C, Alique M, Rodrigues-Diez R, *et al.* Gremlin regulates renal inflammation via the vascular endothelial growth factor receptor 2 pathway. *J Pathol* 2015, 236(4):407-20.
58. Ciuculan L, Sheppard K, Dong L, *et al.* Treatment with Anti-Gremlin 1 Antibody Ameliorates Chronic Hypoxia/SU5416-Induced Pulmonary Arterial Hypertension in Mice. *Am J Pathol* 2013, 183(5):1461-73.
59. Song K, Krause C, Shi S, *et al.* Identification of a key residue mediating bone morphogenetic protein (BMP)-6 resistance to noggin inhibition allows for engineered BMPs with superior agonist activity. 2010, 285(16):12169-80.

60. Sugimoto H, LeBleu VS, Bosukonda D, *et al.* Activin-like kinase 3 is important for kidney regeneration and reversal of fibrosis. *Nat Med* 2012, 18(3):396-404.
61. Shin K, Lim A, Zhao C, *et al.* Hedgehog signaling restrains bladder cancer progression by eliciting stromal production of urothelial differentiation factors. *Cancer Cell* 2014, 26(4):521-33.

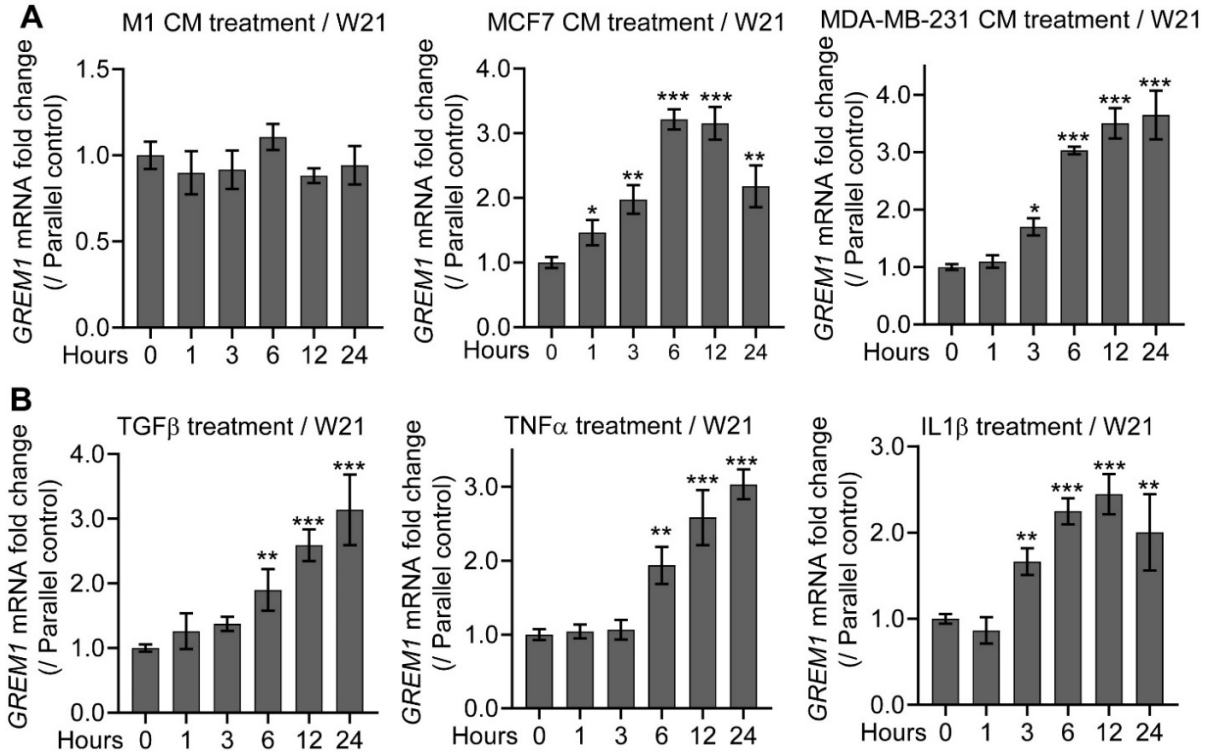
Supplementary Table 1. Quantitative real-time PCR Primers

Genes		Sequence (5' to 3')
<i>ACTA2</i>	Forward	CTGTTCCAGCCATCCTTCATC
	Reverse	CCGTGATCTCCTTCTGCATT
<i>ACVR2A</i>	Forward	GCATCACAAGATGGCCTACC
	Reverse	CCAGGCAAACCTGTAGACTTC
<i>ACVR2B</i>	Forward	ATGTGGACATCCATGAGGAC
	Reverse	TGAAGATCTCCCGTTCACTC
<i>ALK1</i>	Forward	CTGGTTCCGGGAGACTGAGAT
	Reverse	TGCGGGAGGTCATGTCTGA
<i>ALK2</i>	Forward	TGCCTTCGAATAGTGCTGTC
	Reverse	CATCAAGCTGATTGGTGCTC
<i>ALK3</i>	Forward	GGGGTCCGGACTTATGAAA
	Reverse	TACGACTCCTCCAAGATGTGG
<i>ALK4</i>	Forward	GCTCGAAGATGCAATTCTGG
	Reverse	TTGGCATACCAACACTCTCG
<i>ALK6</i>	Forward	CTTGCTGTATTGCTGACCTG
	Reverse	TCAGCCATGATGTAAGACTGG
<i>ALK7</i>	Forward	CGCACTTCAAAAGGGTGTCG
	Reverse	TGATGCCCAACATGCTCCTT
<i>BMP2</i>	Forward	GCAGGCACTCAGGTCAG
	Reverse	ATTCGGTGATGGAAACTGC
<i>BMP4</i>	Forward	TGTCTCCCCGATGGGATTCCCG
	Reverse	AATGGCTCCATAGGTCCCTGCAGTA
<i>BMP6</i>	Forward	CACCCAAGGGCTATGCTGCCAATTA
	Reverse	AGGTGAACCAAGGTCTGCACAATCG
<i>BMP7</i>	Forward	GTGCACTCGAGCTTCATCCA
	Reverse	GATCCGATTCCCTGCCCAAG
<i>BMP15</i>	Forward	AGAACCCGACAAGCAGATGG
	Reverse	AATGGCGTGATTGGGGGAAT
<i>BMPR2</i>	Forward	AACTGTTGGAGCTGATTGGC
	Reverse	CGGTTTGCAAAGGAAAACAC
<i>COL1A1</i>	Forward	CAGCCGCTTCACCTACAGC
	Reverse	TTTGTATTCAATCACTGTCTTGCC
<i>COL1A2</i>	Forward	GGCCCTCAAGGTTTCCAAGG
	Reverse	CACCCTGTGGTCCAACAACCTC
<i>FAP</i>	Forward	CAATGTGGTACTCTGACCAGAACC
	Reverse	TCTGATACAGGCTTGCATCTGC
<i>FNI</i>	Forward	CGTCATAGTGGAGGCACTGA
	Reverse	CAGACATTCGTTCCCACTCA
<i>GAPDH</i>	Forward	TGCACCACCAACTGCTTAGC
	Reverse	GGCATGGACTGTGGTCATGAG

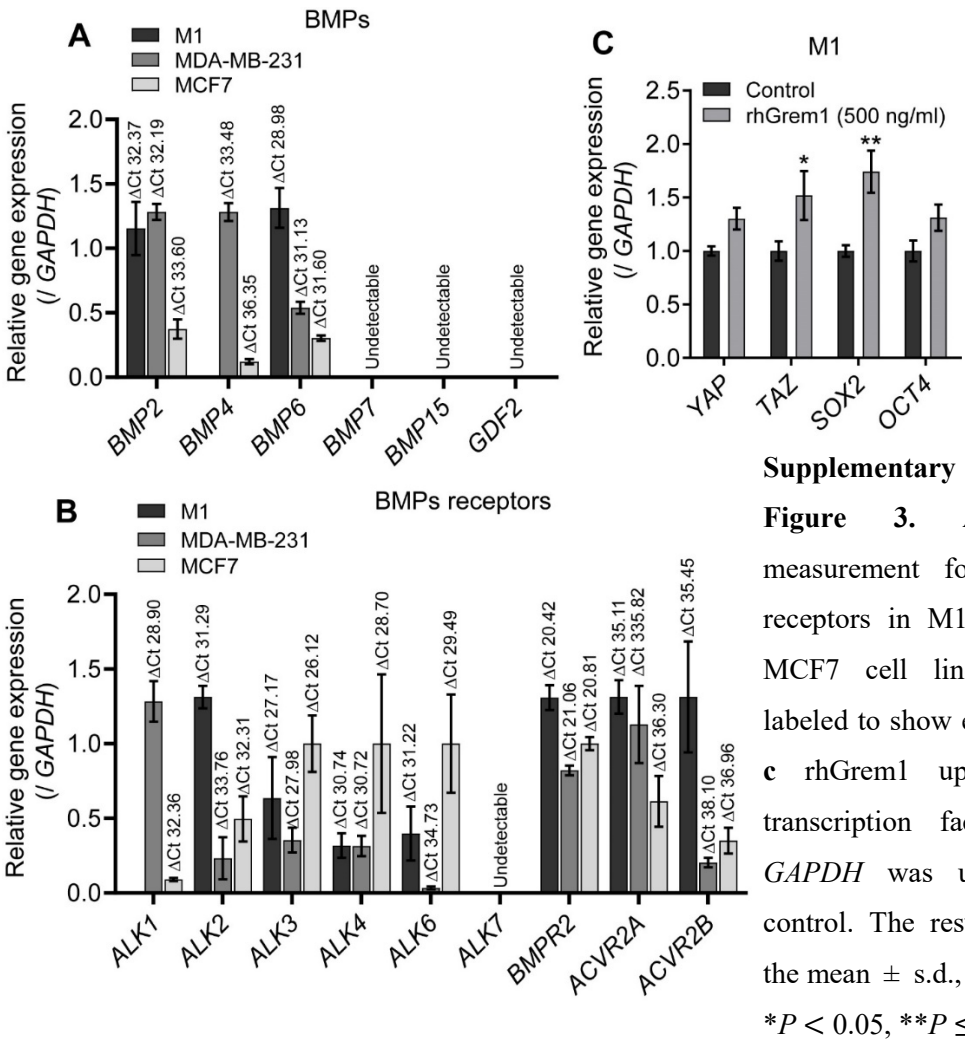
<i>GDF2</i>	Forward	GACGTCCGATAAGTCGACTACGC
	Reverse	AAGATGTGCTTCTGGAAGGGGAA
<i>GREM1</i>	Forward	ACAGTCGCACCATCATCAAC
	Reverse	TAGTGAATTTCTTGGGCTTG
<i>ID1</i>	Forward	CTGCTCTACGACATGAACGG
	Reverse	GAAGGTCCCTGATGTAGTCGAT
<i>ID3</i>	Forward	CACCTCCAGAACGCAGGTGCTG
	Reverse	AGGGCGAAGTTGGGGCCCAT
<i>MMP3</i>	Forward	TGGATGCCGCATATGAAG
	Reverse	CAGAAATGGCTGCATCGA
<i>MMP7</i>	Forward	ACTTCAGGCAGAACATCCAT
	Reverse	ATTGCTAAATGGAGTGGAGG
<i>MMP8</i>	Forward	CTGTATCCACTTTCAGAATGTT
	Reverse	TACAGTGATGGGAAACAATGA
<i>MMP9</i>	Forward	TACTGTGCCTTTGAGTCCG
	Reverse	TTGTCGGCGATAAGGAAG
<i>NCAD</i>	Forward	CAGACCGACCCAAACAGCAAC
	Reverse	GCAGCAACAGTAAGGACAAACATC
<i>PAI1</i>	Forward	CACAAATCAGACGGCAGCACT
	Reverse	CATCGGGCGTGGTGAAGTC
<i>OCT4</i>	Forward	CGAGAAGGATGTGGTCCGAG
	Reverse	AGCCTGGGGTACCAAAATGG
<i>S100A4</i>	Forward	TCTTTCTTGGTTTGATCCTGACT
	Reverse	AGTTCTGACTTGTTGAGCTTGA
<i>SLUG</i>	Forward	ATGAGGAATCTGGCTGCTGT
	Reverse	CAGGAGAAAATGCCTTTGGA
<i>SNAIL</i>	Forward	GCTGCAGGACTCTAATCCAGAGTT
	Reverse	GACAGAGTCCCAGATGAGCATTG
<i>SOX2</i>	Forward	CGGAAAACCAAGACGCTCAT
	Reverse	TGTGCGCGTAAGTGTCCAT
<i>TAZ</i>	Forward	CCCGGCCGGAGAGTACAT
	Reverse	GACTGGTGATTGGACACGGT
<i>TGFB2</i>	Forward	GTGCTCTGTGGGTACCTTGA
	Reverse	GCGCTGGGTTGGAGATGTTA
<i>TGFB3</i>	Forward	CTGGCCCTGCTGAACTTTG
	Reverse	AAGGTGGTGCAAGTGGACAGA
<i>VIM</i>	Forward	CCAAACTTTTCCTCCCTGAACC
	Reverse	CGTGATGCTGAGAAGTTTCGTTGA
<i>YAP</i>	Forward	CGGCAGGCAATGCGGAATATCAAT
	Reverse	ACCATCCTGCTCCAGTGTTGGTAA



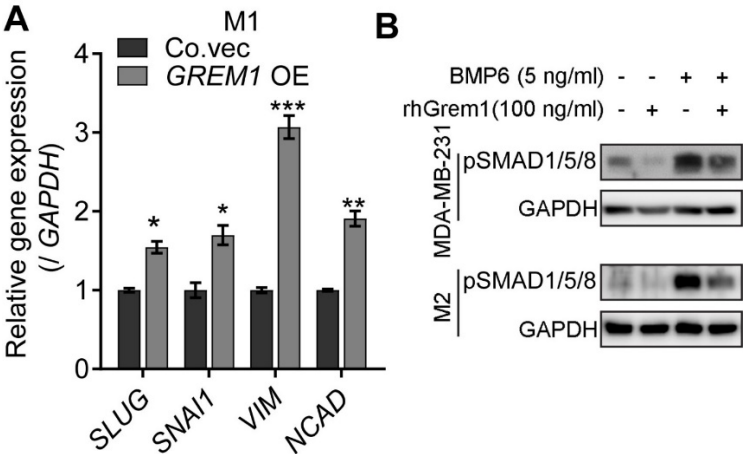
Supplementary Figure 1, related to Figure 1. A, Kaplan-Meier analysis of metastasis free survival based on *GREM1* expression. Endpoint is distant metastasis free survival (MFS). B-E, Kaplan-Meier survival analysis of different breast cancer molecular subtypes, HER2⁺ (B), Triple⁻ (C), ER⁺ (D), and ER⁻ (E). The subjects were divided into 3 quantiles. Endpoint is distant MFS. F, Scatterplot showing the positive correlation between *GREM1* and stromal genes / desmoplastic markers expression in clinical datasets. Pearson's coefficient tests were performed to assess statistical significance.



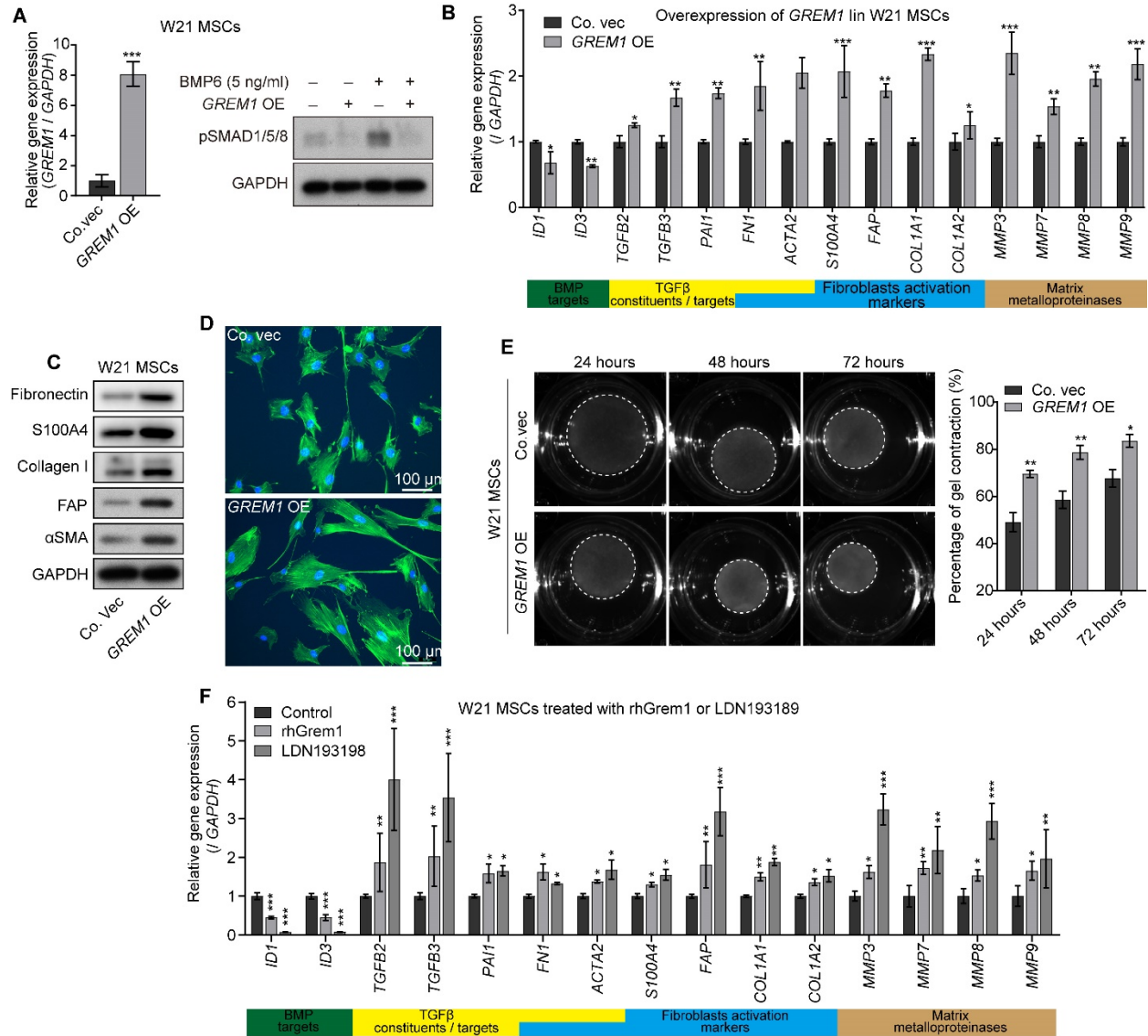
Supplementary Figure 2, related to Figure 2. A, *GREM1* expression in W21 MSCs after treatment with conditioned medium (CM) from breast cell lines (M1, MDA-MB-21, MCF7). Expression was normalized to the parallel time control of normal medium treatment. The results are expressed as the mean \pm s.d, $n = 3$. Student's t test, $*P < 0.05$, $***P \leq 0.001$. **B,** TGFβ3 (5 ng/ml), or TNFα (10 ng/ml), or IL1β (10 ng/ml) induces *GREM1* expression in W21 mesenchymal stem cells (MSCs). Expression was normalized to the parallel time control of buffer treatment. The results are expressed as the mean \pm s.d., $n = 3$. Student's t test, $*P < 0.05$, $**P \leq 0.01$, $***P \leq 0.001$.



Supplementary Figure 3, related to Figure 3. A, B, qRT-PCR measurement for BMPs and BMP receptors in M1, MDA-MB-231 and MCF7 cell lines. Δ Ct values are labeled to show expression abundance. c rhGrem1 upregulates stem cell transcription factors in M1 cells. GAPDH was used as an internal control. The results are expressed as the mean \pm s.d., n = 3. Student's t test, * $P < 0.05$, ** $P \leq 0.01$.

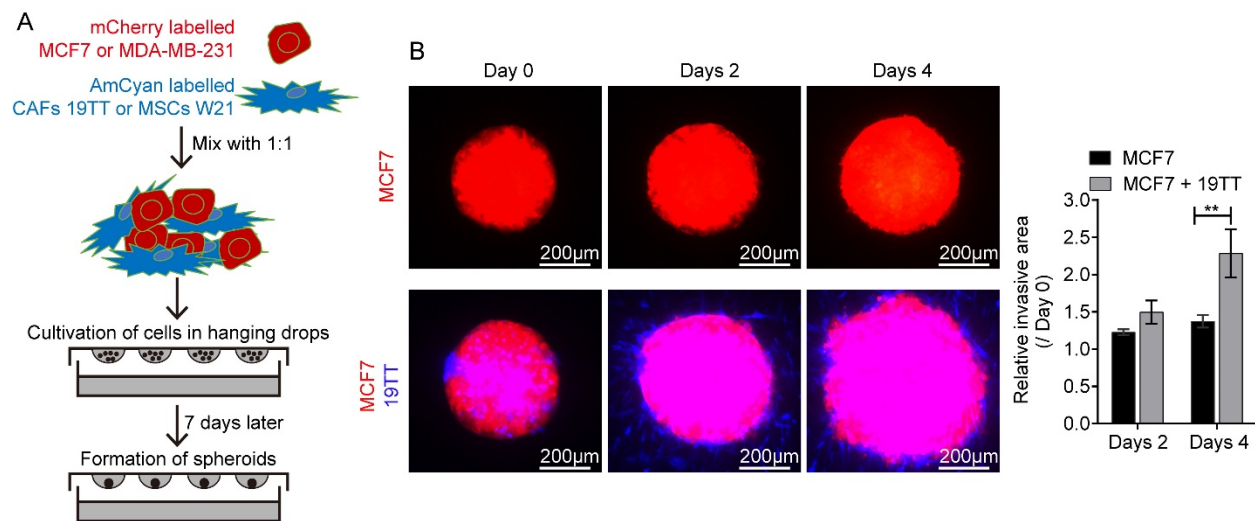


Supplementary 4, related to Figure 4. A, GREM1 OE upregulates the expression of EMT transcription factors and markers in M1 cells. GAPDH was used as an internal control. The results are expressed as the mean \pm s.d., n = 3. Student's t test, * $P < 0.05$, ** $P \leq 0.01$, *** $P \leq 0.001$. B, exogenous administration of rhGrem1 inhibits BMP-induced SMAD1/5/8 phosphorylation (pSMAD1/5/8) in MDA-MB-231 and M2 cell lines.

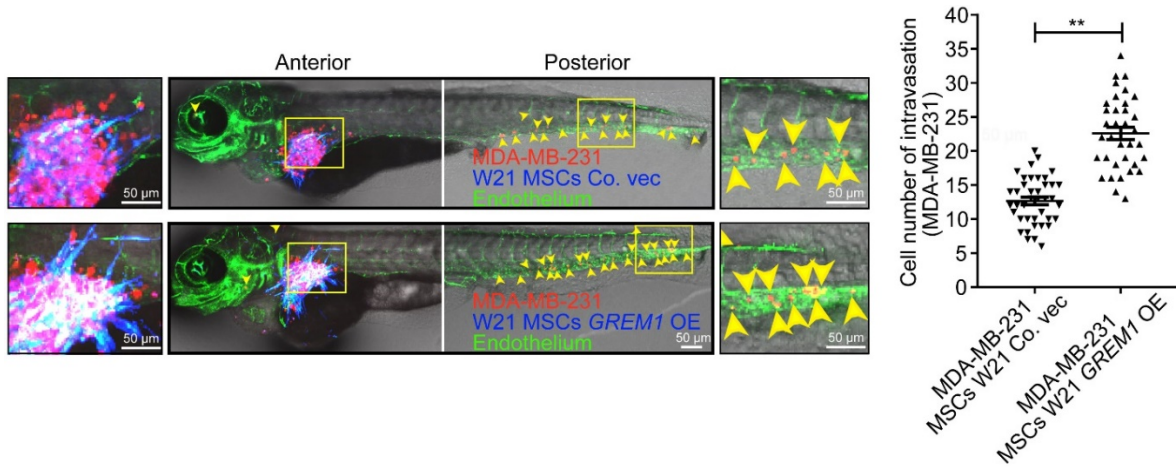


Supplementary Figure 5, related to Figure 5. *GREM1* overexpression (OE) in fetal mesenchymal stem cells (MSCs) W21 shows fibroblast-like characteristics. **A**, Stable *GREM1* OE in MSCs W21 inhibits BMP6 (5 ng/ml) induced SMAD1/5/8 phosphorylation (pSMAD1/5/8). Left, relative mRNA level determined by qRT-PCR. *GAPDH* was used as internal control. The results are expressed as the mean \pm s.d., n = 3. Student's t test, *** $P \leq 0.001$. **B**, qRT-PCR analysis of selected BMP targets, TGF pathway constituents/targets, fibroblasts activation markers, matrix metalloproteinases, in W21 MSCs with/without *GREM1* stable OE. *GAPDH* was used as internal control. The results are expressed as the mean \pm s.d., n = 3. Student's t test, * $P < 0.05$, ** $P \leq 0.01$, *** $P \leq 0.001$. **C**, Western blot to detect indicated proteins level change after *GREM1* OE in W21 MSCs. **D**, W21 MSCs with/without *GREM1* OE were stained with fluorescein-phalloidin (green) to visualize F-actin. DAPI was used for nuclear staining (blue). **E**, Collagen gel contraction assay. W21 MSCs with/without *GREM1* OE were embedded in

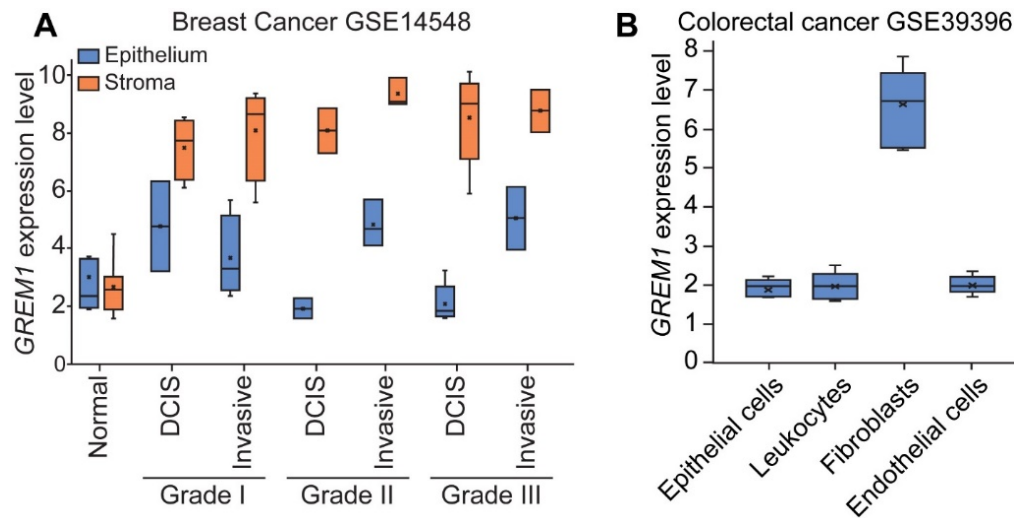
collagen gels. After 24, 48, and 72 h, the area of each gel (white dash circle) was imaged and quantified. Left, representative images of contracted gels. Right, percentage of gel contraction gel. Quantification is shown in Methods. The results are expressed as the mean \pm s.d., $n = 3$. Student's t test, $*P < 0.05$, $**P \leq 0.01$. F, qRT-PCR analysis of selected genes in W21 MSCs after 48 hours treatment with recombinant human Grem1 (rhGrem1) protein (500 ng/ml) or BMP type I receptors inhibitor LDN193198 (120 nM). *GAPDH* was used as internal control. The results are expressed as the mean \pm s.d., $n = 3$. Student's t test, $*P < 0.05$, $**P \leq 0.01$, $***P \leq 0.001$.



Supplementary Figure 6, related to Figure 6. Spheroid invasion assays. **A**, Schematic illustration of spheroid production. Briefly, mCherry-labeled MDA-MB-231 or MCF7 cells (Red) were mixed with AmCyan (converted to blue)-labeled 19TT breast cancer-associated fibroblasts (CAFs) at a ratio of 1:1. Mixtures were cultured for 7 days in hanging drops to obtain spheroids. **B**, 19TT CAFs promotes MCF7 cells invasion. Left, representative images of spheroids at days 0, 2, and 4. Red, MCF7 cells; Blue, 19TT CAFs. Right, the relative invasion area was quantified as area difference at days 2 and 4, relative to day 0. The results are expressed as the as the mean \pm s.d., $n = 8$. Student's t test, $**P \leq 0.01$.



Supplementary Figure 7, related to Figure 7. *GREM1* overexpression (OE) in W21 mesenchymal stem cells (MSCs) promotes breast cancer cells intravasation in zebrafish embryo perivitelline space coinjection model. Perivitelline space co-injection of MDA-MB-231 cells and W21 MSCs with/without *GREM1* stable OE. The panels show representative images. Green, endothelium of zebrafish; Red, mCherry-labelled MDA-MB-231; Blue, converted from AmCyan-labelled W21. Yellow arrowheads point to single intravasated cells in the head and tail regions of zebrafish. Left, cells migration in the perivitelline space; middle, image of zebrafish embryo body; Right, visualization of intravasated cells in the posterior of embryo. The graph shows quantification of the number of intravasated cells in each embryonic body at 3 days post injection (dpi). The results are expressed as the mean \pm s.e.m., $n=2$. Student's t test, $**P \leq 0.01$.



Supplementary Figure 8, related to Figure 1. A, *GREM1* mRNA expression in epithelium and stroma compartments in breast cancer dataset *GSE14548*. Epithelium and stroma were extracted from normal breast, grade I, II, III ductal carcinoma *in situ* (DCIS) and invasive breast cancer tissue using laser capture. **B,** *GREM1* expression in epithelial cells, leukocytes, fibroblasts and endothelial cells in colorectal cancer dataset *GSE39396*. Each specific type of cells were isolated by flow cytometry.

Chapter 4

Synergistic Reactivation of BMP Signaling by MEK Inhibitor and FK506 Reduces Breast Cancer Metastasis

Jiang Ren*, Yanhong Wang*, Josephine Iaria, Peter ten Dijke and Hong Jian Zhu

Manuscript in submission

*These authors contributed equally

Abstract

Transforming growth factor β (TGF β)-SMAD3 signaling is a major driving force for cancer metastasis, while bone morphogenetic protein (BMP)-SMAD1/5 signaling can counteract this response. TGF β -SMAD3 signaling is a major driving force for cancer metastasis, while BMP-SMAD1/5 signaling can counteract this response. We discovered that TGF β abolished BMP-induced SMAD1/5 activation in the highly-invasive breast cancer MDA-MB-231 cells, but to a less extent in the non-invasive and normal breast cells. This suggests an inverse correlation between BMP signaling and invasiveness of tumor cells and TGF β signaling acts in a double whammy fashion in driving cancer invasion and metastasis. Sustained ERK activation by TGF β was specifically observed in MDA-MB-231 cells, and treatment with MEK inhibitor (MEKi) restored BMP signaling. FK506 potently activated BMP, but not TGF β signaling in breast cancer cells. MEKi or FK506 alone inhibited MDA-MB-231 extravasation in zebrafish cancer model. Importantly, when administrated at suboptimal concentrations MEKi and FK506 strongly synergized in promoting BMP-SMAD1/5 signaling and inhibiting cancer cell extravasation. Furthermore, this combination treatment in a mice tumor model potently inhibited tumor self-seeding, liver and bone metastasis, but not lung and brain metastasis. Combining of MEK1 and FK506, or their analogues, may be explored for clinical development of breast cancer.

Keywords: BMP, Breast cancer metastasis, FK506, TGF β , U0126

Introduction

Although substantial progress of early diagnosis and molecular target therapy has been achieved in treating the primary niche of breast cancer patients, a dismal fact remains that over 90% of breast cancer-related deaths are caused by metastatic recurrence at distal organs, commonly bone, brain, lung, liver, and lymph nodes. For cells that contribute to effective metastases, they must successively gain the abilities of escaping the primary site, intravasation into the vasculatures, surviving in the circulation, then extravasation and colonization at the target organs [1]. It has been well-established that transforming growth factor β (TGF β) signaling serves as a major metastasis driver through promoting epithelial-mesenchymal transition (EMT), leading to increased invasion and dissemination of cancer cells, and also through inducing genes that facilitate metastatic colonization [2, 3].

Signaling of other TGF β family members, *i.e.* bone morphogenetic proteins (BMPs) can have a negative effect on EMT and metastatic colonization, indicating a mutual antagonistic role of TGF β and BMP signaling in cancer metastasis [4, 5]. Studies showed that the imbalance between them, towards TGF β signaling [6, 7], as well as BMP antagonists [8, 9] confer the ability of breast cancer cell metastasis. As such, it is worthwhile to interfere with this imbalance artificially; restoring or enhancing BMP signaling activity could be beneficial for reducing metastasis. For instance, activation of BMP4 blocks breast cancer metastasis and BMP4 correlates with good prognosis in patients [10]. Exogenous administration of BMP7 counteracted TGF β -mediated EMT and inhibited the osteolytic bone metastases of breast cancer cells [11]. BMP-7 inhibited TGF β -induced expression of integrin $\alpha\text{v}\beta\text{3}$, which can enhance EMT and expressed strongly in breast cancer cells that metastasize to bone [12].

Signaling by TGF β family is a paradigm of membrane-to-nucleus pathway. Upon ligand-induced heteromeric complex formation of specific type I and II transmembrane serine/threonine kinase receptors, receptor regulated (R-)SMAD2/3 and SMAD1/5/8, acting downstream of TGF β and BMP respectively, are phosphorylated by the activated type I receptor. Phosphorylated R-SMADs (pSMADs) form complexes with SMAD4, which can translocate into the nucleus to regulate genes transcription [13-15]. As SMAD4 is the only common partner, one antagonism between TGF β (-like) and BMP signaling is pSMAD2/3 can compete with pSMAD1/5 for binding SMAD4 [16, 17]. In addition, TGF β could induce a nonfunctional complex comprising

of phosphorylated SMAD1/5 and SMAD3 resulting in inhibition of BMP response in highly-invasive MDA-MB-231 cells [18].

What's more versatile, TGF β -regulated responses can be mediated by several non-canonical SMAD pathways, best illustrated in the activation of phosphatidyl inositol (PI)3K/AKT and early response kinase (ERK) mitogen activated protein kinase (MAPK) [19, 20]. Numerous studies have revealed that the SMAD proteins are a critical platform for integrating RTK/MAPK signals with the TGF β signaling [21]. How non-canonical TGF β signaling affect TGF β and BMP crosstalk remains unclear, as well as subsequent effect on cancer metastasis.

In this study, we found TGF β induced abolishment of the BMP signaling activity in MDA-MB-231 cells. The BMP-SMAD1/5 activation could be restored by MAPK kinase (MEK) inhibitors U0126 or PD98059. Moreover, FK506 was identified as a BMP/SMAD1/5 signaling agonist that inhibited cancer cell extravasation. Notably, suboptimal concentrations of U0126 and FK506 exhibited synergistic effects on restoring BMP signaling both in vitro and in vivo. Furthermore, U0126 and FK506 combination treatment in a strongly cooperative manner reduced extravasation in zebrafish breast cancer model and liver, bone metastasis and tumor self-seeding in mouse breast cancer model. Therefore, future therapies targeting BMP signaling restoration in cancer cells may be worthwhile to be developed for cancer metastasis treatment.

Methods

Cell lines, culture conditions

The human breast cancer cell lines MDA-MB-231 and MCF7, human epidermal carcinoma cell line A431, human head and neck tumor cell line HN5, Madin-Darby canine kidney cell line MDCK, the H-Ras-transformed MDCK (21D1 cells) [22], mouse mammary epithelial cell line NMuMG, and mouse fibroblast cell line NIH3T3 were originally obtained from ATCC (American Type Culture Collection). Doxycycline inducible Ras transformed NIH3T3 fibroblasts [23] and mCherry stable expression MDA-MB-231 cell line had been described before [9, 24]. These cell lines were cultured in Dulbecco's modified Eagle's medium (DMEM, 11965092, ThermoFisher Scientific) supplemented with 10% Fetal Bovine Serum (FBS, 16000044, ThermoFisher Scientific), 100 U/ml Penicillin/Streptomycin (Pen/Strep, 15140148, ThermoFisher Scientific). Human breast epithelial cell line MCF10A [25] was generously provided by Dr. Fred Miller (Barbara Ann Karmanos Cancer Institute, Detroit, USA), and

cultured in DMEM/F12 medium (11039047, ThermoFisher Scientific) supplemented with 5% horse serum (26050088, ThermoFisher Scientific), 20 ng/ml epidermal growth factor (EGF, 01-107, Merck Millipore), 10 mg/ml insulin (91077C, Sigma-Aldrich), 100 ng/ml cholera enterotoxin (C8052, Sigma-Aldrich), and 0.5 mg/ml hydrocortisone (H0135, Sigma-Aldrich) and 100 U/ml Pen/Strep. All cell lines were maintained at 37 °C, 5% CO₂, humidified incubator. All cell lines were monthly tested to verify absence of mycoplasma and human cell lines were authenticated by single nucleotide polymorphism (SNP) analysis.

Cells treatment and small molecule compounds

We obtained recombinant human BMP6/7 (120-06/120-03, PeproTech and from Dr. S. Vukicevics), TGFβ3 (100-36E, PeproTech and A.P. Hinck, University of Pittsburg, USA) and Doxycycline monohydrate (Dox, D1822, Sigma-Aldrich). In certain experiments, cells were received combinational treatments at different priorities with 30 min pretreatment, The compounds that were used in this study: BMP type I receptors inhibitor LDN193189 (SML0559, Sigma-Aldrich) [26], TGFβ type 1 receptor (also termed activin receptor-like kinase (ALK5) inhibitor SB-431542 (S4317, Sigma-Aldrich), MEK inhibitor U0126 (U120, Sigma Aldrich) or PD98059 (9900, Cell Signaling Technology), PI3K inhibitor LY294002 (L9908, Sigma-Aldrich). All small molecule FDA-approved drugs and biologically active compounds were purchased from Sigma-Aldrich, including FK506 (Tacrolimus, F4679). Cells were maintained in serum free medium when receiving treatment, unless otherwise specified.

Adenovirus production

The BMP-SMAD1/5 signaling reporter Ad-Bre-Firefly (F)-luciferase (Luc), TGFβ-SMAD3 signaling reporter Ad-CAGA-Gaussia (G)-Luc, and Wnt signaling reporter Ad-TCF-F-Luc and Ad-CMV-G-Luc adenoviruses were produced and amplified as previously described [27, 28]. Ad-CMV-Flag-SMAD6 viruses were produced similarly for the purpose being infect cultured cells for overexpression of SMAD6 [28].

siRNA-mediated knockdown

MDA-MB-231 cells were transiently transfected with control siRNA (ON-TARGETplus Non-targeting control siRNAs, D-001810-01-05, Dharmacon) or SMAD6 siRNA (SMARTPool, L-015362-00-0010, Dharmacon) using Lipofectamine RNAiMAX (13778030, ThermoFisher

Scientific) according to the manufacturer's protocol. Successful knockdown of SMAD6 was confirmed by western blotting.

Luciferase reporter assay

Ad-Bre-F-Luc/Ad-TCF-F-Luc (multiplicity of infection (MOI): 2000) and Ad-CMV-G-Luc/Ad-CAGA-G-Luc (MOI: 1000) virus infected cells (3000 cells/well approximately) were cultured in a 96-well plate as previously described [28]. Or cells in a 24-well plate, which were seeded 1 day before (5×10^4 cells/well approximately), were co-transfected with 0.1 μ g TGF β -SMAD3-inducible (CAGA)₁₂ or BMP responsive element (Bre) F-Luc transcriptional reporter transcriptional reporter construct and 0.08 μ g β -galactosidase (β gal) expression construct using lipofectamine 3000 (L3000001, ThermoFisher Scientific). After overnight infection or transfection, cells were starved with low serum (0.2%) medium. 8 h later, cells were received conceived treatments. After another overnight incubation, Luc and β gal activities were measured. The Luc activity was presented as relative Luc activity which was normalized based on the G-Luc or β gal activity, or the fold change as compared to the basal reporter level. Representative results of at least three independent biological experiments are shown.

Western blotting

Cells were seeded into a 6-well plate and harvested when they reached 90-100% confluence. The cells were lysed with RIPA buffer containing 1 \times cOmplete Protease Inhibitor Cocktail (11836153001, Roche). Protein concentrations were determined using a bicinchoninic acid protein assay Kit (5000111, Bio-Rad). Proteins were separated by sodium dodecyl sulfate polyacrylamide gel electrophoresis (SDS-PAGE) and transferred onto 45 μ m Polyvinylidene difluoride (PVDF) membrane (IPVH00010, Merck Millipore). Membranes were blocked using 5% skim milk and probed with the respective primary and secondary antibodies. The signal was visualized using Clarity Western ECL Substrate (1705060, Bio-Rad) or exposed to X-ray film (7400, Kodak). The antibodies were raised against the following proteins: phospho-SMAD1/5 (pSMAD1/5, home-made, which recognizes pSMAD1/5, and crossreacts with pSMAD3) [29], phospho-SMAD2 (pSMAD2, home-made) [29], SMAD5 (sc-7443, Santa Cruz), SMAD2 (5339, Cell Signaling Technology), Flag M2 (F3165, Sigma-Aldrich), phospho-ERK1/2 (pERK1/2, 4370, Cell Signaling Technology), ERK1/2 (9102, Cell Signaling Technology), phospho-AKT (pAKT, 9275, Cell Signaling Technology), AKT (9272, Cell Signaling Technology), β -Actin

(A5441, Sigma-Aldrich), glyceraldehyde3-phosphate dehydrogenase (GAPDH, MAB374, Merck Millipore).

Quantitative PCR

Total RNAs were isolated using the NucleoSpin RNA II kit (740955, BIOKE). 1 µg of RNA was reverse transcribed using the RevertAid First Strand cDNA Synthesis Kit (K1621, ThermoFisher Scientific). Quantitative real-time polymerase chain reaction (qRT-PCR) was conducted with GoTaq qPCR Master Mix (A6001, Promega) by CFX Connect Detection System (1855201, Bio-Rad). All target genes expression levels were normalized to *GAPDH/Gapdh*. For Droplet Digital PCR (ddPCR), The samples were placed in the Droplet Reader QX200 (Droplet Digital PCR System). The QuantaSoft software determines the absolute starting copy number in units of copies/µl input sample and then reports the target DNA concentration in the form of copies per µl in the sample.

The sequences of primers for detecting target genes are shown as following. Human *ID1*: Forward, CTGCTCTACGACATGAACGG; Reverse, GAAGGTCCCTGATGTAGTCGAT. Human *ID3*: Forward, CACCTCCAGAACGCAGGTGCTG; Reverse, AGGGCGAAGTTGGGGCCCAT. Human *SMAD6*: Forward, ACAAGCCACTGGATCTGTCC; Reverse, ACATGCTGGCGTCTGAGAA. Human *GAPDH*: Forward, TGCACCACCAACTGCTTAGC; Reverse, GGCATGGACTGTGGTCATGAG. Mouse *Id1*: Forward, ACCCTGAACGGCGAGATCA; Reverse, TCGTCGGCTGGAACACAT. Mouse *Id3*: Forward, GCTGAGCTCACTCCGGAAGT; Reverse, CGGGTCAGTGGCAAAAGC. Mouse *Gapdh*: Forward, TGGCAAAGTGGAGATTGTTGCC; Reverse, AAGATGGTGATGGGCTTCCCG.

Wound healing assay

MDA-MB-231 (5×10^5 cells/well) were cultured in a 6-well plate and pre-treated with the indicated concentration of TGFβ, BMP7 or FK506 for 24h. Scratches were created using a P200 pipette tip to scratch a straight line on the culture plate through the cell monolayer. The culture medium was replaced with 1% serum fresh medium containing the same treatment as before to remove detached cells. Phase-contrast images were acquired at 0 and 16h post-scratch using a microscope equipped with a CCD camera, and ImageJ was used to analyze the closed area.

Embryonic zebrafish xenograft

All zebrafish experiments were carried out according to the international guidelines and was approved by the local Institutional Committee for Animal Welfare (*Dier Ethische Commissie* (DEC)) of the LUMC. The zebrafish xenograft model was established as described before [24, 30]. Briefly, approximately 400 mCherry-labeled MDA-MB-231 cells were injected into the duct of Curvier (DoC) of transgenic zebrafish embryos (*Fli:enhanced green fluorescent protein* (*EGFP*)), whose vasculature is marked in green, at 48h post-fertilization. After verification by microscopy, only correctly injected and viable zebrafish were grouped, and received corresponding treatments by directly administrating compounds into egg water. Xenografted zebrafish embryos were maintained at 34°C after injection, a compromise for both the fish and the human cell lines. 5 days post implantation (dpi), the MDA-MB-231 cells that extravasated individually from circulation into the collagen fibers of the tail fin were imaged and counted under a confocal microscope (SP5 STED, Leica Microsystems). All experiments were repeated at least two times independently, and representative experiments are shown.

Whole mount immunostaining of embryonic zebrafish

Embryos at 3dpi were fixed in 4% paraformaldehyde overnight at 4°C. Embryos were permeabilized with 10 µg/ml proteinase K (AM2546, ThermoFisher Scientific), washed, and blocked with phosphate buffered saline (PBS) containing 0.1% triton, 2% goat serum before incubation with pSMAD1/5 (9516, Cell Signaling Technology) overnight at 4°C in 1% goat serum. Secondary antibody Alexa Fluor 350 goat anti-rabbit IgG (Z25300, ThermoFisher Scientific) was used for detection. Embryos were imaged under a confocal microscope (SP5 STED, Leica Microsystems)

Mice experiments

Mice homozygous for the severe combined immune deficiency spontaneous mutation in DNA dependent protein kinase active subunit $Prkdc^{SCID}$ were purchased from animal resource center (ARC, West Australia). All animal experiments were performed in accordance with National Health Medical Research Council of Australia code of practice for the care and use of animals for scientific purposes and approved by The University of Melbourne Animal Ethics Committee (Ethics ID: 1613813).

For BMP signaling restoration model, mice were challenged with 3×10^6 Ad-Bre-Luc labelled MDA-MB-231-G-luc tumor cells (2 tumors/mouse contralaterally) orthotopically into

mammary fat pads at day 0. At 5 dpi, mice were randomly and evenly divided, followed by daily Bioluminescence imaging and treatment via intraperitoneal (i.p.) injection for 5 days. Bioluminescence signal of mice was measured using an in vivo IVIS imaging system (200 Series, Caliper Life Sciences) after being by administrating 150 mg/kg of D-Luciferin (50227, Sigma-Aldrich) via i.p. injection. The signal intensity was analysed using total flux (photons/second) in the regions of interest and normalized to background signal by Living Image software (V3.2, Caliper Life Sciences).

For metastasis model, mice were challenged with 1×10^6 MDA-MB-231 (left side) and 3×10^6 MDA-MB-231-G-luc (right side) tumor cells in the contralateral fat pads at day 0. Mice were randomly and evenly divided at 5 dpi, followed by daily treatment for 3 weeks. Mice were monitored for body weight and tumor size 2-3 times per week. At the endpoint, immediately after sacrifice of the mice, 1ml whole blood each mouse was collected by cardiac puncture and preserved into tube containing heparin. 5 μ l of the blood samples were lysed and assessed for G-Luc activity, which can represent the degree of circulating tumor cells (CTCs). Blood from mice without MDA-G-LUC tumor implantation was used as a negative control. Unlabeled MDA-MB-231, lung, liver, leg, and brain were harvested for detection of self-seeding and metastasis. Muscle and G-luc labelled tumors were used as negative and positive control, respectively. Three pieces from different sites of all tumors and organs were cut.

Statistics

Data are presented in bar and line graphs as the mean \pm standard deviation (s.d) or mean \pm standard error (s.e.m) as indicated in the figure legends. All statistical analyses were performed Student's *t* test. $P < 0.05$ indicates statistical significance.

Results

TGF β abolishes BMP-induced SMAD1/5 activation in highly-invasive breast cancer cells

To determine TGF β 's effect on SMAD1/5 signaling, MDA-MB-231 cells were infected with adenoviral transcriptional reporter Ad-BRE-F-Luc, where the BMP/SMAD1/5 response element drives firefly luciferase expression, and stimulated with TGF β at different time points. As shown in Figure 1A, SMAD1/5-driven transcription activity was induced by TGF β initially (up to 6h) Western blotting further confirmed TGF β 's stimulatory and inhibitory effects on SMAD1/5 phosphorylation (Figure 1B). The pSMAD1/5 level was increased in the first 0.5h, then was

reduced to levels lower than the baseline (0h) after 2h. unlike pSMAD1/5, pSMAD3 (downstream of TGF β type I receptor activation) continued (above baseline) though there was reduction after peaking, indicating a different dynamic response for SMAD3 and SMAD1/5 signaling upon TGF β stimulation. TGF β had little effect on Wnt pathway according to Ad-TCF-F-Luc transcriptional reporter assay (Figure S1A), confirming the specificity of TGF β on inhibition of SMAD1/5 signaling. In fact, TGF β also suppressed BMP-induced SMAD1/5 phosphorylation in MDA-MB-231 cells. In contrast, this inhibitory effect is much less (Figure 1C) in MCF7 cells, indicating a TGF β 's suppression of BMP-SMAD1/5 signaling is cell context dependent.

To further investigate whether this suppressive effect by TGF β occurs in cells with different invasiveness, we infected highly-invasive breast basal cancer MDA-MB-231 cell line, non-invasive luminal MCF7 cell line or normal mammary epithelial MCF10A cell line with Ad-Bre-F-Luc and Ad-CAGA-G-Luc for 24h, so that SMAD1/5 and SMAD3 signaling could be quantitated in the same cells at the same time respectively. As shown in Figure 1D, TGF β suppressed SMAD1/5 signaling significantly and more importantly inhibited BMP-induced SMAD1/5 signaling to the level lower than the basal level (without treatment) in MDA-MB-231 cells. Whereas, in MCF7 cells, the inhibition intensity is not as strong as seen in MDA-MB-231 cells. Notably, TGF β failed to suppress BMP-induced SMAD1/5 signaling to a level lower than the basal activity in MCF10A cells. Moreover, BMP7 significantly impaired TGF β signaling activity in these two cell lines, which was not observed in MDA-MB-231 cells. Furthermore, TGF β -mediated inhibition of SMAD1/5 signaling could be abolished by TGF β type I receptor inhibitor SB-431542 in a dose-dependent manner (Figure 1E). Taken together, the effectiveness of TGF β suppressing BMP signaling goes in parallel with the tumor cells' invasiveness.

SMAD6 acts as important negative feedback modulator of the BMP/SMAD signaling pathway [31]. To examine the possibility that TGF β blocks BMP signaling by inducing SMAD6 expression. We first showed that *SMAD6* mRNA expression increased with TGF β treatment in MDA-MB-231 cells (Figure S1B). However, only a slightly restoration of TGF β -inhibited SMAD1/5 signaling could be observed when knockdown *SMAD6* by siRNA(Figure S1C, D). Therefore, we reasoned that SMAD6 may weakly contribute to TGF β 's anti-SMAD1/5 signaling effect but not the main cause.

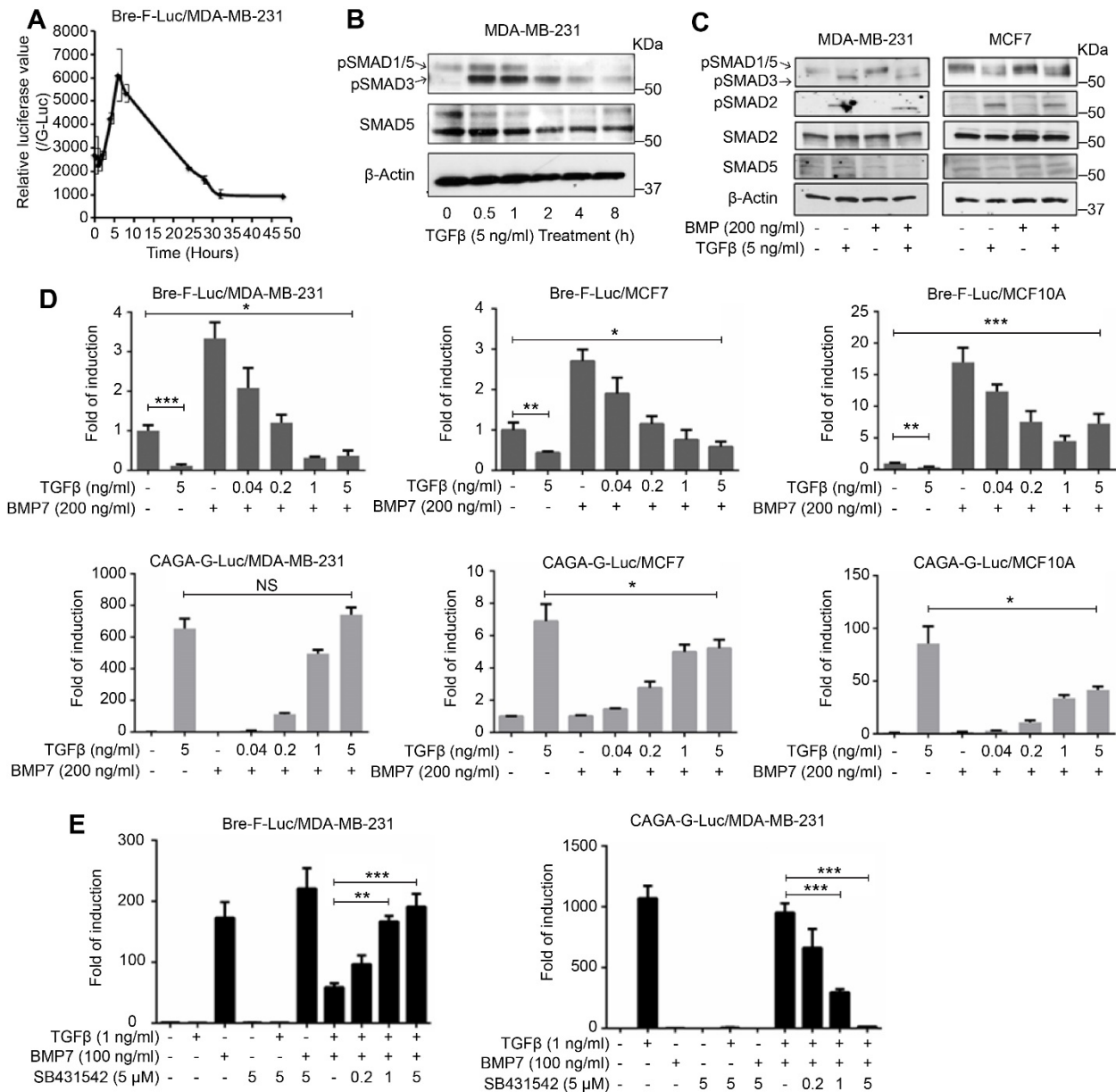


Figure 1. TGFβ impaired BMP signaling activation. **A**, Kinetic response of BMP signaling reporter (Ad-Bre-F (firefly)-Luc) to TGFβ stimulation (5 ng/ml) in MDA-MB-231 cells. The value is normalized to G (Gaussia)-Luc activity. $n = 3$. **B**, Kinetic response of SMAD1/5, SMAD3 phosphorylation (pSMAD1/5, pSMAD3, the home-made used here pSMAD1/5 antibody can well cross act with pSMAD3) to TGFβ stimulation (5 ng/ml) in MDA-MB-231 cells. β-Actin is used as a loading control. **C**, TGFβ suppressed BMP-induced SMAD1/5 phosphorylation (pSMAD1/5) in MDA-MB-231 cells, not in MCF7 cells. β-Actin is used as a loading control. **D**, BMP/TGFβ-SMAD signaling reporter (Ad-Bre-F-Luc/Ad-CAGA-G-Luc) assay in response to BMP/TGFβ alone or combination stimulation in MDA-MB-231, or MCF7, or MCF10A cells. The results are expressed as the mean \pm s.d, $n = 3$. Student's t test, NS, not

significant, $*P < 0.05$, $***P \leq 0.001$. **E**, Impaired response of BMP/SMAD signaling reporter (Ad-Bre-F-Luc) to BMP stimulation by TGF β is restored by TGF β type I receptor inhibitor SB431543 in MDA-MB-231 cells. The value is normalized to G-Luc activity. The results are expressed as the mean \pm s.d, $n = 3$. Student's t test, $**P \leq 0.01$, $***P \leq 0.001$.

MEK inhibitors specifically restore BMP signaling activity

To further explore other possible mechanism of TGF β suppression of SMAD1/5 signaling, we resorted to non-canonical TGF β signaling [19, 20]. Surprisingly, TGF β -induced prolonged ERK1/2 phosphorylation in MDA-MB-231 cells as shown in Figure 2A. TGF β also induced transient AKT phosphorylation suggesting temporary activation of PI3K signaling. Next, two selective small molecule MEK inhibitors (U0126 and PD98059) and PI3K inhibitor (LY294002) were utilized to investigate whether these pathways are involved in TGF β -induced inhibition of SMAD1/5 signaling in MDA-MB-231 cells. As shown in Figure 2B, U0126 or PD98059 treatment significantly enhanced BMP/SMAD1/5-dependent transcription activity, and overcame TGF β mediated inhibitory effect on SMAD1/5 signaling. However, LY294002 treatment had little effect on SMAD1/5 signaling (Figure 2C). Perturbation of TGF β 's activation of AKT and ERK1/2 had no effect on TGF β -SMAD3-dependent transcriptional reporter activity (Figure 2B, C).

For further conformation, we manipulated MAPK/ERK pathway activation independent of TGF β . In A431 and HN5 cells lines, where the EGF receptor (EGFR) is highly expressed [32], EGF stimulation significantly suppressed BMP-induced SMAD1/5 activation. Importantly, U0126 treatment ameliorated such suppression (Figure 2D). Additionally, BMP-induced SMAD1/5 activation in Ras-transformed 21D1 cells was significantly lower than in its parental MDCK cells. TGF β -induced inhibition of SMAD1/5 activity in 21D1 cells could be fully restored by U0126 (Figure 2E). Furthermore, using a doxycycline-inducible-Ras expression NIH3T3 fibroblasts (Figure 2F), similar results were obtained, except U0126 further amplified BMP-SMAD1/5 signaling in inducible NIH3T3 fibroblasts without doxycycline treatment, possibly due to leaky Ras expression in this system [23]. Collectively, these data established that MAPK/ERK activation abolishes BMP-SMAD1/5 activation, which could be reversed by small molecule MEK inhibitors.

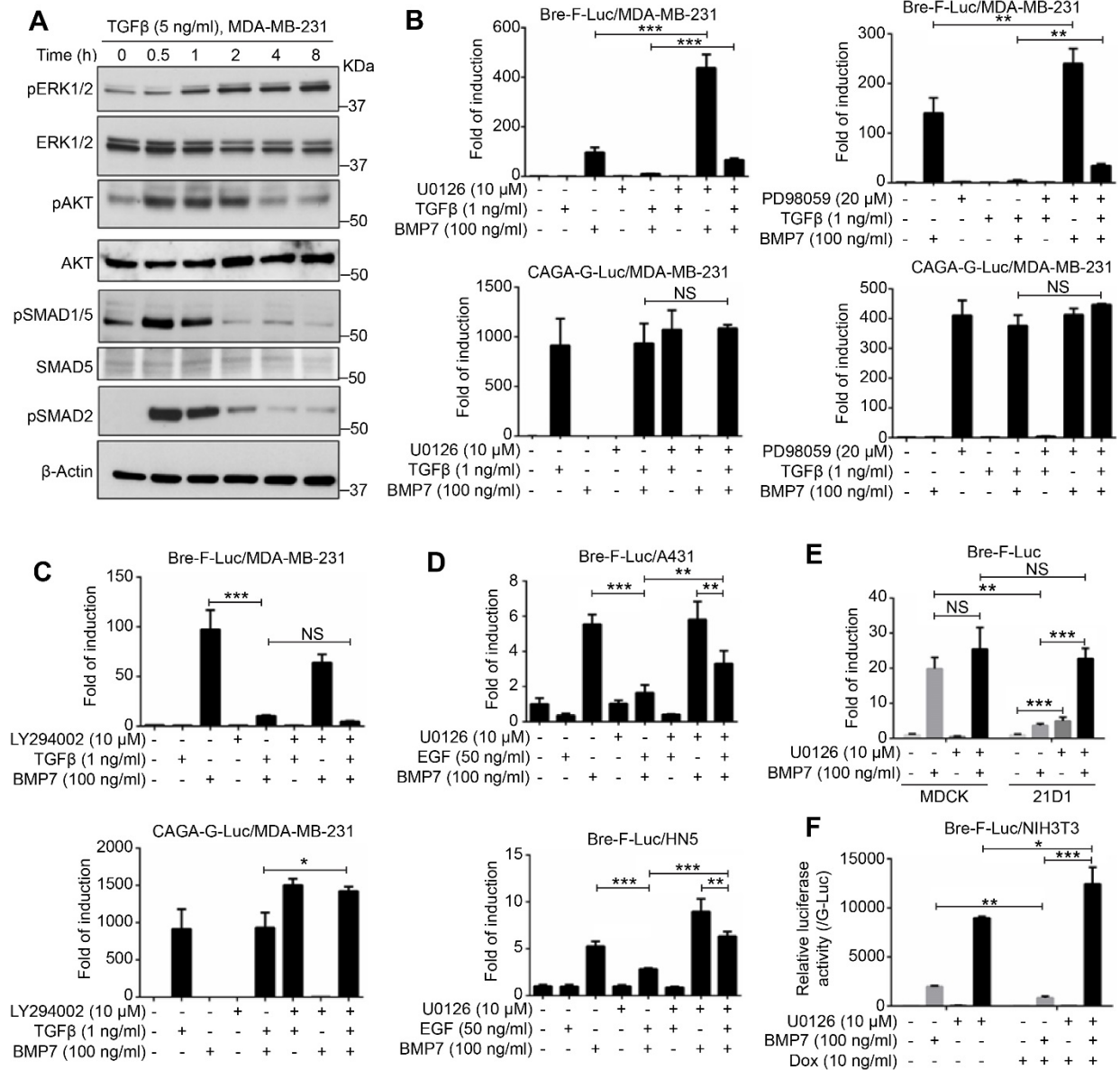


Figure 2. Prolonged ERK1/2 activation induced by TGF β mediated inhibition of BMP signaling. **A**, TGF β induced sustained ERK1/2 activation in MDA-MB-231 cells. The level of ERK1/2, SMAD1/5, SMAD2 phosphorylation (pERK1/2, pSMAD1/5, pSMAD2), ERK1/2, SMAD1/5, were determined by western blotting. β -Actin is used as a loading control. **B**, TGF β -inhibited SMAD1/5 signaling (Ad-Bre-F (firefly)-Luc assay) could be restored by administration of MEK inhibitors, U0126 or PD98059, in MDA-MB-231 cells. SMAD3 signaling (Ad-Bre-G (Gaussia)-Luc assay) is not affected. **C**, PI3K inhibitor LY294002 could not interfere the inhibition of TGF β on SMAD1/5 signaling (Ad-Bre-F-Luc assay) in MDA-MB-231 cells. SMAD3 signaling (Ad-Bre-G-Luc assay) is not affected. The results are expressed as the mean \pm s.d, $n = 3$. Student's t test, NS, not significant, $*P \leq 0.05$, $***P \leq 0.001$. **D**, U0126 restores EGF-inhibited SMAD1/5 signaling (Ad-Bre-F-Luc assay) in EGFR redundant cell lines, A431 and HN5.

The results are expressed as the mean \pm s.d, $n = 3$. Student's t test, $**P \leq 0.01$, $***P \leq 0.001$. **E**, U0126 restores SMAD1/5 signaling (Ad-Bre-F-Luc assay) inhibited by sustain activation of MAPK/ERK in 21D1 cells, which is derived from H-Ras transformed MDCK cells. The results are expressed as the mean \pm s.d, $n = 3$. Student's t test, NS, not significant, $**P \leq 0.01$, $***P \leq 0.001$. **F**, U0126 restores SMAD1/5 signaling (Ad-Bre-F-Luc assay) inhibited by induced activation of MAPK/ERK in doxycycline-inducible-Ras transformed NIH3T3 cells. The results are expressed as the mean \pm s.d, $n = 3$. Student's t test, $*P < 0.05$, $**P \leq 0.01$, $***P \leq 0.001$.

FK506 is a selective BMP-SMAD1/5 agonist in breast cancer cells

We screened for small molecule compounds that can work as a BMP-SMAD1/5 signaling agonist by testing a panel of FDA approved drugs and biologically active compounds for ability

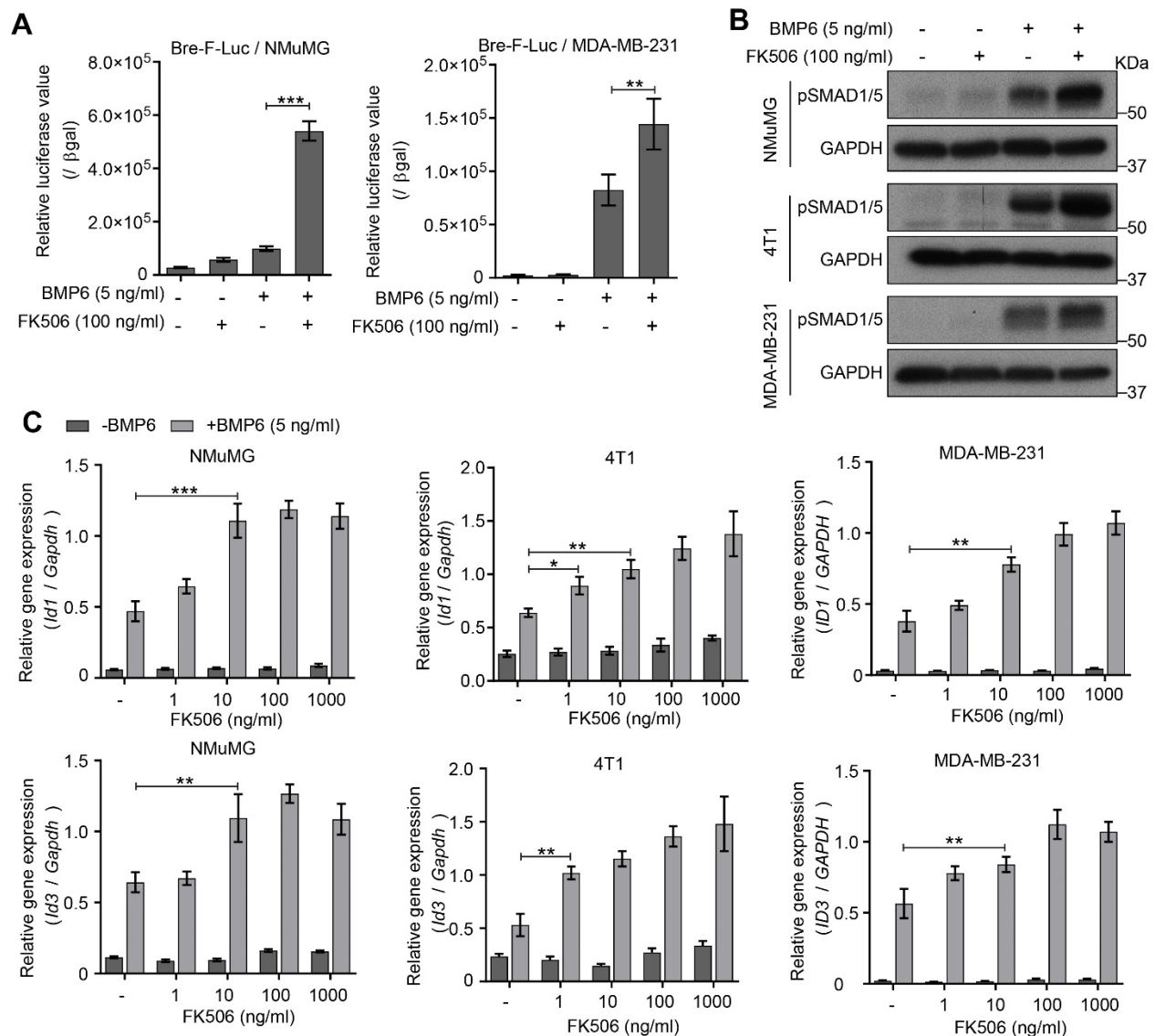


Figure 3. FK506 activates BMP signaling, but not TGF β signaling. **A**, FK506 enhances BMP signaling by Bre-F (firefly)-Luc reporter assay in NMuMG or MDA-MB-231 cells. The value is normalized to β gal activity. The results are expressed as the mean \pm s.d, $n = 3$. Student's t test, $**P \leq 0.01$, $***P \leq 0.001$. **B**, FK506 promotes BMP-mediated SMAD1/5 phosphorylation (pSMAD1/5) by western blotting in NMuMG, or 4T1, or MDA-MB-231 cells. GAPDH is used as a loading control. **C**, FK506 promotes expression of BMP signaling target genes, *Id1/3* in NMuMG, or 4T1 cells, *ID1/3* in MDA-MB-231 cells. *Gapdh* or *GAPDH* is used as an internal control. The results are expressed as the mean \pm s.d, $n = 3$. Student's t test, $*P < 0.05$, $**P \leq 0.01$, $***P \leq 0.001$.

to activate Bre-Luc transcriptional reporter activity in breast NMuMG cells (Figure S3A). The result showed that FK506 (Tacrolimus) is the most potent activator among tested compounds. Indeed, previous study had shown that FK506 can activate BMP signaling in endothelial cells by interfering with binding of negative regulator FKBP12 to BMP type I receptors [33]. We found that FK506 strongly promoted BMP signaling, as shown by increased Bre-Luc reporter activity (Figure 3A), SMAD1/5 phosphorylation (Figure 3B), and BMP/SMAD1/5 target genes (*ID1/3*) expression (Figure 3C) in several tested breast cell lines, NMuMG, 4T1, MDA-MB-231. FK506-mediated promotion of SMAD1/5 phosphorylation could be blocked by addition of a selective BMP type I receptor kinase inhibitor LDN193189 to cells (Figure S3B). We observed that the TGF β -SMAD3 pathway was not affected by FK506 treatment (Figure S3C, D, E). This was contrary what we expected as FKBP12 has been previously reported to bind to all TGF β family type I receptors [34]. Instead, we found that FK506 treatment slightly but significantly inhibited TGF β -SMAD3 signaling in NMuMG cells (Figure S3C, D, E). What's more, FK506 treatment had little effect on TGF β -induced phosphorylation of ERK1/2 in MDA-MB-231 cells (Figure S3F).

The combination of suboptimal dosages of U0126 and FK506 treatment exhibits synergistic effect on BMP signaling restoration *in vitro*

Given that U0126, PD98059 and FK506 were able to restore BMP signaling at 10 μ M, 20 μ M and 100ng/ml, respectively, this may raise a potential risk of side effects on clinical usage. Therefore, we questioned if lower concentration of U0126, or PD98059 or FK506 could synergistically amplify BMP signaling. Cells were incubated with various doses of these drugs in the presence of BMP. As a result, the fold of induction increased with U0126, PD98059 and FK506 treatment in a dose-dependent manner. Even 1 μ M U0126, 4ng/ml FK506 and 2 μ M PD98059 was able to

enhance SMAD1/5 signaling significantly (Figure 4A). Herein, we tried to combine U0126 and FK506 at their suboptimal concentrations to minimize the potential toxicity. As expected, combination of 1 μ M U0126 and 20 ng/ml FK506 amplified BMP-induced SMAD1/5 signaling synergistically. Meanwhile, the combination treatment exhibited synergistic effect on restoration of SMAD1/5 signaling in the presence of TGF β , to extent of higher than BMP single treatment. Again, TGF β -SMAD3 signaling was not influenced by U0126 or/and FK506 stimulation (Figure 4B) in the very same cells where BMP/SMAD1/5 signaling were enhanced.

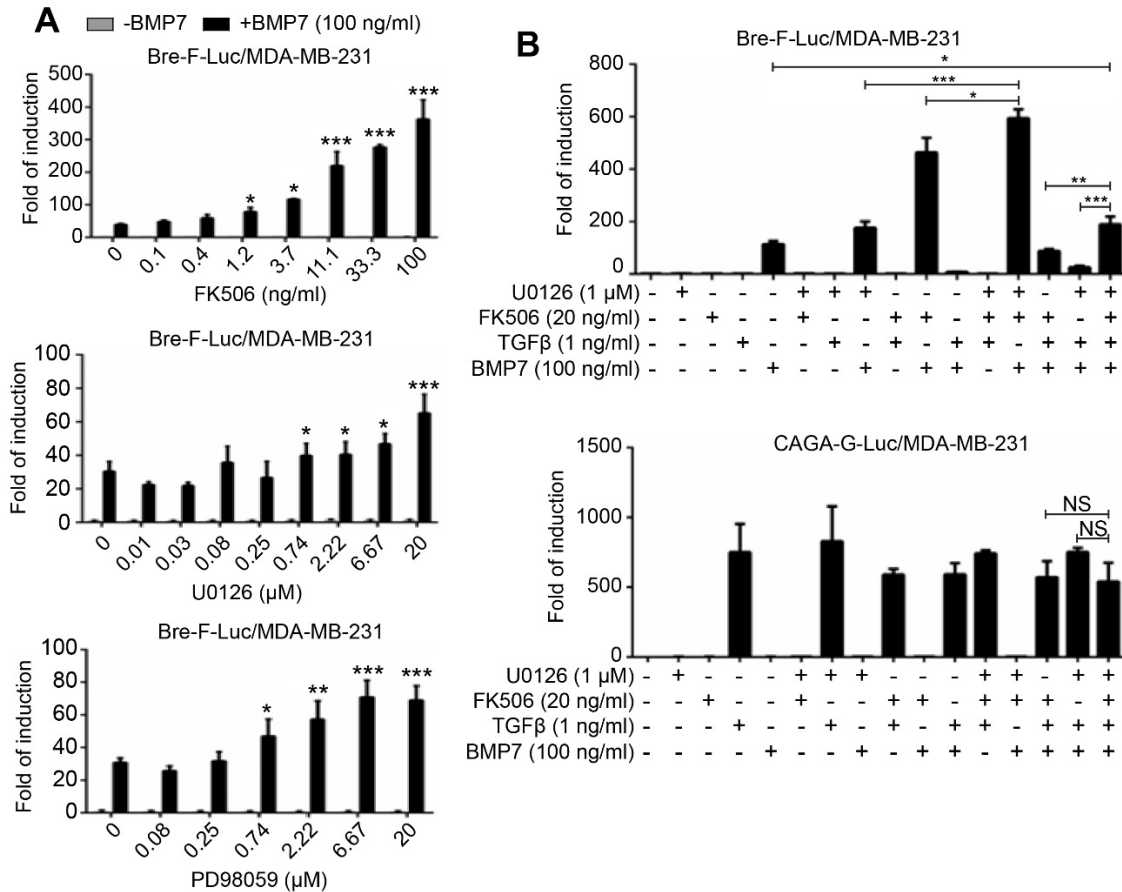


Figure 4. The combination treatment of suboptimal concentration of U0126 and FK506 exhibits synergistic effect on amplification of BMP signaling. **A**, FK506, or U0126, or PD98059 could restore SMAD1/5 signaling (Ad-Bre-F (firefly)-Luc assay) at low dose in MDA-MB-231 cells. The results are expressed as the mean \pm s.d, $n = 3$. Student's t test, $*P < 0.05$, $**P \leq 0.01$, $***P \leq 0.001$. **B**, U0126 and FK506 combination at suboptimal dose shows synergistic effect on amplification of BMP signaling (Ad-Bre-F-Luc assay) in MDA-MB-231 cells. SMAD3 signaling (Ad-CAGA-G (Gaussia)-Luc assay) is not affected. The results are expressed as the mean \pm s.d, $n = 3$. Student's t test, NS, not significant, $*P < 0.05$, $**P \leq 0.01$, $***P \leq 0.001$.

Combination treatment of suboptimal FK506 and U0126 suppresses MDA-MB-231 cells metastasis in zebrafish xenograft model

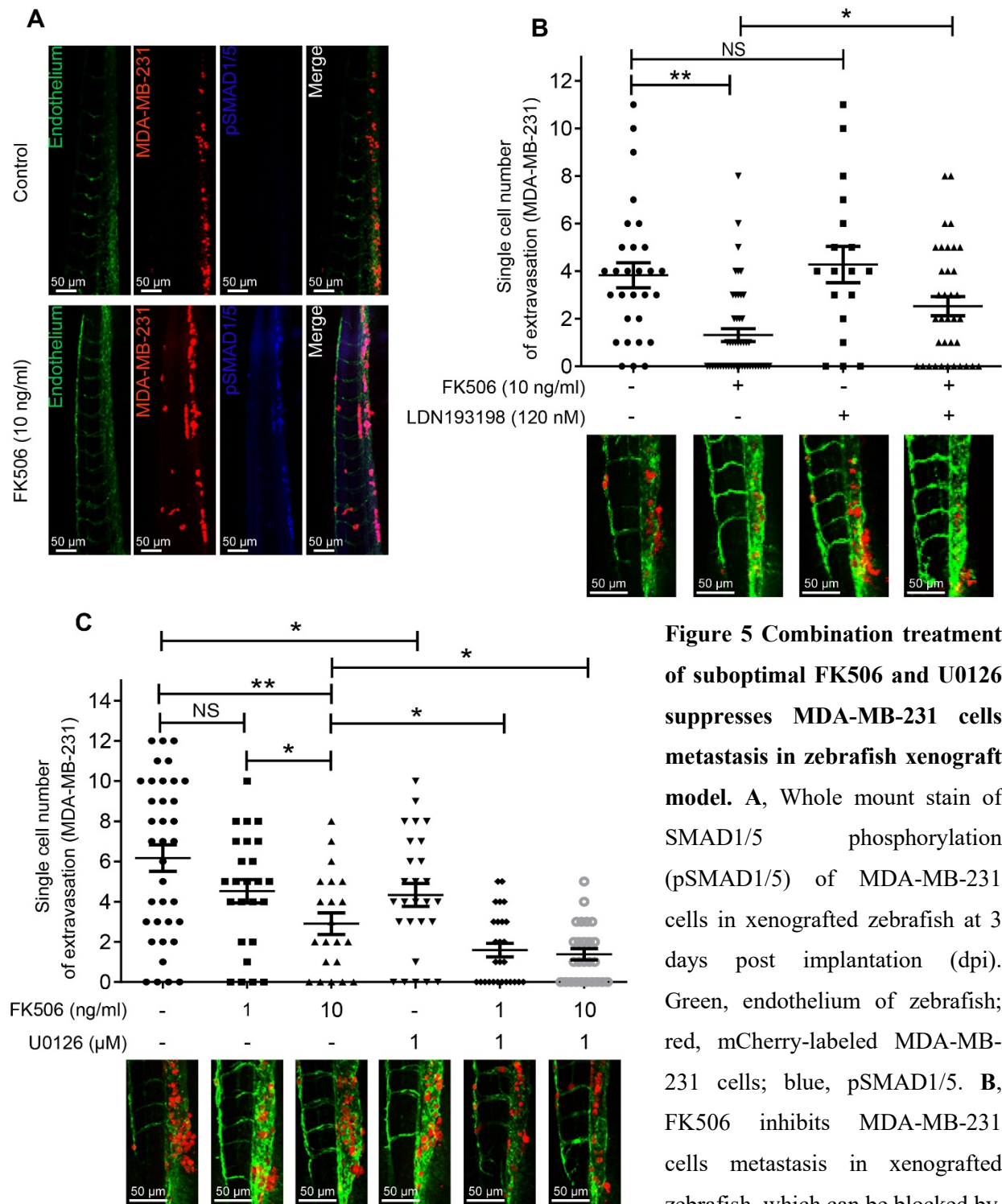


Figure 5 Combination treatment of suboptimal FK506 and U0126 suppresses MDA-MB-231 cells metastasis in zebrafish xenograft model. **A**, Whole mount stain of SMAD1/5 phosphorylation (pSMAD1/5) of MDA-MB-231 cells in xenografted zebrafish at 3 days post implantation (dpi). Green, endothelium of zebrafish; red, mCherry-labeled MDA-MB-231 cells; blue, pSMAD1/5. **B**, FK506 inhibits MDA-MB-231 cells metastasis in xenografted zebrafish, which can be blocked by

LDN193189. The graph shows the quantification of the number of intravasated cells in each embryonic body at 5dpi. The results are expressed as the mean \pm s.e.m, $n = 2$. Student's t test, NS, not significant, $*P$

< 0.05 , $**P \leq 0.01$. The panel shows the representative images. Green, *Fli:EGFP* labelled endothelium of zebrafish; red, mCherry-labeled MDA-MB-231 cells. C, Combination treatment of suboptimal FK506 and U0126 on MDA-MB-231 cells extravasation in xenografted zebrafish. The graph, panel description and statistical analysis are the same as described in B.

We wondered if enhanced BMP signaling functionally affects cancer cell migration *in vitro*. As shown in Figure S3A, FK506 treatment of MDA-MB-231 cells failed to suppress cell migration in wound healing assay. Using zebrafish xenograft model, mCherry labelled MDA-MB-231 cells were injected into zebrafish blood stream. Then zebrafish were subjected to FK506 treatment. Clearly activation of BMP signaling in MDA-MB-231 cells in xenografted zebrafish and in host zebrafish cells could be observed by whole mount immunostaining of pSMAD1/5 at 3dpi upon treatment with FK506 (Figure 5A). At 5dpi, the result showed FK506 decreased number of extravasated cells in the tail fin of zebrafish in a dose dependent manner (Figure S3B). Moreover, BMP type I receptor inhibitor LDN193189 reversed FK506-mediated inhibition of MDA-MB-231 cells metastasis (Figure 5B). These results suggest that activation of SMAD1/5 signaling in MDA-MB-231 and/or zebrafish host cells inhibits extravasation of these cells.

In view of U0126 and FK506 synergistically enhanced BMP signaling *in vitro*, xenografted zebrafish were challenged with combinational treatment to investigate if synergistic inhibition of breast cancer metastasis could be achieved. The result showed that U0126 and FK506 combination at suboptimal dose treatment led to dramatic inhibition of MDA-MB-231 cells metastasis. The number of extravasated cells was reduced by single U0126 treatment. This is probably due to the involvement of MAPK/ERK pathway in regulating cell migration [35]. When looking at the detail, 1 ng/ml FK506 treatment did not inhibit cancer cell metastasis significantly, whereas combining such low dose of FK506 (1 ng/ml) with U0126 displayed significant inhibition effect on MDA-MB-231 cell extravasation (Figure 5C).

FK506 and U0126 treatments suppress tumor self-seeding, liver and bone metastasis in mice model

Then, we sought to study synergistic effect of U0126 and FK506 alone or in combination on metastasis of MDA-MB-231 cells in mice model. G-Luc labelled MDA-MB-231 cells were infected with Ad-Bre-F-Luc reporter and then implanted orthotopically in the mammary fat pads of mice to monitor BMP signaling activation by IVIS imaging (Figure 6A). Mice were imaged and treated daily at 5dpi. The treatment dosages in mice were equivalent to the suboptimal

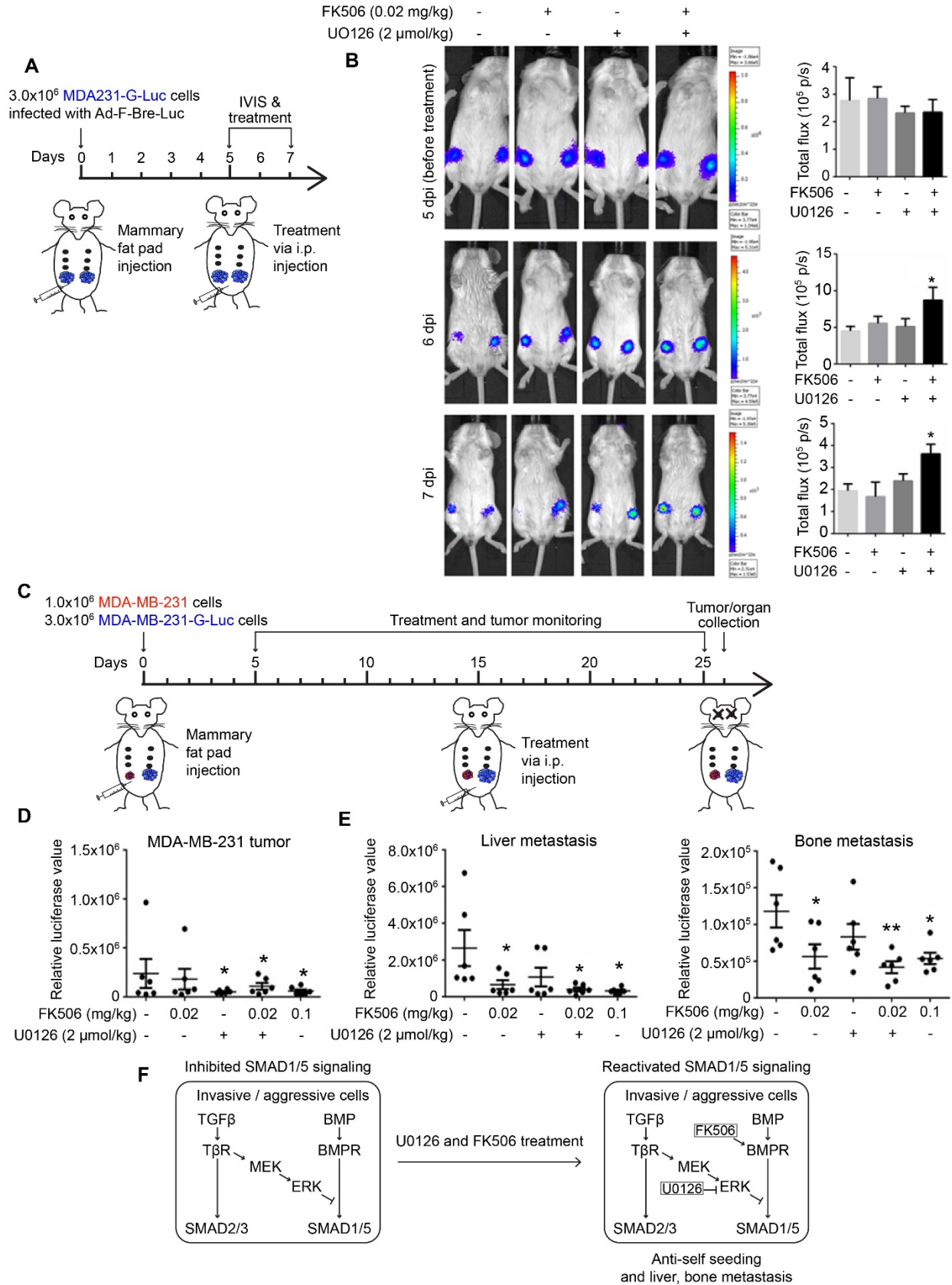


Figure 6. Combination treatment of FK506 and U0126 suppresses tumor self-seeding, liver and bone metastasis in mice. **A**, A diagram of BMP signaling detection experiment. MDA-MB-231-G (Gaussia)-Luc cells were infected with Ad-Bre-F-Luc two days before tumor implantation. 3×10^6 cells were orthotopically injected into the mammary fat pads of immunocompromised SCID mice (2 tumors/mouse contralaterally, 3 mice/group). Daily treatments started at day 5. 24h later, the reporter activity in the tumors was measured by IVIS Lumina imaging system following intraperitoneal (i.p.) injection with 150mg/kg D-Luciferin. **B**, Representative figures (left) and corresponding quantification of the signal in the mammary fat pad area (right) at 5 days post implantation (dpi, before treatment), 6dpi, 7dpi. The results are expressed as the mean \pm s.e.m., Student's *t* test, $*P < 0.05$. **C**, A diagram of breast cancer metastasis experiment. MDA-MB-231 and MDA-MB-231-G-Luc cells were orthotopically injected into mammary fat pads of SCID mice (2 tumors/mouse contralaterally, 6 mice/group) as shown. Daily treatment started at 5 dpi through i.p. injection. 3 weeks later, mice were sacrificed for tumor/organ collection. **D**, **E**, Unlabeled tumor (MDA-MB-231), liver and bone were lysed to determining G-Luc activity. The results are expressed as the mean \pm s.e.m, Student's *t* test, $*P < 0.05$, $**P \leq 0.01$. **F**, Working model. In normal cells, TGF β -SMAD2/3 signaling could not interfere BMP-SMAD1/5 signaling evidently. In invasive/aggressive cells, TGF β inhibits SMAD1/5 signaling via activation of MAPK/ERK pathway. Enhancing BMP-SMAD1/5 signaling by U0126 and FK506 combination treatment reduces cancer cell metastasis.

dosages *in vitro*. 24, 48h after (6, 7dpi), bioluminescent signals in U0126 and FK506 combination treated mice were higher than that in control, while single treatment of U0126 or FK506 had little effect on BMP-SMAD1/5 signaling. This result indicates efficient BMP signaling activation by the combination of suboptimal dosages of these two drugs *in vivo* (Figure 6B).

Next, mice were challenged with MDA-MB-231 and MDA-MB-231-G-Luc tumor cells in contralateral mammary fat pads respectively. Five days later, mice were treated as indicated and monitored for another three weeks (Figure 6C). U0126 or/and FK506 treatment had little effect on primary tumor growth (Figure S4A). Circulating tumor cells (CTCs) were analyzed by measuring the G-Luc activity of lysed blood sample. Interestingly, as shown in Figure S4B, CTCs number in different treatment groups were almost the same. We reasoned that the shedding of tumor cells into the circulation was mainly TGF β -regulated, which was not influenced by U0126/FK506 stimulation as indicated *in vitro*. Previously, CTCs were reported to re-infiltrate an established tumor, in a process termed “tumor self-seeding” [36]. MDA-MB-231

tumors were collected and lysed for detecting tumor self-seeding. The result indicated that U0126, U0126/FK506 combination and higher dose of FK506 treatments significantly reduced MDA-MB-231-G-Luc tumor cells self-seeding. This indicates BMP signaling efficiently suppressed tumor cells colonizing their tumors of origin. Lower dose of FK506 decreased tumor cell self-seeding as well but it was not statistically significant (Figure 6D). In addition, G-Luc activity in mice liver, lung, bone and brain were measured for evaluating intensity of cancer cell metastasis. Both liver and bone metastasis were reduced by low or high dose of FK506 compared to control group. Combination treatment of FK506 and U0126 at low dose further inhibited metastasis compared to low dose of FK506 treatment, even there is no significant difference. U0126 alone did not decrease liver and bone metastasis significantly (Figure 6E). The aforementioned treatments did not lead to significant reduction in lung and brain metastasis (Figure S4C), suggesting that restored BMP signaling plays a differential role in organ specific metastasis. Taken together, enhancement of BMP signaling activity *in vivo* by FK506 and U0126 treatment efficiently suppressed tumor self-seeding and distant organ metastasis especially to liver and bone (Figure 6F).

Discussion

In the present study we found that BMP-SMAD1/5 signaling could be abolished by TGF β in highly metastatic MDA-MB-231 cells, but to a lesser extent in non-invasive MCF7 cells and even weaker inhibitory effect in normal mammary epithelial MCF10A cell. Importantly, chemical activation of BMP-SMAD1/5 signaling inhibited extravasation and metastasis of breast cancer cells. Thus, the TGF β stimulatory effect on the invasion and metastasis of breast cancer cells is not only induced by directly activating SMAD2/3 as reported [2, 3], progressive loss or suppression of BMP-SMAD1/5 signaling by TGF β could be an important factor for metastatic cancer development (Figure 6F).

The underlying mechanism by TGF β inhibits SMAD1/5 activation relates to the its sustained activation of MAPK/ERK in aggressive MDA-MB-231 cells. Challenging of MDA-MB-231 cells with MEK inhibitors, resulted in a reactivation of SMAD1/5 signaling. Consistent with these finding we found that EGF-induced overactivation of MEK in A431 and HN5 cells that express high EGF receptor or activation of MEK by inducible overexpression of active Ras in NIH3T3 fibroblasts elicited a strong inhibition of BMP-SMAD1/5 signaling. Previously, multiple studies have reported BMP signaling and TGF β signaling can antagonize mutually in

physiological process, like tissue morphogenesis and organogenesis, and also in pathological setting, mainly fibrotic and cancerous diseases [5, 37]. This antagonism was reported to occur at the level of common mediator SMAD4 by competing with limiting amounts for this common mediator [17], MAPK/ERK inducing SMAD1/5 phosphorylation in linker region leading a SMAD1/5 cytoplasmic retention [38], by formation of SMAD1/5-SMAD2/3 mixed complexes [39], or by antagonism by a TGF β -induced target genes [40]. All these mechanisms occur downstream of pSMAD1/5, whereas we found that MEK pathway activation inhibits upstream of pSMAD1/5. TGF β -induction of inhibitory SMAD6 that could inhibit BMP-SMAD1/5 response, was found to play, if any, a minor role. Another possibility could be that MEK activation induces an activation of a phosphatase that triggers pSMAD1/5 dephosphorylation. Genetic screening efforts suggest a role for PPM1A phosphatase, which is under current investigation.

In parallel, we identified FK506 as an agonist of BMP-SMAD1/5 signaling in breast cancer cells. This finding is consistent with previous reports in which FK506 is shown to displace the negative regulator FKBP12 from BMP type I receptors [33]. It is not clear to us why FK506 did not activate TGF β -SMAD2/3 signaling in breast cancer cells as FKBP12 has been reported to interact with all TGF β family type I receptors [34]. A possibility is that FK506 has other interaction partners that negatively regulate pSMAD1/5. Multiple FK506 interaction partners have peptidyl-prolyl cis/trans isomerase activity, of which activity is inhibited by FK506 [41]. Peptidyl-prolyl cis/trans isomerase Pin1 was found to stabilize SMAD1 and promote BMP-SMAD1/5 signaling [42]. The slight inhibitory effect of FK506 that we observe may have been caused by the increased BMP-SMAD1/5 signaling antagonizing TGF β -SMAD3 signaling.

Consistent with notion that BMP-SMAD1/5 signaling has a tumor suppressive effect we found that a single dose of MEK inhibitor U0126 or FK506 alone inhibited breast cancer cell extravasation and metastasis. The FK506-induced inhibition of breast cancer cell extravasation was blocked by treatment with BMP type I receptor kinase inhibitor. This is consistent with the action of FK506 promoting BMP type I receptor kinase activity [33]. Of note, a low-dose FK506 was previously shown to activate BMP signaling and inhibit bladder cancer progression [43].

Importantly, we demonstrated a synergistic effect arose in restoring BMP signaling *in vitro/vivo* by combining U0126 and FK506 at suboptimal concentrations. Combination treatment by both small molecules synergistically suppressed breast cancer cells extravasation in zebrafish xenograft model and self-seeding and adaptation to distant organs to liver and bone in mice

(Figure 6F). This could be beneficial to patients who may suffer from high dose drug side effects. FK506 is being used as an immunosuppressant to prevent the rejection of organ transplants. Applying FK506 on cancer patient could weaken the host anti-tumor immunity. Even a good treatment response to anti-PD1 immunotherapy was reported in an advanced urothelial carcinoma patient with kidney transplant who received simultaneously FK506 treatment [44]. Recently, a FK506 analog FKVP without immunosuppressive activity was developed to enhance BMP-SMAD1/5 signaling [23]. We found that FKVP potently activated BMP/SMAD1/5 signaling in mammary epithelial NMuMG cells (Figure S5). Thus, FKVP could be explored as a potential FK506 substitute in treatment of cancer metastasis. For MEK inhibitor, several inhibitors have been approved by FDA, and could be tested as an alternative for U0126.

While U0126 and FK506 co-treatment achieved a strong inhibition of metastasis to liver and bone, no effect was observed for lung and brain metastasis. This suggests that the chemical reactivation of BMP signaling has a differential organ effect on breast cancer homing/reseeding. Different organs likely have different TGF β and BMP bioavailability and thereby influence breast cancer metastasis behavior, and ability of FK506 and U0126 combination to inhibit metastasis. It is a possibility that U0126 and/or FK506 do not reach each organ equally efficient. For example, both compounds may not pass the blood brain barrier efficiently and therefore no effect on brain metastasis by combination treatment was observed.

In conclusion, even though more detailed future studies are required, especially in a clinical setting, before clinical application of our observations can be initiated. Our study provides the feasibility that synergistic activation of BMP signaling by two small molecules at suboptimal dose can achieve a robust decrease in breast cancer metastasis.

Acknowledgements

This study was supported by Cancer Genomics Centre.NL (CGC.NL to PtD) and Chinese Scholarship Council (to JR). We thank Prof. Dr. Paschalis Sideras (Biomedical Research Foundation, Academy of Athens) for valuable discussions, and Maarten van Dinther and Midory Thorikay for technical assistance. We are grateful to Dr. A. Hinck and S. Vukicevic for gift of recombinant ligands and FKVP was kindly provided by Prof. Dr. Jun O. Liu (Johns Hopkins School of Medicine).

Author contributions

PtD and HZ designed and supervised the study. JR and YW conceived experiments and analyzed the majority of the data. JR YW, and JI performed the majority of experiments. JR and YW

prepared the figures, drafted, and wrote the manuscript, which was substantially proof-read, commented, and edited by all authors.

Conflicts of Interest

None of authors has conflict of interest.

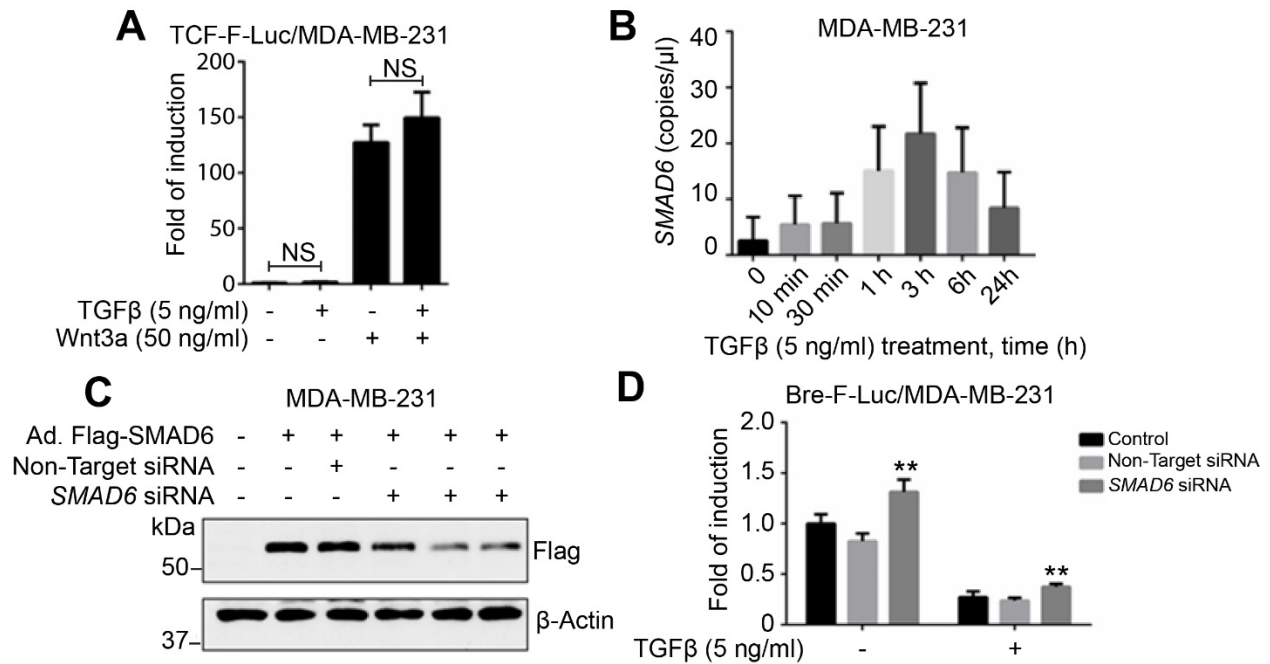
Reference

1. Obenauf AC, Massagué J. Surviving at a distance: Organ-specific metastasis. *Trends in Cancer* 2015;1:76-91.
2. Tsubakihara Y, Moustakas A. Epithelial-mesenchymal transition and metastasis under the control of transforming growth factor β . *Int J Mol Sci* 2018;19:3672.
3. Derynck R, Muthusamy BP, Saetern KY. Signaling pathway cooperation in TGF β -induced epithelial–mesenchymal transition. *Curr Opin Cell Biol* 2014;31:56-66.
4. Ren J, ten Dijke P. Bone Morphogenetic Proteins in the Initiation and Progression of Breast Cancer. *Bone Morphogenetic Proteins: Systems Biology Regulators*, Springer 2017, p.409-33.
5. Wakefield LM, Hill CS. Beyond TGF β : roles of other TGF β superfamily members in cancer. *Nat Rev Cancer* 2013;13:328-41.
6. Scheel C, Eaton EN, Li SH-J, Chaffer CL, Reinhardt F, Kah KJ, *et al.* Paracrine and autocrine signals induce and maintain mesenchymal and stem cell states in the breast. *Cell* 2011;145:926-40.
7. Ehnert S, Zhao J, Pscherer S, Freude T, Dooley S, Kolk A, *et al.* Transforming growth factor β 1 inhibits bone morphogenic protein (BMP)-2 and BMP-7 signaling via upregulation of Ski-related novel protein N (SnoN): possible mechanism for the failure of BMP therapy? *BMC Med* 2012;10:101.
8. Gao H, Chakraborty G, Lee-Lim AP, Mo Q, Decker M, Vonica A, *et al.* The BMP inhibitor Coco reactivates breast cancer cells at lung metastatic sites. *Cell* 2012;150:764-79.
9. Ren J, Smid M, Iaria J, Salvatori DC, van Dam H, Zhu HJ, *et al.* Cancer-associated fibroblast-derived Gremlin 1 promotes breast cancer progression. *Breast Cancer Res* 2019;21:1-19.
10. Eckhardt BL, Cao Y, Redfern AD, Chi LH, Burrows AD, Roslan S, *et al.* Activation of canonical BMP4-SMAD7 signaling suppresses breast cancer metastasis. *Cancer Res* 2020:canres.0743.2019.
11. Buijs JT, Henriquez NV, van Overveld PG, van der Horst G, Que I, Schwaninger R, *et al.* Bone morphogenetic protein 7 in the development and treatment of bone metastases from breast cancer. *Cancer Res* 2007;67:8742-51.

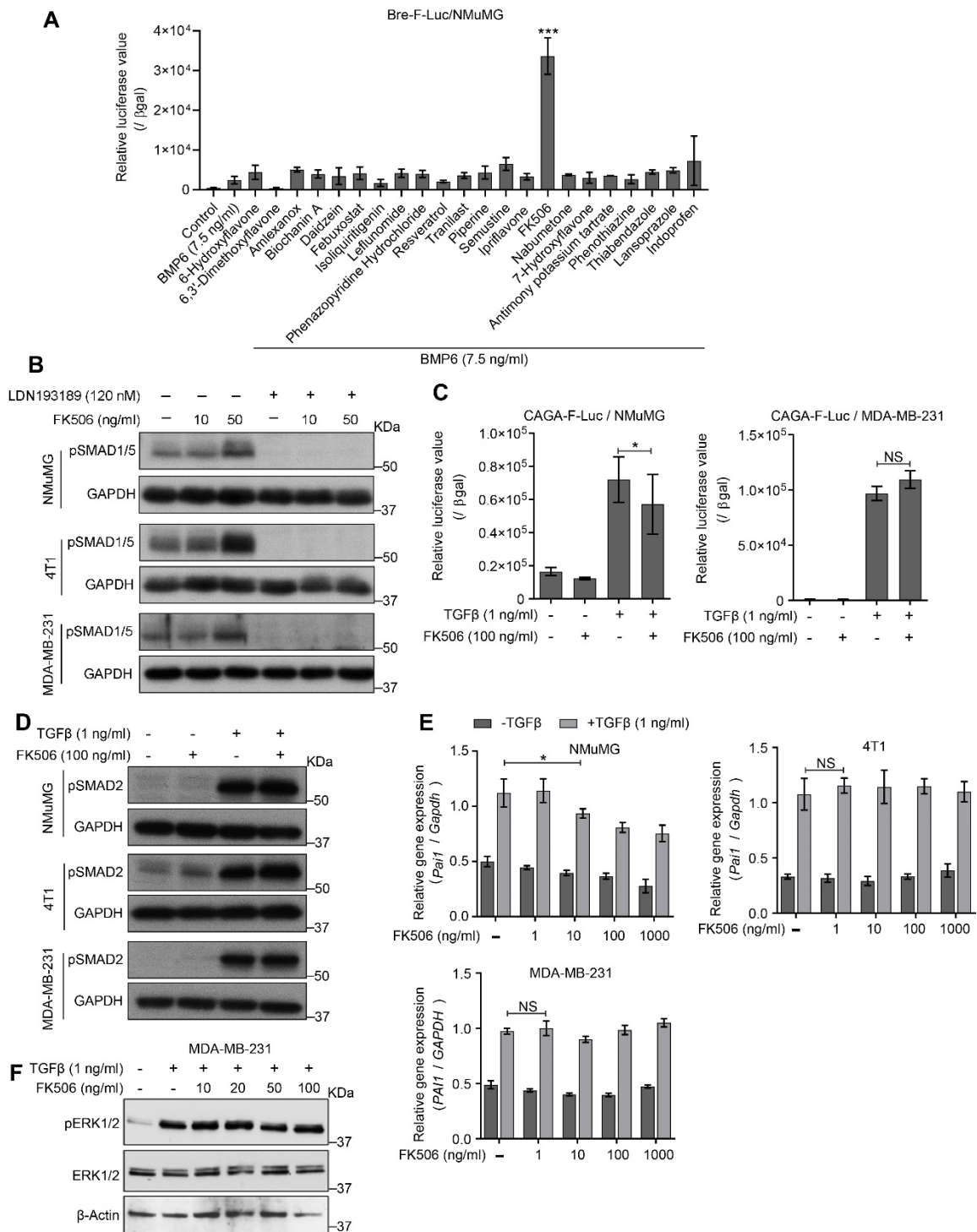
12. Naber HP, Wiercinska E, Pardali E, van Laar T, Nirmala E, Sundqvist A, *et al.* BMP-7 inhibits TGF β -induced invasion of breast cancer cells through inhibition of integrin β 3 expression. *Cell Oncol* 2012;35:19-28.
13. Shi Y, Massagué J. Mechanisms of TGF β signaling from cell membrane to the nucleus. *Cell* 2003;113:685-700.
14. Derynck R, Budi EH. Specificity, versatility, and control of TGF β family signaling. *Sci Signal* 2019;12:eaav5183.
15. Heldin CH, Moustakas A. Signaling receptors for TGF β family members. 2016;8:a022053.
16. Furtado MB, Solloway MJ, Jones VJ, Costa MW, Biben C, Wolstein O, *et al.* BMP/SMAD1 signaling sets a threshold for the left/right pathway in lateral plate mesoderm and limits availability of SMAD4. *Genes Dev* 2008;22:3037-49.
17. Candia AF, Watabe T, Hawley SH, Onichtchouk D, Zhang Y, Derynck R, *et al.* Cellular interpretation of multiple TGF β signals: intracellular antagonism between activin/BVg1 and BMP-2/4 signaling mediated by Smads. *Development* 1997;124:4467-80.
18. Gronroos E, Kingston IJ, Ramachandran A, Randall RA, Vizan P, Hill CS. Transforming growth factor β inhibits bone morphogenetic protein-induced transcription through novel phosphorylated Smad1/5-Smad3 complexes. *Mol Cell Biol* 2012;32:2904-16.
19. Zhang YE. Non-Smad signaling pathways of the TGF β family. *Cold Spring Harb Perspect Biol* 2017;9:a022129.
20. Mu Y, Gudey SK, Landström MJ. Non-Smad signaling pathways. *Cell Tissue Res* 2012;347:11-20.
21. Javelaud D, Mauviel A. Crosstalk mechanisms between the mitogen-activated protein kinase pathways and Smad signaling downstream of TGF β : implications for carcinogenesis. *Oncogene* 2005;24:5742.
22. Liu S, Iaria J, Simpson RJ, Zhu HJ, Signaling. Ras enhances TGF β signaling by decreasing cellular protein levels of its type II receptor negative regulator SPSB1. *Cell Commun Signal* 2018;16:10.
23. Hoppe PS, Coutu DL, Schroeder T. Single-cell technologies sharpen up mammalian stem cell research. *Nat Cell Biol* 2014;16:919-27.
24. Ren J, Liu S, Cui C, ten Dijke P. Invasive Behavior of Human Breast Cancer Cells in Embryonic Zebrafish. *J Vis Exp* 2017;122:e55459.
25. Miller FR, Soule HD, Tait L, Pauley RJ, Wolman SR, Dawson PJ, *et al.* Xenograft model of progressive human proliferative breast disease. *J Natl Cancer Inst* 1993;85:1725-32.
26. Cuny GD, Paul BY, Laha JK, Xing X, Liu JF, Lai CS, *et al.* Structure–activity relationship study of bone morphogenetic protein (BMP) signaling inhibitors. *Bioorg Med Chem Lett* 2008;18:4388-92.

27. Luwor RB, Hakmana D, Iaria J, Nheu TV, Simpson RJ, Zhu HJ. Single live cell TGF β signalling imaging: breast cancer cell motility and migration is driven by sub-populations of cells with dynamic TGF β -Smad3 activity. *Mol Cancer* 2015;14:50.
28. Luwor RB, Wang B, Nheu TV, Iaria J, Tsantikos E, Hibbs ML, *et al.* New reagents for improved *in vitro* and *in vivo* examination of TGF β signalling. *Growth Factors* 2011;29:211-8.
29. Persson U, Izumi H, Souchelnytskyi S, Itoh S, Grimsby S, Engström U, *et al.* The L45 loop in type I receptors for TGF β family members is a critical determinant in specifying Smad isoform activation. 1998;434:83-7.
30. Drabsch Y, He S, Zhang L, Snaar-Jagalska BE, ten Dijke P. Transforming growth factor- β signalling controls human breast cancer metastasis in a zebrafish xenograft model. *Breast Cancer Res* 2013;15:R106.
31. Afrakhte M, Morén A, Jossan S, Itoh S, Sampath K, Westermarck B, *et al.* Induction of inhibitory Smad6 and Smad7 mRNA by TGF β family members. *Biochem Biophys Res Commun* 1998;249:505-11.
32. Luwor R, Baradaran B, Taylor L, Iaria J, Nheu T, Amiry N, *et al.* Targeting Stat3 and Smad7 to restore TGF β cytotstatic regulation of tumor cells *in vitro* and *in vivo*. *Oncogene* 2013;32:2433-41.
33. Spiekerkoetter E, Tian X, Cai J, Hopper RK, Sudheendra D, Li CG, *et al.* FK506 activates BMPR2, rescues endothelial dysfunction, and reverses pulmonary hypertension. *J Clin Invest* 2013;123:3600-13.
34. Wang T, Li BY, Danielson PD, Shah PC, Rockwell S, Lechleider RJ, *et al.* The immunophilin FKBP12 functions as a common inhibitor of the TGF β family type I receptors. *Cell* 1996;86:435-44.
35. Chen H, Zhu G, Li Y, Padia RN, Dong Z, Pan ZK, *et al.* Extracellular signal-regulated kinase signaling pathway regulates breast cancer cell migration by maintaining slug expression. *Cancer Res* 2009;69:9228-35.
36. Kim MY, Oskarsson T, Acharyya S, Nguyen DX, Zhang XH, Norton L, *et al.* Tumor self-seeding by circulating cancer cells. *Cell* 2009;139:1315-26.
37. Dituri F, Cossu C, Mancarella S, Giannelli G. The interactivity between TGF β and BMP signaling in organogenesis, fibrosis, and cancer. *Cells* 2019;8:1130.
38. Kretschmar M, Doody J, Massagué J. Opposing BMP and EGF signalling pathways converge on the TGF β family mediator Smad1. *Nature* 1997;389:618-22.
39. Goumans MJ, Valdimarsdottir G, Itoh S, Lebrin F, Larsson J, Mummery C, *et al.* Activin receptor-like kinase (ALK)1 is an antagonistic mediator of lateral TGF β /ALK5 signaling. *Mol Cell* 2003;12:817-28.

40. Oshimori N, Fuchs E. Paracrine TGF β signaling counterbalances BMP-mediated repression in hair follicle stem cell activation. *Cell Stem Cell* 2012;10:63-75.
41. Rosen MK, Standaert RF, Galat A, Nakatsuka M, Schreiber SL. Inhibition of FKBP rotamase activity by immunosuppressant FK506: twisted amide surrogate. *Science* 1990;248:863-6.
42. Wang DJ, Zhi XY, Zhang SC, Jiang M, Liu P, Han XP, *et al.* The bone morphogenetic protein antagonist Gremlin is overexpressed in human malignant mesothelioma. *Oncol Rep* 2012;27:58-64.
43. Shin K, Lim A, Zhao C, Sahoo D, Pan Y, Spiekerkoetter E, *et al.* Hedgehog signaling restrains bladder cancer progression by eliciting stromal production of urothelial differentiation factors. *Cancer Cell* 2014;26:521-33.
44. Wu C K, Juang G D, Lai HC. Tumor regression and preservation of graft function after combination with anti-PD-1 immunotherapy without immunosuppressant titration. *Ann Oncol* 2017;28:2895-6.
45. Peiffer BJ, Qi L, Ahmadi AR, Wang Y, Guo Z, Peng H, *et al.* Activation of BMP signaling by FKBP12 ligands synergizes with inhibition of CXCR4 to accelerate wound healing. *Cell Chem Biol* 2019;26:652-61.

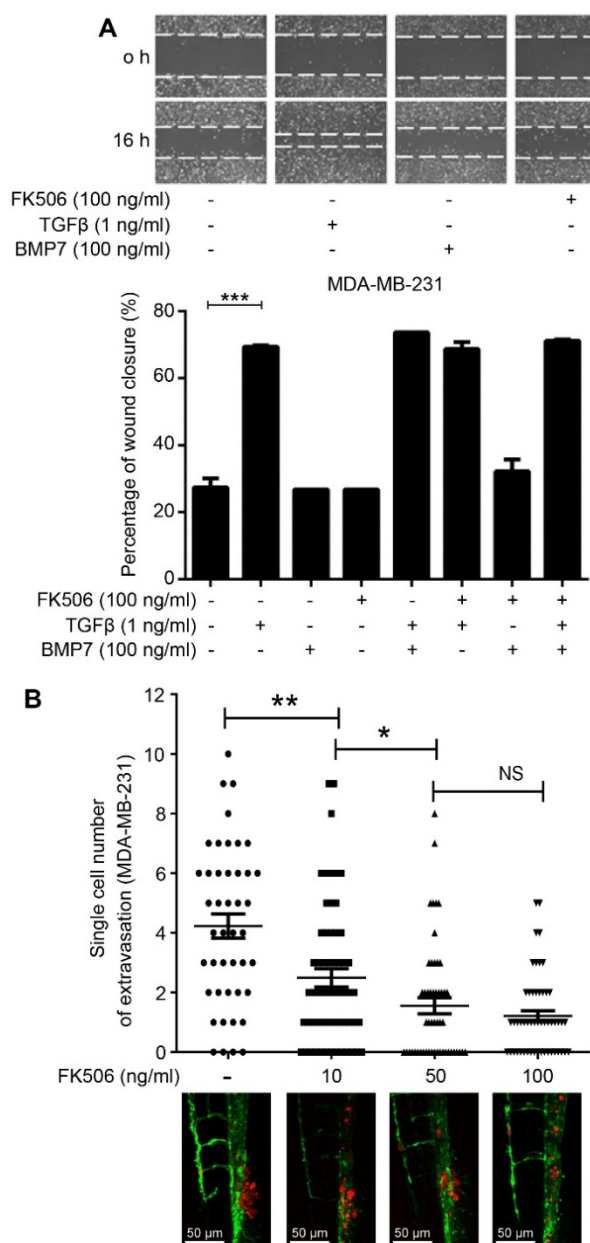


Supplementary Figure 1, related to Figure 1. **A**, Wnt signaling transcriptional reporter (Ad-TCF-F (firefly)-Luc) assay in response to TGFβ or Wnt3a alone, or combination stimulation in MDA-MB-231 cells. The results are expressed as the mean ± s.d, n = 3. Student's t test, NS, not significant. **B**, Droplet digital PCR to determine the kinetic expression level of *SMAD6* to TGFβ stimulation (5 ng/ml) in MDA-MB-231 cells. The results are expressed as the mean ± s.d, n = 3. **C**, siRNA-mediated knockdown of *SMAD6* was measured by western blotting. *SMAD6* overexpressed MDA-MB-231 cells were seeded into 6-well plate and transfected with indicated amount of *SMAD6* siRNA. β-Actin was used as an internal control. **D**, TGFβ-inhibited *SMAD1/5* signaling (Ad-Bre-F-Luc) could be slightly restored by *SMAD6* knockdown in MDA-MB-231 cells. The value is normalized to G-Luc activity. The results are expressed as the mean ± s.d, n = 3. Student's t test, ** $P \leq 0.01$.

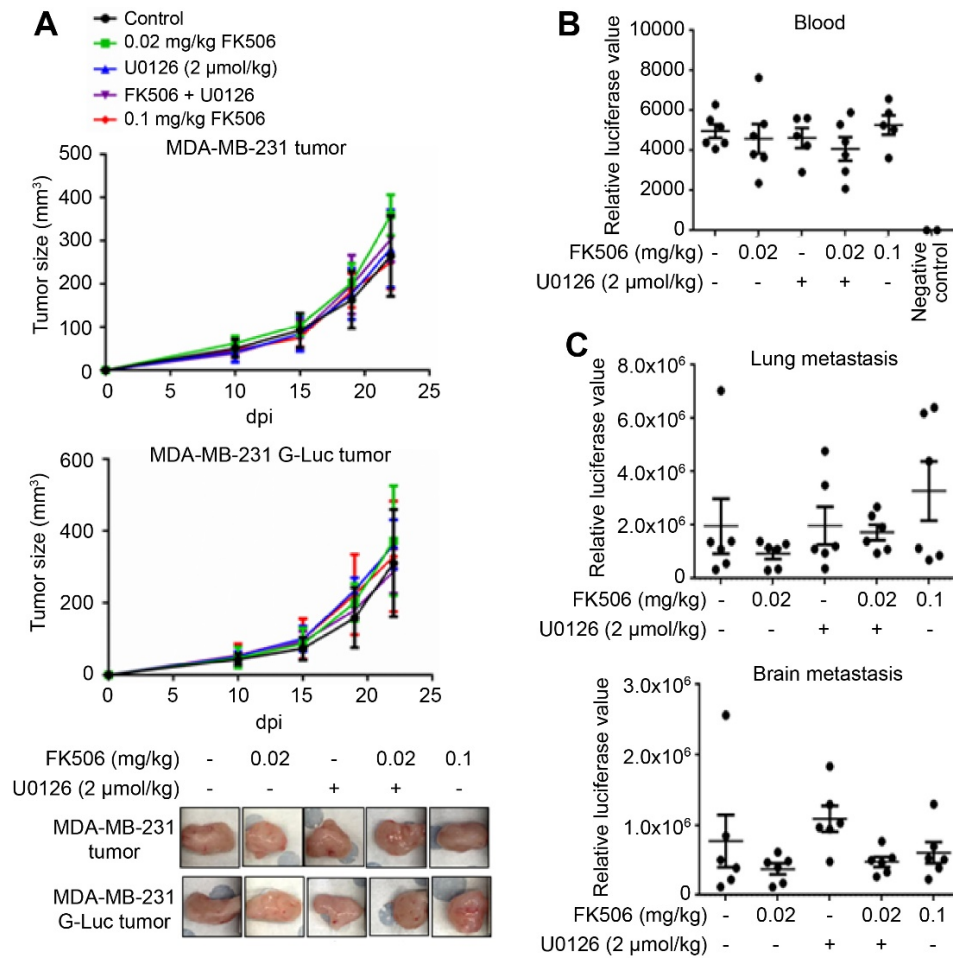


Supplementary Figure 2, related to Figure 3. A, BMP agonist screening in a panel of FDA-approved drugs and bioactive compounds by using Bre-F(firefly)-Luc transcriptional reporter assay. The value is normalized to βgal activity. The results are expressed as the mean ± s.d, n = 3. Student's *t* test, ****P* ≤ 0.001. **B**, BMP type I receptors inhibitor LDN193189 blocks enhancement of FK506 on SMAD1/5 phosphorylation (pSMAD1/5). GAPDH is used as a loading control. Cells were maintained in 10% serum

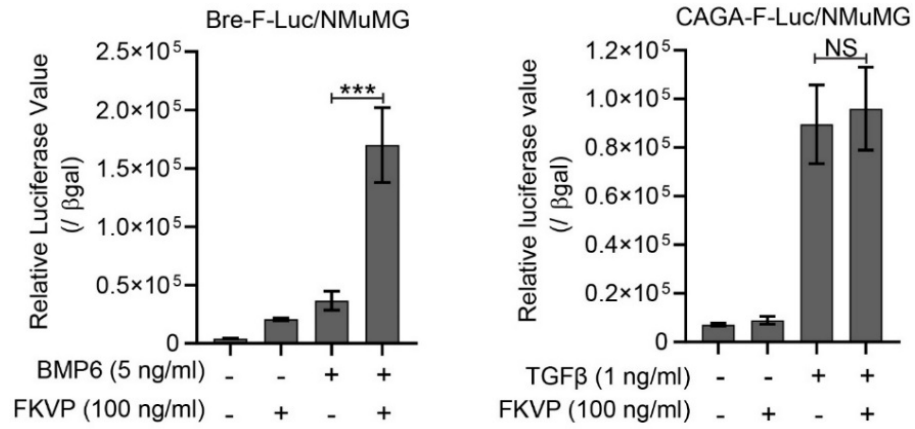
medium when receiving treatment. **C**, CAGA-F-Luc reporter assay in NMuMG or MDA-MB-231 cells. The results are expressed as the mean \pm s.d, n = 3. Student's t test, NS, not significant, $*P \leq 0.05$. **D**, Western blotting to detect SMAD2 phosphorylation (pSMAD2) in NMuMG, or 4T1, or MDA-MB-231 cells after FK506 or/and TGF β treatment. GAPDH is used as a loading control. **E**, Expression of TGF β signaling target genes, *Pail* in NMuMG, or 4T1 cells, *PAIL* in MDA-MB-231 cells after FK506 or/and TGF β treatment. *Gapdh* or *GAPDH* is used as an internal control. The results are expressed as the mean \pm s.d, n = 3. Student's t test, NS, not significant. $*P \leq 0.05$. **F**, FK506 fails to inhibit TGF β -mediated activation of MAPK/ERK signaling. ERK1/2 phosphorylation (pERK1/2) was determined by western blotting. β -Actin is used as a loading control.



Supplementary Figure 3, related to Figure 5. A, Wound healing migration assay of MDA-MB-231 cells. Images were taken at 0 and 16h after scratch. The graph shows the percentage of wound closure. The results are expressed as the mean \pm s.d, n = 3. Student's t test, $***P \leq 0.001$. **B**, Treatment of FK506 on MDA-MB-231 cells invasion/extravasation in xenografted zebrafish at different doses. The graph shows the quantification of the number of extravasated cells in each embryonic body at 5 days after implantation (dpi). The results are expressed as the mean \pm s.e.m, n = 2. Student's t test, NS, not significant, $*P < 0.05$, $**P \leq 0.01$. The panel shows the representative images. Green, *Fli:EGFP* labelled endothelium of zebrafish; red, mCherry-labeled MDA-MB-231 cells.



Supplementary Figure 4, related to Figure 6. A, FK506 and U0126 combination treatment has limited effect on primary tumor growth. Graph shows tumor volume of unlabeled MDA-MB-231 and MDA-MB-231-G (Gaussia)-Luc at the indicated days after treatment (dpi). The panel is representative figures of tumors in different groups at day 25 when the mice were sacrificed. **B,** G-Luc value in 5 μ l of the blood samples of sacrificed mice. Blood from mice without MDA-MB-231-G-Luc tumor implantation was used as a negative control (NC). **C,** Lungs and brains from sacrificed mice were collected and lysed for metastasis analysis by G-Luc activity assay.



Supplementary Figure 5. FK506 analog FKVP shows significant potential in enhancing BMP signaling by Bre-F(firefly)-Luc reporter assay in NMuMG cells, while TGFβ signaling is not affected by CAGA-F(firefly)-Luc assay. The results are expressed as the mean ± s.d, n = 3. Student's t test, NS, not significant, *** $P \leq 0.001$.

Chapter 5

JUNB Governs a Feed-forward Network of TGF β Signaling that Aggravates Breast Cancer Invasion

Anders Sundqvist*, Masato Morikawa*, **Jiang Ren**, Eleftheria Vasilaki,
Natsumi Kawasaki, Mai Kobayashi, Daizo Koinuma, Hiroyuki Aburatani,
Kohei Miyazono, Carl-Henrik Heldin, Hans van Dam, and Peter ten Dijke

Nucleic acids research 2018, 46(3): 1180–1195.

*These authors contributed equally

Abstract

It is well established that transforming growth factor- β (TGF β) switches its function from being a tumor suppressor to a tumor promoter during the course of tumorigenesis, which involves both cell-intrinsic and environment-mediated mechanisms. We are interested in breast cancer cells, in which SMAD mutations are rare and interactions between SMAD and other transcription factors define pro-oncogenic events. Here, we have performed chromatin immunoprecipitation (ChIP)-sequencing analyses which indicate that the genome-wide landscape of SMAD2/3 binding is altered after prolonged TGF β stimulation. *De novo* motif analyses of the SMAD2/3 binding regions predict enrichment of binding motifs for activator protein (AP)1 in addition to SMAD motifs. TGF β -induced expression of the AP1 component JUNB was required for expression of many late invasion-mediating genes, creating a feed-forward regulatory network. Moreover, we found that several components in the WNT pathway were enriched among the late TGF β -target genes, including the invasion-inducing WNT7 proteins. Consistently, overexpression of WNT7A or WNT7B enhanced and potentiated TGF β -induced breast cancer cell invasion, while inhibition of the WNT pathway reduced this process. Our study thereby helps to explain how accumulation of pro-oncogenic stimuli switches and stabilizes TGF β -induced cellular phenotypes of epithelial cells.

Keywords: Breast cancer metastasis, JUNB, TGF β , WNT7B

Introduction

The signaling pathways triggered by the transforming growth factor β (TGF β) family members control a wide range of cellular processes. TGF β signals via heterotetrameric complexes of type I and type II serine/threonine kinase receptors. The activated receptor complex initiates intracellular signaling by phosphorylating receptor-regulated (R-) SMAD proteins (SMAD2 and SMAD3). The activated R-SMADs form heteromeric complexes with SMAD4, which accumulate in the nucleus and control expression of target genes [1-3]. However, SMADs have relatively weak affinity for DNA and in many cases interact with so called master transcription factors to achieve high affinity and target-gene specificity [4, 5]. These interactions alter the intensity, duration and specificity of the TGF β -signaling response, in a context- and cell-type-specific manner [6-8].

TGF β plays a dual role in tumor progression. In normal or premalignant cells TGF β functions as a tumor suppressor by inhibiting cell proliferation and inducing apoptosis. However, in late stages of tumor development, TGF β instead acts as a tumor promoter by stimulating cell motility, invasion, metastasis and tumor stem cell maintenance. This is reflected by the observation that specific types of cancers are insensitive to the cytostatic effect of TGF β due to inactivation of core components in the TGF β pathway [9, 10]. On the other hand, in breast cancer and certain other cancers, defects in the TGF β /SMAD signaling itself are relatively uncommon; instead tumor promoting effects of TGF β /SMAD signaling dominates (reviewed in [11, 12]). In line with this, TGF β is frequently overexpressed in breast cancer and its expression correlates with poor prognosis and metastasis [13]. The influence of TGF β on tumor growth is also affected by crosstalk between the TGF β signaling pathway and a wide variety of signal transduction pathways. For example, the Ras-MAP-kinase (MAPK) pathway [14] regulates cell migration and invasion synergistically with TGF β [8, 11, 15, 16]. Interestingly, transcriptome-wide analysis of mouse primary hepatocytes treated with TGF β revealed that the early TGF β response was characterized by expression of genes involved in cell cycle arrest and apoptosis, while the late gene signature was associated with an aggressive and invasive tumor phenotype that effectively identified clinical relevant subgroups of hepatocellular carcinoma [17].

We previously reported that prolonged stimulation with TGF β induces mesenchymal and invasion-associated genes through interaction between SMAD and activator protein (AP)1 components, in particular JUNB [16]. AP1 transcription factors are targeted by many signal

transduction pathways and regulate a magnitude of cellular processes, including cell proliferation, survival, differentiation, invasion and carcinogenesis, depending on their dimer composition [18-20]. SMAD and AP1 members interact at different levels. For example, TGF β induces the expression of specific AP1 components and reporter assays suggested that the AP1 components JUN and JUNB cooperate with SMAD2/3 to activate TGF β -induced promoters regulated by AP1 binding sites [21, 22], while antagonizing DNA binding of the same SMADs on promoters controlled by SMAD binding sites [23]. However, little is known about the SMADs and AP1 crosstalk at the genome-wide level.

Identification and characterization of signaling molecules that switch TGF β /SMAD signaling from tumor suppression to tumor promotion is critical for the development of therapies targeting the TGF β pathway [24]. To identify SMAD complexes and target genes involved in tumor progression on a genome-wide scale, we performed SMAD2/3 chromatin immunoprecipitation followed by next-generation sequencing (ChIP-seq) and RNA sequencing analyses, both early and late after TGF β stimulation. Our results indicate that most of SMAD2/3 is redirected to different sites on the genome after prolonged TGF β treatment. *De novo* motif analyses predicted enrichment of binding motifs for AP1 and SMAD, or the SMAD Binding Element (SBE) consensus sequence CAGA, in SMAD2/3 binding regions. Moreover, our results suggest that TGF β -induced expression of JUNB via a positive feed-forward mechanism enables a switch of the early TGF β transcriptional program to a late, invasion-mediating program. Furthermore, we found that genes related to WNT signaling pathways are enriched among the late TGF β -target genes. Consistently, modulation of the WNT signaling pathway aggravated TGF β -induced breast cancer cell invasion and metastasis. Our study thereby helps to explain how accumulation of oncogenic stimuli switches TGF β responsiveness in epithelial cells.

Materials and methods

Cell culture

Human breast epithelial MCF10A MII cells were obtained from Dr Fred Miller (Barbara Ann Karmanos Cancer Institute, Detroit, USA) and maintained at 37°C and 5% CO₂ in DMEM/F12 (Gibco), supplemented with 5% fetal bovine serum (FBS) (HyClone), 20 ng/ml epidermal growth factor (EGF) (PeproTech), 100 ng/ml cholera toxin (Sigma-Aldrich), 0.5 μ g/ml hydrocortisone (Sigma-Aldrich), 10 μ g/ml insulin (Sigma-Aldrich). MCF10A MII cells are derived from MCF10A cells by transformation with Ha-Ras. Human breast cancer MDA-MB-

231 cells and human lung cancer A549 cells were obtained from ATCC and maintained at 37°C and 5% CO₂ in DMEM (Sigma-Aldrich), supplemented with 10% FBS (Bio West). Breast cancer Hs578T and BT-549 cells were obtained from ATCC, and maintained as recommended. Briefly, Hs578T cells were cultured at 37°C and 5% CO₂ in DMEM (Gibco) supplemented with 10% FBS (HyClone), and 10 μ g/ml insulin (Gibco), and BT-549 cells were maintained in RPMI-1640 (Gibco), supplemented with 10% FBS (HyClone), and 0.023 IU/ml insulin (Gibco).

Lentiviral transduction

MCF10A MII cells were infected with lentivirus encoding an shRNA sequence against human *JUNB* (TRCN0000014943, TRCN0000014946, TRNC0000014947) selected from the MISSION shRNA library (Sigma-Aldrich). As a control an empty pLKO vector was used. Virus transduction was performed overnight and the infected cells were selected using culture medium containing Puromycin.

Reagents and antibodies

Recombinant human TGF β 3 (a generous gift of Dr K. Iwata, OSI Pharmaceuticals, Inc, New York, USA, or purchased from R&D Systems) was used for stimulation of cells. Epithelial cells that express betaglycan respond similarly to the three TGF β isoforms. Recombinant human WNT7A was from PeproTech. The TGF β type I kinase receptor (TGF β RI) inhibitor SB505124 (ALK5i) and IWP-2 (WNTi), which is an inhibitor of WNT processing and secretion, were purchased from Sigma-Aldrich and Merck Millipore, respectively. Puromycin was purchased from Invivogen and used at a concentration of 0.5 μ g/ml. For siRNA-mediated knockdown, Dharmacon On Target Plus pools of four oligonucleotides (GE Healthcare Life Sciences) was transfected using siLentFect (Bio-Rad) transfection reagent according to manufacturer's instructions at 25 nM final concentration.

Antibodies against the following proteins were used: ERK1/2 (4695, Cell Signaling Technology), phospho-Thr202/Tyr204-ERK1/2 (4370, Cell Signaling Technology), FN1 (F3648, Sigma-Aldrich), JUN (9164, Cell Signaling Technology), JUNB (sc-8051, Santa Cruz), FOS (sc-52, Santa Cruz), FOSB (2251, Cell Signaling Technology), FOSL1 (sc-22794, Santa Cruz), FOSL2 (sc-604, Santa Cruz), MYC (sc-40, Santa Cruz), SMAD2/3 (610843, BD Transduction Laboratories), phospho-Ser465/467-SMAD2 (3108, Cell Signaling Technology), phospho-Ser423/425-SMAD3 (9520, Cell Signaling Technology), SMAD4 (sc-7966, Santa Cruz), α -

TUBULIN (sc-8035, Santa Cruz) and WNT7B (AF3460, R&D Systems). A custom-made JUND antibody was raised in chicken against a synthetic polypeptide CQLLPQHQPAY, corresponding to the unique C-terminal part of JUND (Immune Systems).

Plasmid construction

WNT7A and WNT7B cDNAs were kindly provided by Dr Brad St. Croix. For stable cell line establishment, cDNAs were cloned into an episomal expression vector pPyCAG-IRES-Puro, which contains polyoma Ori and can be propagated episomally in cells [25].

Western blot analysis

MCF10A MII cells were seeded in 6-well-plates (2.5×10^5 cells/well), and starved the following day for 16 h in 0.2% FBS, and cells were then stimulated with 5 ng/ml of TGF β 3 for indicated time-periods. Cells were lysed in 2 \times SDS Laemmli sampler buffer (5% SDS, 25% glycerol, 150 mM Tris-HCl pH 6.8, 0.01% bromophenol blue, 100 mM dithiothreitol (DTT)). Samples were separated by SDS-PAGE, blotted onto nitrocellulose membrane (Amersham Protran, GE Healthcare Life Science), and the chemiluminescent signal was detected using the Immobilon Western kit (Merck Millipore).

3D spheroid collagen invasion assay

One thousand cells, of the indicated cell line, were trypsinized, re-suspended in medium containing 2.4 mg/ml methylcellulose (Sigma-Aldrich) and added into each well of a U-bottom 96-well-plate (Greiner Bio One) allowing the formation of one spheroid per well. Two days after plating, a U-bottom 96-well-plate was coated with neutralized bovine collagen-I (PureCol, Advanced BioMatrix) according to manufacturer's protocol. Spheroids were harvested and embedded in a 1:1 mix of neutralized collagen and medium supplemented with 12 mg/ml of methylcellulose and allowed to polymerize on the top of the neutralized collagen. TGF β 3 and/or recombinant WNT7A were directly added to the embedding solution. After polymerization, medium supplemented with 1.6% FBS was added to the top of the collagen. SB505124 and IWP-2 were added in the medium. Pictures were taken at day 0 and day 2 after embedding and quantified by measuring the area occupied by cells using Adobe Photoshop CS3 software.

Zebrafish maintenance

This study was approved by The Institutional Committee for Animal Welfare of the Leiden University Medical Center (LUMC). Zebrafish and embryos were maintained according to standard procedures. The transgenic fish line Tg (*fli1:EGFP*) was used in this study as described before [26, 27]. All experiments were performed in accordance with approved guidelines and regulations.

Embryo preparation and tumor cell implantation

Tg (*fli1:EGFP*) zebrafish embryos were dechorionated at 2 days post fertilization (dpf). Single cell suspensions of mCherry labelled MCF10A MII, MDA-MB-231 or A549 cells were re-suspended in PBS and kept at 4°C before injection. Cell suspensions were loaded into borosilicate glass capillary needles (1 mm O.D. \times 0.78 mm I.D.; Harvard Apparatus). Injections were performed with a Pneumatic Picopump and a manipulator (WPI). Dechorionated embryos were anaesthetized with 0.003% tricaine (Sigma) and mounted on 10-cm Petri dishes coated with 1% agarose. Approximately 400 cells were injected at the duct of Cuvier (DOC). Injected zebrafish embryos were maintained at 34°C. All the experiments were repeated at least two times and at least 30 embryos were analyzed per group.

Microscopy and analysis

Six days post infection (dpi) embryos were fixed with 4% paraformaldehyde at 4°C overnight. Fixed embryos were analyzed and imaged in PBS with a Leica SP5 STED confocal microscope (Leica). The numbers of clusters formed in caudal hematopoietic tissue (CHT) of each embryo were counted. Confocal stacks were processed for maximum intensity projections with matched software LAS AF Lite. Brightness and contrast of images were adjusted as well.

RNA isolation, cDNA synthesis and quantitative real time-PCR (qRT-PCR)

Total RNA was isolated by RNeasy Kit (Qiagen). cDNA was prepared by using iScript kit (Bio-Rad) using 0.5 μ g of total RNA, according the manufacturer's instructions. The cDNA samples were diluted 10 times in water. qRT-PCR was performed using KAPA SYBR FAST qPCR kit Master Mix (KAPA Biosystems) and BioRad CFX96 real-time PCR detection system according the manufacturer's instructions. qRT-PCR reactions were performed as follow: one cycle of 95°C for 10 min followed by 40 cycles of 95°C for 15 s and 60°C for 30 s, followed by one cycle of 95°C for 15 s and 65°C for 5 s. Relative gene expression was determined using the $\Delta\Delta$ Ct method.

The expression was normalized to the *GAPDH* gene and quantified relative to the control condition. The complete primers list can be found in Table S1 in the Supplementary Data.

Chromatin immunoprecipitation (ChIP)

Cells were cultured in 10-cm plates to ~80–90% confluence, and one plate was used per immunoprecipitation. Cells were fixed in 1% formaldehyde for 10 min at room temperature with swirling. Glycine was added to a final concentration of 0.125 M, and the incubation was continued for an additional 5 min. Cells were washed twice with ice-cold phosphate-buffered saline, harvested by scraping, pelleted, and resuspended in 1 ml of SDS lysis buffer (50 mM Tris-HCl, pH 8.0, 1% SDS, 10 mM EDTA, protease inhibitors (Complete EDTA-free protease inhibitors; Roche Diagnostics)). Samples were sonicated three times for 30 s each time (output H) at intervals of 30 s with a Diagenode Bioruptor sonicator. Samples were centrifuged at 14 000 rpm at 4°C for 10 min. After removal of a control aliquot (whole-cell extract), supernatants were diluted 10-fold in ChIP dilution buffer (20 mM Tris-HCl, pH 8.0, 150 mM NaCl, 2 mM EDTA, 1% Triton X-100). Samples were incubated at 4°C overnight in 2-methacryloyloxyethyl phosphorylcholine polymer-treated 15-ml polypropylene tubes (Assist, Japan) with anti-mouse IgG-Dynabeads that had been preincubated with 5 µg of anti-SMAD2/3 antibody in phosphate buffered saline, 0.5% bovine serum albumin. The beads were then moved to 1.7-ml siliconized tubes (3207; Corning) and washed five times with ChIP wash buffer (50 mM HEPES-KOH, pH 7.0, 0.5 M LiCl, 1 mM EDTA, 0.7% deoxycholate, 1% Igepal CA630) and once with TE buffer, pH 8.0. Immunoprecipitated samples were eluted and reverse cross-linked by incubation overnight at 65°C in elution buffer (50 mM Tris-HCl, pH 8.0, 10 mM EDTA, 1% SDS). Genomic DNA was then extracted with a PCR purification kit (Qiagen). The immunoprecipitated DNA was analyzed by qRT-PCR using locus specific primers (the complete primers list can be found in Table S2 in the Supplementary Data) and normalized to input DNA. Relative fold enrichment corresponded to the SMAD2/3 enrichment in each locus divided by the enrichment in the negative control regions (*hemoglobin β* (*HBB*) promoter and *HPRT1* first intron) and quantified relative to the control- or the siNTC-condition as indicated.

ChIP-sequencing (ChIP-seq) and data analysis

Chromatin isolation, sonication and immunoprecipitation using anti-SMAD2/3 antibody were performed essentially as described (28,29). The library was prepared using NEBNext ChIP-Seq

Library Prep Reagent Set for Illumina (New England Biolabs), KAPA DNA Library Preparation Kits for Illumina (KAPA Biosystems), or IonXpress Plus Fragment Library Kit (Thermo Fisher Scientific). High-throughput sequencing of the ChIP fragments was performed using Genome Analyzer IIX or HiSeq 2000 (Illumina) or Ion Proton sequencer (Thermo Fisher Scientific) following the manufacturer's protocols. Reference files of the human reference sequence assembly (NCBI Build 37/hg19, February 2009) and GTF annotation file were obtained from iGenomes (http://support.illumina.com/sequencing/sequencing_software/igenome.html). All ChIP-seq data sets were aligned using Bowtie (version 1.1.0) [30] with the command '-S -a -best -strata -v 1 -m 1'. SMAD2/3 binding regions were identified using MACS software (Model based analysis of ChIP-seq) (version 1.4.2) [31] with a P-value threshold of 1e-5. Assigning a binding site to the nearest gene within 100 kb from a peak was performed using CisGenome ver2 [32]. De novo motif prediction was performed by MEME-ChIP with a slight modification of the default settings (maximum width: 10) (MEME-ChIP version 4.10; <http://meme.nbcr.net/meme/cgi-bin/meme-chip.cgi>) [33]. The logo plots were generated using the R package seqLogo. Mapping of TFBSs to the specific genomic regions were calculated by the CisGenome. Gene Ontology (GO) enrichment analysis was performed using the Database for Annotation, Visualization, and Integrated Discovery (DAVID v6.7; <http://david.abcc.ncifcrf.gov>) [34]. Biological functions associated with the SMAD2/3 binding sites were predicted using GREAT (Genomic Regions Enrichment of Annotations Tool) [35]. The ChIP-Seq data of H3K4me1, H3K4me3 and corresponding control input DNA of MCF10A cells (SRA045635) [36] were obtained from the Sequence Read Archive (SRA) (<http://www.ncbi.nlm.nih.gov/sra>). The ChIP-Seq data of H3K4me1 and H3K4me3 of HMEC were generated and available from ENCODE consortium [37].

RNA-sequencing (RNA-seq) and data analysis

RNA-seq libraries were prepared essentially as described [38]. In short, mRNA was isolated from 1 μ g total RNA using Dynabeads Oligo(dT) 25 (Life Technologies) and fragmented to 150-200 nt in first strand buffer for 3 min at 94°C. Random hexamer primed first strand was generated in presence of dATP, dGTP, dCTP and dTTP. Second strand was generated using dUTP instead of dTTP to tag the second strand. Subsequent steps to generate the sequencing libraries were performed with the NEBNext kit for Illumina sequencing (New England Biolabs) with minor modifications; after indexed adapter ligation to the dsDNA fragments, the library was

treated with USER (Uracil-Specific Excision Reagent) Enzyme (New England Biolabs) in order to digest the second strand derived fragments. After amplification of the libraries, samples with unique sample indexes were pooled and sequenced using HiSeq 2000 with TruSeq SBS Kit v3 reagent or HiSeq 2500 with TruSeq SBS Kit v4 reagent (Illumina) following the manufacturer's protocols.

Gene expression levels in fragments per kilobase of exon per million fragments mapped (FPKM) were estimated using Tophat/Cufflinks (version 2.0.13 and 2.2.1, respectively) with the default parameter settings [39]. For the analysis and visualization of the data generated by Cufflinks, we used the R package cummeRbund.

Analysis of Breast Cancer clinical datasets

For the analysis of patient datasets from Molecular Taxonomy of Breast Cancer International Consortium (METABRIC) [40], all statistical tests were performed using R software (version 3.2.5, <https://www.r-project.org/>) as described previously [41]. Z-scored expression values of mRNA were obtained from cBioPortal [42, 43] in September 2017. Patients were divided into low and high expressers using the median values of mRNA expression. The overall survival was estimated with the Kaplan-Meier method and differences between groups were evaluated by the log-rank test, using the R package cmprsk. P-values were calculated using Welch's t-test, or unequal variance t-test (* $P < 0.05$, ** $P < 0.01$, *** $P < 0.001$).

Meta-analysis of Breast Cancer datasets were performed using KM plotter (<http://kmplot.com>) (44) with default settings; all subtypes, $n = 3557$; ER+ subjects, $n = 2036$; ER- subjects, $n = 807$; luminal A subtype, $n = 2069$; luminal B subtype, $n = 1166$; HER2-subtype, $n = 239$; basal-like subtype, $n = 668$), and the data sets includes E-MTAB-365, *GSE11121*, *GSE12093*, *GSE12276*, *GSE1456*, *GSE16391*, *GSE16446*, *GSE17705*, *GSE17907*, *GSE19615*, *GSE20194*, *GSE20271*, *GSE2034*, *GSE20685*, *GSE20711*, *GSE21653*, *GSE2603*, *GSE26971*, *GSE2990*, *GSE31448*, *GSE31519*, *GSE3494*, *GSE5327*, *GSE6532*, *GSE7390* and *GSE9195*.

Gene set enrichment analysis (GSEA)

Gene set enrichment analysis (GSEA) analyses were performed using the tool available at <http://www.broadinstitute.org/gsea/index.jsp> [45]. In brief, fold change (log2) in gene expression

from two experimental conditions were calculated and the list was then used as a ranked list in the Pre-Ranked function of the GSEA software.

Statistical analysis

For ChIP-qPCR and qRT-PCR at least three independent experiments were performed and results are shown by dot plot chart. The differences between experimental groups were analyzed using Welch's t-test, with $*P < 0.05$, $**P < 0.01$ and $***P < 0.001$ being considered significant. Collagen invasion assays contained $n \geq 6$ spheroids for each condition, and was repeated at least twice with similar results. Data are presented as means \pm SD. The differences between experimental groups were analyzed using Welch's t-test, with $*P < 0.05$, $**P < 0.01$ and $***P < 0.001$ being considered significant. For the zebrafish experiments statistical analysis was performed using Prism 4 software (GraphPad La Jolla, USA). Results are expressed as the mean \pm SEM. Student's t-test or one-way analysis of variance (ANOVA) were performed followed by the Tukey's method for multiple comparison. $P < 0.05$ was considered to be statistically significant ($*0.01 < P < 0.05$, $**0.001 < P < 0.01$, $***P < 0.001$).

Results

SMAD2/3 are redirected to different sites after prolonged TGF β treatment

To identify both early and late SMAD-containing complexes and target genes involved in tumor progression, we first conducted SMAD2/3 ChIP-seq in MCF10A MII breast cancer cells after 1.5 and 16 h of TGF β treatment. Analysis of three well known TGF β /SMAD target genes, *SERPINE1*, *laminin β (LAMB3)* and *matrix metalloprotease (MMP)2*, as expected, showed enriched SMAD2/3 binding in specific regions of the gene loci, including the SMAD2/3 binding site that was previously identified in the *SERPINE1* promoter in HaCaT keratinocytes [46] (Figure 1A). TGF β -dependent SMAD2/3 binding to these three genes was also detected by ChIP-qPCR analysis (Figure S1A). Interestingly, at the late time point SMAD2/3 was found to bind to different regions of the *SERPINE1* and *LAMB3* loci, whereas in the *MMP2* gene locus SMAD2/3 binding to the binding site located 40 kb upstream of the transcription start site (TSS) was lost (Figure 1A). Moreover, overall SMAD2/3 recognized more target sites after 16 h of TGF β stimulation (3280 sites) compared to 1.5 h stimulation (2206 sites), and only ~ 700 SMAD2/3 binding sites overlapped between the two time points (Figure 1B), suggesting that the activated SMAD2/3 proteins (Figure 1C) were redirected to different binding sites over the

genome at the late time point. Furthermore, there were no differences in preferences of SMAD2/3 binding sites on the genome between the two conditions; ~35% of the SMAD2/3 binding sites were located in the introns of known genes and ~10% in the promoter regions within 10 kb upstream of known TSSs (Figure 1D).

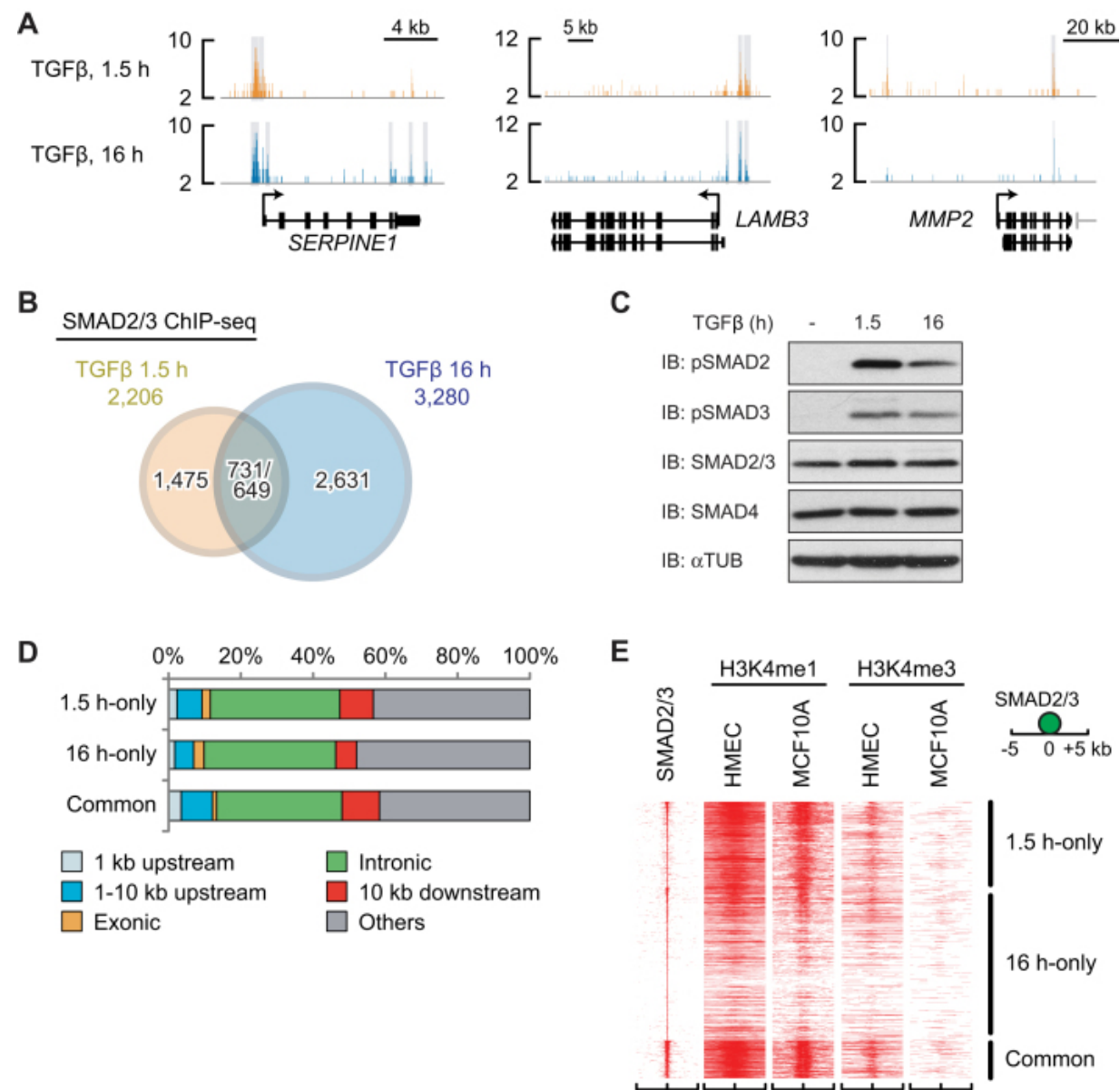


Figure 1. SMAD2/3 are redirected to different sites in MCF10A MII after prolonged TGFβ treatment. **A**, Genomic loci of *SERPINE1* (*plasminogen activator inhibitor 1*, or *PAI-1*), *MMP2* and *LAMB3* genes are shown together with the results of SMAD2/3 ChIP-seq data. The direction of transcription is shown by the arrow beginning at the transcription start site (TSS). Statistically significant regions are marked by a gray-colored box. **B**, A Venn diagram indicating overlap of SMAD2/3 binding

sites of MCF10A MII cells after 1.5 and 16 h TGF β (5 ng/ml) treatment. The numbers of overlapped regions are not identical, since some of the peaks are not on a one-by-one correspondence. **C**, Western blots for phospho-SMAD2/3 in MCF10A MII cells after 0, 1.5 and 16 h TGF β (5 ng/ml) treatment. **D**, Distribution of SMAD2/3 binding sites in MCF10A MII cells relative to known genes in the human genome (hg19). **E**, Heat map representation of the location of the indicated histone marks in breast HMEC and MCF10A epithelial cells within the 10-kb region surrounding the center of the SMAD2/3 peaks. SMAD2/3 binding sites were ordered based on the strength of binding (y axis). The presence of epigenetic marker [36, 37] is displayed.

We next compared our SMAD2/3 binding data with previously reported enhancer data in non-stimulated normal human mammary epithelial cells (HMEC) and parental MCF10A cells [36, 37]. The SMAD2/3 binding sites shared between cells stimulated 1.5 and 16 h overlapped well with the previously identified enhancer regions characterized by H3K4me1 (Figure 1E and Figure S1B). The 1.5 h-only sites also overlapped with these H3K4me1 marks, but the 16 h-only sites did not (Figure 1E and Figure S1B). In contrast, fewer SMAD2/3 peaks overlapped with the previously reported promoter regions characterized by H3K4me3. This could mean that after 1.5 h TGF β stimulation, SMAD2/3 preferentially binds to enhancer regions already accessible in non-stimulated normal mammary epithelial cells, but after 16 h prefers different regions. In fact, distinct gene ontologies (GOs) were enriched in the genes associated with 16 h-only sites compared with those of 1.5 h-only sites (Figure S1C).

To validate whether the changes in SMAD2/3 binding indeed result in changes in target gene programs, we performed RNA-seq transcriptome analysis after short (1.5 h) and long (16 h) periods of TGF β stimulation of MCF10A MII cells and compared with unstimulated cells. Consistent with the SMAD2/3 binding profiles, RNA-seq data revealed that more genes were strongly induced at the late time point compared to the early time point (Figure 2A). Gene set enrichment analysis (GSEA) based on Kyoto encyclopedia genes and genomes (KEGG)-defined pathways confirmed that genes associated with GOs like the TGF β signaling pathway were enriched among the early TGF β target genes with SMAD2/3 binding sites, whereas genes within Focal adhesion and MAPK signaling pathways were enriched among the late TGF β target genes (Figure 2B–E).

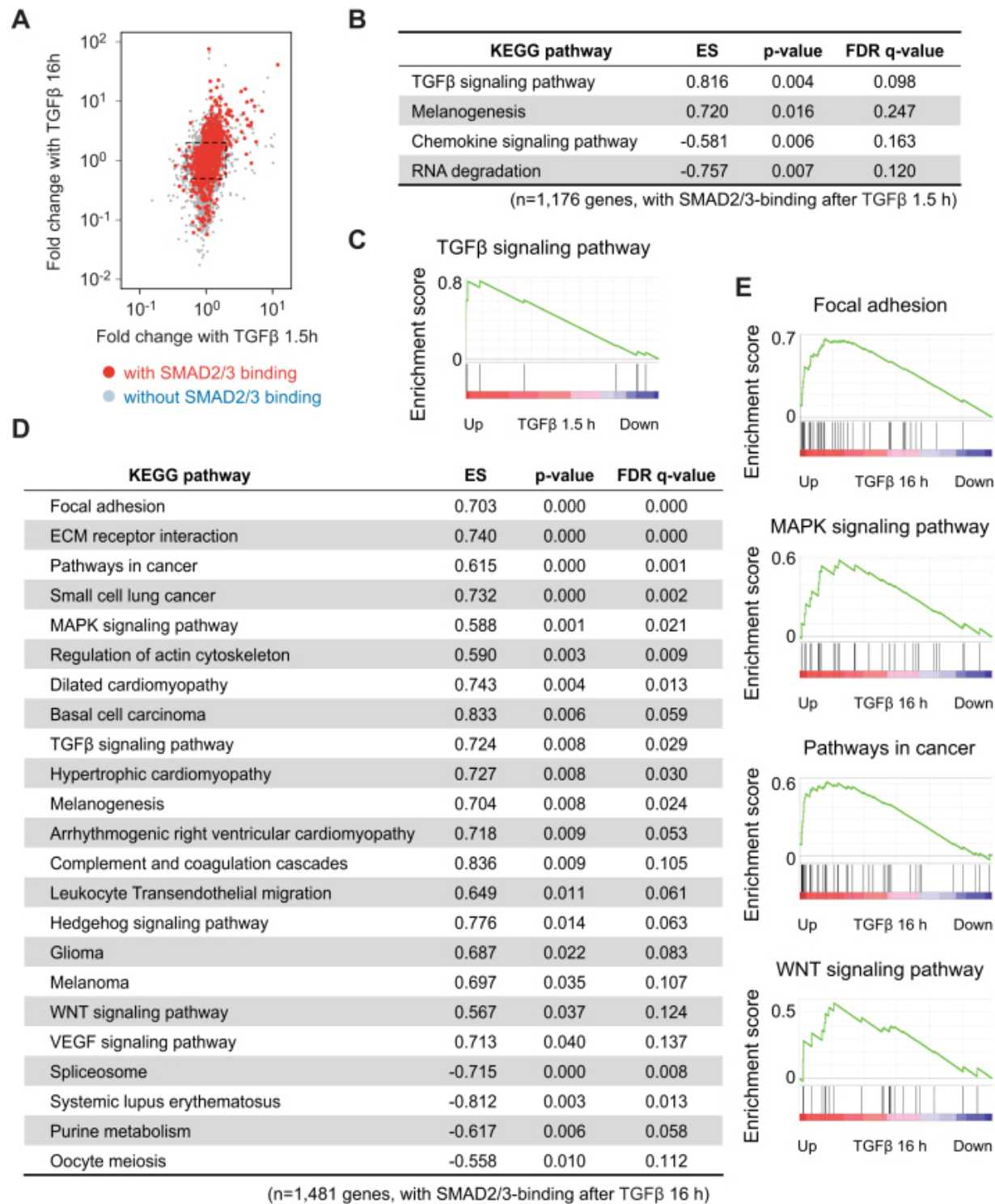


Figure 2. Identification of a late TGFβ target gene signature. **A**, Scatter plot representing fold change after TGFβ (5 ng/ml) treatment. Each point represents values of a gene. Genes with a SMAD2/3 binding within 50 kb from gene bodies after 16 h TGFβ treatment are colored red. A dot square represents 2-fold change of gene expression. **B-E**, Gene set enrichment analysis (GSEA) of expression changes of

SMAD2/3 target genes after 1.5 h (**B** and **C**) and 16 h (**D** and **E**) of TGF β (5 ng/ml) treatment. The SMAD2/3 target genes were pre-rank-ordered according to their fold change (log2) after TGF β treatment for the indicated time periods, and analyzed based on KEGG signaling pathway enrichment. Gene sets with a *P*-value < 5% and an FDR *q*-value < 25% were considered significant. (**C** and **E**) Enrichment score (ES) is plotted on the y axis.

JUNB is a critical AP1 component for SMAD2/3 binding after TGF β stimulation

An explanation for the changes in SMAD2/3 binding at 16 h might be that DNA binding factors that are modulated by TGF β -SMAD signaling at early time points subsequently redirect SMAD2/3 to different binding sites on the genome as a part of a feed-forward loop, e.g. by interacting with SMAD2/3 and/or affecting its chromatin accessibility. To obtain more clues on this, we performed *de novo* motif prediction analysis. Interestingly, AP1 binding motifs were identified as the major recognition elements among both the early and late sites, with higher significance than SBEs (Figure 3A).

We next analyzed the expression profiles of AP1 at protein and mRNA levels (Figures 3B and Figure S2A). Both JUN, JUNB, FOS, FOSB and FOSL2 were strongly induced after TGF β treatment, while FOSL1 was suppressed at the mRNA level but unaffected at the protein level, in line with our previous findings (16). Moreover, in these cells JUNB was most critical for TGF β -induced invasion as well as induction of some invasion-associated genes (16). It is also of note that JUNB gene amplification occurred in 1–14% of breast cancer patients (Figure S2B) (40, 42, 43). In addition, patients with JUNB amplification had a trend of poorer prognosis (Figure S2C), although this was not statistically significant because of the small number of cases. We therefore decided to functionally assess the role of JUNB in the recruitment of SMAD2/3 to the late TGF β -induced gene program.

We first analyzed again the three well known TGF β /SMAD target genes, *SERPINE1*, *LAMB3*, and *MMP2*. Knock-down of JUNB strongly inhibited the recruitment of SMAD2/3 to the *SERPINE1* and *LAMB3* gene loci after 16 h of TGF β stimulation (Figure 3C and Figure S2D), while SMAD2/3 recruitment to the *MMP2* gene locus was not affected. Moreover, knock-down of JUNB inhibited TGF β -induced mRNA expression of *SERPINE1* and *LAMB* after prolonged TGF β stimulation, but not of *MMP2*, and phosphorylation of SMAD 2 and 3 was hardly influenced (Figure 3D). The late JUNB-dependent binding of SMAD2/3 to the *SERPINE1* and *LAMB3* gene loci (Figure 3C and Figure S1A), correlated with enhanced binding of JUNB to the

same gene loci (Figure 3E). Based on these results, we hypothesized that JUNB may determine the target- and time-specificity of SMAD complexes as a co-binding factor for a specific subset of invasion genes.

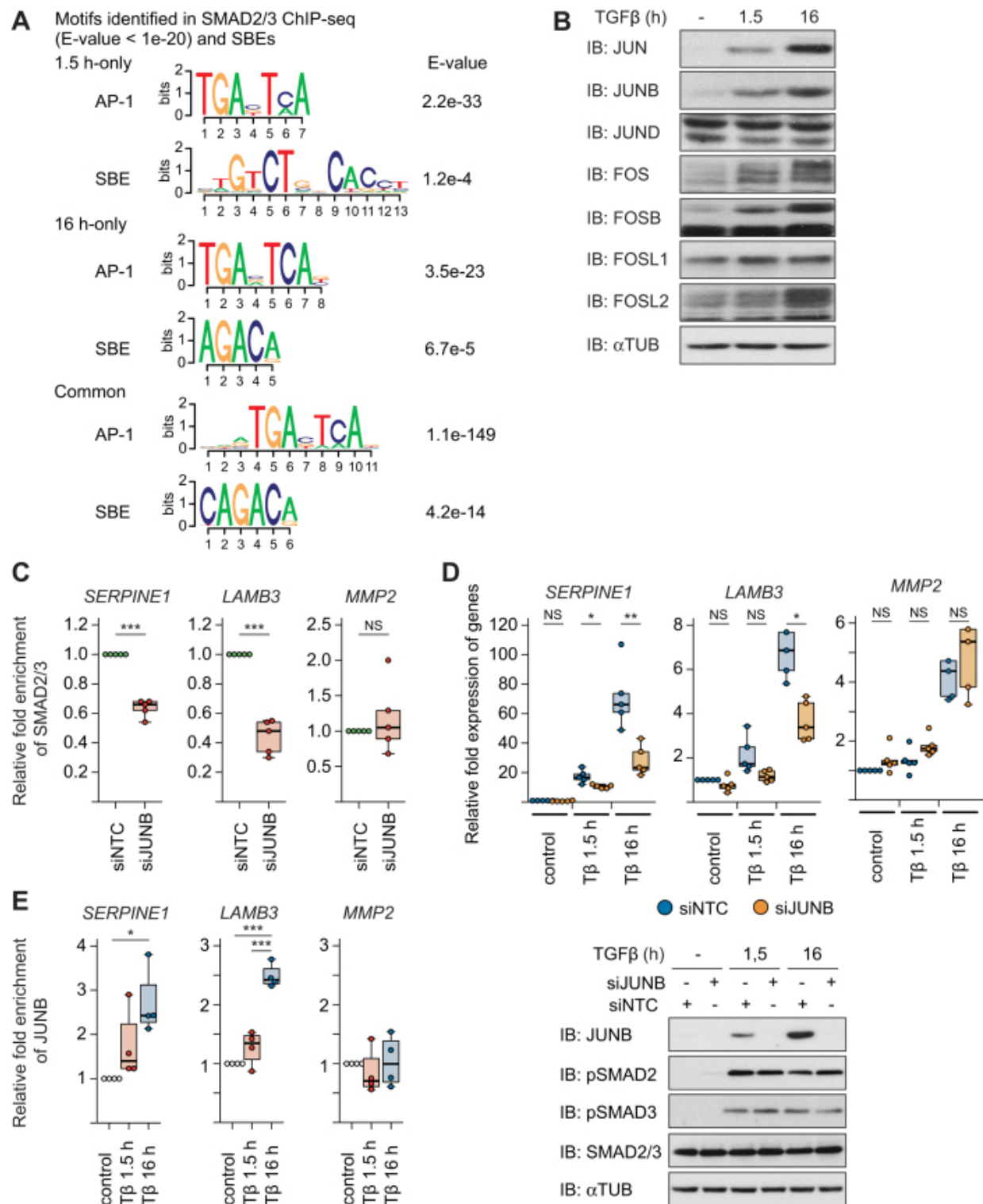


Figure 3. JUNB is a critical AP1 component for SMAD2/3 binding after TGF β stimulation. **A**, Motifs enriched in the SMAD2/3 binding sites. Motifs which resemble the motif of AP1 were identified as well as SBE. **B**, Western blots of various AP1 components in MCF10A MII cells after no TGF β treatment (-), or TGF β (5 ng/ml) treatment for 1.5 or 16 h. **C**, ChIP-qPCR showing SMAD2/3 binding to the indicated gene loci in MCF10A MII cells transfected with non-targeting control (siNTC) or specific JUNB siRNA and stimulated for 16 h with TGF β (5 ng/ml). Results of five independent experiments are shown by dot plot chart; *** P < 0.001 versus siNTC. **D**, qRT-PCR analysis (top) and Western blot control (bottom) to investigate the role of JUNB in TGF β -induced gene expression. MCF10A MII cells were transfected with non-targeting control (siNTC) or specific JUNB siRNA and stimulated for 1.5 or 16 h with TGF β (5 ng/ml). Results of five independent experiments are shown by dot plot chart; * P < 0.05, ** P < 0.01. **E**, ChIP-qPCR showing time-dependent recruitment of JUNB to the indicated gene loci in MCF10A MII cells before (-) or after TGF β treatment (1.5 or 16 h). Results of three independent experiments are shown by dot plot chart; * P < 0.05, *** P < 0.001.

A JUNB-mediated feed-forward mechanism regulates genes associated with cell adhesion and invasion, and controls invasion in zebrafish xenograft models

To characterize the significance of JUNB for TGF β -SMAD-target genes on a genome-wide scale, we performed RNA-seq transcriptome analysis in JUNB-knock-down MCF10A MII cells (Figure 4A and Figure S3A). We found that several well-characterized TGF β -SMAD-target genes associated with cell adhesion, invasion and mesenchymal phenotype, e.g. *fibronectin (FN)1* and *integrin α (ITGA)2*, were dependent on JUNB-induction (Figure S3B), which was also confirmed by GO analysis (Figure S3C). Interestingly, 20 genes appeared in the core-enriched genes of the pathway ‘Pathways in cancer’ in GSEA analysis (Figure 4B and C), at least 8 of which, *FN1*, *ITGA2*, *ITGA6*, *LAMA3*, *LAMB3*, *LAMC2*, *collagen (COL) 4A1*, and *COL4A2*, are known target genes of TGF β (8, 47–49). In addition, genes in the WNT signaling pathway were enriched, which is discussed.

Taken together, the gene set analysis presented above, and the observation that JUNB is required for efficient expression of selected TGF β -SMAD-target genes associated with cell invasion and mesenchymal phenotype ([16], Figures 3D and 4C), suggest that a late SMAD/JUNB-induced gene program is critical for TGF β -induced invasion and cancer progression. In line with this hypothesis, we previously found transient siRNA-mediated knock-down of *JUNB* to result in strongly reduced TGF β -induced invasion of MCF10A MII spheroids in collagen [16]. To further validate these data, we stably knocked down *JUNB* with lentiviral

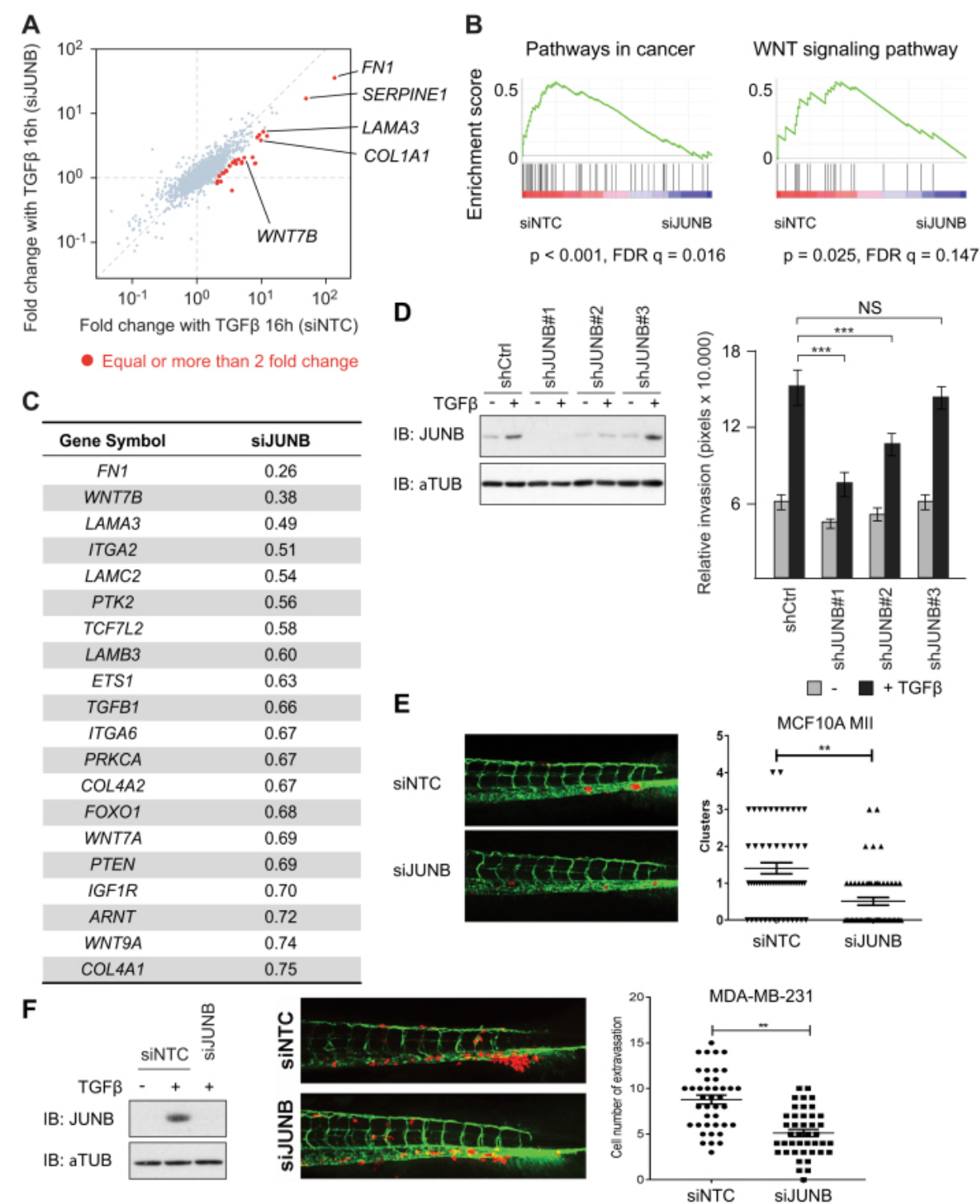


Figure 4. A JUNB-mediated feed-forward mechanism regulates genes associated with cell adhesion, invasion and controls invasion in a zebrafish model. **A**, Scatter plot representing fold change after TGFβ (5 ng/ml) treatment. Each point represents values of a gene. Genes whose induction after 16 h TGFβ (5 ng/ml) treatment was attenuated more than 50% with siJUNB treatment are colored red. **B**,

GSEA of expression changes of SMAD2/3 target genes after manipulation of JUNB expression. The SMAD2/3 target genes were pre-rank-ordered according to their fold change (\log_2) between siNTC and siJUNB, and analyzed based on KEGG signaling pathway enrichment. Gene sets with P -value $< 5\%$ and FDR q -value $< 25\%$ were considered significant. Enrichment score (ES) is plotted on the y axis. **C**, A list of core-enriched genes of the pathway 'Pathways in cancer', which contribute most to the enrichment score of the pathway. **D**, Stable knock-down of JUNB in MCF10A MII cells with three distinct shJUNB expressing lentiviral vectors. Whereas #1 is efficient, #3 does not inhibit JUNB expression. Left: Western blot analysis. Right: collagen invasion of MCF10A MII spheroids stably expressing the sh control (Ctrl) or three distinct shJUNB lentiviral constructs. Spheroids were embedded in collagen in the absence or presence of TGF β (5 ng/ml) as indicated. Relative invasion was quantified as the mean area that the spheroids occupied 36 h after being embedded in collagen. Data represent means \pm SD ($n \geq 6$ spheroids per condition) and are representative of three independent experiments; *** $P < 0.001$. **E** and **F**, MCF10A MII (**E**) or MDA-MB-231 (**F**) mCherry cells transfected with non-targeting control (siNTC) or specific JUNB siRNA (siJUNB) were injected into the ducts of Cuvier (DoC) of 48 h post-fertilization (hpf) zebrafish embryos. Left: representative images of zebrafish at 6 days post-injection (dpi). Right: quantification of invasive cell cluster numbers in non-targeting and *JUNB* knock-down cells injected zebrafish larvae. (**F**) Most left, western blot control of knock-down efficiency.

vectors, which showed that decreased levels of JUNB correlate with decreased collagen invasion (Figure 4D). To examine the importance of JUNB in breast cancer cell invasion in vivo, we used an embryonic zebrafish xenograft invasion model [27]. We have previously demonstrated that TGF β signaling is critical for MCF10A MII invasion in this model [50]. Importantly, knock-down of *JUNB* with siRNA resulted in reduced invasion compared to non-targeting siRNA control groups (Figure 4E). Moreover, knock-down of *JUNB* also resulted in reduced zebrafish invasion of the TGF β -dependent metastatic human breast cancer cell line MDA-MB-231 [51, 52] (Figure 4F). These results confirm that JUNB is important for breast cancer invasion.

Since tumorigenesis is a long-term event, we next verified whether a more extended TGF β exposure, up to 72 h, results in a similar 'late-stage' TGF β -induced gene expression program as 16 h treatment. As exemplified in Figure S4A, the data obtained for these later time points were consistent with the data obtained at 16 h. In addition, since we identified the mesenchymal marker fibronectin as one of the main JUNB-dependent genes (Figure 4A, C and Figure S3B), we examined the effect of JUNB depletion in the human pulmonary adenocarcinoma cancer cell line A549, which undergoes epithelial-mesenchymal transition (EMT) in response to prolonged

TGF β stimulation. The expression of various TGF β -induced mesenchymal and/or EMT controlling genes was severely reduced by *JUNB* knock-down in these pulmonary adenocarcinoma cells (Figure S4B), and *JUNB* was also found to be critical for invasion of A549 cells in the zebrafish xenograft model (Figure S4C). This further confirms the pro-oncogenic potential of JUNB in TGF β induced invasion.

Activation of the WNT signaling pathway strengthens the TGF β -induced migratory phenotype

Interestingly, we also found that genes related to the WNT signaling pathway were enriched among the late TGF β target genes, in addition to the genes associated with adhesion and invasion (Figures 2E and 4B). We therefore focused on the most prominent JUNB-dependent WNT pathway and breast cancer associated gene in the list, *WNT7B*, and examined its importance in TGF β -induced cell migration and invasion. Our SMAD2/3 ChIP-seq and -qPCR analysis showed enhanced TGF β -induced binding of SMAD2/3 to the *WNT7B* locus in a time-dependent manner (Figure 5A and Figure S5A). In line with this, *WNT7B* expression was preferably induced after prolonged TGF β -treatment (Figure 5B). Moreover, *WNT7B* was induced after prolonged TGF β stimulation in a SMAD4- and JUNB-dependent manner (Figure 5C). The late JUNB-dependent expression of *WNT7B* and the time-dependent recruitment of SMAD2/3 to the *WNT7B* locus (Figure 5A), correlated with enhanced binding of JUNB to the same gene locus after 16 h of TGF β stimulation (Figure 5D). Together, these results identify *WNT7B* as a JUNB-mediated late TGF β -SMAD-target gene.

To directly test if *WNT7B* is important for TGF β -induced invasion, we performed collagen invasion assays. Addition of the TGF β type I kinase receptor (TGF β RI) inhibitor SB505124 almost completely blocked TGF β -induced collagen invasion of MCF10A MII spheroids, as expected (Figure 5E). Addition of the general WNT-inhibitor IWP-2 [53] also significantly inhibited TGF β -induced invasion. To directly evaluate the role of *WNT7B*, we generated MCF10A MII cells stably expressing *WNT7B* (Figure S5B). Exogenous expression of *WNT7B* enhanced both basal and TGF β -induced invasion (Figure 5E). Consistent with this finding, addition of recombinant WNT7A, which was also one of the late TGF β target genes (Figure 4C) and shares 82% amino acid identity with *WNT7B*, or expression of WNT7A, enhanced both basal and TGF β -induced invasion (Figure S5C and S5D). Interestingly, addition of the TGF β RI inhibitor SB505124 strongly inhibited TGF β -induced invasion also in *WNT7B* expressing cells

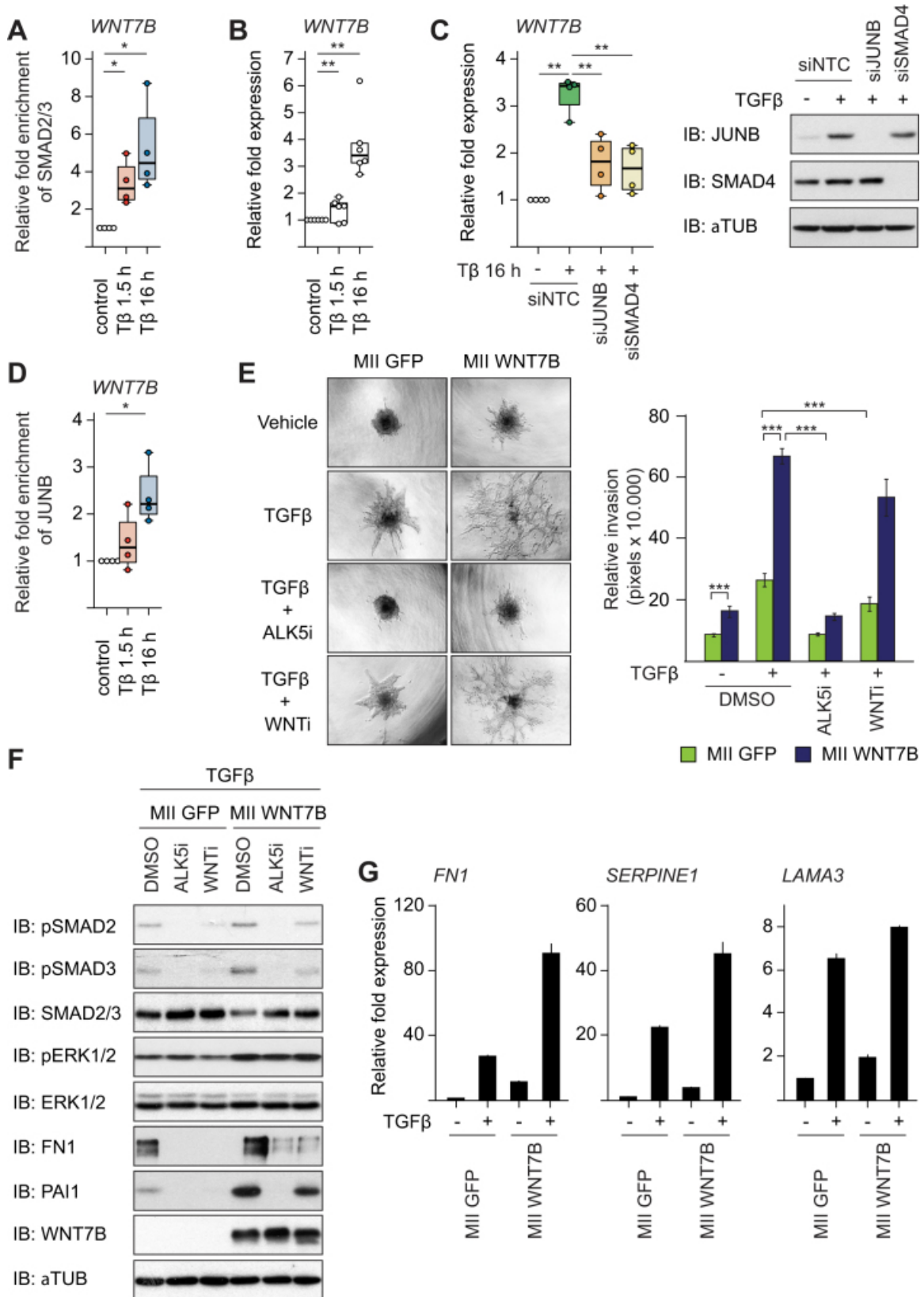


Figure 5. Activation of the WNT signaling pathway strengthens the TGF β -induced migratory phenotype. **A**, ChIP-qPCR showing time-dependent recruitment of SMAD2/3 binding to the *WNT7B* gene locus in MCF10A MII before (-) or after TGF β (5 ng/ml) treatment (1.5 and 16 h). Results of four independent experiments are shown by dot plot chart; * $P < 0.05$. **B**, qRT-PCR analysis showing time-dependent *WNT7B* mRNA expression in MCF10A MII before (-) or after TGF β (5 ng/ml) treatment (1.5 or 16 h). Results of six independent experiments are shown by dot plot chart; ** $P < 0.01$. **C**, Left: qRT-PCR analysis of *WNT7B* mRNA expression in MCF10A MII cells transfected with the indicated control (siNTC) or JUNB and SMAD4 specific siRNAs, and stimulated for 16 h with TGF β (5 ng/ml). Results of four independent experiments are shown by dot plot chart; ** $P < 0.01$ versus siNTC TGF β 16 h. Right: Western blot control of knock-down efficiency. **D**, ChIP-qPCR showing time-dependent recruitment of JUNB to the *WNT7B* gene locus in MCF10A MII before (-) or after TGF β (5 ng/ml) treatment (1.5 and 16 h). **E**, Collagen invasion assay of MCF10A MII spheroids stably expressing control GFP or ectopic WNT7B-MYC. Spheroids were embedded in collagen in the absence or presence of TGF β , the TGF β RI inhibitor (ALK5i) SB505124 (2.5 μ M) or the WNT inhibitor (WNTi) IWP-2 (5 μ M), as indicated. Left: representative pictures of spheroids taken 36 h after being embedded in collagen. Right: relative invasion was quantified as the mean area that the spheroids occupied 36 h after being embedded in collagen. Data represent means \pm SD ($n \geq 6$ spheroids per condition) and are representative of three independent experiments; *** $P < 0.001$. **F**, Western blot analysis of the MCF10A MII cells stably expressing control GFP or ectopic WNT7B-MYC. Cells were treated for 12 h with TGF β (5 ng/ml) in the absence or presence of DMSO control, the TGF β RI inhibitor (ALK5i) SB505124 (2.5 μ M) or the WNT inhibitor (WNTi) IWP-2 (5 μ M), as indicated. **G**, qRT-PCR target gene analysis of the cells shown in **E** and **F**, treated for 16 h with TGF β (5 ng/ml) as indicated. A representative results of three independent experiments is shown.

(Figure 5E), suggesting that WNT7B stabilizes the TGF β -induced migratory phenotype of epithelial cells, rather than merely functioning as a downstream mediator of TGF β signaling. In line with this notion, we found enhanced levels of TGF β -induced phospho-SMAD2 and 3 in WNT7B overexpressing cells, whereas the general WNT-inhibitor IWP-2 reduced this phosphorylation, and also in the parental cells (Figure 5F). In addition, the WNT7B overexpressing cells contained increased levels of activated phosphorylated ERK1/2 and the expression of various TGF β /SMAD-induced invasion genes was enhanced (Figure 5G). This indicates that WNT7B increases invasion/migration to a large extent by enhancing TGF β type I receptor mediated signaling.

WNT7B promotes breast cancer cell invasion

To investigate the role of WNT7B in invasion and metastasis *in vivo*, we again used the zebrafish embryo xenograft model. Embryos injected with MCF10A MII cells stably expressing WNT7B showed a significant increase in invasive cell numbers compared to control cells (Figure 6A). This result demonstrates that WNT7B expression stimulates MCF10A MII invasion in zebrafish.

To further address the clinical significance of WNT7B expression in breast cancers, we analyzed patient datasets from the Molecular Taxonomy of Breast Cancer International Consortium (METABRIC) [40]. We found that higher expression of the WNT7B gene was linked with shorter overall survival (Figure 6B). Moreover, high expression of WNT7B correlated with poorer prognosis in a cohort of ER⁺ tumors, especially in those of luminal type, but not of basal-like or triple negative breast cancers (TNBC). The WNT7B-high subgroup had higher mRNA expression of FN1 and COL1A1, well-established markers for the mesenchymal phenotype or tumor invasiveness (Figures 4A and 6C). In addition, we performed *in silico* meta-analysis of published microarray datasets using the Kaplan-Meier plots website [44], which also indicated that mRNA expression of WNT7B predicted poorer outcome especially in ER⁺ patients (Figure S6A).

To verify whether ER⁻ negative tumor cells have a similar genome-wide SMAD2/3 binding landscape as ER⁺ cells, we performed SMAD2/3 ChIP-seq analysis in the TNBC lines Hs-578-T and BT-549 (Supplementary Figure S6B). In Hs-578-T cells SMAD2/3 did not bind the WNT7B locus (Supplementary Figure S6B), while SMAD2/3 binding was observed in the WNT7B locus of BT-549 cells. However, in contrast to MCF10A MII cells, the number of SMAD2/3 binding sites was higher at 1.5 h than at 16 h with about 50% overlap (Figure S6C). Moreover, although the AP1 motif was enriched in the SMAD2/3 binding sites in BT-549 (Figure S6D), the data suggests that there is no JUNB-mediated redirection of SMAD2/3 in BT-549. Thus, our data showed heterogeneity among the TNBC cell lines.

The selective association in the ER⁺ group may be explained by the finding that TGF β mainly functions as a tumor suppressor in the ER⁺ group, but as a tumor promoter in the ER⁻ group of the breast cancer patients [13]. Our data thus suggest that inhibition of the JUNB-mediated feed-forward loop may restore the tumor suppressive roles of TGF β . It also implies that

the feed-forward loop and/or activation of WNT7B signaling pathway may be a biomarker for the use of TGF β inhibitors for tumor treatment.

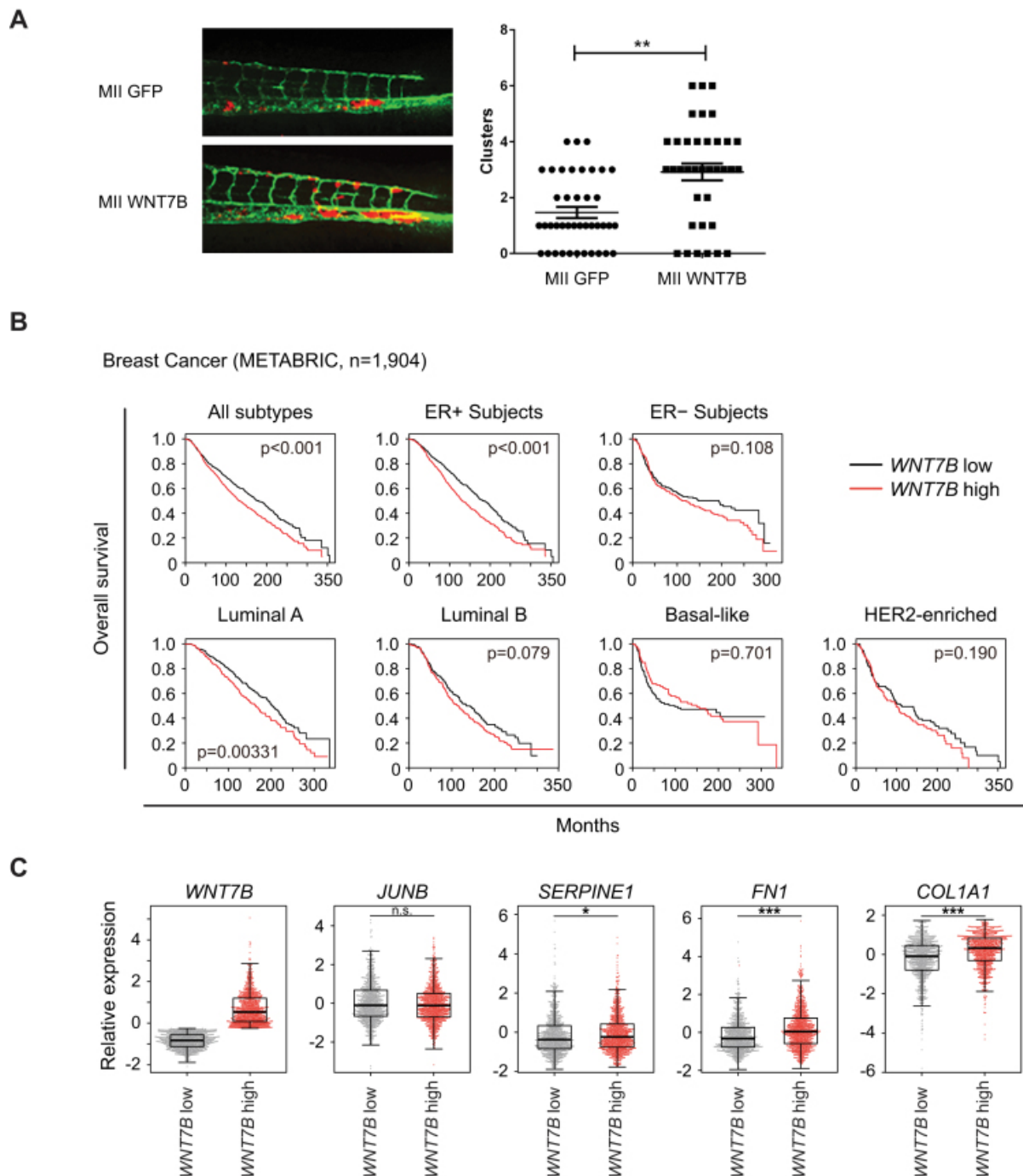


Figure 6. WNT7B promotes breast cancer cell invasion. A, MCF10A MII mCherry stably expressing control GFP (MII GFP) or ectopic WNT7B-MYC (MII WNT7B) were injected into the DoC of 48-hpf zebrafish embryos. Left: representative images of zebrafish at 6 days post-injection (dpi). Right: quantification of invasive cell cluster numbers in GFP or WNT7B-MYC expressing MCF10A MII cells

injected zebrafish larvae. **B**, Kaplan-Meier analysis of overall survival of breast cancer datasets from Molecular Taxonomy of Breast Cancer International Consortium (METABRIC) [40]; all subtypes, $n = 1904$; ER $^{+}$ subjects, $n = 1445$; ER $^{-}$ subjects, $n = 429$; luminal A subtype, $n = 679$; luminal B subtype, $n = 461$; HER2 $^{-}$ subtype, $n = 220$; basal-like subtype, $n = 199$). Survival analysis was performed using a log-rank test. **C**, Z-scored expression values of mRNA were obtained with cBioPortal [42, 43]. (*** $P < 0.001$; n.s. not significant, Welch's t-test).

Discussion

It is well established that during the later stages of tumorigenesis TGF β promotes tumor progression by enhancing migration, invasion and survival of tumor cells, by stimulating extracellular matrix deposition and tissue fibrosis, perturbing immune surveillance, stimulating angiogenesis and promoting EMT [8, 11, 15]. One of the contributing factors is the effect of TGF β on the tumor microenvironment, which in turn affects the tumor cells. In addition, sequential acquisition of genomic mutations changes the TGF β responsiveness of cancer cells in a cell-intrinsic manner [54]. For instance, in pancreatic cancer where SMAD4 mutations are common, loss of SMAD4 enables escape from cytostatic TGF β effects or lethal effects associated with TGF β -induced-EMT [55]. In breast cancer cells, however, SMAD mutations are rare [56, 57]. This suggests that DNA-binding co-factors for SMADs, including JUNB, cause quantitative and/or qualitative changes in SMAD signaling and thereby play essential roles in the switch of the cancer-associated functions of TGF β , from cytostasis/apoptosis to tumor-promotion.

We have previously demonstrated that SMAD3, SMAD4 and the AP1 components JUN, JUNB, FOS and FOSL1 cooperatively regulate several established TGF β -target genes with a known function in EMT and invasion, including *MMPI1*, *MMP9*, *SNAIL* and *SERPINE1*, and enhance TGF β -induced collagen invasion of MCF10A MII spheroids (16). The ChIP-seq and RNA-seq analyses in the current study show that the strong and prolonged induction of JUNB by TGF β redirects SMAD2/3 to different target sites and thereby plays a major role in the activation of late TGF β target genes as critical component of a feed-forward regulatory network. Interestingly, AP1 has previously been reported to potentiate chromatin accessibility of the glucocorticoid receptor (GR) in a murine mammary epithelial cells [58], and in human breast cancer cells to colocalize on the genome with YAP/TAZ/TEAD, Hippo pathway transducers and transcription factors [59]. Since critical roles of AP1 components in breast cancer have been well documented, especially in the aggressive clinical subtype TNBC [60], induction of AP1 by

TGF β may potentiate aggressive phenotypes of breast cancer cells through other signaling pathways *in vivo*, in addition to the feed-forward network of TGF β .

Interestingly, our list of late TGF β target genes was enriched with signaling components of the WNT pathway (Figures 2E and 4B). It has been reported that a small portion of breast cancers (~10%) express 30-fold higher levels of WNT7B compared with normal or benign breast tissues [61]. In addition, recent data suggest that WNT7B is associated with anchorage-independent growth of breast cancer cells [62]. The importance of crosstalk between TGF β and WNT signaling pathways has been established [63, 64]. For acquisition of mesenchymal phenotypes in the breast TGF β and WNT signaling pathways (both canonical and non-canonical) collaborate to activate mesenchymal genes and function in an autocrine fashion [65]. Similarly, activation of canonical WNT signaling is required for TGF β -mediated fibrosis [66]. Furthermore, it was recently shown that WNT7A is secreted by breast tumor cells that promote fibroblast recruitment and conversion to a cancer-associated fibroblast (CAF) phenotype, which promotes metastasis [67]. WNT7A-mediated CAF activation was mediated via enhanced TGF β receptor signaling and not via classical WNT receptor signaling. This suggests that the JUNB-mediated feed-forward network of TGF β is further stabilized by WNT ligands, resulting in more migratory and mesenchymal cell phenotypes. In line with this, we found enhanced ERK1/2 and SMAD2/3 phosphorylation, and enhanced TGF β target gene expression in cells stably expressing WNT7B (Figure 5F and G), indicating that WNT7B increases invasion/migration in part by enhancing TGF β type I receptor mediated signaling.

It should be noted that when we examined the role of canonical WNT signaling, as measured by TCF/LEF-dependent transcriptional reporter activity, we only found less than a two-fold increase by WNT7B (Figure S5E). However, MII cells show autocrine TGF β (-related) signaling [16, 68] and our RNA sequencing analysis showed that both *WNT7A*, *WNT7B* and *WNT9A* besides being induced by TGF β (Figure 4C) already show relatively high basal expression.

In accordance with our analysis, high expression of WNT7B mRNA was associated with poorer outcomes of ER⁺ breast cancer patients in a recent large-scale clinical study and meta-analysis (Figure 6B and C, and Figure S6A). In line with this, SMAD2/3 ChIP-seq analysis in the TNBC lines Hs-578-T and BT-549 (Figure S6B and C) showed that the binding patterns of

SMAD2/3 in these TNBC cell lines are different from MII cells and, in addition, heterogeneity among the TNBC cell lines.

In summary, our study presents a model how JUNB mediates a TGF β signaling feed-forward network in which WNT7B plays an effector role in specific breast cancer subtypes to promote breast cancer invasion (Figure S7).

Availability

ChIP- and RNA-seq raw data are available in Gene Expression Omnibus under accession number *GSE83788*.

Acknowledgements

We thank our colleagues, in particular Aristidis Moustakas and Oleksander Voytyuk, for their valuable discussion, Martijn Rabelink, Sijia Liu, Kaori Shiina and Hiroko Meguro for technical assistance, the ENCODE Consortium for data use, and Leiden Genome Technology Center in Leiden University Medical Center for sequencing.

Funding

Swedish Cancer Foundation [090773, 100452, 2016/445]; Swedish Research Council [2015-02757]; Kanae Foundation for Research Abroad; ITO Genboku and SAGARA Chian Memorial Scholarship (to M.M.); The Japan Society for the Promotion of Science (JSPS) (to N.K.); KAKENHI Grants-in-Aid for Scientific Research (S) [15H05774] (to K.M.). Funding for open access charge: Swedish Research Council [2015-02757].

References

1. Heldin CH, Miyazono K, ten Dijke P. TGF β signalling from cell membrane to nucleus through SMAD proteins. *Nature* 1997, 390(6659):465-71.
2. Kang JS, Liu C, Derynck R. New regulatory mechanisms of TGF β receptor function. *Trends Cell Biol* 2009, 19(8):385-94.
3. Shi Y, Massagué J. Mechanisms of TGF β signaling from cell membrane to the nucleus. *Cell* 2003, 113(6):685–700.
4. Massagué J, Seoane J, Wotton D. Smad transcription factors. *Genes Dev* 2005, 19(23):2783-810.
5. Ross S, Hill CS. How the Smads regulate transcription. *Int. J. Biochem. Cell Biol* 2008, 40(10):383-408.
6. Akhurst RJ, Padgett RW. Matters of context guide future research in TGF β superfamily signaling. *Sci Signal* 2015, 8(399):re10.

7. Ikushima H, Miyazono K. TGF β signal transduction spreading to a wider field: a broad variety of mechanisms for context-dependent effects of TGF β . *Cell Tissue Res* 2012, 347(1):37-49.
8. Massagué J. TGF β signalling in context. *Nat Rev Mol Cell Biol* 2012, 13(10):616-30.
9. Roberts AB, Wakefield LM. The two faces of transforming growth factor β in carcinogenesis. *Proc Natl Acad Sci U S A* 2003, 100(15):8621-23.
10. Akhurst RJ, Derynck R. TGF β signaling in cancer—a double-edged sword. *Trends Cell Biol* 2001, 11(11):S44–51.
11. Ikushima H, Miyazono K. TGF β signalling: a complex web in cancer progression. *Nat Rev Cancer* 2010,10(6):415-24.
12. Padua D, Massagué J. Roles of TGF β in metastasis. *Cell Res* 2009, 19(1):89-102.
13. Moses H, Barcellos-Hoff M.H. TGF β biology in mammary development and breast cancer. *Cold Spring Harb Perspect Biol* 2011, 3(1):a003277.
14. Garraway LA, Lander ES. Lessons from the cancer genome. *Cell* 2013, 153(1):17-37.
15. Sundqvist A, ten Dijke P, van Dam H. Key signaling nodes in mammary gland development and cancer: Smad signal integration in epithelial cell plasticity. *Breast Cancer Res* 2012, 14(1):204.
16. Sundqvist A, Zieba A, Vasilaki E, *et al.* Specific interactions between Smad proteins and AP-1 components determine TGF β -induced breast cancer cell invasion. *Oncogene* 2013, 32(31):3606-15.
17. Coulouarn C, Factor VM, Thorgeirsson SS. Transforming growth factor- β gene expression signature in mouse hepatocytes predicts clinical outcome in human cancer. *Hepatology* 2008, 47(6):2059-67.
18. van Dam H, Castellazzi M. Distinct roles of Jun: Fos and Jun: ATF dimers in oncogenesis. *Oncogene* 2001, 20(19):2453-64.
19. Ozanne BW, Spence HJ, McGarry LC, *et al.* Transcription factors control invasion: AP-1 the first among equals. *Oncogene* 2007, 26(1):1–10.
20. Shaulian E, Karin M. AP-1 as a regulator of cell life and death. *Nat Cell Biol* 2002(5), 4:E131-6.
21. Qing J, Zhang Y, Derynck R. Structural and functional characterization of the transforming growth factor- β -induced Smad3/c-Jun transcriptional cooperativity. *J Biol Chem* 2000, 275(49):38802-12.
22. Zhang Y, Feng XH, Derynck R. Smad3 and Smad4 cooperate with c-Jun/c-Fos to mediate TGF β -induced transcription. *Nature* 1998, 394(6696):909-13.
23. Javelaud D, Mauviel A. Crosstalk mechanisms between the mitogen-activated protein kinase pathways and Smad signaling downstream of TGF β : implications for carcinogenesis. *Oncogene* 2005, 24(37):5742-50.
24. Akhurst RJ, Hata A. Targeting the TGF β signalling pathway in disease. *Nat Rev Drug Discov* 2012, 11(10):790-811.

25. Niwa H, Masui S, Chambers I, *et al.* Phenotypic complementation establishes requirements for specific POU domain and generic transactivation function of Oct-3/4 in embryonic stem cells. *Mol Cell Biol* 2002, 22(5):1526-36.
26. Lawson ND, Weinstein BM. *In vivo* imaging of embryonic vascular development using transgenic zebrafish. *Dev Biol* 2002, 248(2):307-18.
27. He S, Lamers GE, Beenakker JW, *et al.* Neutrophil-mediated experimental metastasis is enhanced by VEGFR inhibition in a zebrafish xenograft model. *J Pathol* 2012, 227(4):431-45.
28. Isogaya K, Koinuma D, Tsutsumi S, *et al.* A Smad3 and TTF-1/NKX2-1 complex regulates Smad4-independent gene expression. *Cell Res* 2014, 24(8):994-1008.
29. Morikawa M, Koinuma D, Mizutani A, *et al.* BMP sustains embryonic stem cell self-renewal through distinct functions of different Krüppel-like factors. *Stem Cell Rep* 2016, 6(1):64-73.
30. Langmead B, Trapnell C, Pop M, *et al.* Ultrafast and memory-efficient alignment of short DNA sequences to the human genome. *Genome Biol* 2009, 10(3):R25.
31. Zhang Y, Liu T, Meyer CA, *et al.* Model-based analysis of ChIP-Seq (MACS). *Genome Biol* 2008, 9(9):R137.
32. Ji H, Jiang H, Ma W, *et al.* An integrated software system for analyzing ChIP-chip and ChIP-seq data. *Nat Biotechnol* 2008, 26(11):1293-1300.
33. Machanick P, Bailey TL. MEME-ChIP: motif analysis of large DNA datasets. *Bioinformatics* 2011, 27(12):1696-7.
34. Huang da W, Sherman BT, Lempicki RA. Systematic and integrative analysis of large gene lists using DAVID bioinformatics resources. *Nat Protoc* 2009, 4(1):44-57.
35. McLean CY, Bristor D, Hiller M, *et al.* GREAT improves functional interpretation of cis-regulatory regions. *Nat Biotechnol* 2010, 28(5):495-501.
36. Hong CP, Choe MK, Roh TY. Characterization of chromatin structure-associated histone modifications in breast cancer cells. *Genomics Inform* 2012, 10(3):145-52.
37. The ENCODE Project Consortium, An integrated encyclopedia of DNA elements in the human genome. *Nature* 2012, 489(7414):57-74.
38. Parkhomchuk D, Borodina T, Amstislavskiy V, *et al.* Transcriptome analysis by strand-specific sequencing of complementary DNA. *Nucleic Acids Res* 2009, 37(18):e123.
39. Trapnell C, Roberts A, Goff L, *et al.* Differential gene and transcript expression analysis of RNA-seq experiments with TopHat and Cufflinks. *Nat Protoc* 2012, 7(3):562-78.
40. Pereira B, Chin SF, Rueda OM, *et al.* The somatic mutation profiles of 2,433 breast cancers refines their genomic and transcriptomic landscapes. *Nat Commun* 2016, 7:11479.

41. Vasilaki E, Morikawa M, Koinuma D, *et al.* Ras and TGF β signaling enhance cancer progression by promoting the Δ Np63 transcriptional program. *Sci Signal* 2016, 9(442):ra84.
42. Cerami E, Gao J, Dogrusoz U, *et al.* The cBio cancer genomics portal: an open platform for exploring multidimensional cancer genomics data. *Cancer Discov* 2012, 2(5):401-4.
43. Gao J, Aksoy BA, Dogrusoz U, *et al.* Integrative analysis of complex cancer genomics and clinical profiles using the cBioPortal. *Sci Signal* 2013, 6(269):p11.
44. Györfy B, Lanczky A, Eklund AC, *et al.* An online survival analysis tool to rapidly assess the effect of 22,277 genes on breast cancer prognosis using microarray data of 1,809 patients. *Breast Cancer Res Treat* 2010, 123(3):725-31.
45. Mootha VK, Lindgren CM, Eriksson KF, *et al.* PGC-1 α -responsive genes involved in oxidative phosphorylation are coordinately downregulated in human diabetes. *Nat Genet* 2003, 34(3):267-73.
46. Koinuma D, Tsutsumi S, Kamimura N, *et al.* Chromatin immunoprecipitation on microarray analysis of Smad2/3 binding sites reveals roles of ETS1 and TFAP2A in transforming growth factor β signaling. *Mol Cell Biol* 2009, 29(1):172-86.
47. Roberts AB, Sporn MB, Assoian RK, *et al.* Transforming growth factor type β : rapid induction of fibrosis and angiogenesis in vivo and stimulation of collagen formation *in vitro*. *Proc Natl Acad Sci U S A* 1986, 83(12):4167-71.
48. Imitola J, Massagué J. Transforming growth factor- β stimulates the expression of fibronectin and collagen and their incorporation into the extracellular matrix. *J Biol Chem* 1986; 261(9):4337-45.
49. Pickup M, Novitskiy, Moses HL. The roles of TGF β in the tumour microenvironment. *Nat Rev Cancer* 2013, 13(11):788-99.
50. Drabsch Y, He S, Zhang L, *et al.* Transforming growth factor- β signalling controls human breast cancer metastasis in a zebrafish xenograft model. *Breast Cancer Res* 2013, 15(6):R106.
51. Petersen M, Pardali E, van der Horst G, *et al.* Smad2 and Smad3 have opposing roles in breast cancer bone metastasis by differentially affecting tumor angiogenesis. *Oncogene* 2010, 29(9):1351-61.
52. Deckers M, van Dinther M, Buijs J, *et al.* The tumor suppressor Smad4 is required for transforming growth factor β -induced epithelial to mesenchymal transition and bone metastasis of breast cancer cells. *Cancer Res* 2006, 66(4):2202-9.
53. Chen B, Dodge ME, Tang W, *et al.* Small molecule-mediated disruption of Wnt-dependent signaling in tissue regeneration and cancer. *Nat Chem Biol* 2009, 5(2):100-7.
54. Vogelstein B, Papadopoulos N, Velculescu VE, *et al.* Cancer genome landscapes. *Science* 2013, 339(6):1546-58.

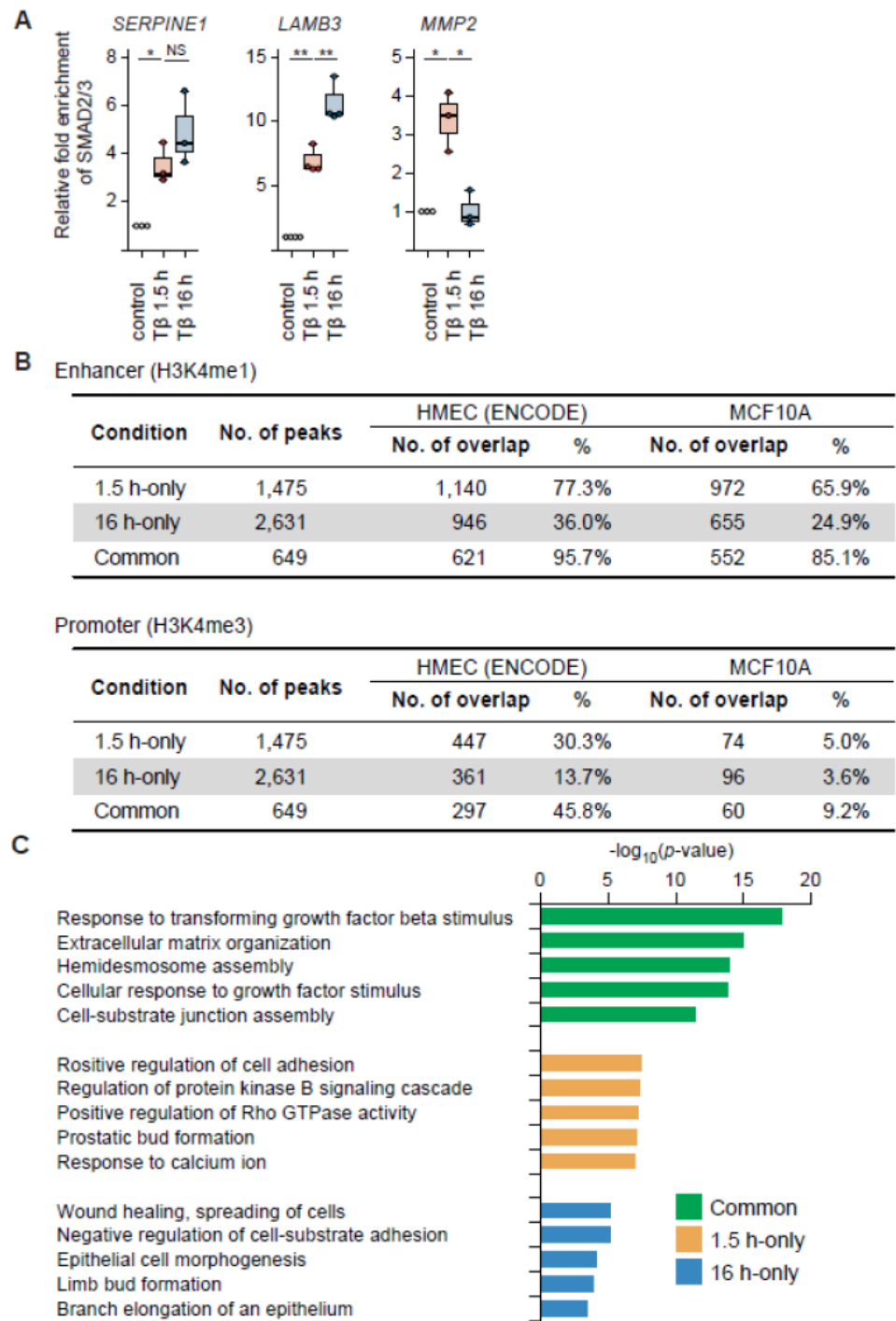
55. David CJ, Huang YH, Chen M, *et al.* TGF β tumor suppression through a lethal EMT. *Cell* 2016, 164(5):1015-30.
56. Cancer Genome Atlas Network, Comprehensive molecular portraits of human breast tumours. *Nature* 2012, 490(7418):61–70.
57. Stephens PJ, Tarpey PS, Davies H, *et al.* The landscape of cancer genes and mutational processes in breast cancer. *Nature* 2012, 486(7403):400-4.
58. Biddie SC, John S, Sabo PJ, *et al.* Transcription factor AP1 potentiates chromatin accessibility and glucocorticoid receptor binding. *Mol Cell* 2011, 43(1):145-55.
59. Zanonato F, Forcato M, Battilana G, *et al.* Genome-wide association between YAP/TAZ/TEAD and AP-1 at enhancers drives oncogenic growth. *Nat Cell Biol* 2015, 17(9):1218-27.
60. Zhao C, Qiao Y, Jonsson P, *et al.* Genome-wide profiling of AP-1-regulated transcription provides insights into the invasiveness of triple-negative breast cancer. *Cancer Res* 2014, 74(14):3983-94.
61. Huguet EL, McMahon JA, McMahon AP, *et al.* Differential expression of human Wnt genes 2, 3, 4, and 7B in human breast cell lines and normal and disease states of human breast tissue. *Cancer Res* 1994, 54(10):2615-21.
62. Ni M, Chen Y, Lim E, *et al.* Brown M. Targeting androgen receptor in estrogen receptor-negative breast cancer. *Cancer Cell* 2011; 20(1):119-31.
63. Labbé E, Letamendia A, Attisano L. Association of Smads with lymphoid enhancer binding factor 1/T cell-specific factor mediates cooperative signaling by the transforming growth factor- β and Wnt pathways. *Proc Natl Acad Sci U S A* 2000, 97(15):8358-63.
64. Nishita M, Hashimoto MK, Ogata S, *et al.* Interaction between Wnt and TGF β signalling pathways during formation of Spemann's organizer. *Nature* 2000, 403(6771):781-5.
65. Scheel C, Eaton EN, Li SH, C *et al.* Paracrine and autocrine signals induce and maintain mesenchymal and stem cell states in the breast. *Cell* 2011, 145(6):926-40.
66. Akhmetshina A, Palumbo K, Dees C, *et al.* Activation of canonical Wnt signalling is required for TGF β -mediated fibrosis. *Nat Commun* 2012, 3:735.
67. Avgustinova A, Iravani M, Robertson D, *et al.* Tumour cell-derived Wnt7a recruits and activates fibroblasts to promote tumour aggressiveness. *Nat Commun* 2016, 7:10305.
68. Wiercinska E, Naber HP, Pardali E, *et al.* The TGF β /Smad pathway induces breast cancer cell invasion through the up-regulation of matrix metalloproteinase 2 and 9 in a spheroid invasion model system. *Breast Cancer Res Treat* 2011, 128(3):657-66.

Supplementary Table S1. Primer sequences used for qRT-PCR. Primer sequences used for qRT-PCR are shown. Fw, forward primer; Rev, reversed primer.

Name		Sequence
<i>CDH2</i>	Fw	5'-CCTGCTTCAGGCGTCTGTAGA-3'
	Rev	5'-TCATGCACATCCTTCGATAAGACT-3'
<i>FERMT1</i>	Fw	5'-CTTGGTTCAGTGACAGCCCT-3'
	Rev	5'-GGAGTCTAGCCAACCTGCAT-3'
<i>FNI</i>	Fw	5'-CATCGAGCGGATCTGGCCC-3'
	Rev	5'-GCAGCTGACTCCGTTGCCCA-3'
<i>GAPDH</i>	Fw	5'-GGAGTCAACGGATTTGGTCGTA-3'
	Rev	5'-GGCAACAATATCCACTTTACCA-3'
<i>ITGA2</i>	Fw	5'-GCTGGTGCTCCTCGGGCAA-3'
	Rev	5'-TGGTCACCTCGGTGAGCCTGA-3'
<i>LAMA3</i> transcript variants 2 and 4	Fw	5'-CCTGGGGCAGTGTCTGGGCT-3'
	Rev	5'-TCCCGCGGTGTTGTGCTGAC-3'
<i>LAMB3</i>	Fw	5'-ACGGCAGAACACACAGCAAGGA-3'
	Rev	5'-ACCGGGTCCTCCCAACAAGCA-3'
<i>LAMC2</i> transcript variant 1	Fw	5'-CATCTGATGGACCAGCCTCTC-3'
	Rev	5'-GCAGTTGGCTGTTGATCTGG-3'
<i>MMP1</i>	Fw	5'-CCAAATGGGCTTGAAGCT-3'
	Rev	5'-GTAGCACATTCTGTCCCTAA-3'
<i>MMP2</i>	Fw	5'-AGATGCCTGGAATGCCAT-3'
	Rev	5'-GGTTCTCCAGCTTCAGGTAAT-3'
<i>SERPINE1</i>	Fw	5'-GAGACAGGCAGCTCGGATTC-3'
	Rev	5'-GGCCTCCCAAAGTGCATTAC-3'
<i>SNAIL</i>	Fw	5'-CACTATGCCGCGCTCTTTC-3'
	Rev	5'-GCTGGAAGGTAACTCTGGATTAGA-3'
<i>SNAIL2</i>	Fw	5'-ATGAGGAATCTGGCTGCTGT-3'
	Rev	5'-CAGGAGAAAATGCCTTTGGA-3'
<i>WNT7B</i>	Fw	5'-AAGCTCGGAGCACTGTCATC-3'
	Rev	5'-ACTGGTACTGGCACTCGTTG-3'

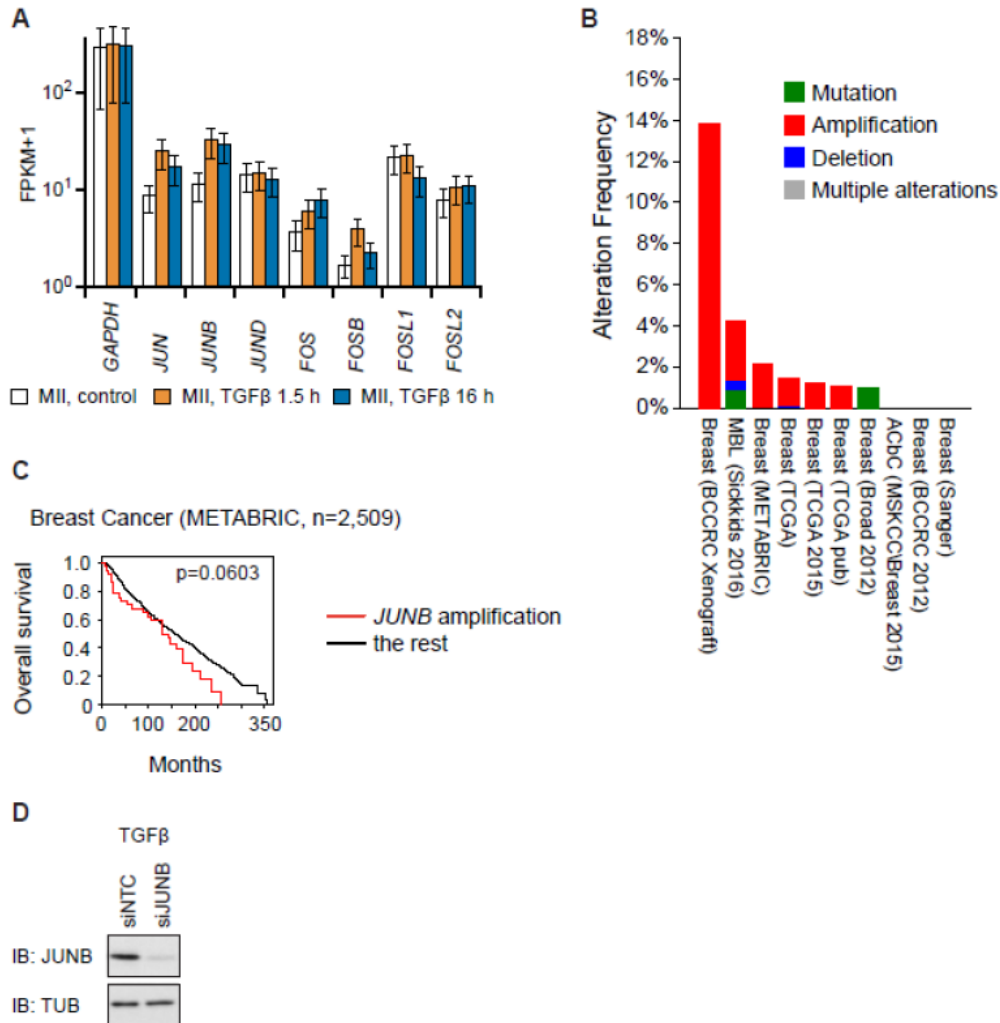
Supplementary Table S2. Primer sequences used for ChIP-qPCR. Primer sequences used for ChIPqPCR are shown. Fw, forward primer; Rev, reversed primer.

Name	Sequence
<i>HBB</i> Fw	5'-AACGTGATCGCCTTTCTC-3'
<i>HBB</i> Rev	5'-GAAGCAGAACTCTGCACTTC-3'
<i>HPRT1</i> Fw	5'-TGTTTGGGCTATTTACTAGTTG-3'
<i>HPRT1</i> Rev	5'-ATAAAATGACTTAAGCCCAGAG-3'
<i>SERPINE1</i> Fw	5'-GCAGGACATCCGGGAGAGA-3'
<i>SERPINE1</i> Rev	5'-CCAATAGCCTTGGCCTGAGA-3'
<i>LAMB3</i> Fw	5'-TTGCCCTGCACTACAACACA-3'
<i>LAMB3</i> Rev	5'-GTAACACACCAGGCCCACTT-3'
<i>MMP2</i> Fw	5'-TCCCAGGCCTGCCCATGTCA-3'
<i>MMP2</i> Rev	5'-GGAGCTGGTGGGTGGAAAGCC-3'
<i>WNT7B</i> Fw	5'-TCACCCATGACTCACTTGGC-3'
<i>WNT7B</i> Rev	5'-AGGTCTCTTCCGCTCTCAGT-3'

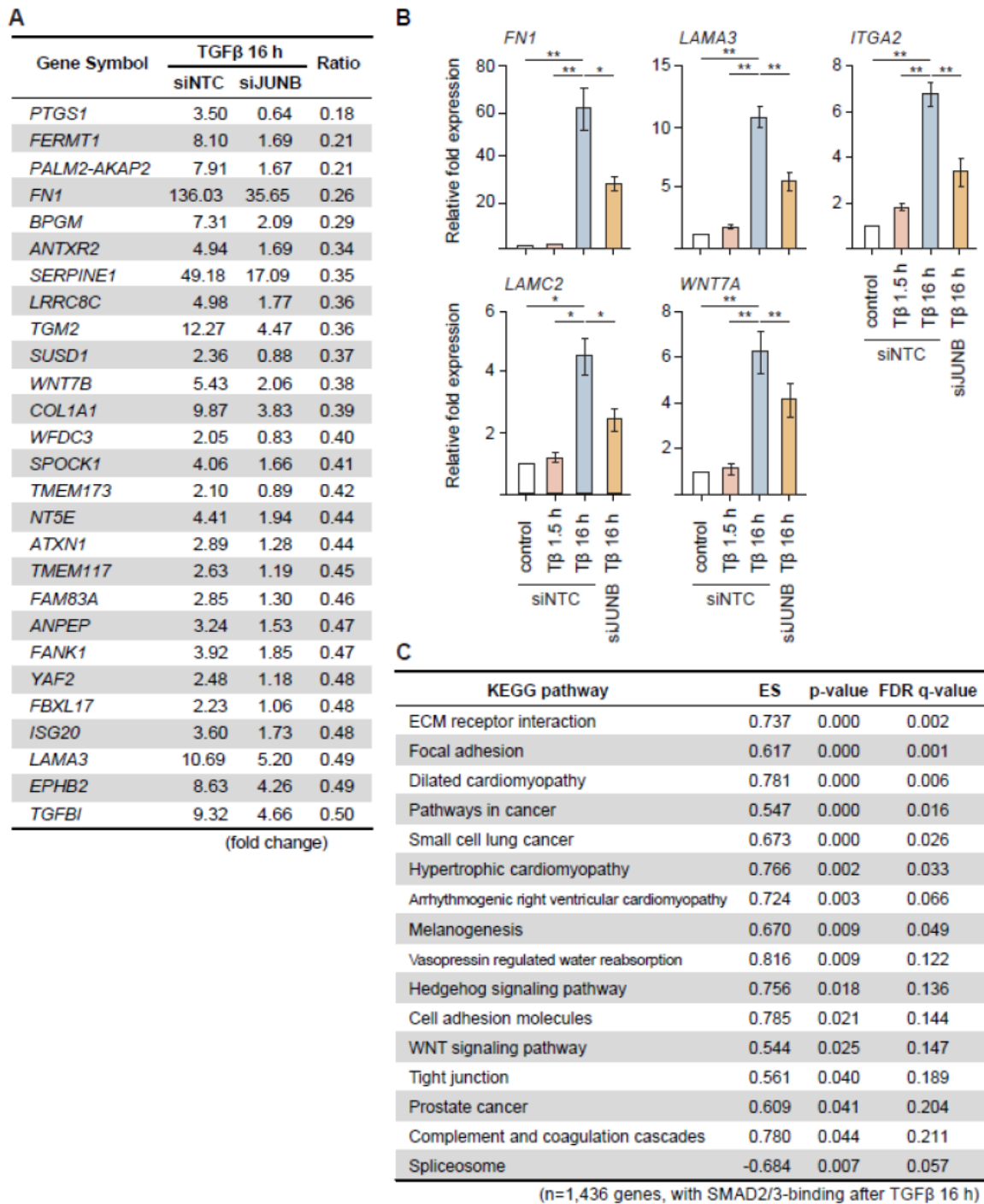


Supplementary Figure S1. SMAD2/3 are redirected to different sites in MCF10A MII after prolonged TGFβ treatment. (A) ChIP-qPCR showing time-dependent recruitment of SMAD2/3 to the SMAD binding site close to the *SERPINE1* transcription start site (TSS), the binding site approximately 5 kb upstream of the *LAMB3* TSS, and to the intronic binding site in the *MMP2* gene locus, in MCF10A MII cells after no treatment, or treatment with TGFβ (5 ng/ml) for 1.5 h or 16 h. Results of three independent experiments are shown by dot plot chart; * $P < 0.05$, ** $P < 0.01$. (B) Quantification of

overlap between the SMAD2/3 binding sites and histone marks in breast epithelial cells, related to Figure 1E. (C) Functional annotation of SMAD2/3 binding regions, performed using GREAT (35). The top five over-represented categories belonging to Gene Ontology (GO) biological process, which describes the biological processes associated with gene function, are presented. The x axis represents binomial raw (uncorrected) P -values in $(-\log_{10})$.

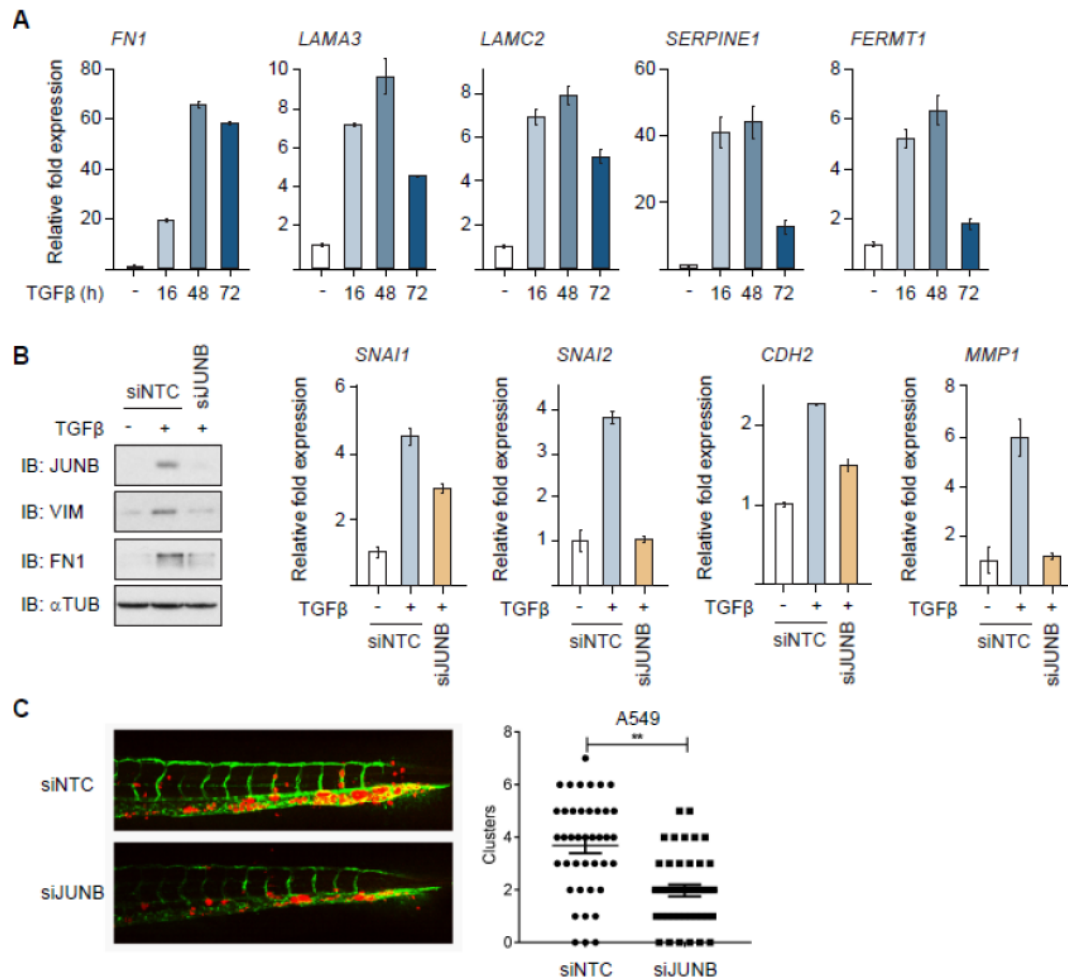


Supplementary Figure S2. JUNB is a critical AP1 component for SMAD2/3 binding after TGF β stimulation. (A) Expression levels of indicated genes in MCF10A MII cells after 1.5 h and 16 h TGF β (5 ng/ml) treatment are shown in FPKM (fragments per kilobase of exon per million fragments mapped) values (data represent FPKM \pm 95% confidence interval). (B and C) Frequency of JUNB gene alterations (mutation, amplification and deletion) in breast cancer datasets using cBioPortal (40, 42, 43). Patients with JUNB amplification had a trend of poorer prognosis (C), although this was not statistically significant because of the small number of the cases. (D) Western blot control of JUNB knockdown efficiency of Figure 3C.

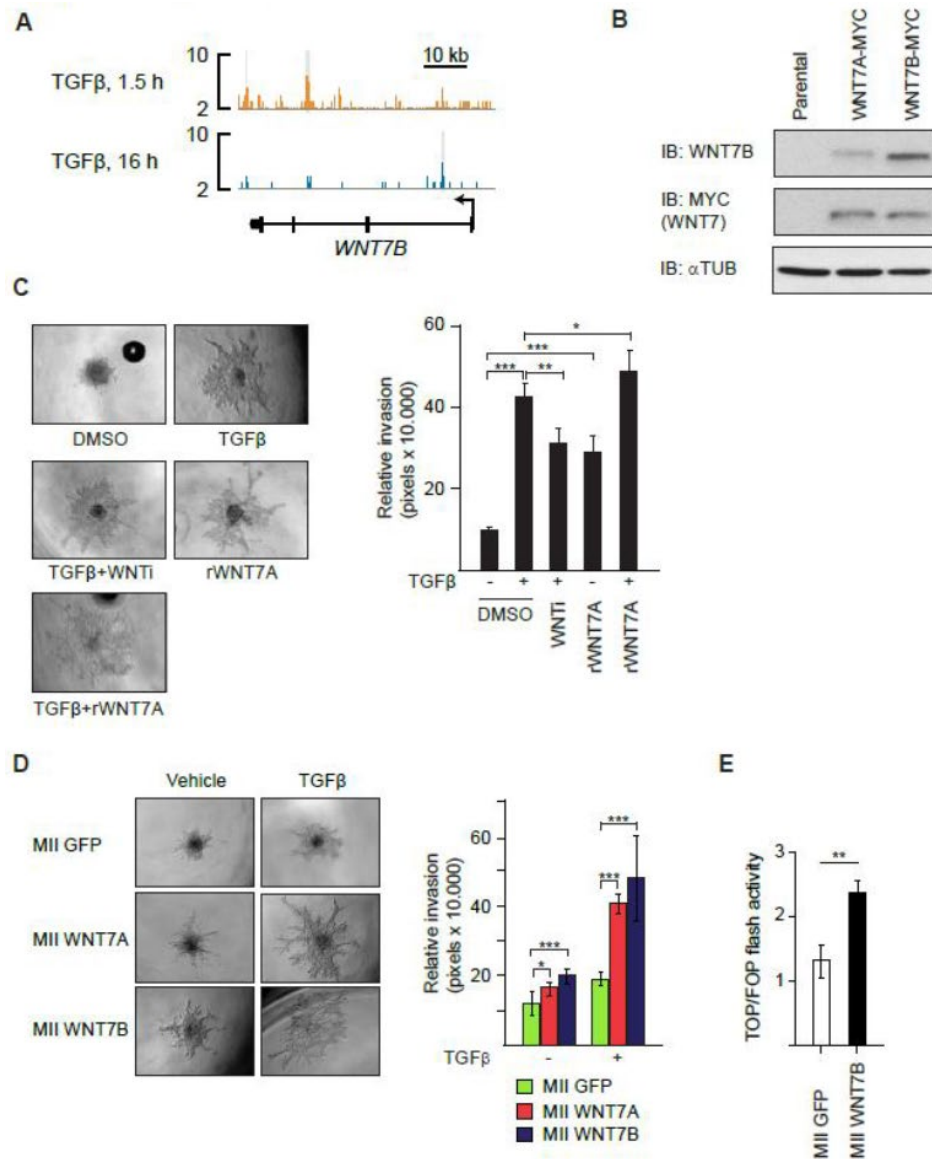


Supplementary Figure S3. A JUNB-mediated feed-forward mechanism regulates genes associated with cell adhesion and invasion. (A) A list of genes whose induction after 16 h TGFβ (5 ng/ml) treatment was attenuated more than 50 % with siJUNB treatment. See also Figure 4A. (B) qRT-PCR validation of identified JUNB target genes. MCF10A MII cells were transfected with non-targeting control (siNTC) or specific JUNB siRNA and stimulated for 1.5 h or 16 h with TGFβ (5 ng/ml). Results of three independent experiments are shown; * $P < 0.05$, ** $P < 0.01$. (C) GSEA of expression changes of

SMAD2/3 target genes after manipulation of JUNB expression. The SMAD2/3 target genes were pre-rank-ordered according to their fold change (log2) between siNTC and siJUNB, and analyzed based on KEGG signaling pathway enrichment. Gene sets with p -value < 5% and FDR q -value < 25% were considered significant. See also Figure 4B.

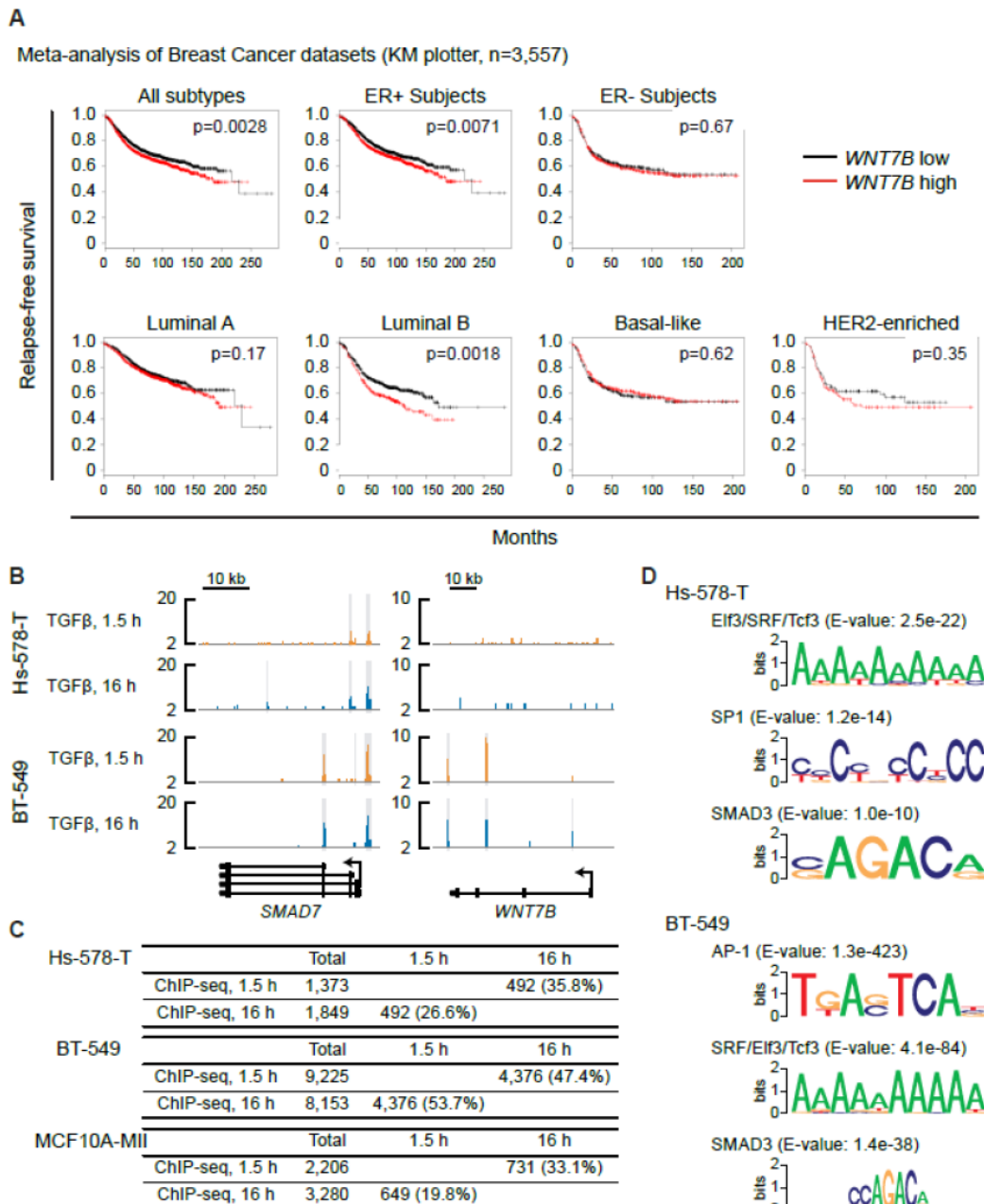


Supplementary Figure S4. JUNB regulates genes associated with EMT and invasion. (A) qRT-PCR analysis of late TGFβ-induced gene expression. MCF10A MII cells were stimulated for 16, 48 or 72 h with TGFβ (5 ng/ml). A representative results of three independent experiments is shown. (B) Western blot (left) and qRT-PCR (right) analysis of A549 human pulmonary adenocarcinoma cells transfected with non-targeting control (siNTC) or specific JUNB siRNA and treated with TGFβ (5 ng/ml) for 48 h (left) or 16 h (right) as indicated. (C) A549 mCherry cells transfected with non-targeting control (siNTC) or specific JUNB siRNA were injected into the ducts of Cuvier (DoC) of 48 hours post-fertilization (hpf) zebrafish embryos. Left: representative images of zebrafish at 6 days post-injection (dpi). Right: quantification of invasive cell cluster numbers in nontargeting and JUNB knock-down cells injected zebrafish larvae.

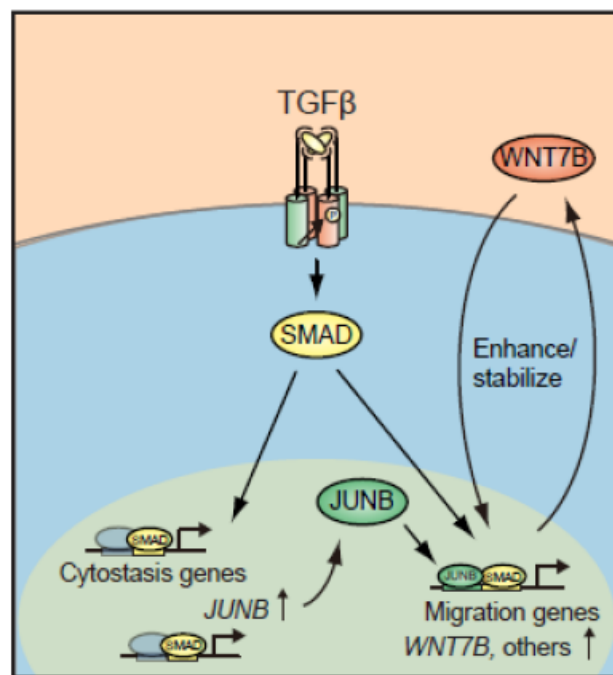


Supplementary Figure S5. Activation of the WNT signaling pathway strengthens the TGFβ-induced migratory phenotype. (A) Genomic locus of the *WNT7B* gene shown together with the results of SMAD2/3 ChIP-seq data obtained in MCF10A MII cells. The direction of transcription is shown by the arrow beginning at the TSS. Statistically significant regions are marked by a gray-colored box. (B) Western blot for WNT7A and WNT7B in MCF10A MII cells stable expressing control GFP or MYCtagged WNT7A (WNT7A-MYC) or WNT7B (WNT7B-MYC). (C) Collagen invasion assay of MCF10A MII spheroids. Spheroids were embedded in collagen in the absence or presence of TGFβ (5 ng/ml), recombinant WNT7A (300 ng/ml) or the WNT inhibitor (WNTi) IWP-2 (5 μM), as indicated. Left: representative pictures of spheroids taken 36 h after being embedded in collagen. Right: relative invasion was quantified as the mean area that the spheroids occupied 36 h after being embedded in collagen. Data represent means ± SD (n ≥ 6 spheroids per condition) and are representative of two

independent experiments; $*P < 0.05$, $**P < 0.01$, $***P < 0.001$. (D) Collagen invasion assay of MCF10A MII spheroids stably expressing control GFP, WNT7A or WNT7B. Spheroids were embedded in collagen in the absence or the presence of TGFβ (5 ng/ml). Left: representative pictures of spheroids taken 36 h after being embedded in collagen. Right: relative invasion was quantified as the mean area that the spheroids occupied 36 h after being embedded in collagen. Data represent means \pm SD ($n \geq 6$ spheroids per condition) and are representative of two independent experiments; $***P < 0.001$. (E) Canonical WNT signaling activity as measured by a TCF/LEF driven transcriptional luciferase reporter plasmid system in the MCF10A MII cells stably expressing control GFP or ectopic WNT7B-MYC.



Supplementary Figure S6. ChIP-seq of TNBC cell lines and meta-analysis of published microarray datasets of Breast Cancer patients. (A) Kaplan-Meier analysis of relapse-free survival of breast cancer datasets, generated using KM plotter (35); all subtypes, $n=3,557$; ER⁺ subjects, $n=2,036$; ER subjects, $n=807$; luminal A subtype, $n=2,069$; luminal B subtype, $n=1,166$; HER2⁻ subtype, $n=239$; basal-like subtype, $n=668$). Survival analysis was performed using a log-rank test. (B) Genomic loci of *SMAD7* and *WNT7B* are shown together with the results of SMAD2/3 ChIP-seq data obtained in the TNBC cells Hs-578-T and BT-549. The direction of transcription is shown by the arrow beginning at the TSS. Statistically significant regions are marked by a gray-colored box. (C) The number of SMAD2/3 binding sites and overlap between 1.5 h and 16 h. The number of ChIP-seq peaks in each time point is presented. The number of peaks overlapping with other conditions is also presented, together with the percent to the total. (D) Motifs enriched in the SMAD2/3 binding sites in TNBCs treated with TGF β for 1.5 h.



Supplementary Figure S7. Working model. The TGF β /SMAD-mediated induction of JUNB in premalignant cells causes redirection of SMAD binding to different sites on the genome which results in the activation of an invasion-mediating transcriptional program via a self-enabling mechanism. This self-enabling TGF β /SMAD/JUNB-dependent transcriptional program will contribute to make the cell more migratory/invasive. One example of a TGF β and JUNB-induced target gene activated by this mechanism is WNT7B. We suggest that in late phases of breast cancer the JUNB/WNT7B signaling pathway contributes to the tumor promoting function of TGF β .

Chapter 6

Combined Inhibition of TGF β Signaling and the PD-L1 Immune Checkpoint Is Differentially Effective in Tumor Models

Heng Sheng Sow*, **Jiang Ren***, Marcel Camps, Ferry Ossendorp, and Peter ten Dijke

Cells 2019, 8(4):E320.

*These authors contributed equally

Abstract

Antibodies blocking the programmed death-ligand 1 (PD-L1) have shown impressive and durable responses in clinical studies. However, this type of immunotherapy is only effective in a subset of patients and not sufficient for rejection of all tumor types. In this study, we explored in two mouse tumor models whether the antitumor effect could be enhanced by the combined blockade of PD-L1 and transforming growth factor- β (TGF β), a potent immunosuppressive cytokine. The effect of anti-PD-L1 mouse monoclonal (mAb) and a TGF β type I receptor small molecule kinase inhibitor (LY364947) was evaluated in the highly immunogenic mouse MC38 colon adenocarcinoma and the poorly immunogenic mouse KPC1 pancreatic tumor model. In the MC38 tumor model, LY364947 monotherapy did not show any antitumor effect, whereas treatment with anti-PD-L1 mAb significantly delayed tumor outgrowth. However, combination therapy showed the strongest therapeutic efficacy, resulting in improved long-term survival compared with anti-PD-L1 mAb monotherapy. This improved survival was associated with an increased influx of CD8⁺ T cells in the tumor microenvironment. In the KPC1 tumor model, LY364947 did not enhance the antitumor effect of anti-PD-L1 mAb. Despite this, delayed KPC1 tumor outgrowth was observed in the LY364947-treated group and this treatment led to a significant reduction of CD4⁺ T cells in the tumor microenvironment. Together, our data indicate that an additive anti-tumor response of dual targeting PD-L1 and TGF β is dependent on the tumor model used, highlighting the importance of selecting appropriate cancer types, using in-depth analysis of the tumor microenvironment, which can benefit from combinatorial immunotherapy regimens.

Keywords: Anti-PD-L1 mAb; LY364947; Mouse syngeneic tumor models

Introduction

Immune checkpoint molecules are gaining prominence as targets for cancer immunotherapy, demonstrating durable remission of patients with metastatic lesions [1]. Last year the Nobel prize for physiology and medicine was awarded to James P. Allison and Tasuku Honjo “for their discovery of cancer therapy by inhibition of negative immune regulation” [2]. Antibodies targeting programmed death ligand 1 (PD-L1) such as atezolizumab, avelumab, and durvalumab have received regulatory approval [3-6]. Despite showing remarkable durable remissions, these antibodies only demonstrate their efficacy in a subset of specific cancer types [7]. In order to increase the therapeutic efficacy, many on-going preclinical and clinical studies are evaluating anti-PD-L1 mAb in combination with other immunostimulatory agents or cancer-modulating drugs. An important strategy is to down-regulate the immune suppression that is elicited by the tumor microenvironment to allow immunotherapy to be effective.

Transforming growth factor- β (TGF β) is an immunosuppressive cytokine which is often produced in large quantities by many cell types in the tumor microenvironment, including tumor cells [8,9]; regulatory T cells [10, 11]; and myeloid suppressor cells [12, 13]. TGF β is well known for its pleiotropic role from initiating to promoting tumor development [14-17] and it has a negative effect on anti-tumor immunity by suppressing the effector functions of several immune effector cells such as neutrophils, macrophages, natural killer (NK) cells, CD8 cells, and CD4 T cells [16, 18-20]. Together with other cytokines such as interleukin (IL)-2 and IL-6, TGF β also induces the generation and recruitment of regulatory T cells to further suppress the antitumor T and NK cell responses [21, 22]. Moreover, it is also known for its role in regulating and promoting the accumulation of stiff fibrillary extracellular matrix composed of collagen [23], resulting in hindered drug transport [24] and infiltration of immune cells [25-27] into the tumor. Most importantly, high serum levels of three TGF β isoforms, TGF β 1, TGF β 2, and TGF β 3, correlate with poor clinical outcome [28-32].

As such, it is plausible that TGF β inhibition, through reducing immune suppression and decreasing deposition of matrix collagen content, could potentially improve infiltration of activated immune effector cells and delivery of drug into the tumor microenvironment. In this study, we investigated if the treatment of TGF β receptor 1 selective small molecule kinase inhibitor, termed LY364947 [33], can enhance the antitumor efficacy of anti-PD-L1 mAb in

immunogenic (MC38 colorectal tumor) and poorly immunogenic (KPC1 pancreatic tumor) tumor models.

Materials and Methods

Cell culture

The mouse breast cancer TUBO cell line was a gift from Prof Guido Forni [34]; mouse pancreatic tumor cell lines KPC1 and KPC3 were obtained from Dr Thorsten Hagemann (Queen Mary, University of London). B16OVA, a variant of the melanoma B16F10 tumor line that expresses full-length OVA, was a gift from K. L. Rock (University of Massachusetts Medical Center, Worcester, MA, USA). EL4 and B16F10 cell lines were obtained from ATCC (Rockville, MD, USA). RMA is a mutagenized derivative of RBL-5, a Rauscher MuLV-induced T lymphoma cell line [35]. The MC38 tumor cell line is derived from a primary mouse colon carcinoma [36]. The C3 tumor cell line was generated by transfection of B6 mouse embryonic cells (MEC) with the complete HPV16 genome and maintained as previously described [37]. All tumor cell lines were cultured in Iscove's modified Dulbecco's medium (IMDM) (Lonza, Allendale, NJ, USA) supplemented with 10% heat-inactivated fetal bovine serum (FBS) (Greiner, Bio-One, Frickenhausen, Germany), 2 mM l-glutamine (Gibco, Invitrogen, Blijswijk, The Netherlands), 25 μ M 2-mercaptoethanol (Merck, Darmstadt, Germany), and 100 IU/mL penicillin/streptomycin (Gibco). Dulbecco's modified Eagle's medium (DMEM) supplemented with 10% heat-inactivated FBS (Greiner, Bio-One, Frickenhausen, Germany) and 100 U/mL penicillin/streptomycin (Gibco) were used to culture human embryonic kidney (HEK)293 cells. HEK293 cells were obtained from ATCC (Rockville, MD, USA). All cell lines in our studies were maintained at 37 °C, with 5% CO₂, in a humidified incubator and were free of mycoplasma.

Mice

Wild-type (WT) C57Bl/6 female mice were purchased from Charles River (L'Arbresle, France) and maintained under specific pathogen-free (SPF) animal facilities of the Central Animal Facility (PDC) of the Leiden University Medical Center (LUMC). Mice were 8–9 weeks old at the beginning of each experiment. The health status of the animals was monitored over time. Animals tested negative for all agents listed in the Federation of European Laboratory Animal Science Associations (FELASA) guidelines for SPF mouse colonies [38]. All animal studies were approved by the animal ethics committee of LUMC. Experiments were performed

recommendations and guidelines set by LUMC and the Dutch Act on Animal Experimentation and EU Directive 2010/63/EU (Guidelines on the Protection of Experimental Animals).

Syngeneic tumor studies

MC38 colon adenocarcinoma cancer cells (4×10^5 cells) were injected subcutaneously into 8–12-week-old mice in 100 μ L of phosphate buffered saline (PBS). Then, 200 μ g of anti-PD-L1 mAb (clone MIH5) were injected intraperitoneally at days 6, 8, and 11 after inoculation. LY364947 was purchased from Selleckchem (Huston, TX, USA) and dissolved in dimethylsulfoxide (DMSO) to make final concentration of 20 mg/mL. Then, 10 mg/kg of LY364947 were injected intraperitoneally at days 6, 8, and 11 and once every three days after cancer cell inoculation. The KPC1 pancreatic cancer cell line was generated from Kras^{LSL-G12D/+}, Trp53^{LSL-R172H/+}, Pdx1-Cre (KPC) mice and was a gift from Thorsten Hagemann (Queen Mary University of London). The tumor cells (1×10^5 cells) were injected subcutaneously into 8–12-week-old mice in 100 μ L of PBS. At days 9, 11, and 14 post tumor inoculation, mice were injected intraperitoneally with 200 μ g of anti-PD-L1 mAb (clone MIH5). For the LY364947 or combination group, mice received 10 mg/kg of LY364947 (intraperitoneally) at day 9 and once every day post tumor inoculation. All tumors were measured twice weekly using calipers. Mice were sacrificed when tumors reached a size of 100 mm² to avoid unnecessary suffering. Both cell lines were mycoplasma and mouse antibody production (MAP)-tested before the start of tumor studies.

Flow cytometry

Harvested tumors were manually minced into small pieces with scalpels before incubating with 350 μ g/mL Liberase TL (Roche) for 20 min at 37 °C and filtered through a 70- μ m cell strainers (BD Biosciences, Bedford, MA, USA) to obtain single cell suspension. The cells were subjected to Ammonium-Chloride-Potassium (ACK) lysis (5 min) before staining with 10% normal mouse serum and anti-mouse CD16/CD32 antibody (clone 2.4G2) to block Fc receptor for IgG (Fc γ Rs). Single-cell suspensions of tumor-infiltrating lymphocytes were stained using the following antibodies: CD8 α (clone 53-6.7), CD4 (clone L3T4), CD3 ϵ (clone 145-2c11), CD11b (clone M1/70), F4/80 (clone BM8), CD45.2 (clone 104), Ly6G (clone 1A8), PD-L1 (clone MIH5), LAG-3 (C9B7W), and CTLA-4 (9H10). Then, 7-AAD staining (Invitrogen, Carlsbad, CA, USA) was used to exclude dead cells. All stained cells were analyzed on a LSRII cytometer (BD) and data analysis was performed with FlowJo Software v10 (Tree Star, San Carlos, CA, USA).

mTGFβ1 ELISA

Briefly, tumor cell lines were cultured in 24-well plates in complete IMDM until 80% confluent. Cells were washed twice with PBS and cultured in IMDM supplemented with 1% FBS (not heat-inactivated) for 24 h at 37 °C. Supernatants were collected and stored at −20 °C until further analysis. Total mTGFβ1 levels were measured by using a Mouse TGFβ1 duoset ELISA kit according to the manufacturer's instructions (#DY1679, R&D Systems, Minneapolis, MN, USA).

CAGA luciferase reporter assay

To produce conditional medium (CM), MC38, KPC1, KPC3, and B16F10 cells were washed two times with PBS at 70–80% confluency and incubated in serum-free DMEM medium for 24 h. CM was then collected and passed through a 0.45-mm Syringe Filter (SLHP033RB, Merck Millipore, Billerica, MA, USA). HEK293 cells were seeded at approximately 5×10^4 cells per well into a 24-well plate. The next day, cells in each well were co-transfected with 0.1 μg TGFβ/SMAD inducible (CAGA)12 luciferase transcriptional reporter construct, which encodes 12 repeats of the AGCCAGACA sequence (identified as a SMAD3/SMAD4-binding element in the human PAI-1 promoter [39]), and 0.08 μg β-galactosidase construct (driven by a cytomegalovirus promoter) using five times of polyethyleneimine in quantity. After overnight incubation, HEK293 cells were starved with serum free medium. Eight hours later, serum free media were removed and replaced by CM. A TGFβ treatment (5 ng/mL, 8420-B3, R&D SYSTEMS, Minneapolis, MN, USA) was also performed that served as a standard. After another overnight incubation, luciferase and β-galactosidase activities were measured. The luciferase activity was normalized based on the β-galactosidase activity. Representative experiments indicating the mean and standard deviation of triplicate values are shown.

Western blot

Approximately 2.5×10^5 of MC38 and KPC1 cells were plated in 6-well plate in complete medium and incubated overnight at 37 °C. The next day, the complete medium was replaced with 0.2% FBS medium and further incubated at 37 °C for eight hours. Cells were then treated with 1 μg/mL of LY364947 for 30 min before stimulating with 5 ng/mL of TGFβ3 for 2 h. Cells were lysed in radioimmunoprecipitation assay buffer (RIPA) sampler buffer (50 mM Tris-HCl (pH 8.0) with 150 mM NaCl, 1.0% Nonidet P-40, 0.5% sodium deoxycholate, and 0.1% sodium dodecyl sulfate) containing cOmplete™ Protease Inhibitor Cocktail (11697498001, Roche, Basel,

Switzerland). Protein concentration was determined using a DC™ Protein Assay Kit (5000111, Bio-Rad, Hercules, CA, USA). An equal amount of protein was subjected to sodium dodecyl sulfate–polyacrylamide gel electrophoresis and blotted onto a polyvinylidene difluoride membrane (IPVH00010, Merck Millipore). Membrane was probed with phospho-SMAD2 antibody [40] (homemade) and GAPDH antibody (AB2302, Merck Millipore, Billerica, MA, USA). The chemiluminescent signal was detected using the Clarity™ Western ECL Substrate (Hercules, CA, USA) and visualized using the ChemiDoc Imaging Systems (17001402, Bio-Rad, Hercules, CA, USA).

***In vitro* cell proliferation assay**

MC38 and KPC1 cells were plated in a 96-well plate, with 2×10^3 cells/well approximately, and incubated overnight. Cells were treated with vehicle control, or 1 μg/mL of LY364947, or 5 ng/mL of TGFβ3, or a LY364947 and TGFβ3 combination. The cell proliferation was determined by CellTiter 96 AQueous Non-Radioactive Cell Proliferation Assay (MTS) (G5421, Promega BioSciences, Madison, WI, USA) following the manufacturer's protocol. Absorbance was measured at 490 nm over 5 consecutive days using VICTORX Multilabel Plate Reader (2030-0050, Perkin Elmer, Waltham, MA, USA). Each group was evaluated in five repeats, and a cell growth curve was plotted.

Statistical analyses

Data were analyzed using Prism 7.0 GraphPad Prism 7.0 (GraphPad Software, La Jolla, CA, USA). To determine statistical significance between two groups, an unpaired Student's t-test was performed. Significance between more than two groups was evaluated by one-way ANOVA. Kaplan-Meier method and the log-rank (Mantel-Cox) test were used to determine statistical differences in the survival of mice.

Results

Colorectal and pancreatic cancer cells produce high levels of mTGFβ1

In order to select mouse tumor models to investigate the therapeutic efficacy of combining TGFβ inhibitor and anti-PD-L1 mAb, we measured mTGFβ1 production by various mouse tumor cell lines. As illustrated in Figure 1A, ELISA analysis revealed that both pancreatic (KPC1) and colorectal (MC38) cancer cell lines produced high levels of latent mTGFβ1 protein. Using a transcriptional reporter assay, we observed that MC38 but not KPC1 cells secreted elevated

amounts of active mTGFβ (Figure 1B). Due to the high level of production of latent and/or active mTGFβ, MC38 and KPC1 were selected for in vivo analysis. We first evaluated the TGFβ/SMAD2 response and efficacy of the small molecule inhibitor LY364947 targeting the TGFβRI serine/threonine kinase activity in both cell lines when cultured in vitro. TGFβ potently stimulated the phosphorylation of SMAD2 (pSMAD2) in MC38 and KPC1 cell lines and this was blocked by LY364947 (Figure 1C). Despite these inhibitory effects, the proliferation of tumor cells remained unaffected by LY36947 and/or TGFβ treatment (Figure 1D). Next, the effect of LY364947 treatment in vivo was determined by investigating intra-tumoral levels of

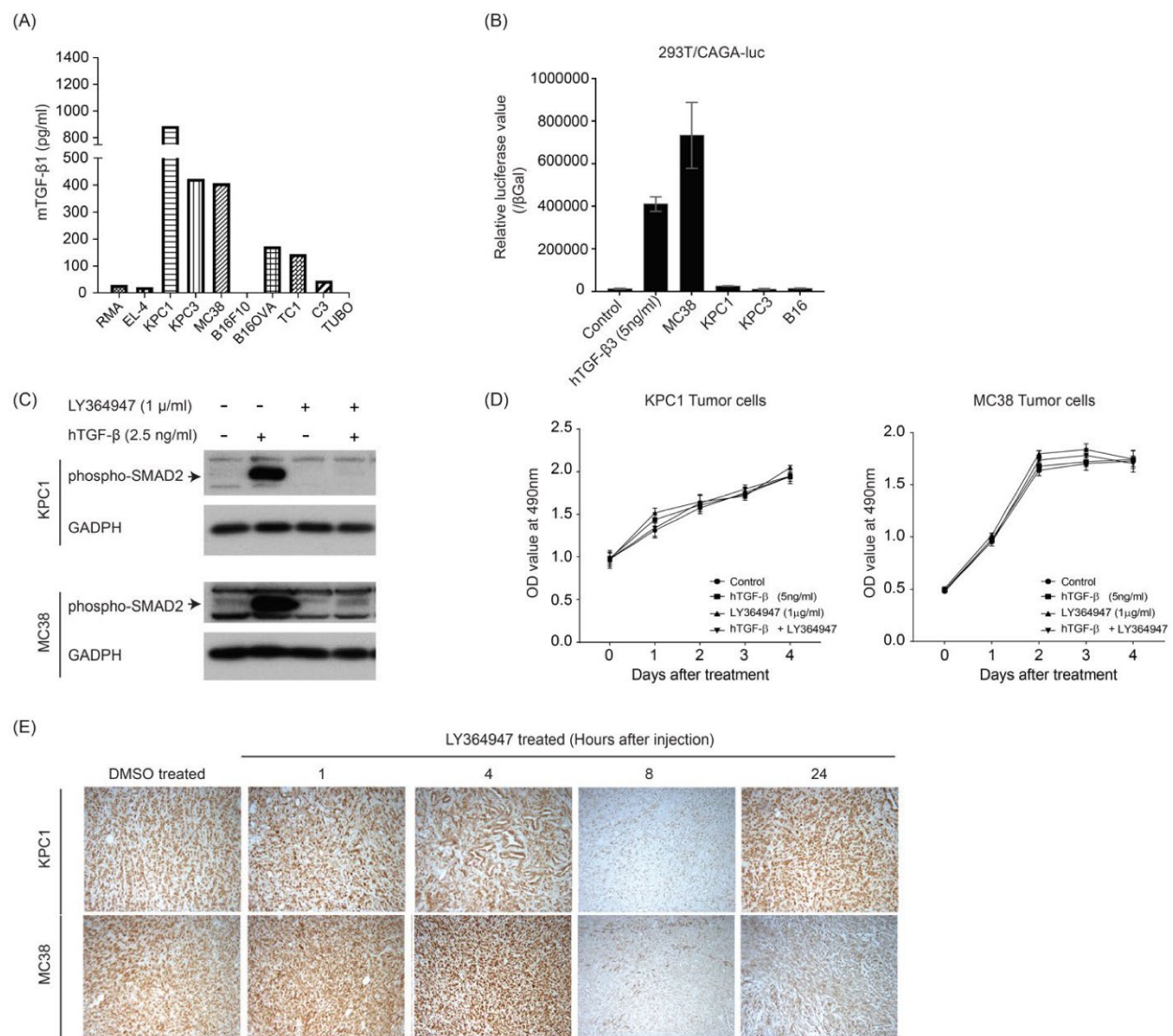


Figure 1. Production level of transforming growth factor-β (TGFβ) by various preclinical mouse tumor models and the potency of LY364947 to inhibit TGFβ-mediated cellular SMAD2

phosphorylation. Latent (A) and active (B) TGF β in the conditioned media of cancer cell lines was assessed by TGF β 1 ELISA and transcriptional CAGA-luciferase reporter assay, respectively. (C) Immunoblotting of phospho-Smad2 of KPC1 and MC38 tumor cell lines after TGF β and/or LY364947 treatment. glyceraldehyde 3-phosphate dehydrogenase (GAPDH) was measured as loading control. (D) Effect of the TGF β and/or LY364947 on the proliferation of KPC1 and MC38 tumor cell lines. (E) Established MC38 or KPC1 tumor-bearing C57Bl/6 mice were administered LY364947 or DMSO, respectively. At 1, 4, 8, and 24 h after the injection, mice were sacrificed and tumors were analyzed by immune-histochemical staining for phospho-SMAD2.

pSMAD2 after intraperitoneal (i.p.) injection of LY364947 in mice bearing either established MC38 or KPC1 tumors (Figure 1D). Histology analysis using phospho-SMAD2 antibody revealed strong phosphorylation of SMAD2 in control DMSO and 1 and 4 h post LY364947-treated MC38 and KPC1 tumors. Decreased TGF β -induced SMAD2 phosphorylation was observed in 8 h post LY364947-treated tumors and this inhibitory effect of LY364947 appeared to last longer in MC38 than KPC1 tumors.

TGF β kinase inhibitor LY364947 improves therapeutic efficacy of Anti-PDL1 mAb

The MC38 colon adenocarcinoma syngeneic model on a C57BL/6 background is highly immunogenic and it has been demonstrated to be sensitive to anti-PD-L1 immune checkpoint

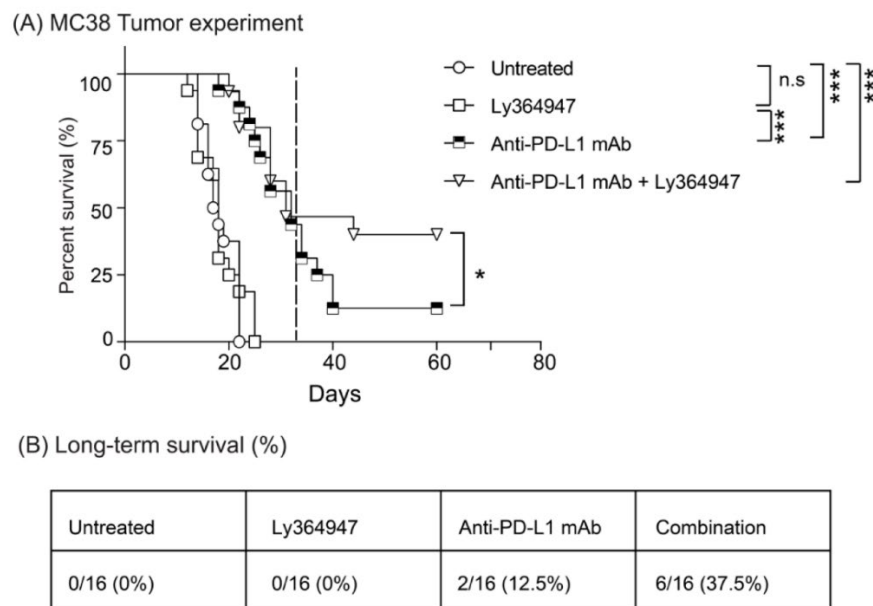


Figure 2. LY364947 improves anti-PDL1 mAb therapy. (A) MC38 tumor-bearing mice were treated with 200 μ g anti-PDL1 mAb i.p. (MIH5; days 8, 10, and 13) and/or 10 mg/kg TGF β receptor kinase

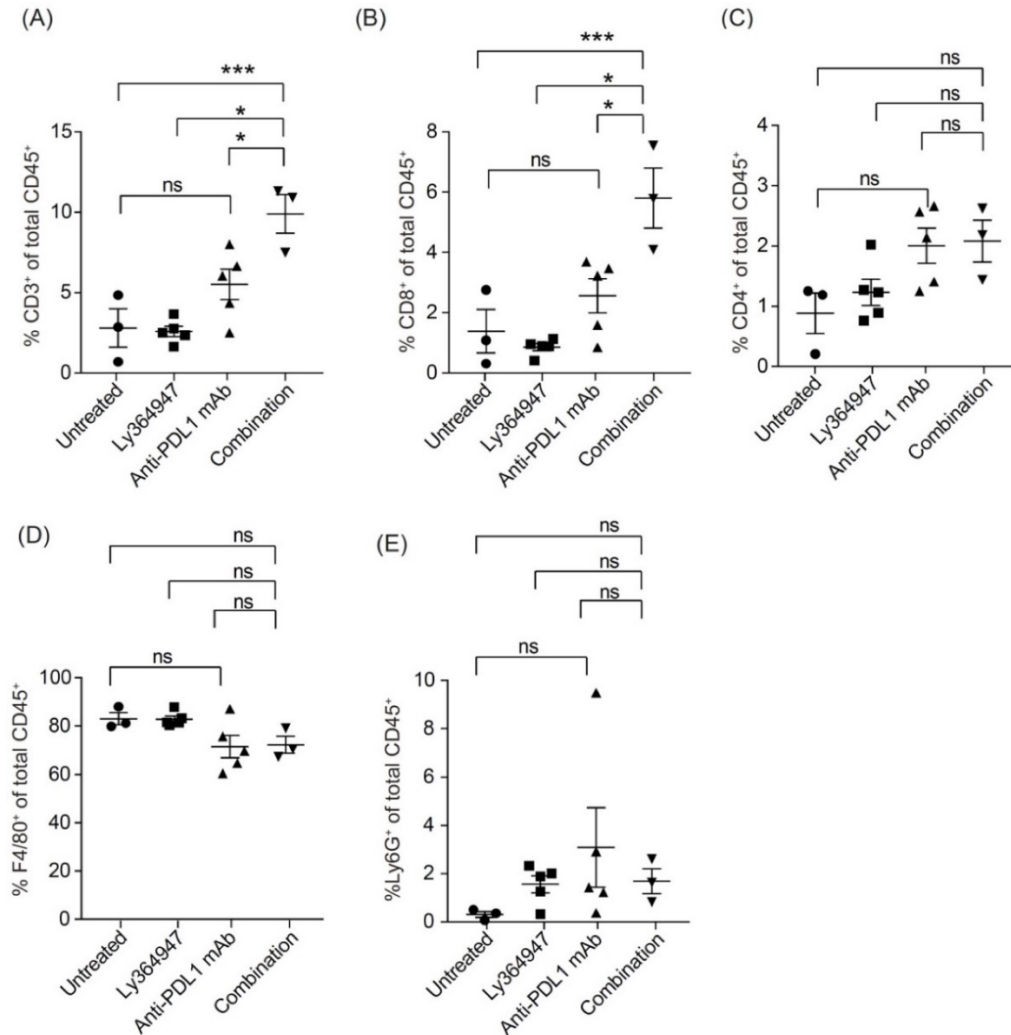
inhibitor i.p. (LY364947; days 8, 10, 13, and every three days). Data presented as Kaplan–Meier survival curves with a total of 16 animals per group. Dashed line represents day 31. The log-rank test was used to determine the statistical significance of the survival. (B) Percentage of mice bearing subcutaneous MC38 treated with indicated regimens that rejected the tumor and survived tumor-free-long-term. Data compiled from two independent experiments, 16 mice per group. PDL1: programmed death-ligand 1. (* $P < 0.05$; *** $P < 0.001$, n.s., non-significant).

monotherapy [41,42]. To test if LY364947 boosts the antitumor effect of anti-PD-L1 mAb, we examined the anti-tumor effect of these treatments on subcutaneously growing MC38 tumors in immune-competent C57BL/6 mice. As shown in Figure 2A, LY364947 induced little therapeutic effect, whereas treatment with anti-PDL1 mAb or combination therapy significantly delayed tumor outgrowth, leading to prolonged overall survival. Beyond day 31, the survival rate of mice treated with combination therapy showed significantly higher survival rate than mice receiving anti-PD-L1 mAb (Figure 2A). These data suggest that the blockade of TGF β receptor activity enhanced the anti-tumor immunity of anti-PD-L1 mAb therapy, leading to improved overall long-term survival in the immunogenic MC38 tumor model (Figure 2B).

Effect of combination therapy on the MC38 tumor microenvironment

To investigate the mechanism of action of anti-PDL1 mAb and LY364947 in the MC38 tumor model, we first analyzed the impact of the therapies on the frequency of immune cells in the tumor microenvironment of MC38 tumors by flow cytometry. As shown in Figure 3A, treatment with combined therapy of LY364947 and anti-PDL1 mAb led to a higher frequency of tumor-infiltrating CD3⁺ T cells. CD8⁺ (Figure 3B, Figure S1A) but not CD4⁺ (Figure 3C). T cells were accountable for the higher frequency to tumor-infiltrating T cells. Moreover, blockade of TGF β had no effect on the frequency of Foxp3⁺ CD4⁺ T cells (Figure S2A). Frequencies of F4/80⁺ macrophages (Figure 3D) and Ly6G⁺ granulocytes (Figure 3E) were not significantly affected by LY364947 and combination therapy. Our results support previously reported studies which show that the combination of TGF β and PD-L1 blockade increased the percentages of CD8⁺ T effector cells in the tumor bed [27] which correlates with the improved tumor eradication of the combination treatment.

Figure 3. Combining TGF β receptor kinase inhibitor LY364947 with anti-PDL1 mAb modulates infiltration of T cells in the tumor. Mice with established MC38 were treated with anti-PD-L1 mAb



(200 μ g; days 8, 10, and 13) and/or LY364947 (10 mg/kg; days 8, 10, 13, and 14). Tumors were harvested at day 15 and analyzed for the percentages of CD3 (A), CD8 (B), CD4 (C) T lymphocytes, (D) F4/80⁺ macrophages, and Ly6G⁺ granulocytes (E) by flow cytometry. Bars represent mean \pm SEM. Statistical significance was determined by one-way ANOVA (* $P < 0.05$; *** $P < 0.001$; ns, non-significant).

TGF β Inhibitor Delays KPC1 Pancreatic Tumor Outgrowth

Unlike the MC38 colorectal tumor model which is known to have high mutational load [43], the KPC tumors, which are derived from the KPC transgenic mouse strain which drives pancreatic ductal adenocarcinoma (PDA) tumorigenesis by expression of a combination of strong oncogenes, is a poorly immunogenic tumor due to a low mutational burden [44]. To investigate the potential checkpoint inhibitors in this PDA model, we examined the expression of

programmed cell death protein 1 (PD-1), cytotoxic T-lymphocyte-associated protein 4 (CTLA-4), and lymphocyte-activation gene 3 (Lag-3) on T cells within the KPC tumor microenvironment. In KPC tumor, the infiltrating T cells were predominantly CD4⁺ and majority of them expressed PD-1 (Figure 4A). These data suggest that blockade of PD-1/PD-L1 may improve antitumor immunity in KPC1 tumor model. We therefore tested the effect of anti-PD-L1 mAb and LY364947 on KPC1 pancreatic tumor outgrowth. Treatment with anti-PD-L1 mAb did not impact tumor outgrowth. In contrast, treatment with LY364947 or combination therapy significantly reduced tumor outgrowth as compared to untreated group (Figure 4B). This suggest that anti-tumor effect was most likely elicited by blocking of TGF β signaling pathway. Moreover, flow cytometric analysis revealed a decrease of total CD3⁺ T cells, particularly CD4⁺ T cells (Figure 4C; Figure S1B), but no detectable decrease of Foxp3⁺ CD4⁺ T cells (Figure S2B). No reduction was observed of granulocytes and macrophages (Figure 4C).

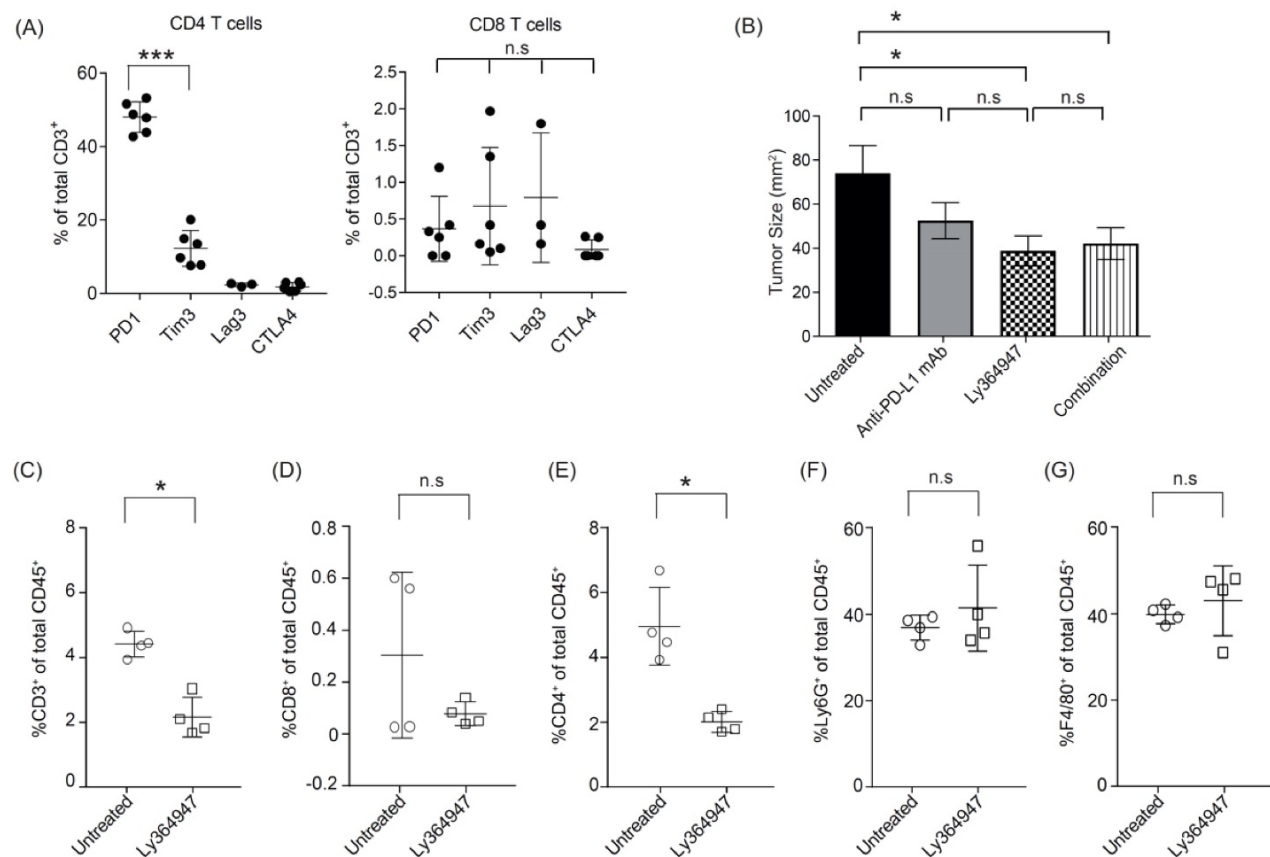


Figure 4. Antitumor effect of LY364947 in KPC1 tumor model. (A) Established KPC1 tumors were harvested at day 17 and analyzed for the percentages of PD-1⁺; Tim3⁺; Lag3⁺; CTLA4⁺ CD4⁺ or CD8⁺ T

cells. (B) KPC1-tumor bearing mice were treated with 200 μ g anti-PDL1 mAb (MIH5; days 8, 10, and 13) and/or 10 mg/kg TGF β inhibitor (LY364947; day 8 and once every day). Data are represented as mean of tumor size $\text{mm}^2 \pm \text{SEM}$ at day 23. Statistical significance was determined by two-way ANOVA (* $p < 0.05$; *** $p < 0.001$; n.s., non-significant). Data from one experiment, eight mice per group. (B) Mice with established KPC1 were treated with LY364947 (10 mg/kg; day 10 to 15). Tumors were harvested at day 16 and analysed for the percentages of (C) CD3 $^+$, (D) CD8 $^+$, (E) CD4 $^+$ T lymphocytes, (F) Ly6G $^+$ granulocytes, and (G) F4/80 $^+$ macrophages. Statistical significance was determined by Student's t-test (* $p < 0.05$; n.s, non-significant).

Discussion

Experimental tumor models are essential preclinical step for the development and evaluation of cancer immunotherapy strategies. From our studies with the MC38 and KPC1 tumor models, one key finding that emerged is that tumor immunogenicity is a dominant feature predicting responsiveness to dual targeting of TGF β signaling and PD-L1. In an immunogenic MC38 tumor model, blocking PD-L1 significantly delayed MC38 tumor outgrowth. However, combination LY364947 with anti-PD-L1 mAb further improved overall survival versus anti-PD-L1 mAb monotherapy (**Figure S3**). The antitumor activity of this combination therapy is consistent with the findings of multiple recent studies using immunogenic tumor models which demonstrated the improvement of anti-PD-L1 mAb when it is combined TGF β receptor kinase inhibitor galunisertib [45, 46]. In all studies investigating the therapeutic efficacy of galunisertib in the colon adenocarcinoma model, galunisertib was injected at high amounts (from 75 mg/kg to 800 mg/kg) and frequent intervals. This might explain the limited antitumor effect of LY364947 (10 mg/kg) monotherapy on MC38 tumor outgrowth observed in our study. Nonetheless, we show that the anti-tumor activity of the combination therapy is associated with higher levels of tumor-infiltrating CD8 $^+$ T cells. This observation is in agreement with the finding of Mariathasan *et al.* [27] who demonstrated that the main mechanism of action of TGF β is to increase T-cell infiltration into MC38 tumor. Together, these data suggest that co-administration of TGF β and PD-L1 blocking agents may provide a subset of colorectal cancer patients a more favorable outcome.

On the other hand, a combined effect of anti-PD-L1 mAb and LY364947 was not observed in poorly immunogenic KPC1 tumor model; blocking of TGF β resulted in significant reduction of KPC1 tumor outgrowth, in contrast to the anti-PD-L1 mAb-treated group, which was not

effective in this model (**Figure S3**). This lack of antitumor efficacy is similar to the lack of responses observed in KPC tumor bearing animal treated with anti-PD1 and/or anti-CTLA-4 mAb [47]. The limited effect of immune checkpoint inhibitors in this tumor model may be due to the low mutational burden and absence of potential neoepitopes derived from tumor mutations [44]. This model is reminiscent of most human pancreatic cancers with similar low numbers of mutations [48]. For this reason, the KPC pancreatic tumor model has a high potential of translational relevance for examining therapeutic efficacy of anti-PD-L1 mAb and LY364947. However, a small cohort of pancreatic cancer patients has been shown to have a relatively high mutational burden [49, 50]; this may have an impact on the therapeutic efficacy of anti-PD-L1 mAb and LY364947. Therefore, study with an alternative pancreatic tumor cell line such as Pan02 (derived from Pancreatic ductal adenocarcinoma (PDAC) tumor induced by implanting 3-methyl-cholanthrene in the pancreas of C57Bl/6 mice) [51] that has a higher mutational burden may help address this question.

More evidence is emerging that targeting TGF β can elicit beneficial effects in halting the pancreatic tumorigenic process. In a study by Principe and colleagues [52], global loss of TGF β signaling protected against pancreatic tumor development via inhibition of tumor-associated fibrosis, stromal TGF β 1 production, and restoration of anti-tumor CD8 $^{+}$ T cells responses. Here we showed that the treatment with LY364947 independent of the established subcutaneous KPC1 tumor decreases the relative amount of CD4 $^{+}$ T cells within the tumor microenvironment. The potential role of CD4 $^{+}$ T cells in promoting pancreatic tumorigenesis has been reported by Alam *et al.* who showed that the p38 MAP kinase inhibitor induced a reduction in the percentage of CD4 $^{+}$ tumor infiltrating lymphocytes (TILs) producing tumor necrosis factor (TNF)- α , retinoic acid-related orphan receptor (ROR γ t), interferon γ (IFN γ), and interleukin (IL)-17, and was associated with improved survival in KPC tumor-bearing animals. A significant delay in pancreatic intraepithelial neoplasia (PanIN) was reported in spontaneous pancreatic tumor model KC mice that received weekly CD4-depleting antibodies [53]. Although TGF β might also be expected to reduce the regulatory CD4 $^{+}$ T cells (Tregs) cell population [11, 54], our data suggest that the numbers of Tregs are not strongly affected by LY364947 and therefore future investigations are warranted to reveal the subsets of CD4 T cells that are affected by the TGF β inhibitor as this would guide the development of therapeutic strategies to target specific tumor-promoting CD4 $^{+}$ T cells in pancreatic tumors.

Clinical studies with galunisertib (LY2157299 monohydrate) have demonstrated its safety and potential antitumor activity [55-57]. It is currently under clinical development in combination with checkpoint inhibitors in patients with non-small cell lung carcinoma (NSCLC), hepatocellular carcinoma (HCC) (NCT02423343), or pancreatic cancer (NCT02734160). In addition, there is an ongoing phase I/II study of galunisertib in combination with the anti-PD-1 antibody nivolumab in participants with advanced refractory solid tumors and in recurrent or refractory non-small cell lung cancer or hepatocellular carcinoma (metastatic and/or unresectable; NCT02423343). Anti-PDL1 mAb therapy is very effective but not all patients respond to this as single agent. The objective response rate with approved anti-PD-L1 mAb as monotherapy is ~20% in urothelial carcinomas [58-60], ~15% in non-small-cell lung cancer (NSCLC) [61, 62], and ~30% in Merkel cell carcinoma [5, 6]. Targeting TGF β pathway inhibition represents an attractive strategy to enhance immune checkpoint blockade. Indeed, a recent study has shown that lack of response to atezolizumab (anti-PD-L1 mAb) in metastatic urothelial cancer patients was associated with active TGF β signaling in peritumoral stroma and especially in patients with T cells excluded from the tumor parenchyma [27]. However, it is unclear whether lack of response to PD-L1 checkpoint blockade is also correlated with active TGF β signaling in other patients of different tumor types. Furthermore, even though the combination of TGF β blockade and checkpoint inhibitors has been demonstrated in multiple preclinical studies, their therapeutic efficacy varies across a range of syngeneic tumors [27, 45, 46, 63-65]. Together, our studies indicate that adequate immune phenotyping of the various tumor models is critical for both rational model selection and data interpretation. This is critical as TGF β has diverse and profound effects on the immune system, and therefore knowledge of the mechanisms by which TGF β interferes in different tumor models may improve the current TGF β -based immunotherapeutic approaches for specific tumor types.

Author Contributions

Designed and supervised the study: F.O. and P.t.D. Conducted the experiments and processed the data: H.S.S., J.R., and M.C. Analysis and interpretation of data: H.S.S., J.R., F.O., M.C., F.O., and P.t.D. The draft of the manuscript was written by HSS. All authors have read and approved the final version of the manuscript

Funding

This work was supported by Cancer Genomics Center Netherlands and Chinese Scholarship Council.

Acknowledgments

The authors thank the staff of the Central Animal Facility (PDC) of the Leiden University Medical Center (LUMC) for excellent animal care and breeding.

Conflicts of Interest

The authors declare no conflict of interest.

References

1. Wei, SC, Duffy, C.R. Allison, JP. Fundamental Mechanisms of Immune Checkpoint Blockade Therapy. *Cancer Discov* 2018, 8(9):1069–86.
2. Smyth, MJ, Teng MW. 2018 Nobel Prize in physiology or medicine. *Clin Transl Immunol* 2018, 7(10):e1041.
3. Lu J, Lee-Gabel L, Nadeau MC, *et al.* Clinical evaluation of compounds targeting PD-1/PD-L1 pathway for cancer immunotherapy. *J Oncol Pharm Pract N* 2015, 21(6):451-67.
4. Lee SM, Chow LQ. A new addition to the PD-1 checkpoint inhibitors for non-small cell lung cancer-the anti-PDL1 antibody-MEDI4736. *Transl Lung Cancer Res* 2014, 3(6):408-10.
5. Kaufman HL, Russell J, Hamid O, *et al.* Avelumab in patients with chemotherapy-refractory metastatic Merkel cell carcinoma: A multicentre, single-group, open-label, phase 2 trial. *Lancet. Oncol.* 2016, 17(10):1374-85.
6. Kaufman HL, Russell JS, Hamid O, *et al.* Updated efficacy of avelumab in patients with previously treated metastatic Merkel cell carcinoma after ≥ 1 year of follow-up: JAVELIN Merkel 200, a phase 2 clinical trial. *J Immunother Cancer* 2018, 6(1):7.
7. Strauss J, Madan RA, Gulley JL. Considerations for the combination of anticancer vaccines and immune checkpoint inhibitors. *Exp Opin Biol Ther* 2016, 16(7): 895-901.
8. Pickup M, Novitskiy S, Moses HL. The roles of TGF β in the tumour microenvironment. *Nat Rev Cancer* 2013, 13(11):788-99.
9. Liu VC, Wong LY, Jang T, *et al.* Tumor evasion of the immune system by converting CD4⁺CD25⁻ T cells into CD4⁺CD25⁺ T regulatory cells: Role of tumor-derived TGF β . *J Immunol* 2007, 178(5):2883-92.
10. Ghiringhelli F, Menard C, Terme M, *et al.* CD4⁺CD25⁺ regulatory T cells inhibit natural killer cell functions in a transforming growth factor- β -dependent manner. *J Exp Med* 2005, 202(8):1075-85.
11. Wan YY, Flavell RA. ‘Yin-Yang’ functions of transforming growth factor- β and T regulatory cells in immune regulation. *Immunol Rev* 2007, 220(1):199-213.
12. Yang L, Huang J, Ren X, *et al.* Abrogation of TGF β signaling in mammary carcinomas recruits Gr-1⁺CD11b⁺ myeloid cells that promote metastasis. *Cancer Cell* 2008, 13(1):23-35.

13. Shvedova AA, Kisin ER, Yanamala N. *et al.* MDSC and TGF β are required for facilitation of tumor growth in the lungs of mice exposed to carbon nanotubes. *Cancer Res* 2015, 75(8):1615-23.
14. Flavell RA, Sanjabi S, Wrzesinski SH *et al.* The polarization of immune cells in the tumour environment by TGF β . *Nat Rev Immunol* 2010, 10(8):554-67.
15. Li MO, Flavell RA. TGF β : A master of all T cell trades. *Cell* 2008, 134(3):392-404.
16. Yang L, Pang Y, Moses HL. TGF β and immune cells: An important regulatory axis in the tumor microenvironment and progression. *Trends Immunol* 2010, 31, 220-27.
17. Yoshimura A, Wakabayashi Y, Mori T. Cellular and molecular basis for the regulation of inflammation by TGF β . *J Biochem* 2010, 147(6):781-92.
18. Caja F, Vannucci L. TGF β : A player on multiple fronts in the tumor microenvironment. *J. Immunotoxicol* 2015, 12(3): 300-7.
19. Park HY, Wakefield LM, Mamura M. Regulation of tumor immune surveillance and tumor immune subversion by TGF β . *Immune Netw* 2009, 9(4):122-6.
20. Sanjabi S, Oh SA, Li MO. Regulation of the Immune Response by TGF β : From Conception to Autoimmunity and Infection. *Cold Spring Harbor Perspect Biol* 2017, 9 (6):a022236.
21. Winkler I, Wilczynska B, Bojarska-Junak A, *et al.* Regulatory T lymphocytes and transforming growth factor β in epithelial ovarian tumors-prognostic significance. *J Ovarian Res* 2015, 8, 39.
22. Wu M, Chen X, Lou J, *et al.* TGF β 1 contributes to CD8⁺ Treg induction through p38 MAPK signaling in ovarian cancer microenvironment. *Oncotarget* 2016, 7(28):44534-44.
23. Guido C, Whitaker-Menezes D, Capparelli C, *et al.* Metabolic reprogramming of cancer-associated fibroblasts by TGF β drives tumor growth: Connecting TGF β signaling with “Warburg-like” cancer metabolism and L-lactate production. *Cell Cycle* 2012, 11(16):3019-35.
24. Papageorgis P, Stylianopoulos T. Role of TGF β in regulation of the tumor microenvironment and drug delivery. *Int J Onco* 2015, 46(3):933-43.
25. Dangerfield J, Larbi KY, Huang MT, *et al.* PECAM-1 (CD31) homophilic interaction up-regulates α 6 β 1 on transmigrated neutrophils in vivo and plays a functional role in the ability of α 6 integrins to mediate leukocyte migration through the perivascular basement membrane. *J Exp Med* 2002, 196(9):1201-11.
26. Sorokin L. The impact of the extracellular matrix on inflammation. *Nat Rev Immunol* 2010, 10(10):712-23.
27. Mariathasan S, Turley SJ, Nickles D, *et al.* TGF β attenuates tumour response to PD-L1 blockade by contributing to exclusion of T cells. *Nature* 2018, 554(7693):544-8.
28. Hawinkels LJ, Verspaget HW, van Duijn W, *et al.* Tissue level, activation and cellular localisation of TGF β 1 and association with survival in gastric cancer patients. *Br J Cancer* 2007, 97(3):398-404.

29. Wu Y, Su M, Zhang S, *et al.* Abnormal expression of TGF β type II receptor isoforms contributes to acute myeloid leukemia. *Oncotarget* 2017, 8(6):10037-49.
30. Seystahl K, Papachristodoulou A, Burghardt I, *et al.* Biological Role and Therapeutic Targeting of TGF β 3 in Glioblastoma. *Mol Cancer Ther* 2017, 16(6):1177-86.
31. Principe DR, Doll JA, Bauer J, *et al.* TGF β : Duality of function between tumor prevention and carcinogenesis. *J Nat Cancer Inst* 2014, 106(2):djt369.
32. Bruna A, Darken RS, Rojo F, *et al.* High TGF β -Smad activity confers poor prognosis in glioma patients and promotes cell proliferation depending on the methylation of the PDGF-B gene. *Cancer Cell* 2007, 11(2):147-60.
33. Sawyer JS, Anderson BD, Beight DW, *et al.* Synthesis and activity of new aryl- and heteroaryl-substituted pyrazole inhibitors of the transforming growth factor- β type I receptor kinase domain. *J. Med Chem* 2003, 46(19):3953-6.
34. Rovero S, Amici A, Di Carlo E, *et al.* DNA vaccination against rat her-2/Neu p185 more effectively inhibits carcinogenesis than transplantable carcinomas in transgenic BALB/c mice. *J Immunol* 2000, 165(9):5133-42.
35. Ljunggren HG, Kärre K. Host resistance directed selectively against H-2-deficient lymphoma variants. Analysis of the mechanism. *J Exp Med* 1985, 162, 1745-59.
36. Corbett TH, Griswold DP Jr, Roberts BJ, *et al.* Tumor induction relationships in development of transplantable cancers of the colon in mice for chemotherapy assays, with a note on carcinogen structure. *Cancer Res* 1975, 35(6):2434-9.
37. Feltkamp, MC, Smits HL, Vierboom MP, *et al.* Vaccination with cytotoxic T lymphocyte epitope-containing peptide protects against a tumor induced by human papillomavirus type 16-transformed cells. *Eur J Immunol* 1993, 23(9):2242-9.
38. Feinstein R, Gallagher A, Illgen-Wilcke B, *et al.* FELASA recommendations for the health monitoring of mouse, rat, hamster, guinea pig and rabbit colonies in breeding and experimental units. *Lab Anim* 2014, 48(3):178-92.
39. Dennler S, Itoh S, Vivien D, *et al.* Direct binding of Smad3 and Smad4 to critical TGF β -inducible elements in the promoter of human plasminogen activator inhibitor-type 1 gene. *EMBO J* 1998, 17, 3091-100.
40. Persson U, Izumi H, Souchelnytskyi S, *et al.* The L45 loop in type I receptors for TGF β family members is a critical determinant in specifying Smad isoform activation. *FEBS Lett* 1998, 434(11):83-7.
41. Kleinovink JW, Marijt KA, Schoonderwoerd MJA, *et al.* PD-L1 expression on malignant cells is no prerequisite for checkpoint therapy. *Oncoimmunology* 2017, 6(4):e1294299.

42. Sow HS, Benonisson H, Breukel C, *et al.* Fc γ R interaction is not required for effective anti-PD-L1 immunotherapy but can add additional benefit depending on the tumor model. *Int J Cancer* 2019, 144(2):345-54.
43. Yadav M, Jhunjhunwala S, Phung QT, *et al.* Predicting immunogenic tumour mutations by combining mass spectrometry and exome sequencing. *Nature* 2014, 515(7528):572-6.
44. Evans RA, Diamond MS, Rech AJ, *et al.* Lack of immunoediting in murine pancreatic cancer reversed with neoantigen. *JCI Insight* 2016, 1(14):e88328.
45. Tauriello DVF, Palomo-Ponce S, Stork D, *et al.* TGF β drives immune evasion in genetically reconstituted colon cancer metastasis. *Nature* 2018, 554(7693):538-43.
46. Holmgaard, RB, Schaer DA, Li Y, *et al.* Targeting the TGF β pathway with galunisertib, a TGF β RI small molecule inhibitor, promotes anti-tumor immunity leading to durable, complete responses, as monotherapy and in combination with checkpoint blockade. *J Immunother Cancer* 2018, 6(1):47.
47. Winograd R, Byrne KT, Evans RA, *et al.* Induction of T-cell Immunity Overcomes Complete Resistance to PD-1 and CTLA-4 Blockade and Improves Survival in Pancreatic Carcinoma. *Cancer Immunol Res* 2015, 3(4):399-411.
48. Alexandrov LB, Nik-Zainal S, Wedge DC, *et al.* Signatures of mutational processes in human cancer. *Nature* 2013, 500(7463):415-21.
49. Grassi E, Durante S, Astolfi A, *et al.* Mutational burden of resectable pancreatic cancer, as determined by whole transcriptome and whole exome sequencing, predicts a poor prognosis. *Int J Oncol* 2018, 52(6):1972-80.
50. Humphris JL, Patch AM, Nones K, *et al.* Hypermutation In Pancreatic Cancer. *Gastroenterology* 2017, 152(1):68-74.
51. Corbett TH, Roberts BJ, Leopold,WR, *et al.* Induction and chemotherapeutic response of two transplantable ductal adenocarcinomas of the pancreas in C57BL/6 mice. *Cancer Res* 1984, 44(2):717-26.
52. Principe DR, DeCant B, Mascarinas E, *et al.* TGF β Signaling in the Pancreatic Tumor Microenvironment Promotes Fibrosis and Immune Evasion to Facilitate Tumorigenesis. *Cancer Res* 2016, 76(9):2525-39.
53. McAllister F, Bailey JM, Alsina J, *et al.* Oncogenic Kras activates a hematopoietic-to-epithelial IL-17 signaling axis in preinvasive pancreatic neoplasia. *Cancer Cell* 2014, 25(5):621-37.
54. Konkel JE, Zhang D, Zanvit P, *et al.* Transforming Growth Factor- β Signaling in Regulatory T Cells Controls T Helper-17 Cells and Tissue-Specific Immune Responses. *Immunity* 2017, 46(4):660-74.

55. Dragovich T, Huberman M, Von Hoff DD, *et al.* Erlotinib plus gemcitabine in patients with unresectable pancreatic cancer and other solid tumors: Phase IB trial. *Cancer Chemother Pharmacol* 2007, 60(2):295-303.
56. Fujiwara Y, Nokihara H, Yamada Y, *et al.* Phase 1 study of galunisertib, a TGF β receptor I kinase inhibitor, in Japanese patients with advanced solid tumors. *Cancer Chemother Pharmacol* 2015, 76(6):1143-52.
57. Ikeda M, Takahashi H, Kondo S, *et al.* Phase 1b study of galunisertib in combination with gemcitabine in Japanese patients with metastatic or locally advanced pancreatic cancer. *Cancer Chemother Pharmacol* 2017, 79(6):1169-77.
58. Rosenberg JE, Hoffman-Censits J, Powles T, *et al.* Atezolizumab in patients with locally advanced and metastatic urothelial carcinoma who have progressed following treatment with platinum-based chemotherapy: A single-arm, multicentre, phase 2 trial. *Lancet* 2016, 387(10031):1909-20.
59. Balar AV, Galsky MD, Rosenberg JE, *et al.* Atezolizumab as first-line treatment in cisplatin-ineligible patients with locally advanced and metastatic urothelial carcinoma: A single-arm, multicentre, phase 2 trial. *Lancet* 2017, 389(10064):67-76.
60. Powles T, O'Donnell PH, Massard C, *et al.* Efficacy and Safety of Durvalumab in Locally Advanced or Metastatic Urothelial Carcinoma: Updated Results From a Phase 1/2 Open-label Study. *JAMA Oncol* 2017, 3(9):e172411.
61. Rittmeyer A, Barlesi F, Waterkamp D, *et al.* Atezolizumab versus docetaxel in patients with previously treated non-small-cell lung cancer (OAK): A phase 3, open-label, multicentre randomised controlled trial. *Lancet* 2017, 389(10066):255-65.
62. Fehrenbacher L, Spira A, Ballinger M, *et al.* Atezolizumab versus docetaxel for patients with previously treated non-small-cell lung cancer (POPLAR): A multicentre, open-label, phase 2 randomised controlled trial. *Lancet* 2016, 387(10030):1837-46.
63. Knudson KM, Hicks KC, Luo X, *et al.* M7824, a novel bifunctional anti-PD-L1/TGF β Trap fusion protein, promotes anti-tumor efficacy as monotherapy and in combination with vaccine. *Oncoimmunology* 2018, 7(5):e1426519.
64. Principe DR, Park A, Dorman MJ, *et al.* TGF β blockade augments PD-1 Inhibition to promote T-cell mediated regression of pancreatic cancer. *Mol Cancer Ther* 2019, 18(3):613-20.
65. Terabe M, Robertson FC, Clark K, *et al.* Blockade of only TGF β 1 and 2 is sufficient to enhance the efficacy of vaccine and PD-1 checkpoint blockade immunotherapy. *Oncoimmunology* 2017, 6(5):e1308616.

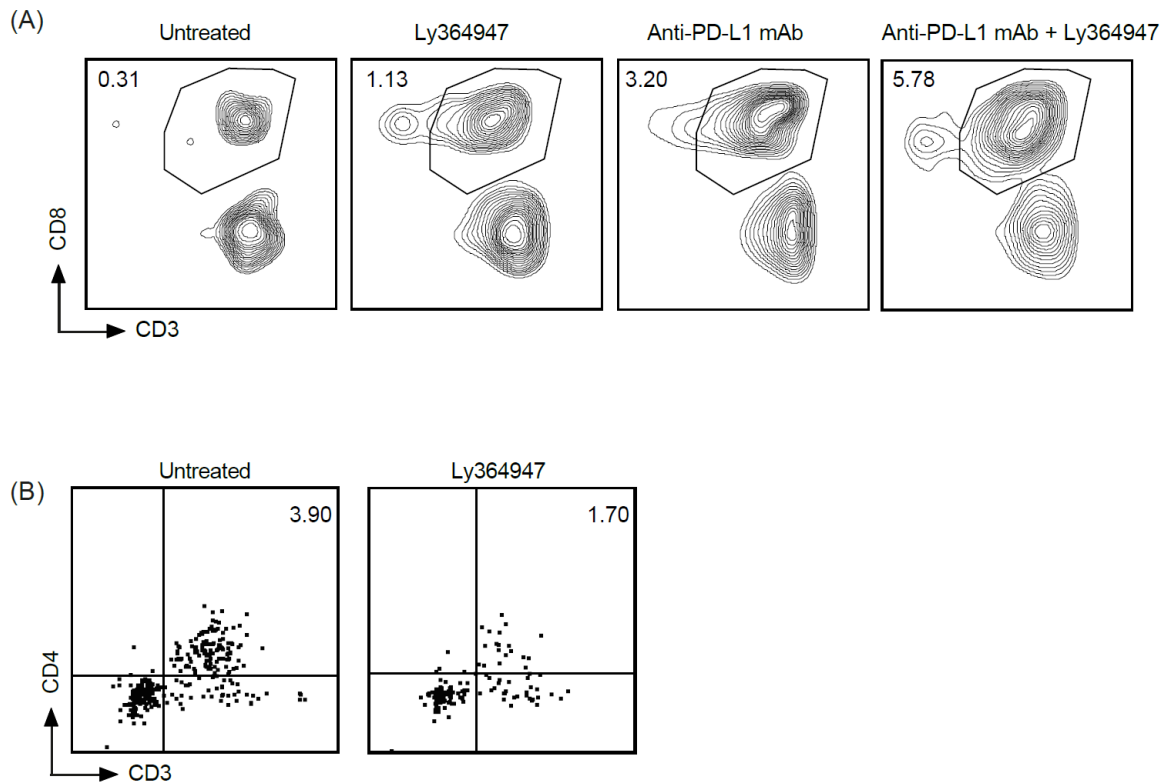


Figure S1. Flow cytometric analysis of T cells in the tumor microenvironment. (A) Representative plots show the frequency of CD8⁺ T cells (plotted against the frequency of CD45⁺ cells) in MC38 tumor. (B) Representative plots show the frequency of CD4 T⁺ cells (plotted against the frequency of CD45⁺ cells) in KPC1 tumor

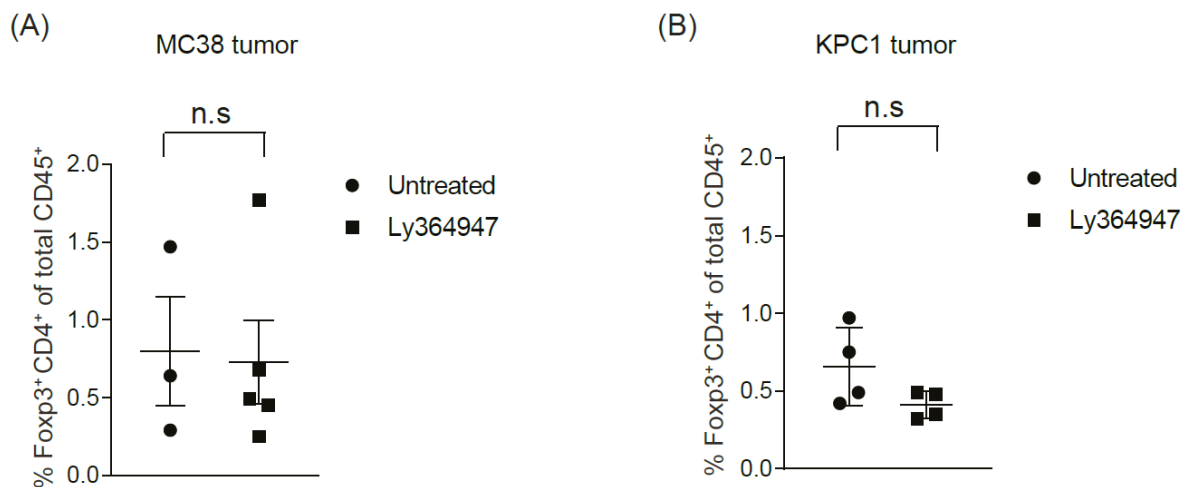


Figure S2. No detectable reduction of tumor infiltrating Foxp3⁺ CD4⁺ T cells upon treatment with LY364947. Flow cytometry analysis of frequency of Foxp3⁺ CD4⁺ T cells in (A) MC38 and (B) KPC1 tumors. Statistical significance was determined by Student's t-test (n.s, non-significant).

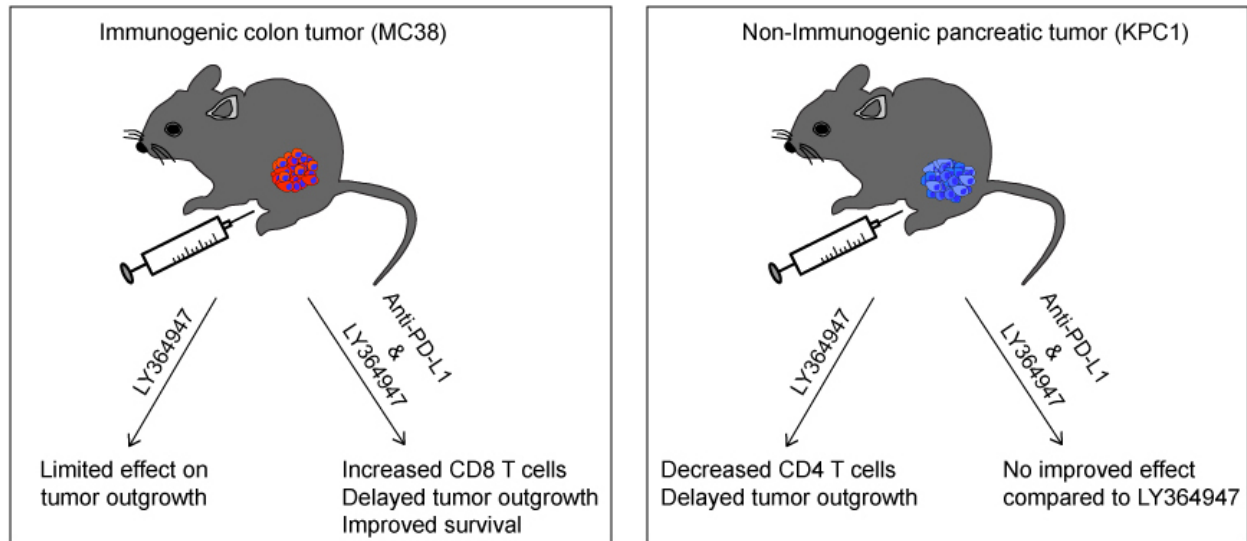


Figure S3. Working model. Tumor immunogenicity is a determinant factor to predict efficiency of dual inhibition of TGFβ and PD-L1 signaling. In an immunogenic MC38 tumor model, inhibition of TGFβ signaling further improved overall survival of anti-PD-L1 treatment. Higher levels of CD8⁺ T cells infiltrate in tumors received combination treatment. However, the enhancement effect of combination treatment is not observed in Non-immunogenic KPC1 tumor model.

Summary and Perspectives

The main aim of my thesis was to reveal the anti-/pro-invasive metastatic role of BMP/TGF β signaling in breast cancer and explore possible therapeutic interventions.

To do so, we first wanted to establish a rapid and inexpensive model in our laboratory to investigate the (potential) functional role of genes and proteins that regulate or mediate the tumor-suppressive and tumor-promoting effects of TGF β family members in breast cancer cells. We opted for zebrafish embryo models in which we injected fluorescently labeled cancer cells (and fibroblasts). In embryos in which the immune system has not yet developed, human/mouse cells are not rejected [1, 2]. At the embryonic stage, the transplanted cells can be easily visualized, as the zebrafish are transparent, particularly casper mutant zebrafish [3]. Human/mouse cells communicate with the zebrafish host. By using genetically engineered *flil:EGFP* zebrafish [4], all vessels are labeled in green, allowing us to easily track the migration and invasion of cancer cells. Two zebrafish models were established: (1) one in which cells were injected into circulation via the duct of Cuvier, which allows us to examine the level of extravasation of cancer cells into the avascular tail fin area; and (2) one in which cells were injected into the perivitelline space, which allows us to examine how cancer cells intravasate into the bloodstream. Moreover, the latter model also allows us to assess the effect of cancer cells in promoting angiogenesis surrounding the grafted tumor mass (**Chapter 2**). Moreover, we further adapted the perivitelline space model by coinjecting breast cancer cells with fibroblasts/cancer associated fibroblasts (CAFs), as discussed in **Chapter 3**. This allows us to look *in vivo* at the effect of the interplay of breast cancer cells and CAFs on the intravasation of cancer cells. Moreover, by adding drugs/small-molecule compounds to the egg water, zebrafish xenograft models are very amendable to pharmacological (and toxicity) studies.

In **Chapter 3**, by analyzing all secreted BMP antagonists in clinical breast cancer datasets, we found a strong correlation between high *GREM1* mRNA expression and poor distant metastasis-free survival of breast cancer patients. Analysis of many breast cancer cell lines surprisingly showed that nearly all cell lines had no detectable *GREM1* expression. Further analysis of different cells in the breast cancer tumor microenvironment showed that *GREM1* was exclusively and highly expressed in CAFs at the invasion front. *Grem1* maintains stemness and promotes invasion of breast cancer cells in a paracrine manner. In addition, *Grem1* mediates the fibrogenic activation of CAFs in an autocrine manner, suggesting that *GREM1* expression can serve as a marker for activated fibroblasts in the cancer stroma. TGF β secreted by tumor cells

was found to be a strong promotor of *GREM1* expression in CAFs, and Grem1 appeared to be capable of inducing TGF β and TGF β target genes in CAFs, thereby creating a feed-forward loop. Moreover, activated CAFs strongly promoted breast cancer cell invasion. In this study, we tried but failed to produce a Grem1-neutralizing nanobody that inhibits breast cancer progression. However, our failure does not mean impossible. Further efforts to develop neutralizing antibodies or small molecular compounds that can block the function of Grem1 are still warranted. We also wondered whether Grem1 was upregulated in the serum of (breast) cancer patients and whether it could be used as a diagnostic or prognostic marker.

After showing that Grem1 is a factor in the tumor microenvironment that could restrict BMP signaling and promote CAF activation, thereby creating a favorable niche for breast cancer cells to invade and metastasize, we continued to explore the intrinsic cellular factors that could regulate BMP signaling in breast cancer cells, which are detailed in **Chapter 4**. We found that progressive loss or suppression of BMP-SMAD1/5 signaling by TGF β -induced activation of MAPK/ERK could be an important factor for metastatic cancer development. We hypothesized that MEK activation induces the activation of a phosphatase, which triggers pSMAD1/5 dephosphorylation. Our ongoing genetic screening attempt suggests that the phosphatase PPM1A may be a candidate. A parallel study shows that FK506 potentially activates BMP signaling in breast cancer cells, whereas TGF β signaling is not affected. Next, we demonstrated that a synergistic effect arose upon restoration of BMP signaling *in vitro* and *in vivo* by combining U0126 and FK506 at suboptimal concentrations. A strong inhibition of cancer cell metastasis was thereby observed.

In **Chapter 5**, we investigated the effector function of a component of the AP1 transcription complex, *i.e.*, JUNB, the expression of which is strongly induced by TGF β in breast cancer cells. We found that JUNB is required for the expression of many late invasion-mediating genes, and in particular, signaling components of the WNT pathway are induced. WNT7B was shown to potentiate TGF β -induced breast cancer cell invasion, creating a feed-forward regulatory network. Intriguingly, we found enhanced MAPK/ERK activation in cells stably expressing WNT7B upon TGF β stimulation. Thus, linking these results to those in **Chapter 4**, the question can be raised as to whether the WNT7B or WNT pathway can create a feed-forward regulatory network that is also involved in sustained MAPK/ERK activation and BMP signaling inhibition in response to TGF β stimulation.

Cancer immunotherapy is emerging as an efficient cancer treatment that improves the prognosis of patients with a broad variety of hematological and solid malignancies [5, 6]. Specifically, the application of immune checkpoint inhibitors (ICIs) was shown to boost the immune system and eradicate cancer cells of patients [6]. However, only a few cancer patients respond to ICIs therapy (less than 10-15%). TGF β is a potent immune suppressor within the tumor microenvironment, and recent studies have revealed roles of TGF β in tumor immune evasion and poor responses to cancer immunotherapy. TGF β also regulates the generation and effector functions of many immune cell types [7]. Importantly, TGF β -activated CAFs are the main determinant for ICIs failure in colorectal and metastatic urothelial cancer [8, 9]. Thus, targeting TGF β pathway inhibition represents an attractive strategy to enhance immune checkpoint blockade. Our key finding, detailed in **Chapter 6**, is that tumor immunogenicity is a dominant feature predicting responsiveness to dual inhibition of TGF β signaling and PD-L1. In an immunogenic MC38 tumor model, inhibition of TGF β signaling further improved the overall survival induced by anti-PD-L1 mAb treatment. The antitumor activity of the combination treatment is associated with higher levels of CD8⁺ T cells infiltration in tumors than were seen in tumors treated with either agent as a monotherapy. However, an enhancement effect of combination treatment was not observed in the poorly immunogenic KPC1 tumor model. As mentioned, TGF β -induced activation of CAFs can work as a physical stromal barrier and prevent immune cell infiltration. We found that Grem1 is a contributor of CAFs activation, as detailed in **Chapter 3**. We are therefore keen to explore whether a Grem1-neutralizing antibody can improve the treatment efficiency of ICIs in immune-excluded and immune-desert tumors.

Overall, our studies elucidated the possibility of manipulating BMP/TGF β signaling to achieve inhibition of breast cancer metastasis, including boosting BMP signaling via blockade of the BMP antagonist Grem1 extracellularly or via stimulation of small-molecule compounds intracellularly, preventing TGF β signaling to allow accumulation of pro-oncogenic stimuli. We also highlight the importance of selecting appropriate cancer types when adopting dual inhibition of PD-L1 and TGF β signaling. I hope my research will aid in more efficient clinical cancer therapies.

References

1. Konantz M, Balci TB, Hartwig UF, *et al.* Zebrafish xenografts as a tool for in vivo studies on human cancer. *Ann N Y Acad Sci* 2012, 1266(1):124-37.

2. Mizgirev I, Revskoy S. Generation of clonal zebrafish lines and transplantable hepatic tumors. *Nat Protoc* 2010, 5(3): 383-94.
3. White RM, Sessa A, Burke C, B *et al.* Transparent adult zebrafish as a tool for in vivo transplantation analysis. *Cell Stem Cell* 2008 , 2(2):183-9.
4. Lawson ND, Weinstein BM. *In vivo* imaging of embryonic vascular development using transgenic zebrafish. *Dev Biol* 2002, 248(2):307-18.
5. Dance A. Cancer immunotherapy comes of age. *Science* 2017, 355(6330):1220-2.
6. Baumeister SH, Freeman GJ, Dranoff G, *et al.* Coinhibitory pathways in immunotherapy for cancer. *Annu Rev Immunol* 2016, 34:539-73.
7. Ganesh K, Massagué J. TGF β inhibition and immunotherapy: Checkmate. *Immunity* 2018, 48(4):626-8.
8. Mariathasan S, Turley SJ, Nickles D, *et al.* TGF β attenuates tumour response to PD-L1 blockade by contributing to exclusion of T cells. *Nature* 2018, 554(7693):544-8.
9. Tauriello DVF, Palomo-Ponce S, Stork D, *et al.* TGF β drives immune evasion in genetically reconstituted colon cancer metastasis. *Nature* 2018, 554(7693):538-43.

Addendum

Nederlandse Samenvatting

List of Abbreviations

List of Publications

Curriculum Vitae

Acknowledgments

Nederlandse Samenvatting

Het belangrijkste doel van mijn proefschrift was het onthullen van de rol van BMP/TGF β -signalering tijdens invasie en uitzaaiingen bij borstkanker en daarnaast mogelijke therapeutische interventies te onderzoeken. In **hoofdstuk 2** geven we een inleidende beschouwing over de rol van BMP in kanker.

Hiervoor hebben we eerst een snel en goedkoop model in ons laboratorium opgezet waarmee de (potentiële) functionele rol van genen en eiwitten werd onderzocht die de tumoronderdrukkende en tumorbevorderende effecten van TGF β -familieleden in borstkankercellen reguleren. We kozen voor zebra vis embryo modellen, waarin we fluorescent-gemarkeerde kankercellen injecteerden (**hoofdstuk 2**). Door embryo's te gebruiken waarin het immuunsysteem zich nog niet heeft ontwikkeld, worden de menselijke/muizencellen niet opgeruimd. In het embryonale stadium kunnen de getransplanteerde cellen gemakkelijk worden gevisualiseerd, aangezien de zebra vissen transparant zijn. Door genetisch gemanipuleerde Fli1:EGFP-zebra vissen te gebruiken, worden alle vaten in het groen gemarkeerd, zodat de migratie en invasie van kankercellen gemakkelijk kan worden gevolgd. Er zijn twee zebra vismodellen opgezet: (1) cellen werden via het kanaal van Cuvier in circulatie gebracht, wat ons in staat stelde om extravasatie van kankercellen te onderzoeken, (2) cellen werden in de perivitelline ruimte geïnjecteerd, waardoor we intravasatie konden bestuderen. Bovendien maakte het laatste model het ook mogelijk om tumor angiogenese te volgen (**hoofdstuk 2**). Verder hebben we het perivitelline ruimte model gebruikt voor co-injectie van borstkankercellen met fibroblasten / kanker geassocieerde fibroblasten (CAFs) in **hoofdstuk 3**. Dit heeft ons in staat gesteld om de interactie van borstkankercellen en CAFs te bestuderen.

Na het goedkope en snelle model zijn we vervolgens uitgescheiden BMP-antagonisten in een klinische model voor borstkanker gaan onderzoeken. Expressieniveaus van BMP-antagonisten in borstkanker samples werden geanalyseerd, waaruit bleek dat er een sterke correlatie is tussen hoge *GREM1* mRNA expressie en een slechte metastase-vrije overleving van borstkanker patiënten (**hoofdstuk 3**). Uit verdere analyse van verschillende borstkanker omgevingscellen bleek dat *GREM1* uitsluitend en hoog tot expressie kwam in CAFs aan het invasiefront. Wij vonden dat *Grem1* stamceleigenschappen handhaaft en invasie van borstkankercellen op een paracrine wijze bevordert. Ook stimuleert *Grem1* de fibrogene activering van CAFs op een

autocrine wijze. TGF β uitgescheiden door tumorcellen bleek een sterke promotor van GREM1 expressie in CAFs, en Grem1 bleek in staat te zijn CAFs tot TGF β secretie aan te zetten.

Nadat was aangetoond dat Grem1 een factor is in de tumor micro-omgeving die BMP-signalering zou kunnen beperken en CAF-activatie kan bevorderen, onderzochten we de intrinsieke cellulaire factoren die BMP-signalering in borstkankercellen reguleren (**hoofdstuk 4**). We ontdekten dat onderdrukking van BMP-SMAD1/5 signalering door TGF β -geïnduceerde activering van MAPK/ERK een belangrijke factor kan zijn voor de ontwikkeling van gemetastaseerde kanker. Parallele studies toonden aan dat het medicijn FK506 het BMP signaal krachtig activeert in borstkankercellen. Vervolgens hebben we aangetoond dat door de medicijnen U0126 en FK506 te combineren bij suboptimale concentraties, een sterke stimulatie van het BMP-signaal plaatsvindt. De combinatie van U0126 en FK506 gaf een sterke remming van kankerceluitzaaiing.

In **hoofdstuk 5** onderzochten we de effectorfunctie van JUNB, een component van het AP1-transcriptiecomplex, waarvan de expressie sterk wordt geïnduceerd door TGF β in borstkankercellen. We vonden dat JUNB nodig is voor expressie van vele late invasie-betrokken genen, en dat in het bijzonder signaleringscomponenten van het WNT-traject werden geïnduceerd.

De kankerimmunotherapie ontpopt zich als een efficiënte kankerbehandeling, die de prognose verbetert van patiënten met een breed scala aan hematologische en solide maligniteiten. In het bijzonder is dit aangetoond door behandeling van kankerpatiënten met immuun controle remmers zoals aPD-L1 (immunotherapie). Echter, nog steeds het merendeel van de kankerpatiënten reageren niet op deze immunotherapie. TGF β is een krachtige immuunsuppressor, en het falen van immunotherapie kan te wijten zijn aan hoge expressie van TGF β in tumoren. Onze belangrijkste bevinding in **hoofdstuk 6** is dat tumorimmunogeniciteit een dominant kenmerk is wat responsiviteit voorspelt op dubbele remming van TGF β -signalering en aPD-L1. In een hoog immunogeen colorectaal tumormodel (MC38) gaf de additionele remming van TGF β signalering een verdere verbetering op de algehele overleving na behandeling met aPD-L1. Echter, dit verbeterde effect van combinatie therapie werd niet waargenomen in het laag immunogene pancreas kanker (KPC1) tumor model.

Samenvattend, heb ik door gebruik te maken van verschillende (pre)-klinische modellen, de rol van verschillende componenten van de BMP/TGF β -signaleringscascade tijdens

tumorceluitzaaiingen onderzocht. Ik heb de moleculaire mechanismen van twee therapeutische interventies die metastasen verminderen in deze cascade achterhaald, en ik heb de rol van TGF β -gemedieerde eiwitten JUNB en Gremlin in borstkankercellen en tumor-omgevingscellen bestudeerd. Ik hoop dat de resultaten van mijn onderzoek in de toekomst zullen bijdragen tot een meer efficiëntere behandeling van kankerpatiënten.

List of Abbreviations

α SMA	α -smooth muscle actin
ACVR2A/B	activin receptor, type II A/B
ALDH	aldehyde dehydrogenase
ALK	activin receptor-like kinase
AP	activator protein
ATCC	american type culture collection
β gal	β -galactosidase
BAMBI	BMP and activin membrane-bound inhibitor
BMP	bone morphogenetic protein
BMPRIA/B	bone morphogenetic protein receptor, type I A/B
BMPRII	bone morphogenetic protein receptor, type II
BRE	BMP response elements
BSA	bovine serum albumin
CAFs	cancer associated fibroblasts
ChIP	chromatin immunoprecipitation
CHT	caudal hematopoietic tissue
CM	conditional medium
COL	collagen
CSC	cancer stem cell
CTC	circulating tumor cell
CTLA	cytotoxic T-lymphocyte-associated protein
CTGF	connective tissue growth factor
dpf/i	days post fertilization/injection
DAN	differential screening-selected gene aberrative in neuroblastoma
D/LCIS	ductal/lobular carcinoma in situ
Doc	Duct of cuvier
ECM	extracellular matrix
EGF	epidermal growth factor
EGFP	enhanced green fluorescent protein
EGFR	EGF receptor
EMT	epithelial–mesenchymal transition
ER	estrogen receptor
ERK	extracellular signal-regulated kinase
FAP	fibroblast activation protein

FACS	fluorescence-activated cell sorting
FBS	fetal bovine serum
FGF	fibroblast growth factor
FN	fibronectin
FOX	forkhead box
fRMA	frozen robust multiarray analysis
FSP1	fibroblast-specific protein 1
GAPDH	glyceraldehyde 3-phosphate dehydrogenase
G-CSF	granulocyte colony stimulating factor
GDF	growth and differentiation factor
GO	gene ontology
Grem	Gremlin
GSEA	Gene set enrichment analysis
HER	human epidermal growth factor receptor
HMEC	human mammary epithelial cells
HGF	hepatocyte growth factor
hpf/i	hours post fertilization/injection
ICIs	immune checkpoint inhibitors
ID	inhibitor of differentiation
IHC	immunohistochemical
IL	interleukin
i.p.	intraperitoneal
ISH	<i>in situ</i> hybridization
JAK	janus kinase
JNK	c-Jun NH ₂ -terminal kinase
KEGG	Kyoto encyclopedia genes and genomes
LAG	lymphocyte-activation gene
MAPK	mitogen-activated protein kinase
MFS	metastasis-free survival
MMP	matrix metalloprotease
MOI	multiplicity of infection
MSCs	mesenchymal stem cells
NF-κB	nuclear factor-κB
NK	natural killer
OCT	octamer-binding transcription factor
OPG	osteoprotegerin

PD-L1	programmed death-ligand 1
PI3K	phosphoinositide 3-kinase
PK	protein kinase
pRb	retinoblastoma protein
PRDC	protein related to Dan or Cerberus
pSMAD	phospho-SMAD
PTEN	phosphatase and tensin homolog
PTHrP	parathyroid hormone-related protein
PTP	protein tyrosine phosphatase
qRT-PCR	quantitative real-time polymerase chain reaction
RANKL	nuclear factor- κ B ligand
RGM	repulsive guidance molecule
s.d	standard deviation
s.e.m	standard error
SMAD	small mothers against decapentaplegic
SMURF	SMAD ubiquitin regulatory factor
SNP	single nucleotide polymorphism
SOX	SRY-related HMG-box
STAT	signal transducers and activators of transcription
TAZ	tafazzin
TGF β	transforming growth factor β
TGFBRI/II	TGF β receptor, type I/II
TNBC	triple negative breast cancer
TNF α	tumor necrosis factor α
THBS	thrombospondin
ZEB1	E-box-binding homeobox 1

List of Publications

1. **Ren J**, Smid M, Iaria J, Salvatori DC, van Dam H, Zhu HJ, Martens JW, ten Dijke P. Cancer-associated fibroblast-derived Gremlin 1 promotes breast cancer progression. *Breast Cancer Res* 2019, 21(1):109.
2. Sow HS*, **Ren J***, Camps M, Ossendorp F, ten Dijke P. Combined inhibition of TGF β signaling and the PD-L1 immune checkpoint is differentially effective in tumor models. *Cells* 2019, 8(4):E320.
3. **Ren J**, ten Dijke P. Bone morphogenetic proteins in the initiation and progression of breast cancer. *Bone Morphogenetic Proteins: Systems Biology Regulators*, Springer 2017, p.409-33.
4. **Ren J***, Liu S*, Cui C, ten Dijke P. Invasive behavior of human breast cancer cells in embryonic zebrafish. *J Vis Exp* 2017, (122):e55459.
5. Sundqvist A*, Morikawa M*, **Ren J**, Vasilaki E, Kawasaki N, Kobayashi M, Koinuma D, Aburatani H, Miyazono K, Heldin CH, van Dam H, ten Dijke P. JUNB governs a feed-forward network of TGF β signaling that aggravates breast cancer invasion. *Nucleic Acids Res* 2017, 46(3):1180-95.
6. Li Y, Drabsch Y, Pujuguet P, **Ren J**, van Laar T, Zhang L, van Dam H, Clément-Lacroix P, ten Dijke P: Genetic depletion and pharmacological targeting of α v integrin in breast cancer cells impairs metastasis in zebrafish and mouse xenograft models. *Breast Cancer Res* 2015, 17(1):28.
7. **Ren J***, Wang Y*, Iaria J, ten Dijke P, Zhu HJ: Synergistic reactivation of BMP signaling by MEK inhibitor and FK506 reduces breast cancer metastasis. (Manuscript in submission)

*These authors contributed equally

Curriculum Vitae

Jiang Ren (任江) was born on 10th of December 1987 in Longzhong, Sichuan province, China. He finished Master study in State Key Laboratory of Biotherapy at West China hospital, Sichuan university, China (September, 2010-June, 2013). His Masters research project focused on immunotherapy of lung cancer in humanized mouse model. Thereafter, he worked 1 year as a Research Assistant in State Key Laboratory of Biotherapy. During that period, he mainly performed pharmacokinetic preclinical studies on newly discovered therapeutic compounds. In September, 2014, he started his PhD research in the group of Prof. Dr. Peter ten Dijke. While his initial studies focused on the role of the BMP pathway in breast cancer cell invasion and metastasis, in subsequent research projects he examined the effector role of JUNB in TGF β /SMAD-induced breast cancer invasion and whether targeting TGF β can improve therapy with immune checkpoint inhibitors.

Acknowledgments

It is the time! No matter how gorgeous the words are, they couldn't capture my tremendous appreciation to those that have all contributed.

I would like to express my sincere gratitude to my supervisor Prof. Dr. Peter ten Dijke! Many thanks for the opportunity to be a member of your excellent team where I learnt and benefited a lot. His mentorship and kindness has guided, motivated and supported me throughout my PhD training.

I am grateful to all my kind teammates. Midory, Maarten and Gerard for their enormous help. Sijia, Yihao, Gonzalo, Amaya, Miriam, Chuannan, Mary Jin, Jing, Prasanna, Marten, Dieuwke, Sharon, Maureen for their daily help. And best wishes to new friend Yifan, Abhishek.

Special thanks for suggestion and comments from great scientists Dr. Hans van Dam, Dr. David Baker, Dr. Laila Ritsma, Prof. Dr. Alfred Vertegaal, Prof. Dr. Marie-Jose Goumans, Prof. Dr. John Martens, Prof. Dr. Daniela Salvatori, Dr. AG Jochemsen, Dr. Annemarthe van der Veen, and Dr. Manuel Goncalves.

Many thanks my collaborators Hengsheng, Marcel, Yanhong.....

Many thanks go to Julia, Willem, Martijn, Annelies, Steve, Jin, Qian, Ruud, Roman, Baoxu..... for all the help!

Also thanks the committee members of my thesis defense for their valuable time!

I am greatly indebted to my family for their endless support and love!

Thanks to China! Thanks to The Netherlands! Thanks to LUMC! Thanks to M/CCB!
Thanks to TGF β /BMP superfamily!

